UNIVERSITÉ DE STRASBOURG

ÉCOLE DOCTORALE 414

Laboratoire de Neurosciences Cognitives et Adaptatives - UMR7364

THÈSE présentée par :

Laura TZEPLAEFF

Soutenue le : **16 décembre 2021**

Pour obtenir le grade de : **Docteur de l'université de Strasbourg**

Discipline / Spécialité : Biologie / Neurosciences

Memory dysfunctions and associated epigenetic and transcriptomic changes in an ALS/FTD mouse model linked to a FUS mutation

Etude des dysfonctionnements de la mémoire et des modifications épigénétiques et transcriptomiques associées, dans un modèle murin de SLA/DFT lié à une mutation de la protéine FUS

THÈSE dirigée par (codirection) :

Mme BOUTILLIER Anne-Laurence	Directrice de Recherches, Université de Strasbourg
M. DUPUIS Luc	Directeur de Recherches, Université de Strasbourg

RAPPORTEURS :

M. FISCHER André	Professeur Docteur, University Medical Center, Göttingen
Mme SUBERBIELLE Elsa	Chargée de Recherches, Université de Toulouse

AUTRES MEMBRES DU JURY :

M. VAN DEN BOSCH Ludo	Professeur, Center for Brain & Disease Research, Leuven
Mme GODIN Juliette	Chargée de Recherches, Université de Strasbourg
M. MONASSIER Laurent	Directeur de Recherches, Université de Strasbourg

REMERCIEMENTS

Durant ces 4 années de thèse, j'ai eu la chance d'être en contact avec de nombreuses personnes qui m'ont soutenu tout au long de mon parcours. Ça serait une erreur de dire que cet aboutissement n'est que le résultat d'une seule personne. Chacun, à votre manière, vous avez contribué à l'aboutissement de mes études et de ce projet professionnel. Ce chapitre peut vous paraître un peu long mais il m'était important de remercier chaque personne comme il se doit.

Cette aventure a tout d'abords commencé grâce à mes deux co-directeurs de thèse **Anne-Laurence BOUTILLIER (Laurette)** et **Luc DUPUIS**. A l'époque, bien que la SLA et les maladies neurodégénératives n'étaient pas un début pour moi, je n'avais jamais entendu parler de ChIP-seq et d'analyses bio-informatiques. Merci de m'avoir tout de même fait confiance et d'avoir cru en ma motivation pour assurer toutes ces tâches. Ça a été un grand chalenge ! Mais aujourd'hui, la technique de Chip-seq n'a presque plus de secret pour moi, même pour FUS qui nous a donné du fil à retordre ! Grâce à vous, j'ai pu m'ouvrir et apprendre de nouvelles choses tous les jours.

Laurette, je retiens tout particulièrement le temps que tu m'as accordé pour la préparation de mes multiples présentations orales ainsi que le soutient lors de l'écriture de mes différents abstracts. L'attention que tu as apportée à chacun de ces projets a largement contribué à l'obtention de la Bourse de déplacement pour les NeuroFrance de Marseille et du Prix de la meilleure présentation orale du Neuropole. Ceci a largement contribué à booster ma confiance quant à mes capacités. Je te remercie aussi de m'avoir fait participer à la réalisation de publications sur des projets parallèles, notamment sur le projet ThyTau, Bmal1 ou Cafeine.

Luc, je me souviens en particulier de la période des demandes de 4ème années. Nous avons travaillé ensemble pour mettre en place deux dossiers et j'ai beaucoup apprécié ta manière d'organiser et de planifier ce projet. Ça a été une énorme surprise, par la suite, de voir notre demande auprès de la FRM acceptée. Là encore, c'était extrêmement valorisant de réaliser que notre projet intéressait. J'ai appris que même lorsque la possibilité de succès est très faible, il faut tout de même essayer. Car parfois, oui, on gagne ! Merci pour tes discussions rassurantes à la fin de ma thèse lorsque la pression et le stress étaient au plus haut.

Un énorme merci à mes rapporteurs de thèses **André FISCHER** et **Elsa SUBERBIELLE**, et pour le temps qu'ils accorderont à la lecture de ce rapport. Sans nul doute, vos commentaires

contribueront à la qualité du manuscrit final. Je suis aussi très reconnaissante que vous ayez accepté de faire partie de mon jury de thèse le jour de ma soutenance avec **Juliette GODIN** et **Ludo VAN DEN BOSCH**. J'ai hâte d'échanger sur le projet avec vous quatre, et je suis sûre que nos discussions seront très enrichissantes. Un grand merci à **Laurent MONASSIER**, qui a gentiment accepté d'endosser le rôle de président du jury au dernier moment et qui a permit à ma thèse d'avoir lieu malgré les imprévus liés au COVID19.

Le côté positif de travailler en codirection c'est que j'ai eu la chance d'être en contact avec deux fois plus de collègues. Chacun avec des personnalités, des idées et des qualités très différentes. Merci à tous mes collègues pour nos nombreuses discussions en labmeeting ou concernant les projets scientifiques !

Au LNCA, notamment merci à **Karine MERIENNE** pour nos nombreuses discussions sur les sujets d'épigénétiques pour mon premier papier, ainsi que d'avoir fait partie de mon jury de comité de suivi de thèse avec **Valérie BUEE-SCHERRER**.

Un énorme merci à **Isabel PAIVA**, la meilleure collègue et amie portugaise ! Tu as été un énorme support tout au long de ma thèse, que ce soit lors de discussions scientifiques, concernant mon futur et ma vie personnelle, ou lors de nos cours de portugais. En dehors les discussions enrichissantes, tu as été très présente pour la mise en place ou l'amélioration de plusieurs protocoles, ainsi que pour les analyses de nos données. Tu m'as même remplacé avec **Iris GRGURINA** lorsque j'ai dû me mettre à l'écriture de mon manuscrit. Merci à toutes les deux, vous m'avez été indispensables ! Merci à **Rafael ALCALA VIDA**, sans toi j'aurais été perdue dans de nombreux domaines scientifiques. Comment isoler des noyaux par FACS ? Comment faire sans fixation ? Comment marche un ChIP- ou un ATAC-seq ? Et comment on analyse tout ça ? Isabel et toi vous avez toujours une réponse à apporter et vous êtes toujours heureux d'aider avec le sourire. Merci à vous deux d'avoir participé à la relecture de mon manuscrit et d'avoir été de bons compagnons pour prendre soin de nos souris !

Je remercie **Jonathan SEGUIN**, qui a permis d'analyser nos multiples résultats de ChIP-seq et qui m'a transmis de nombreux scripts qui me permettent maintenant d'être un peu plus autonome quant à l'analyse de ces données. Merci pour nos discussions, tes explications et ton aide continuelle, même après ton départ du LNCA. Merci à **Charles DECRAENE** d'avoir pris le relais sur les analyses de nos données, principalement via tes compétences concernant les RNA-seq. Et

merci d'avance pour les futures discussions et analyses qui seront nécessaires à la publication de nos différents projets.

Merci à **Brigitte COSQUER**, la personne à ne surtout pas oublier ! Tu es les petites mains discrètes du labo, mais indispensable à la réalisation de tous nos projets. Toujours prête, bien organisée et présente même lorsque le COVID m'a bouclée à la maison. Perfusions, immuno- ou Golgi, aucun problème pour toi. Mais que ferait-on sans toi ? En dehors du travail, tu as toujours été un bon support lors des petits coups de mou ou de doute.

Merci à **Anne PEREIRA DE VASCONCELOS** pour les conseils concernant le comptage des épines dendritiques. Ça n'a pas été une mince affaire ! Merci à **Jean-Christophe CASSEL** qui a toujours eu sa porte ouverte pour discuter des petits soucis de la vie scientifique. Merci à ma collègue la plus récente, **Laurine BOCH**, qui a partagé mon bureau, de nombreuses discussions et mes galères sur Azymaze. Heureusement, tu avais aussi toujours du temps pour boire un verre ou manger de bonnes choses. Dans notre bureau, je souhaite aussi la bienvenue à Elodie **PANZER**, qui lors de son Master nous à déjà prouvé qu'elle fera une collègue et amie formidable. Merci à mes anciennes collègues, et notamment à **Xiaolan WANG**, toujours souriante et volontaire. Tu as été ma collègue de jour et de nuit pour les expériences sur le cycle circadien. J'espère que depuis que tu es Docteur tu peux passer des nuits plus paisibles. Merci à **Estelle SCHUELLER** et **Caroline LOTZ**, notamment concernant les tests et analyses comportementales sur les souris. Merci aux autres membres du groupe, présents ou déjà partis, notamment **Ali AWADA**, **Baptiste BRULE**, **Marion PELLEN**, **Marie-Muguet KLEIN, Aurélie SALVADORI** et les autres avec qui j'ai eu moins le temps de collaborer et de connaître.

La recherche scientifique est un milieu de collaboration. Outre mon groupe de recherche, j'ai aussi énormément apprécié les échanges avec les autres membres du labo. Je remercie **Chantal MATHIS** pour avoir accepté de participer à la rédaction de ma deuxième publication et à la relecture de cette partie du manuscrit. Merci à **Karine HERBAUX**, qui, comme Brigitte, assure le bon fonctionnement du labo et a été d'une grande aide pour la résolution de nombreux petits soucis. Comme le labo le dit si bien, vous êtes un peu nos mamans et l'ambiance agréable du LNCA ne serait pas la même sans vous deux. Merci de nous soutenir et de nous remonter le moral régulièrement. Je remercie **Catherine KRIEGER** qui gère d'une main de maître toute la paperasse du labo et qui a toujours sa porte ouverte pour répondre à nos questions administratives. Un énorme merci à **Aminé ISIK** qui est la meilleur dans la gestion des animaux, des repros et des phénotypages, mais avec qui nous pouvons aussi passer de très bons moments de discussion. Merci

à **Marie-Dominique MARINUTTI**, depuis que tu es arrivée, tu as toujours une histoire improbable à nous raconter, mais toujours avec ta bonne humeur et ton grand sourire. Je te souhaite tout le courage du monde pour le comptage des épines dendritiques. Merci à **Anne-Sophie AUBRY**, nous n'avons pas seulement partagé un bureau mais aussi quelques bons moments pour se plaindre et se détendre autour d'un verre avec Laurine et **Matthieu AGUILERA**. Merci aussi à **Florian SCHOUKROUN** qui, même tard le soir, est présent pour te sortir de mauvaises situations dans le labo. Merci à **Vincent DOUCHAMPS** pour nos discussions dans la cuisine sur l'avenir du milieu scientifique. Je remercie aussi **Wilf GARDNER** et **Cristiana PISTONO** avec qui j'ai partagé le bureau un petit moment. Merci à **Samy CASTRO** qui nous a rejoint plus tard au labo, mais à qui nous avons présenté toutes les spécialités françaises les unes après les autres : croziflette, raclette, choucroute et autres. Et ce n'est pas fini ! Merci aux animaliers **George EDOMWOYNI** et **Daniel EGESI**, mais principalement à **Olivier BILDSTEIN** toujours présent pour nous aider, que ce soit avec les animaux ou pour regonfler une roue de vélo.

Outre les collègues, j'ai aussi rencontré de réels amis lors de ma thèse. Je pense notamment à **Laura DURIEUX** et **Christopher BORCUK,** mais surtout à deux filles un peu folles et pétillantes qui sont toujours présentes pour moi, **Gaëlle AWAD** et **Caroline CORREIA**. Je ne compte plus les Escape Games que nous avons effectués ensemble, les soirées jeux de société, les Halloweens et Nouvels Ans. Autant de bons moments que je n'ai pas la place de lister ici. Un deuxième merci à Gaëlle et Caroline pour le soutient qu'elles m'ont apporté lors de ma fin de thèse. Même si j'étais moins disponible, elles sont venues me rendre visite, m'ont préparé des repas et se sont révélées être des amis exceptionnels !

Même si j'ai principalement été présente au LNCA, j'ai eu la chance de travailler quelque temps à la Fac de médecine au sein de l'INSERM 1118 où j'ai rencontré un grand nombre de personnes essentielles à la mise en place de ce projet.

Je tiens à remercier **Salim MEGAT** pour nos échanges sur les analyses bio-informatiques des projets FUS. Nous avons pu notamment échanger durant nos quelques jours de ChIP-seq H3K27me3. Merci pour le temps que tu passes à remanier, analyser et intégrer nos résultats pour la mise en place des publications. Merci à **Stéphane DIETERLE** pour avoir effectué des manips complémentaires sur le projet. Tu gères les fractionnements nucleo-cytoplasmics comme personne ! Je t'ai confié mes échantillons en toute sérénité. Merci à toi et **Gina PICCHIARELLI** pour m'avoir présenté aux autres membres de votre labo lorsque je suis arrivée. Surtout, je suis

heureuse que nous ayons réussi tous ensemble à mettre au point le ChIP-seq de FUS. Grosse réussite !

Merci à **Raphaelle CASSEL** pour les discussions sur le projet et le futur. J'apprécie le temps que tu m'as accordé pour la relecture de mon manuscrit ainsi que ton aide quant à la mise en place de tests comportementaux. Tes conseils m'ont été d'une grande aide. Merci aussi à **Félicie LORENC** et **Margueritte JAMET,** notamment pour nos discussions intéressantes aux dernières JR7 SLA. Merci à **Sylvie GROSCH** pour tes conseilles sur les immuno quand je suis arrivée dans le labo et merci à toi pour assurer la suite de ces manips après mon départ. Merci à **Caroline ROUAUX**, à chacune de mes présentations tu as toujours de bonnes questions qui permettent de bonnes discussions sur le projet. Merci à **Chantal SELLIER** pour les expériences sur cultures cellulaires qui permettront, je l'espère, de mieux comprendre le mystère FUS-ETS.

Merci à **Aurore BRUNET** avec qui je me suis tout de suite bien entendue dans le labo et au cours de nos déplacements professionnels. J'ai particulièrement apprécié les quelques jours à Paris pour les JR5 SLA ou lors du meeting franco-allemand-suisse en Allemagne, notamment avec d'autres membres du labo : **Matei BOLBOREA**, **Alexandra BOUSCARY**, **Thibaut BURG**, **Haoyi LIU**, **Cyril QUESSADA**, **Inmaculada SANJUAN RUIZ** et **Geoffrey STUART LOPEZ**. Merci aux autres membres du labo qui ont été présents, que ce soit pour le travail, l'administratif ou le bon temps passé ensemble : **Frédérique RENE**, **Claudia DE TAPIA**, **Marc-Antoine GOY**, **Brigitte KUENEMANN** et **Marie-Josée RUIVO**. Merci à vous tous pour la fête de Noël et le barbecue estival !

J'aimerais aussi remercier mes amis de longue date, qui sont restés dans le monde scientifique (ou pas). **Patrik POLGARI** présent depuis toujours, mais aussi principalement mes collègues du parcours franco-allemand, notamment la présentement canadienne **Anne-Gabrielle SIEMONSMEIER**, et la très joviale **Pauline GRAFF**. Je remercie aussi **Kenny SCHUMACHRER** et **Marine HEMMERLE**, qui ont tous deux répondu présents pour participer et interagir lors de mes cours d'UE langue scientifique. J'aimerais particulièrement remercier **Joern PÜTZ**, l'organisateur de ce parcours franco-allemand, qui a largement contribué à ma réussite. Tu m'as fait confiance il y a maintenant presque 10 ans et, grâce à toi, j'ai pu effectuer des expériences scientifiques internationales exceptionnelles et découvrir le monde de l'enseignement pendant 3 ans. En passant, merci à tous mes élèves qui étaient présents aux cours, que ce soit sur le campus ou en visio. Vous étiez là pour apprendre, mais moi aussi j'ai grandi et appris tellement de choses à travers vos exposés et nos discussions. Je ne regrette pas mon

engagement quand je vois le compte rendu si élogieux que vous avez fait sur nos cours d'UE langue scientifique.

Pour terminer, j'aimerais remercier d'une manière toute particulière les membres de ma famille et mon entourage. Vous n'avez pas participé de manière scientifique au projet, mais vous m'avez tenu la main tout au long de ce chemin semé d'embuches. Je remercie mes parents **Evelyne** et **Ivan TZEPLAEFF** qui m'ont accueilli tous les weekends chez eux pour que je puisse me changer les idées. Merci pour tous ces bons moments en famille, avec mon grand frère **Mikaël TZEPLAEFF** et mamie **Micheline HERRMANN** autour d'un dîner, d'un film, d'un jeu ou lors d'une balade avec ce chien tellement attendu depuis 15 ans. **Cannelle**, qui m'occupe tous les dimanche matin lors de longues promenades et de cours d'éducation canine. On se demande qui apprend le plus à l'école ? Elle ou moi ? Bien sûr je pense aussi à tous les autres membres de ma famille qui m'accompagnent de loin. Une grosse pensée pour vous tous.

Une mention toute particulière pour **Théo MEYER**, un jeune homme fantastique qui me supporte depuis plus de 10 ans. Je tiens à préciser que pour ta part, ta participation n'a pas été que psychologique. Tu as été impliqué dans un certain nombre de mes projets tout en me soutenant lors de mes formations à l'analyse bio-informatique et des différents langages de programmation. Merci pour ton aide sur les scripts qui m'ont permis d'ordonner et d'analyser les datas des différents tests comportementaux (Actographie, water maze, test d'objet), mais aussi sur les scripts qui me permettent aujourd'hui d'être un peu plus autonome sur mes analyses de séquençages. Ta passion pour l'électronique et l'élaboration des scripts m'a inspiré et m'a poussé à faire de même dans ma carrière. Il est aussi indispensable de rappeler, que même absent lors de mes dernières semaines d'écriture, tu m'as fait livrer deux semaines de nourriture provenant de chez Picard pour m'éviter de mourir de faim. Mais qu'aurais-je donc fait sans toi ? Tout simplement merci d'être là, toi et toute ta famille qui a une place toute particulière dans mon cœur. I love you.

CONTENTS

LIST OF FIGURES

ABBREVATIONS

a.a. = amino acids
AC = Anterior Cingular cortex
ALS = Amyotrophic lateral sclerosis
AMPA = α-amino-3-hydroxy-5-methyl-4-isoxazolepropionic acid
Arc = activity-regulated cytoskeleton associated protein
BDNF = Brain-derived neurotrophic factor
BIBD = Basophilic inclusion body disease
Bmal1 = Brain and muscle arnt-like 1
C9ORF72 = Chromosome 9 open reading frame 72
CA = Cornus ammonis
CaMKII = Calcium/calmodulin dependent protein kinase II
CBD = Corticobasal degeneration
CBP = CREB binding protein
CCNF = Cyclin F
ChIP = Chromatin Immuno Precipitation
CHMP2B = Charged Multivesicular Body Protein 2B
CHCHD10 = Coiled-coil-helix-coiled-coil-helix domain containing 10
CLIP = Crosslinking Immuno Precipitation
CLOCK = Circadian Locomotor Output Cycles Kaput
Cry = Cryptochrome Circadian Regulator
CRE = cAMP response element
CREB = cAMP Response Element binding protein
DEG = Differential enriched genes
DG = Dental gyrus
DNA = Deoxyribonucleic acid
DNA-PK = DNA protein kinase
DSB = double strand break
dsDNA = double strand DNA
dsRNA = double strand RNA
e.g. = example given
E = Nuclear export signal
ETS = E-Twenty six
fALS = familial ALS
fFTD = familial FTD
FUS = Fused in Sarcoma
FTD = Frontotemporal dementia
FTLD = Frontotemporal lobar degeneration
GNAT = Gcn5-related N-acetyltransferases
H = Hilus
H2a = Histone 2a
H2b = Histone 2b
H3 = Histone 3
H3K9ac = Histone 3 lysine 9 acetylated
H3K9me3 = Histone 3 lysine 9 trimethylation
H3K14ac = Histone 3 lysine 14 acetylated
H3K27ac = Histone 3 lysine 27 acetylated
H3K27me3 = Histone 3 lysine 27 trimethylation
H3K36me3 = Histone 3 lysine 26 trimethylation
H4 = Histone 4
H4K12ac = Histone 4 lysine 12 acetylated
HAT = Histone acetyl transferase
HDAC = Histone deacetylase
HDM = Histone demethylase
HMEG = Histone mark enriched genes
HMT = Histone methyl transferase
HR = Homologous recombination
IEG = immediate early genes
IL = Infralimbic cortex
iPSC = induced pluripotent stem cells
K = Lysine
KAT = Lysine acetyltransferases
KDM = Lysine demethylase
KMT = Lysine methyltransferase
LigIII = DNA ligase IIIa
LINE-1 = Long interspersed nuclear element 1
LLPS = Liquid-liquid phase separation
LMN = Lower motor neurons
LTD = Long Term Depression
LTM = Long Term Memory
LTP = Long Term Potentiation
MAPK = Mitogen-Activated Protein Kinase
MWM = Morris Water Maze
MYST = MOZ, yeast YBF2, SAS2, and TIP60

mPFC = medial Prefrontal Cortex
mRNA = messenger RNA
NAD+ = Nicotinamide adenine dinucleotide
nfvPPA = Nonfluent variant of PPA
NBS1 = Nibrin
NES = Nuclear export signal
NHEJ = Non-homologous end joining
NIFID = Neuronal intermediate filament inclusion disease
NLS = Nuclear localization signial
NMDA = N-methyl-D-aspartate
NOR = Novel object recognition
OiP = Object-in-place
OL = Object location
p-ATM = phosphorylated Ataxia-telangiectasia Mutated
p-Elk1 = phospho-Elk1
PARP-1 = Poly(ADP-ribose) polymérase 1
Per = Period
PFC = Prefrontal cortex
PKA = Protein Kinase A
PL = Prelimbic cortex
PPA = Primary progressive aphasia
PRMT = Protein methyltransferase
PSP = Progressive supranuclear palsy
PGRN = Progranuline/granuline
PY-NLS = Proline-Tyrosine NLS
QGSY = Glutamine Glycine Serine Tyrosine-rich region
R = Arginine
RGG = Arginine Glycine rich domain
RNAPolII = RNA polymerase II
RRM = RNA recognition motif
S = Serine
sALS = sporadic ALS
sFTD = sporadic FTD
SG = Stratum Granulosom
SIRT = Sirtuins
SL = Stratum lucidum
SLM = Stratum lacunosom molecular
SMi = Stratum molecular inner
SMo = Stratum molecular outer
SO = Stratum oriens
SOD1 = Copper/zinc superoxide dismutase 1
SP = Stratum pyramidal
SQSTM1 = Sequestosome 1/ p62
SR = Stratum radiatum
SRE = Serum Response Element
SRF = Serum response factor
SSB = single strand break
ssDNA = single strand DNS
STM = Short Term Memory
svPPA = Semantic variant of PPA
T = Tyrosine
TBK1 = TANK-binding kinase 1
TIA1 = T cell-restricted intracellular antigen-1
TDP43 = TAR-DNA-binding protein
TNPO1 = Transporti 1 / Karyopherin β2
TOM = Temporal order memory
TSS = Transcription start site
UBQLN1 = Ubiquilin 1
UMN = Upper motor neurons
UTR = Untranslated region
VCP = Valosin containing protein gene
WT = Wild Type
XRCC-1 = X-ray repair cross-complementing protein 1
Y = Tyrosin
ZnF = Zinc finger motif
γH2AX = gamma H2AX
53BP1 = 53 binding protein 1

I. Publications

1. Chatterjee, S., Cassel, R., Schneider-Anthony, A., Merienne, K., Cosquer, B., **Tzeplaeff, L.**, Sinha, S.H., Kumar, M., Chaturbedy, P., Eswaramoorthy, M., Le Gras, S., Keime, C., Bousiges, O., Dutar, P., Petsophonsakul, P., Rampon, C., Cassel, J.-C., Buée, L., Blum, D., Kundu, T.-K., Boutillier, A.-L. (2018). Reinstating plasticity and memory in a tauopathy mouse model with an acetyltransferase activator. EMBO Mol. Med. e8587.

2. Boutillier, A.-L., **Tzeplaeff, L.**, and Dupuis, L. (2019). The dark side of HDAC inhibition in ALS. EBioMedicine 41, 38–39.

3. Scekic-Zahirovic, J., Sanjuan-Ruiz, I., Kan, V., Megat, S., De Rossi, P., Dieterlé, S., Cassel, R., Jamet, M., Kessler, P., Wiesner, D., **Tzeplaeff, L.**, Demais, V., Sahadevan, S., Hembach, K.-M., Muller, H.-P., Picchiarelli, G., Mishra, N., Antonucci, S., Dirrig-Grosch, S., Kassubek, J., Rasche, V., Ludolph, A., Boutillier, A.-L., Roselli F, Polymenidou M, Lagier-Tourenne C, Liebscher S, Dupuis L.. (2021). Cytoplasmic FUS triggers early behavioral alterations linked to cortical neuronal hyperactivity and inhibitory synaptic defects. Nat. Commun. 12, 3028.

4. Wang, X.-L., Kooijman, S., Gao, Y., **Tzeplaeff, L.**, Cosquer, B., Milanova, I., Wolff, S.E.C., Korpel, N., Champy, M.-F., Petit-Demoulière, B., Goncalves Da Cruz, I., Sorg-Guss, T., Rensen, P.-C.-N., Cassel, J.-C., Kalsbeek, A., Boutillier, A.-L., Yi, C.-X. (2021). Microglia-specific knock-down of Bmal1 improves memory and protects mice from high fat diet-induced obesity. Mol. Psychiatry.

Publications in preparation :

5. **Tzeplaeff, L.**, Seguin, J., Cosquer, B., Le Gras, S., Plassard, D., Megat, S., Dieterlé, S., Alcala Vida R., Cassel, J.-C., Merienne, K., Dupuis, L*. and Boutillier, A.-L*. Memory dysfunctions and associated epigenetic and transcriptomic changes in an ALS/FTD mouse model linked to a FUS mutation.* Equal contribution (In preparation for Neuron)

6. Paiva, I., Seguin, J., Cosquer, B., Plassard, D., Le Gras, S., **Tzeplaeff, L.**, Alcala-Vida, R., Merienne, K., Cassel, J.-C., Blum, D., Buée, L., Kundu, T.-K., Boutillier, A.-L.. Dysregulation of the cholesterol pathway alters epigenomic signatures of hippocampal neurons in Alzheimer's disease. (In preparation)

7. Cellai, L., Paiva, I., Mériaux, C., Poncelet, L., Papegaey, A., Drobecq, H., Le Gras, S., Schneider, M., Malik, E.M., Müller, C.E., Faivre, E., Carvalho, K., Gomez-Murcia, V., Vieau, D., Thiroux, B., Eddarkaoui, S., Lebouvier, T., Schueller, E., Seguin, J., **Tzeplaeff, L.**, Stauber, J., Lopes, L.V., Buée, L., Buée-Scherrer, V., Cunha, R.A., Ait-Belkacem, R., Sergeant, N., Annicotte, J.-S., Boutillier, A.-L., Blum, D. Genome-wide effects of regular caffeine intake on hippocampal metabolism and learning-dependent transcription. (In Revision, in J Clin Invest.)

Other projets in preparation :

1. Behavioral characterization of *Fus*$^{\Delta NLS/+}$ mice
2. A kinetic study of spatial learning transcriptomic in normal and pathological adult mouse hippocampus
3. Epigenomic/transcriptomic signatures in the pathological FTD/ALS brain in response to the positive effect of environmental enrichment.
4. ChIP-seq FUS in muscle cells (C2C12). (In collaboration with Luc Dupuis, INSERM 118)
5. Behavioral characterization of a conditional C9ORF72 knockout in neurons. (collaboration with Nicolas Charlet-Berguerand, IGBMC Strasbourg)

II. Communications

1. Posters presentations

- **Tzeplaeff L**. , Seguin J., Cosquer B., Cassel J.-C., Dupuis L., Boutillier A.-L. Memory dysfunctions in *Fus*$^{\Delta NLS/+}$ mice and associated transcriptomic changes. NeuroFrance 2019 at Marseille, France, Followship from the University of Strasbourg, 22.05.19 - 24.05.19

- **Tzeplaeff L.** , Seguin J., Cosquer B., Cassel J.-C., Dupuis L., Boutillier A.-L. Memory dysfunctions in *Fus*$^{\Delta NLS/+}$ mice and associated transcriptomic changes. Doctoneuro at Strasbourg, France. 13.09.19.

- **Tzeplaeff L.** , Seguin J., Cosquer B., Cassel J.-C., Dupuis L., Boutillier A.-L. Memory dysfunctions in *Fus*$^{\Delta NLS/+}$ mice and associated transcriptomic and epigenetic changes. 5ème Journée de la Recherche sur la SLA et les Maladies du Neurone Moteur at Paris, France. 17.10.19-18.10.19.

- **Tzeplaeff L.** , Seguin J., Cosquer B., Cassel J.-C., Dupuis L., Boutillier A.-L. Memory dysfunctions in *Fus*$^{\Delta NLS/+}$ mice and associated transcriptomic and epigenetic changes. 10 years celebration of the French-German biology school degree, at Saarbrucken, Germany. 01.11.19-02.11.19.

- **Tzeplaeff L.** , Seguin J., Legras S., Plassard D., Megat S., Cosquer B., Merienne K, Cassel J.-C, Dupuis L., Boutillier A.-L. Memory dysfunctions in Frontotemporal dementia *Fus*$^{\Delta NLS/+}$ mouse model and associated epigenetic and transcriptomic changes. NeuroFrance 2021 at Strasbourg, France (visio), 19.05.21 – 21.05.21.

2. Oral presentations

- **Tzeplaeff L.** Spatial memory dysfunctions in heterozygous knockin *Fus*$^{\Delta NLS/+}$ mice. French, German and Swiss meeting on ALS-FTD at Gunzburg, Germany, 28.02.19 - 02.03.19.

- **Tzeplaeff L.** Memory dysfunctions in Frontotemporal dementia *Fus*$^{\Delta NLS/+}$ mouse model and associated epigenetic and transcriptomic changes. Neuropole of Strasbourg, award of the best communication. 10.01.20.

- **Tzeplaeff L.** Dysfonctionnements de la mémoire chez les souris *Fus*$^{\Delta NLS/+}$ et modifications épigenetiques et transcriptomiques associées. 6ème Journée de la Recherche sur la SLA et les Maladies du Neurone Moteur at Paris, France (visio). 21.10.20 - 22.10.20.

- **Tzeplaeff L.** Dysfonctionnements de la mémoire chez les souris *Fus*$^{\Delta NLS/+}$ et modifications épigenetiques et transcriptomiques associées. 7ème Journée de la Recherche sur la SLA et les Maladies du Neurone Moteur at Paris, France (visio). 12.10.21 - 13.10.21.

PREFACE

In this thesis, we will be focusing on the role of the *Fused in sarcoma* (FUS) protein in memory deficits and associated transcriptomic and epigenomic alterations in the context of two neurodegenerative diseases: Amyotrophic lateral sclerosis (ALS) and Frontotemporal dementia (FTD).

ALS is characterized by the predominant death of upper motor neurons in the motor cortex and lower motor neurons in the spinal cord. These patients demonstrate progressive muscle weakness finally resulting in respiratory failure ultimately causing the death withing 2 to 5 years after onset of symptoms.
FTD is the second most common type of young onset dementia after Alzheimer disease. Patients are marked by the predominant atrophy and neuronal death of the frontal and temporal cortex with predominant behavioral and language disorders. Despite their differences in symptoms, ALS and FTD are parts of the same spectrum due to common features in neuropathology and genetics causes. Among all FTD and ALS patients, approximately 30% demonstrate simultaneous motor deficit and cognitive impairment or criteria for dementia. These patients are poorly characterized in the literature and are usually associated with worsen disease progression and shorter lifespan.

Mutations in the gene encoding for the DNA/RNA binding protein *Fused in sarcoma* (*FUS*) have been linked to early onset and severe cases of familial ALS (5%) and to a small subset of sporadic cases (1%). In these patients, the FUS protein that is physiologically nuclear, is mislocalized and aggregated in the cytoplasm. Such abnormality of FUS is also observed in cases of ALS without mutation, as well as in sporadic cases of FTD (10%).

FUS protein is involved with all steps of gene expression, including transcription, alternative splicing, and mRNA transport. FUS has also been associated to DNA damage repair pathways, epigenetic modifications, and several neuronal and synaptic functions. However, how FUS mutations affect these nuclear pathways remain largely uncharacterized.

This manuscript is composed of an introduction that aims to present the major concepts on which my thesis is based. First, I started with the concept of learning and memory, then I presented epigenetic histone post-translational modifications and their role in the memory process. To continue, I introduced both ALS and FTD diseases and focused on the particular FUS ALS and FTD disease variants before giving a full introduction on the physiological functions of the FUS protein. Finally, in two independent parts, I presented the behavioral alterations observed in the different FUS-linked mouse models and the epigenetic alterations associate to FUS dysfunctions. The introduction section will be followed by the objectives of my thesis and my scientific contributions presented as two articles in preparation. Since none of our studies has been published yet, I then discussed the meaningful of our result in a general discussion. The first part of the discussion is mainly focused on the characterization of behavioral alterations observed in our mouse model (mainly discussion of the publication 2). The second part aims to expose the potential mechanisms underlying the molecular and behavioral alterations in the presence of FUS mutation (mainly discussion of the publication 1). In the third and last part I discussed the validity of our model in the ALS-FTD spectrum and the implication of our results in terms of existing epigenetic therapeutic approaches.

During my thesis, I had the chance to collaborate on another paper that show that FUS mislocalization is sufficient to induce cortical synaptic defects that could lead to FTD-like symptoms in our mouse model (Scekic-Zahirovic et al., 2021). I also participated to the writing of a comment that discusses the potential negative effect of HDAC inhibitors treatment in the context of ALS (Boutillier et al., 2019). Both of these studies are discussed in the discussion part and are available in the Annex section. The Annex section also comprises two published papers in which I participated along my thesis. Detailed information about my contribution in these papers are exposed at the beginning of the Annex section.

INTRODUCTION

Part 1: Learning and memory

Life is constant learning, and memory is crucial to construct who we are, our identity, our thoughts, and our ability to adapt to new situations. Learning is described as the process through which we obtain new knowledge and information, while memory is defined as the process that allows us to remember these newly acquired information and experiences. Learning and memory are thought to be closely related since no memory can take place without proper learning. Learning is constructed and based on three important steps: (1) acquisition, (2) consolidation and (3) recall. Acquisition is the process by which information is introduced or presented for the first time. Consolidation refers to the fact that the information is retained and that the memory becomes stable. Finally, recall is the ability to access and retrieve this information over time. Memory can be distinguished in very different forms and differs depending on the duration of the storage and the type of information.

I. Types of memories

Amount the distinct types of memories (Figure 1), we can distinguish short term memory (STM) from long term memory (LTM) depending on the length of time the information is stored. According to Miller's law (1956 & 1989), STM is a process by which the brain can approximately hold about 7±2 items in mind (e.g., telephone number that has just been recited) for a short period. The duration of STM last usually a few seconds but can be maintained up to minutes in presence of rehearsal and when no distracting task is present to disrupt the process. In opposition, LTM can store an unlimited number of items and keep them up to a lifetime. We can further distinguish the recent LTM (stored for hours to a few days) from the remote LTM (stored for weeks, months, and up to a lifetime). The transition between the recent and the remote LTM requires activation of different consolidation processes in different brain regions (systemic consolidation), which will be further discussed later in the manuscript. LTM is distinguished into two subtypes according to the type of information and the way these are stored and recalled: declarative explicit memory, including semantic and episodic memory, and nondeclarative implicit memory.

In 1949, Gilbert Ryle, an English philosopher, proposed in his book "The Concept of Mind" a distinction of LTM separating the declarative knowledge (explicit memory, knowing that) from the non-declarative procedural knowledge (implicit memory, knowing how). Declarative memory is the process in which we consciously collect information on events and facts, and which can be stored and retrieved explicitly through oral expression. In contrast, nondeclarative memory is acquired in a nonconscious way and is stored and recalled implicitly through motor tasks and performances. Non-declarative memory is sometimes referred to as procedural memory and manifest, for example, through the learning of "how to tie your shoes?" or "how to bike?". Later, declarative explicit memory has been further divided in episodic memory (remembering personal and specific event of the past) and in semantic memory (general knowledge). Semantic memory refers to general knowledge about the world that we accumulate throughout our life, at school or through novel experiences for example (facts, ideas, meaning and concepts), unrelated to specific experiences. It is easy to say that Paris is the capital of France but it is much more difficult to remember when we learned this concept. In comparison, episodic memory is based on our memory of personal life experience, where we can recreate any giving point (what happened? Where and when it happened? And with whom this particular event took place).

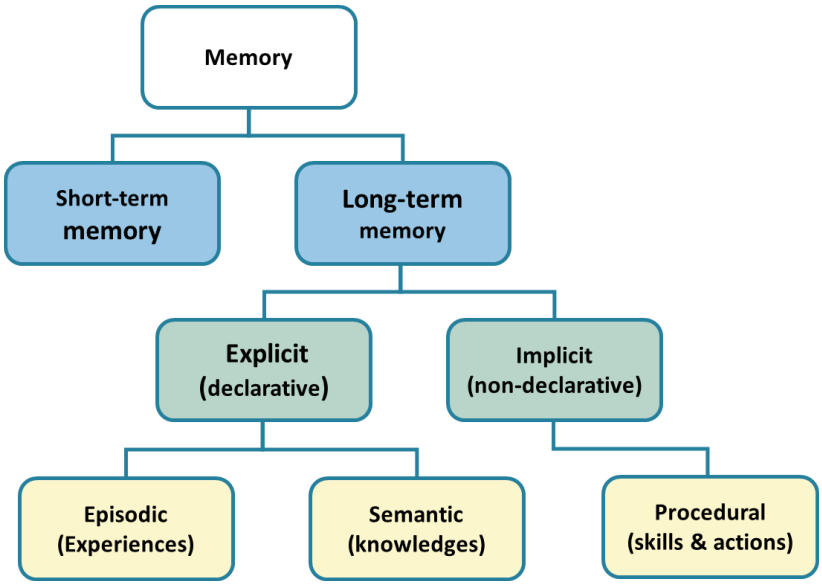

Figure 1: Classification of the different types of memories

The different types of memory are divided in two groups according to the duration of the information storage (Short-term and Long-term memory). The long-term memory is itself divided into explicit and implicit memory, respectively, if the information can be restored in a declarative (knowing that) or non-declarative manner (knowing how). The declarative explicit memory includes both episodic memory (remembering personal and specific event of the past) and in semantic memory (general knowledge).

II. Long term episodic-like memory in rodents

According to Tulving (1985), episodic memory is evolutionarily the most recent memory and only humans have acquired this form of memory. Episodic memory relies on the ability to relate to any given point of an event (When the memory happened? Where it was? And what or who was present?). Unfortunately, rodents and other non-humans do not have the ability to talk and obviously cannot explicitly relate any personal past experiences and memories. However, using behavioral task challenging mice on the What, Where and When questions, we can mimic episodic memory. In this manuscript, we will speak of "episodic-like" memory when referring to rodents' episodic memory, with rodents referring mainly to mice and rats. In the next part of this chapter, we will present two well standardized task to study "episodic-like" memory in rodents: the object test paradigm and the Morris Water Maze spatial paradigm.

1. Object Test to study episodic-like memory in rodents

How can we visualize and study an "episodic-like memory" in rodents that would closely reflect episodic memory in Humans? Using rodents' preference for novelty, studies demonstrate that they can distinguish between a combination of objects presented (What?), the position of objects (Where?), and which items/events have been experienced first (When?). The What-Where-When being the three components of episodic-like memory in rodents and non-humans.

A. Novel object recognition (What?)

Novelty preference in rodents is used to study the recognition capacity based on the distinction between a new object or situation and a previously explored one (What?), Figure 2 A. The novel object recognition (NOR) is a well-standardized paradigm used to study the effect of a specific drug on rodent memory or to study the effect of genetic mutations and environmental influence on memory. In this task, rodents are exposed to at least two similar objects in a closed arena and get to explore them for a set amount of time. This is called the acquisition phase. The rodent is then placed back in its cage for a fixed period of time. One of the objects is replaced by another one in the arena and the animal is then put back into the device for the so-called recall phase or

probe trial, again during a set amount of time, during which the time that the rodent spent on exploring the new object is recorded. If the rodent memory is functioning normally, novelty preference will be reflected by increased time exploring the new object as compared to time exploring the old/familiar object. If not, this can be the sign of memory deficit. As in all memory tests, many parameters need to be controlled to avoid any bias. For example, an animal exploring more the old object is not necessarily senile, he could be anxious or neophobic. This is why many different criteria are assessed such as the time spent in the center of the device or along the walls. Experimental procedure described here (Lueptow, 2017).

B. Object location (Where?)

Based on the same instinctive preference for novelty, we can also study if rodents can determine a change in object position (Where?) and not a change in the object itself, with the so-called object location task (OL), Figure 2 B. As in the NOR, this task is divided into two phases: the acquisition one and the recall one during which the memory is evaluated. During the first phase, mice are exposed to several objects that are in a specific place and then returned to their cage. However, during the recall, one of the previous objects is moved to a new location. If the memory is working well, the animal will spend more time exploring the moved object compared to the others. If not, we can suspect alteration of the “where” component of episodic-like memory.

C. Object in place (What and Where?)

The object in place task (OIP) can be used to assess two distinct aspects of the episodic-like memory in mice (What and Where?) at the same time, Figure 2 C. In this task, at least two highly different objects are presented to mice during the acquisition phase. For the probe test, one of the two objects remains unchanged and the other is replaced by the same version of this first object. Thus, animals are then exposed to two identical objects with one being already here previously and the other one being a new one. Here again, the time exploring the new object will reflect the ability of mice to discriminate which object has been changed and where it was. To assess this test, we need to ensure that animals are able to perform the NOR and the OL tasks correctly and that they can recognize the “what” and the “where” aspect alone. Indeed, any alteration in the NOR and OL will decrease abilities in the OIP task. However, each task relies on

communication between different brain regions and any conclusion on the OIP task without evaluating the NOR and OL can lead to misleading conclusions.

D. Temporal order memory (What and When?)

The last aspect of the episodic-like memory is the "When?" component, Figure 2 D. As it is not possible to test this aspect alone, a combination of the NOR with the introduction of different period of time between object presentations is required to determine if mice can identify the order in which items/events have been experienced. In the temporal order memory task (TOM), two identical objects are presented to the mice during the acquisition phase. After some time, another couple of identical objects are presented at the same place to the same animal, this is the second acquisition phase. Finally, one copy of each pair of objects is presented to the animal. Mice with intact memory will spend less time exploring the object they have recently seen and more time exploring the one they have not seen for a long time (i.e., the first pair of objects). If both objects are explored similarly this might reflect an inability of the mouse to analyze time and the "when" aspect of episodic-like memory. For this task, the NOR task and the "what" component needs to be previously validated to ensure proper recognition of each object by the animal.

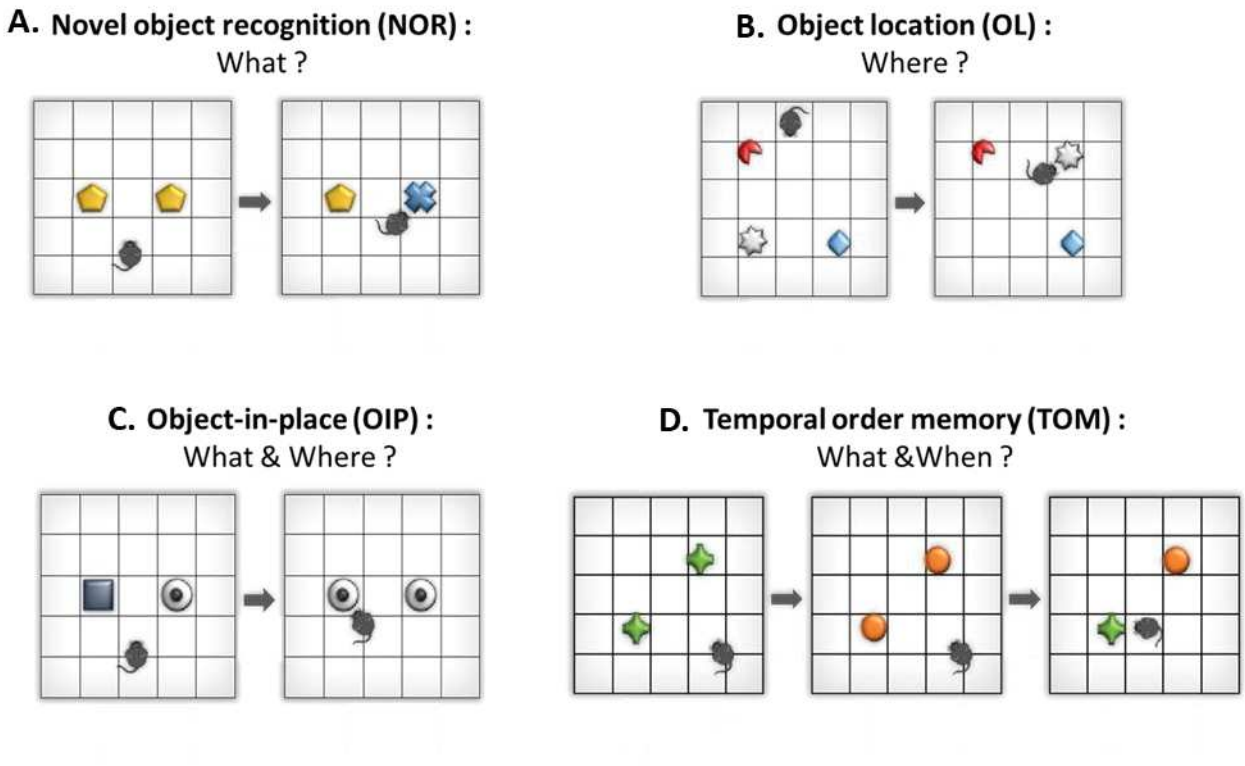

Figure 2: Episodic-like memory paradigm

Memory paradigm in mice allowing to test the What, Where and When component of the episodic-like memory. (**A**) Novel object recognition (NOR). (**B**) Object location (OL). (**C**) Object-in-place (OIP). (**D**) Temporal order memory (TOM). (Adapted from Estelle Schueller PhD Thesis, University of Strasbourg).

2. Spatial memory evaluation in rodents: Morris Water Maze task

A. Standard procedure

The Morris Water Maze (MWM) spatial task was invented by Richard Graham Michael Morris (Morris et al., 1982) (Morris, 1984). Today, this is one of the most used paradigms to evaluate spatial learning and memory in rodents (Figure 3). The MWM is a large circular pool, virtually split into four quadrants (named according to the four cardinal points: South-Est (SE), North-Est (NE), South-West (SW) and North-West (NW)) and containing a submerged hidden platform just under the water. The water is cloudy to avoid the obvious visualization of the escape platform. In this test, R. Morris relied on the “escape from water” motivation to induce learning which is a strong one for mice.

The MWM paradigm is separated into two steps, each of them is designed to test either the learning abilities of animals (acquisition of the platform location) or the memory retention (recall of the platform location, or probe trial). During acquisition, animals are trained to find the location of the hidden platform, helped by distal visual-spatial cues place in the room and on the wall. Thus, days after days, rodents can adapt their behavior to develop strategies to find the platform, whatever the introduction point into the maze (e.g., NW, NE, SW and SE). Learning efficiency is measured by parameters such as escape latency and swimming distance to the platform. The shorter the time to reach the platform, the more the animal encodes its location relative to distal cues.

Once rodents have learned the correct position of the platform, it is removed from the pool to probe their memory recall. Animals are placed back in the pool for a set amount of time (usually 60s), and some variables are recorded to determine the quality of the memory. The time spent in the target quadrant, the time spent in a virtual zone around the platform (Annulus), the number of crossing in the annulus or platform former location and the average distance of the animal from the former platform location during the Probe (Maei et al., 2009) are evaluated. Depending on when the Probe trial takes place, we can study different types of memory. We can assess the probe just after the acquisition phase or after few minutes to test the short-term memory or test different aspects of the LTM such as recent LTM (e.g., hours, days) or the remote LTM (e.g. weeks, months).

The MWM spatial task is thus a well-standardized test to evaluate learning and memory, but it can also be used to study the impact of a mutation (in transgenic animals), lesions or drug administration. This paradigm is also widely used to study the effect of molecules or the involvement of a specific gene, brain region, or other protein and receptors, in learning and memory consolidation.

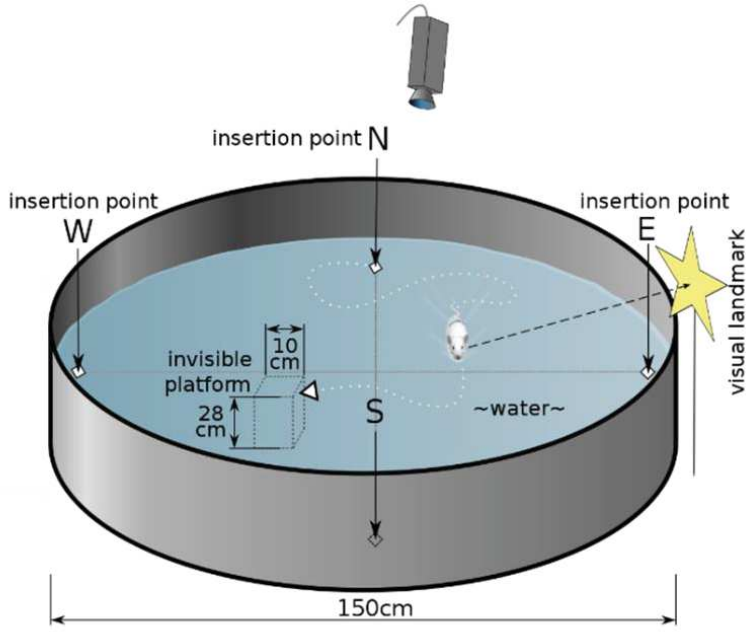

Figure 3: Morris Water Maze

The Morris Water Maze (MWM) disposal is composed of a circular pool surrounded by visual cues. The pool is virtually separated in 4 quadrant (South-Est (SE), North-Est (NE), South-West (SW) and North-West (NW)) with a 10cm large platform located in the middle of one of the four quadrant. Animals are trained to find this platform starting from different point locations (N, E, S or W). A camera is located above the pool to record all trials during the experiment.

B. Variation of the MWM

Variations of the MWM have been proposed and developed over time to study other aspects of memory. For example, a visible platform, or a platform with a cue on it, can be used to test the visual abilities, the maximum swim speed for motor abilities, or the motivation of rodents. Additional Probe tests can be interspersed along the acquisition phase to assess levels of memory consolidation. Repeated Probe tests can be further performed to determine how long the rodents need to completely extinguish the memory of the platform location. Of note, ability to forget (extinction) some information is essential to be able to learn new ones and too much of extinction of memory can be deleterious if it happens inappropriately (e.g., in case the information is still necessary). Thus, the capacity to forget an information and shift strategy (flexibility) in a changing environment is an essential ability. Another test named “reversal” allows determining if an animal can extinguish its initial learning by changing the platform location at the end of the acquisition phase. This test also allows us to study flexibility by examining the

strategy used by the animal to learn the new platform location (Nolan and Lugo, 2018). It is also possible to replace the platform by a smaller one to test the accuracy of the memory (Broening et al., 2001). Working memory can be assessed by changing the location of the platform day after day, so that the rodents need to learn the platform position for each day (Wisman et al., 2008). Another version of the MWM is used to test the discrimination learning with several visible platforms but only one being the goal platform. This version has been developed to test non-spatial learning. Thus, the MWM task allows for multiple testing and had become an important, even dominant, method of learning and memory assessment in rodents.

III. The hippocampus and the medial prefrontal cortex

Decades of research have revealed that two brain regions, the hippocampus, and the medial prefrontal cortex (mPFC), are essential for the encoding, consolidation, and retrieval of episodic memories. This will be discussed in the next chapters.

1. The hippocampus

A. Hippocampal structure and layer organization

The hippocampus is located in the temporal lobe, one in each cerebral hemisphere of the mammals' brain. This brain structure plays a key role in integrating information from short-term memory to long-term memory, as well as in spatial memory. The hippocampus is composed of two parts: the Cornus Ammonis (CA) and the dentate gyrus (DG). The CA region is further divided in three subregions, CA1, CA2 & CA3. In some descriptions, the end part of the CA3 regions running into the hilus is referred as CA4, but this will not be discussed in this manuscript. The hippocampus arises from the cortex that reduces its number of layers from six layers to five (CA3), four (CA1 & 2), or three (DG) layers. Each of these layers contains distinct cell types that give rise to unique and specific axonal fiber pathways in the hippocampus. Neurons in the CA regions are pyramidal neurons, while neurons in the DG are referred to as granular neurons.

Pyramidal neurons of CA1, 2 and 3 are found in the principal layer of the CA region, the pyramidal layer (stratum pyramidal, SP). In the CA3, the basal part of the pyramidal neurons orients their dendrites in direction of the deepest layer, the stratum oriens (SO), while the apical part projects through the most superficial layers, first the stratum lucidum (SL) and deeper to the stratum radiatum (SR) and the stratum lacunosum molecular (SLM). The CA1 and CA2 regions have the same layer organization, except that the stratum lucidum is absent.

The principal layer of the DG is the granular cell layer (stratum granulosum, SG), made of very densely packed granular neurons. The dendrites of those neurons extend in the most superficial zone of the DG, the molecular layer (the outer- and inner stratum molecular, SMo and SMi), and their axon project in direction of the deepest layer of the DG, named the hilus (H). See Figure 4.

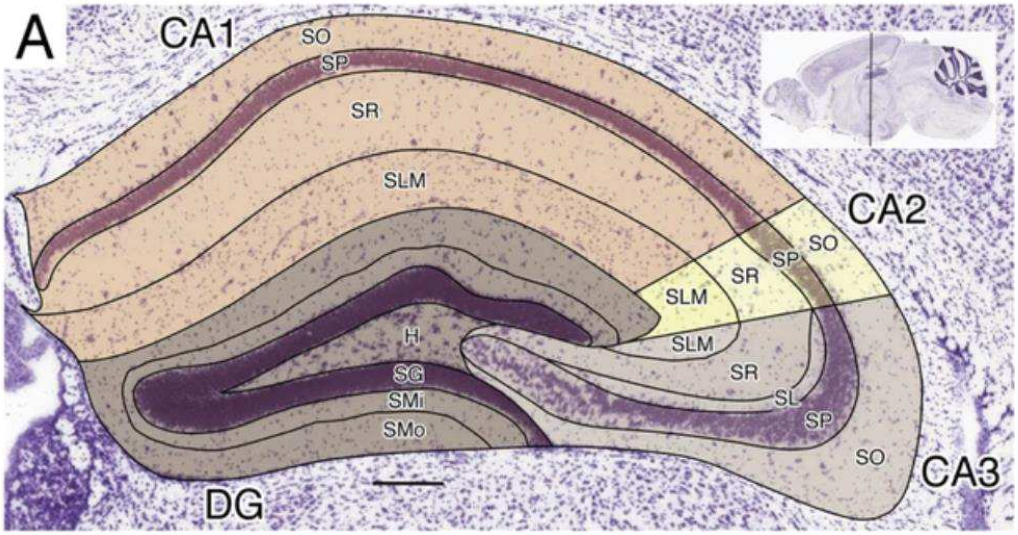

Figure 4: Hippocampal regions and their cortical layers

Coronal section of the mouse hippocampus showing the four main regions: the dental gyrus (DG), the cornus ammonis 1, 2 and 3 (CA1, CA2 and CA3). The DG is composed, from the deepest to the most superficial layers, of the hilus (H), the stratum granulosum (SG) and the molecular layer (inner- and outer-; SMi SMo). All the CA regions are constituted, from the deeper to the more superficial layers, of the stratum lacunosom molecular (SLM), the stratum radiatum (SR) the stratum pyramidal (SP) and the stratum oriens (SO). The CA3 regions is made of a supplementary layer, the stratum lucidum (SL) located between the SP and the SR layers (Wheeler et al., 2015).

B. Hippocampal connectivity: the direct (mono-synaptic) and indirect (tri-synaptic) pathways

Connections inside the hippocampus are mainly organized in a unidirectional manner, from the DG to the CA1. The major Input of the hippocampus arrives from different brain regions through the entorhinal cortex (EC), a six-layer cortical region in the medial temporal lobe. The major output is sent by CA1 to the subiculum region, located between the CA1 region of the hippocampus and the EC. Both, the subiculum and the EC, in addition to the DG and the CA region of the hippocampus form all together the hippocampal formation.

Input Information of the hippocampus arises from the superficial layers II and III of the EC and travels through two different pathways, either through the direct pathway to the CA1, or through the indirect pathway, the so-called tri-synaptic system.

The indirect pathway is also called the tri-synaptic circuit because it includes three different major cell groups: granule cells of the DG, pyramidal cells of the CA3 region and pyramidal cells of the CA1 region. Granular cells of the DG and pyramidal cells of the CA3 region receive input from the EC. This projection is named the perforant pathway. In addition to the perforant pathway, CA3 receives information from the granular cells of the DG through the mossy fiber projection. The CA3 pyramidal neurons either connect to the other hemisphere of the brain through the fimbria fornix or project to CA1 *via* the Schaffer collateral. CA1 pyramidal neurons then send output information to other subcortical and cortical regions *via* the subiculum and deeper layers V and IV of the EC

In contrast, the direct pathway is a monosynaptic circuit that originates from the entorhinal cortex and that connects directly to the CA1 hippocampal region before sending back projections to the subiculum and other brain regions. See scheme Figure 5.

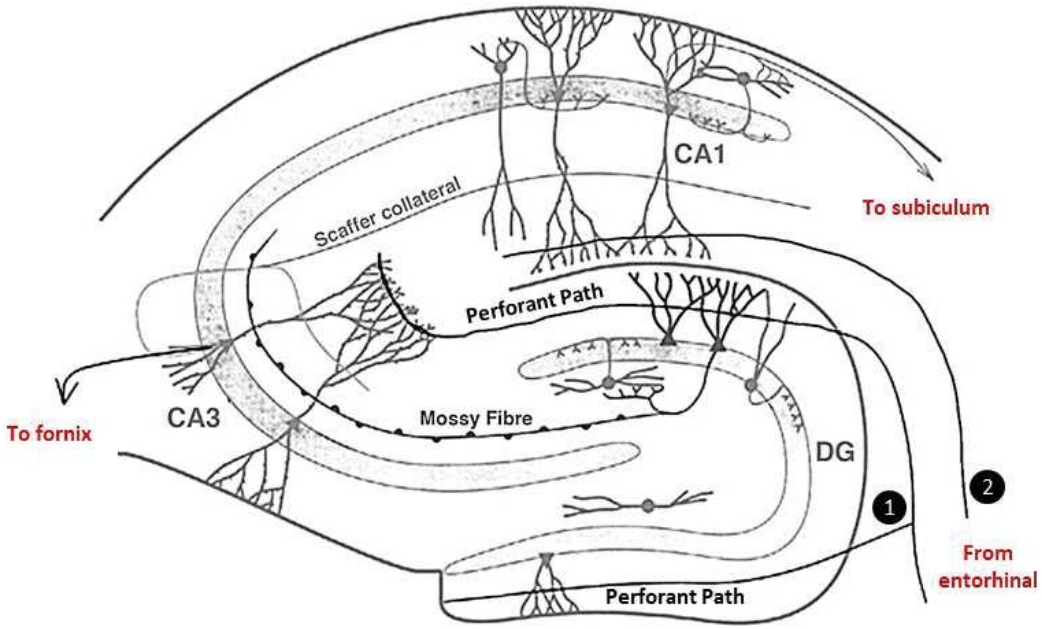

Figure 5: The hippocampal mono and tri-synaptic circuit organization

The entorhinal cortex is a major source of inputs to the hippocampus. The monosynaptic direct pathways project information from the entorhinal cortex directly to the pyramidal cells of the CA1 region (2). In contrast, the trysynaptic indirect pathway projects from the entorhinal cortex to the granular cells of the dental gyrus *via* the perforant pathway (1), to pyramidal cells of the CA3 region *via* the mossy fiber projection and finally to pyramidal cells of the CA1 region *via* the Schaffer collateral. The major output of the CA1 is the subiculum. Interhemispheric communications are possible due to the projection from the CA3 region to the other side of the hippocampus *via* the fornix. Adapted from (Daumas et al., 2009).

2. Medial prefrontal cortex

The medial prefrontal cortex (mPFC) is located in the anterior part of the frontal lobe of the brain, in front of the motor and premotor cortical regions. In the mouse, the mPFC is composed of three subregions, from the most dorsal part to the ventral part: the anterior cingulate cortex (AC), the prelimbic cortex (PL) and the infralimbic cortex (IL), Figure 6.

Studies of afferent projections to the mPFC revealed different implications of the dorsal and ventral regions of the mPFC. There is a shift from predominantly cortical non-limbic afferences in the dorsal mPFC, to increased limbic afferences in the ventral mPFC. For example, the IL region receives preferential afference from limbic regions, suggesting involvement in stress response, while the PL receives more afference from cortical regions suggesting a greater implication with cognitive functions. Interestingly, the three different regions of the mPFC receive direct

projection from the hippocampal region CA1, mostly the ventral part (Hoover and Vertes, 2007). Information from the other hippocampal regions first travels *via* direct axon projection from the subiculum and the entorhinal cortex. Of note, it is established that the mPFC, at least the PL and the IL, has no direct projection to the hippocampus and requires to relay information in other brain regions before reaching the hippocampus (Vertes, 2004) (Jones and Witter, 2007) (Cassel et al., 2013).

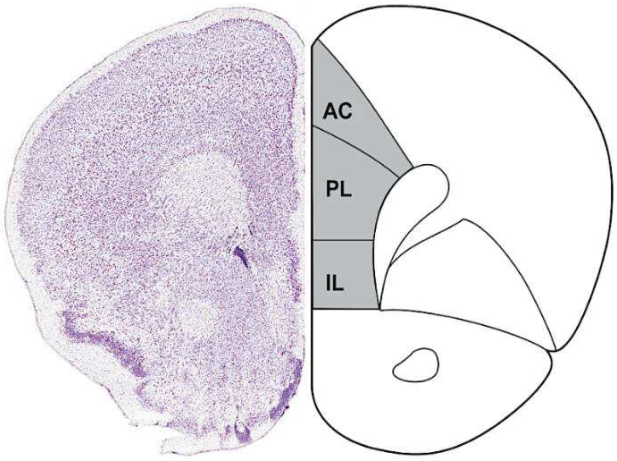

Figure 6: mPFC regions of the mouse brain

Coronal section of the medial prefrontal cortex (mPFC) and delimitation showing the position of the anterior cingulate cortex (AC), prelimbic cortex (PL) and infralimbic cortex (IL). (Blazon, 2018).

3. The Hippocampus and the medial prefrontal cortex: Two main brain regions associated with learning and memory processes

In this part of the manuscript I will discuss the implication of the hippocampus and the medial prefrontal cortex in the previously describes memory task, the different object test and MWM.

As early as 1982, R. Morris demonstrated that a complete hippocampal lesion significantly impaired learning in the spatial MWM task (Morris et al., 1982). Years later, it has been shown that some hippocampal neurons respond to a particular object, while others respond to another one in a specific location during an object recognition task (Manns and Eichenbaum, 2009). In agreement with this study, other authors demonstrated the involvement of the hippocampus in the OL task (Oliveira et al., 2010) (Barker and Warburton, 2011). It remains unclear if the hippocampus is crucial for proper NOR task since some studies demonstrate that hippocampal

lesion altered recognition memory (Clark et al., 2000) while others failed to observe any deficit after hippocampal inactivation (Oliveira et al., 2010) (Barker and Warburton, 2011) (Langston and Wood, 2010). However, these conflicting results might be due to differences in the protocol (lesion vs. inactivation). Barker and Warburton also demonstrated the involvement of the hippocampus in the OIP task (using 4 objects in the task), and in the TOM task (Barker and Warburton, 2011). The network underlying novelty detection in the OIP seems to be different when containing only two objects. In this situation, the hippocampus is no longer required for the proper execution of the task (Langston and Wood, 2010). In conclusion, hippocampus plays a role in remembering item-location association as well as temporal component, and thus, integrates contextual, temporal and object information as a whole.

The mPFC has also been proposed to be essential for LTM consolidation and retrieval. Indeed, as it is essential for proper MWM remote LTM (Teixeira et al., 2006) (Lopez et al., 2012), for OR with a 24h delay between acquisition and recall (Akirav and Maroun, 2006) and in the TOM task (Barker and Warburton, 2011). Lesion of the mPFC also induced deficit in a variant of the OL task (DeVito and Eichenbaum, 2010) and a variant of the OIP task involving several objects (Kesner and Ragozzino, 2003). The mPFC has also been involved in some aspects of executive functions. Executive functions regroup, different processes such as planning and decision making, cognitive flexibility, sustained attention and inhibitory response (inhibit inappropriate behavior in a particular situation, e.g., accelerating if the traffic light is red). For example, the mPFC is essential for cognitive flexibility in planning and resolving problems in the context of the MWM reversal learning (Latif-Hernandez et al., 2016). For more information on the mPFC implication in the different executive and cognitive functions, see the review (Dalley et al., 2004). Finally, the involvement of the mPFC in recent LTM is under debate since it was found involved in some studied (Cholvin et al., 2016), and not in others (Latif-Hernandez et al., 2016).

Thus, the hippocampus and the frontal cortex are two brain structures playing an essential role for the proper memory retention, and therefore their involvement in the consolidation process will be further discussed in the next chapters.

IV. Systemic and synaptic consolidation

The process in which new information becomes more stable over time to build LTM information is called consolidation. Depending on the temporal dynamics, we can distinguish a rapid and a long-lasting consolidation process. The rapid, or synaptic consolidation process, arises through the genesis of new synapses or synapses reorganization, this occurs after the first minute to hours after the learning process. In contrast, the systemic consolidation is a much slower process that can last from days to years and rely on the gradual reorganization of the brain regions that supports the information. Thus, to transform a memory from a labile state to a more permanent one, both synaptic and systemic consolidation need to take place.

1. Systems consolidation of memory

Systems consolidation of memory postulates that the circuit and brain networks activated upon learning are changing and reorganizing over time for the maintenance of long-term memory. This theory arises from the well-known patient H.M. and the discovery of other patients with lesions in the hippocampus that preferentially demonstrate alterations in recent memories but preserved remote memory (Scoville and Milner, 1957) (Penfield and Milner, 1958). These studies demonstrated that the hippocampus has a time-limited role in the storage and retrieval of semantic and episodic memories. The Systems consolidation theory proposes that recent memories are initially hippocampal-dependent, but as these memories mature, they become increasingly dependent on other brain regions, such as cortical regions (including the mPFC known to have an important role in processing remote memory). During the last decades, the principle of systems consolidation of memory has been widely accepted, yet the exact mechanistic process is still under debate and gave rise to different conflicting theories.

A. The standard model and the multiple trace theory: What is the role of the hippocampus?

The standard model (Marr, 1971) and the multiple trace theory (Nadel and Moscovitcht, 1997) are the two most popular theories (Figure 7). Both of them agreed that semantic and episodic memories are first encoded in the hippocampus and will be forgotten unless the content of

memories is transferred and redistributed across the cortex. The ensemble of neurons across the brain manifesting learning-induced changes is called an engram. The term engram was first introduced 100 years ago by Richard Semon (Semon, 1921). He described the engram as a population of neurons activated together in response to a specific stimulus, thus resulting in physical and chemical changes strengthening their connectivity. Both theories of the systems consolidation model propose that the transfer of this engram depends on circuit reactivation between the hippocampus and the cortical network during the sleep process or each time the memory is recalled. Thus, repetitive reactivation of the hippocampo-cortical networks will strengthen the engram and progressively activate a cortico-cortical network representing itself the entire memory information. However, the two theories differ on the continuous involvement of the hippocampus regarding the recall of remote memories. The standard theory proposes that the recall of the remote memory might be fully independent of hippocampal activation and that it becomes strictly dependent on cortico-cortical network reactivation (Figure 7 A). In contrast, the multiple trace theory proposes that, while semantic memory can be fully supported by the cortico-cortical network, episodic memory will always require, at least partially, reactivation of the hippocampal network and hippocampo-cortical circuits (Figure 7 B). Furthermore, in this model, each activation of the hippocampo-cortical network will activate a new population of neurons, thus the older a memory, the larger the engram, the easier it is to recover it. In contrast, the more recent a memory is the more vulnerable it is. For more information see reviews (Frankland and Bontempi, 2005) (Squire et al., 2015) (Tonegawa et al., 2018). Nevertheless, in the particular context of spatial learning, the hippocampus appears always necessary (Teixeira et al., 2006), which was also confirmed by recent studies from our laboratory (Cholvin et al., 2016) (Klein et al., 2019).

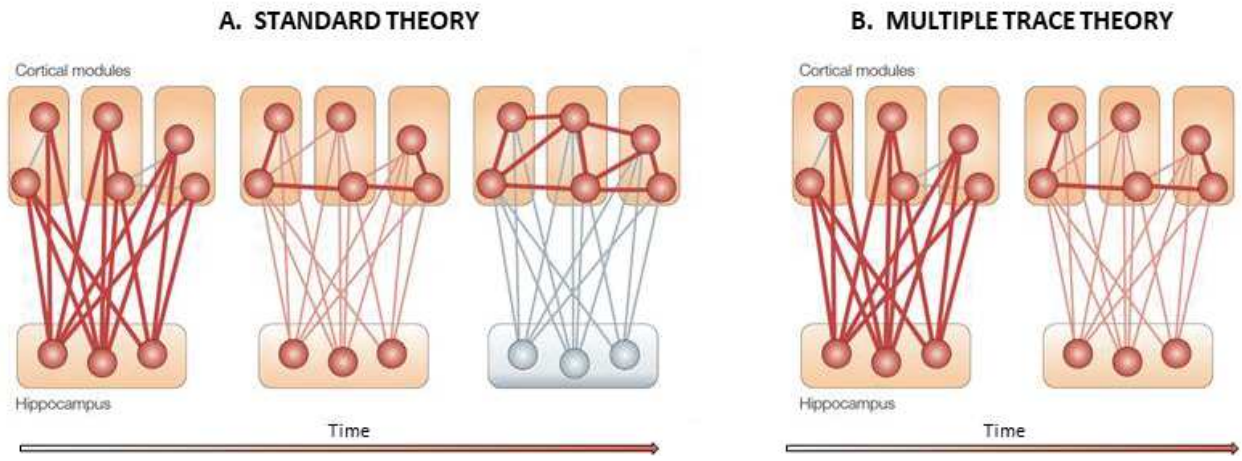

Figure 7: The standard theory and the multiple trace theory

Model of the Standard theory (A) and the multiple trace theory (B). The two theories differ considering the implication of the hippocampus during remote memory. Adapted from (Frankland and Bontempi, 2005).

B. The medial frontal cortex, an essential actor for remote memory

What could be the cortical areas required for remote long term memory retrieval? The mPFC located in the anterior part of the brain seems to be an interesting candidate. In 1999, Bontempi and collaborators were the first to demonstrate different brain activation patterns in recent and remote memory (Bontempi et al., 1999). In this study, while the hippocampal region is highly activated after 5-days of memory retention, its activation was much lower after a delay of 25 days. In contrast, they observed increased activation in different frontal cortex areas and the anterior cingulate cortex of the mPFC. Specific inhibition of the hippocampal output information to the mPFC (*via* the entorhinal cortex) during learning, demonstrated impaired remote memory but no impact on recent memory retrieval (Kitamura et al., 2017). In the specific context of spatial learning, other studies demonstrated the importance of the mPFC in remote memory retrieval through studies on immediate early genes expression patterns. The c-fos gene is an immediate early gene that is rapidly transcribed, leading to increased c-FOS protein after neuronal stimulation (Sheng and Greenberg, 1990) (Cullinan et al., 1995) (Bisler et al., 2002) (Zangenehpour and Chaudhuri, 2002). Thus, the expression of this protein can give information of brain structures activated at different steps of the learning process, as well as their level of activation. A high expression of the c-Fos protein was observed in the mPFC after remote but not recent memory (Teixeira et al., 2006) (Lopez et al., 2012). One of these two studies also

demonstrates that inactivation of the anterior cingulate cortex in the mPFC blocks the expression of remote memory but has no effect on recent memory (Teixeira et al., 2006).

Several evidence also proposed involvement of the mPFC in recent memory. While NMDA lesion of the mPFC demonstrate involvement of this structure in both recent and remote fear memory (Quinn et al., 2008), muscimol inactivation in the mPFC also reveal its role during recent and remote memory in the MWM (Cholvin et al., 2016). In conclusion, this data suggests that the mPFC is needed for both recent and remote memory, with many studies pointing out a greater involvement of the mPFC in remote memory. This information is supported by the study of Quinn and collaborators showing a weak but significant impairment in recent memory and a stronger impairment in remote memory after mPFC lesion (Quinn et al., 2008). For more information on the topic see review (Euston et al., 2012).

2. Synaptic consolidation

The efficiency of systems consolidation relies on other consolidation processes taking place much earlier and faster in the brain. The consolidation of synapses begins directly after the acquisition of new information and is described as the process that generates new synapses, reorganizes and strengthens ones already construct/formed.

Synapses represent the junction point between two neurons. This junction is favorable to induce communication and exchange of information between neurons. Chemical molecules can be release *via* vesicles from the pre-synapse button to then interact with receptors on the membrane of the post-synaptic button. Those synapses are not fixed, as they can modify their morphology and their functions in response to a particular situation. This is called synaptic plasticity. Thus, increased synaptic communication is termed long-term potentiation (LTP) while decreasing synapse efficiency is named long-term depression (LTD). While LTP results in increasing size of synapses and strengthening the communication, LTD is associated with synaptic weakening and elimination of synapses that are not activated anymore. A balance between the strengthening and the pruning (i.e., process of synapse elimination) of synapses is required in the brain for correct memory consolidation. Briefly, after neuronal stimulation, presynaptic neurons release neurotransmitters in the synaptic cleft. Glutamate, which is the most common excitatory

neurotransmitter in the central nervous system, binds to both the α-amino-3-hydroxy-5-methyl-4-isoxazolepropionic acid (AMPA) receptor and the N-methyl-D-aspartate (NMDA) receptor on the post-synaptic neuron. Their principal function is to allow the passage of ions through their channels. AMPA receptor channel opens as soon as glutamate is bound, allowing increased sodium and potassium in the post-synaptic neuron and then membrane depolarization. NMDA receptor needs two conditions to open, (1) that glutamate bound and (2) that the membrane is already strongly depolarized. If so, NMDA receptor channels allow sodium and potassium entry as well as calcium entrance in the post-synaptic neuron. LTP is induced when a long-lasting neuronal activation, as well as a repeated or a strong acute neuronal stimulation, occurs and is responsible for a high glutamatergic release from the presynaptic neuron and a large calcium entry into the postsynaptic neuron. After LTP, a few changes at the scale of the synapse are observed. Morphologically, the size of the head of the postsynaptic spine is growing due to increased branching of the cytoskeleton, and functionally the addition of new AMPA glutamatergic receptors. These spines are then referred to as mature. In opposite, LTD induces reduction of the spine head and diminution of AMPA receptor number (Figure 8). For more details see Review (Kennedy, 2016).

Thus, neuronal stimulation leads to changes in total or mature spine number in different brain regions upon learning conditions. For example, increased total spine numbers were observed in both the hippocampus and the mPFC following different learning paradigm (Restivo et al., 2009) (Klein et al., 2019). Interestingly, synaptic changes arise much faster in the hippocampus than in the mPFC. Indeed, increased spine density and change in morphology are already observed during recent memory retrieval. These changes are only visible in the mPFC during remote memory retrieval. No change in spine density is observed in the hippocampus in response to remote fear conditioning (Restivo et al., 2009), while the hippocampus still presents increased spine density in the context of MWM remote memory (Klein et al., 2019). Two conclusions can thus be raised. First, these findings are in accordance with the systemic consolidation theory, claiming that the mPFC is required much later in the consolidation process. Second, the hippocampus is indeed necessary for the recall of remote spatial memory. Several studies demonstrate a correlation between the number of mature spines and learning and memory capacities. Indeed, aging (Halbach et al., 2006) and neurodegenerative diseases (Sephton et al.,

2014) (Chatterjee et al., 2018) (Doria et al., 2018) mouse models displayed altered spine number and/or morphology of dendritic spines in specific brain area.

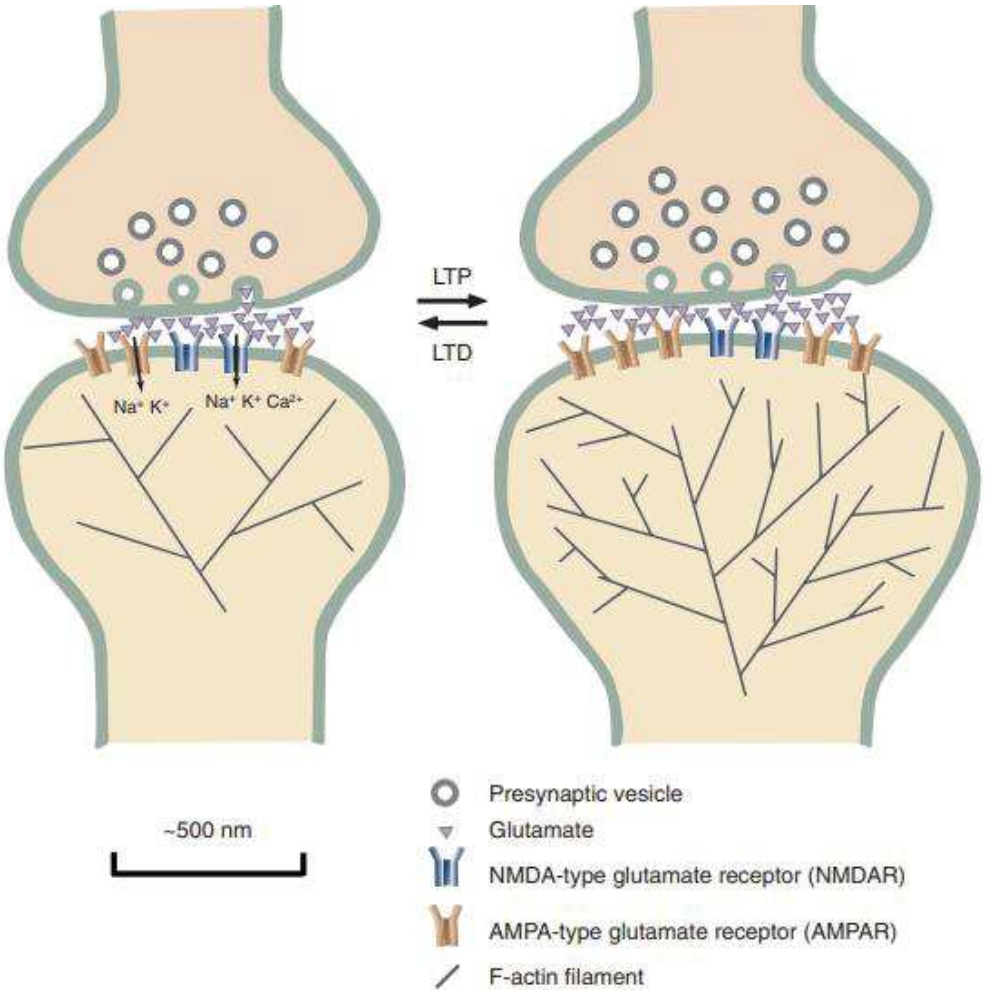

Figure 8: Synaptic rearrangement upon LTP and LTD

Increased communication between synapses induces long term potentiation (LTP) as well as morphological and functional synaptic changes. LTP result in increased presynaptic vesicle release of glutamate neurotransmitter, but also increased cytoskeleton branching, growing of the post-synaptic head and increased expression of AMPA glutamate receptor. Long term depression (LTD), in contrast, result in the opposite mechanism. (Kennedy, 2016).

V. Molecular pathways underlying transcription-related long-term memory

There are many genetic changes that take place during learning and that are essential for the formation of long-term cortical memory. The construction of long-term memory and the consolidation of these memories is dependent on *de novo* protein synthesis. Indeed, when

transcription is abolished using protein synthesis inhibitors (e.g.: anisomycin), LTM is impaired (Remaud et al., 2014) (Dubue et al., 2015).

Gene transcription is not uniquely required at a specific time point. All along the consolidation process, distinct groups of genes are transcribed. While some genes are expressed later (late response genes), others are induced very rapidly after neuronal stimulation. Those genes are called immediate early genes (IEG). They are rapidly and transiently activated after neuronal stimulation (Sheng and Greenberg, 1990) (Cullinan et al., 1995) (Bisler et al., 2002) (Zangenehpour and Chaudhuri, 2002). In this manuscript, we will focus on some of the very well know molecular cascades responsible for IEG expressions, the learning-associated activation of nuclear CREB and Elk-1, with a particular focus on the Elk1 transcription factor.

1. The CREB transcription factor pathway

The cAMP Response Element binding Protein (CREB) is an essential transcription factor in the context of IEG expression and memory consolidation. Briefly, calcium entry, triggered by LTP activity, is responsible for the activation of several calcium-dependent kinases, including the calcium/calmodulin-dependent protein kinase II (CAMPKII) and Protein kinase A (PKA). The role these proteins is to phosphorylate other proteins, such as CREB. The CREB protein is constitutively present in the nucleus where it plays a transcriptional role. It's phosphorylation at the serine residue 133 is responsible of the recruitment of the co-activator proteins CBP (CREB-binding protein) and p300 which has been proposed to increase the transcription of CREB-dependent genes (Kwok et al., 1994; Parker et al., 1996). See review (Mayr and Montminy, 2001). CREB recognizes the specific cAMP response element (CRE) DNA region found on genomic regions of IEG (e.g. zif268/Egr-1, c-fos, c-jun, c-myc) and other effectors essential for synaptic plasticity (e.g. Brain-derived neurotrophic factor (BDNF) and activity-regulated cytoskeleton-associated protein (Arc)), see review (Carlezon et al., 2005). IEG are themselves responsible for the expression of late response genes responsible for the translation of new structural proteins, enzymes, membrane receptors, and ion channels, as well as several neurotransmitters, all participating in synaptic plasticity, excitatory/inhibitory balance, and memory consolidation (Figure 9). See review (Yap and Greenberg, 2018).

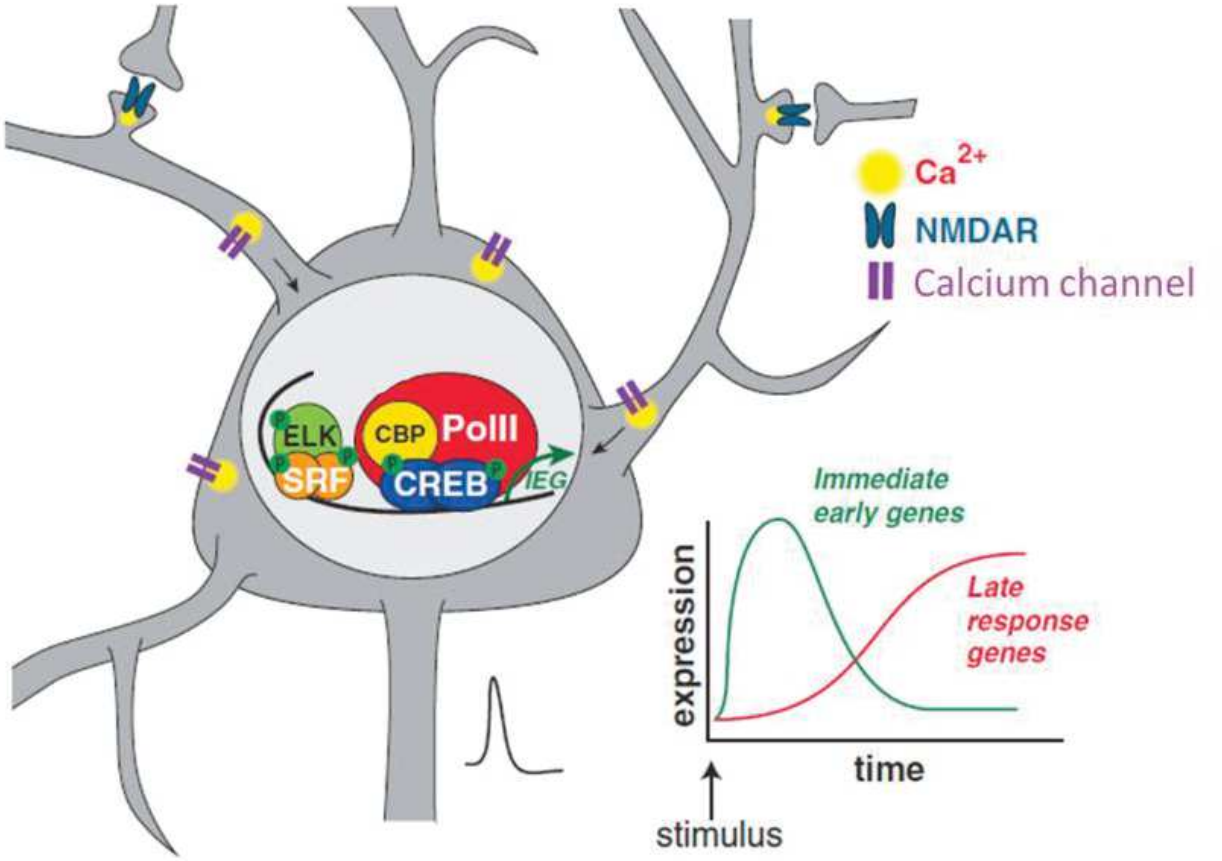

Figure 9: Immediate early and late response gene expression mediated by CREB and Elk

Neuronal activation *via* NMDA receptors leads to calcium entry in the neurons. Calcium influx induces the activation (phosphorylation) of ELK, SRF and CREB which regulates the expression of immediate early genes (IEG). Then, IEG regulate the expression of late response genes. CBP = cAMP-response-element-binding-protein-binding protein, polII = RNA polymerase II. Adapted from (Yap and Greenberg, 2018).

2. The Elk-1 transcription factor pathway

Elk1 is a member of the ETS (E-Twenty-six) family that is found abundantly in the central nervous system. While Elk1 is exclusively expressed in the nucleus in non-neuronal cells, it is also present in the cytoplasm and neurites of mature neurons. Outside of the nucleus Elk1 is found to colocalize with microtubule to regulate microtubule organization (Kelle et al., 2019) and with mitochondria for proapoptotic functions (Barrett et al., 2006).

However, upon neuronal stimulation, Elk1 is phosphorylated and translocated to the nucleus to ensure transcriptional activities (Lavaur et al., 2007). Elk1 phosphorylation (p-Elk1) is ensured by

the MAPK family (e.g. JNK, p38, or ERK) (Cavigelli et al., 1995) (Enslen et al., 1998) (Cruzalegui et al., 1999). In contrast, Elk1 is also susceptible to be post-translationally modified by SUMOylation, resulting in cytoplasmic transport of Elk1 and thus, inability to further insure transcriptional functions (Salinas et al., 2004). See Figure 10.

In the nucleus, Elk1 transcriptional activity arises from the complex formation between one TCF and two SRF (Serum response factor) proteins, TCF being a subgroup of ETS family including Elk1, 3 (NET/Sap2), and 4 (Sap1). The Elk1/SRF complex is known to recognize SRE (Serum response element) domain on the genome. Most of the IEG contain an SRE domain in their promotor (ex: c-fos, junB, erg-1, and Nur77, the murine homolog of the human NR4A1 gene) (Figure 9 and Figure 10). Inhibiting or in contrast increasing the activity of the complex has a direct impact on c-fos expression. A high number of Elk-1 targets encode for transcription factors and components of the basal transcription machinery. Thus, Elk1 is essential not only for the expression of transcription factors but for the general transcription itself. See review (Besnard et al., 2011).

p-Elk1 seems to be tightly related to learning. In the hippocampus, increased Elk1 phosphorylation is observed after Long term potentiation induction or after contextual fear conditioning in hippocampal neurons (Davis et al., 2000) (Sananbenesi et al., 2002). One-trial avoidance learning is also associated with a specific increase in the phosphorylation of ERK, Elk-1, CREB, and c-Fos expression in the hippocampus (Cammarota et al., 2000). Importantly, the specific inhibition of Elk-1 phosphorylation, and subsequent nuclear translocation, was associated with a defect in the glutamate-induced expression of IEGs bearing SRE site(s) on their promoters, such as c-fos, junB, and zif 268 (Lavaur et al., 2007).

In pathological conditions, Elk1-dependent gene transcription is altered. Aβ treatment to recapitulate Alzheimer disease in culture cells, resulted in decreased phosphorylation of critical transcription factors, such as CREB and Elk-1, and reduce the transcriptional activity of CRE- and SRE- dependent genes under BDNF induction (Tong et al., 2004). Elk1 hyperphosphorylation is observed in a mouse model of Huntington disease (Roze et al., 2008), and in a cellular model of Synucleopathie, the synuclein indirectly interact with Elk1 via ERK which results in decrease p-Elk1 (Iwata et al., 2001). Also, Phosphorylation of Threonine 17 was identified in various brain tissues from patients with those three neurodegenerative diseases (Sharma et al., 2016a).

The phosphorylation of both CREB and Elk1 also induces recruitment of other coactivators, such as CBP (Arias et al., 1994) (Nissen et al., 2001). Besides its co-activator function, CBP has a role in epigenetic mechanisms directly impacting chromatin conformation and transcription through post-translational histone core modification (Wang et al., 2009). The different histone modifier enzymes and the involvement of histone post-translational modification in the context of learning and memory will then be discussed in the next chapter.

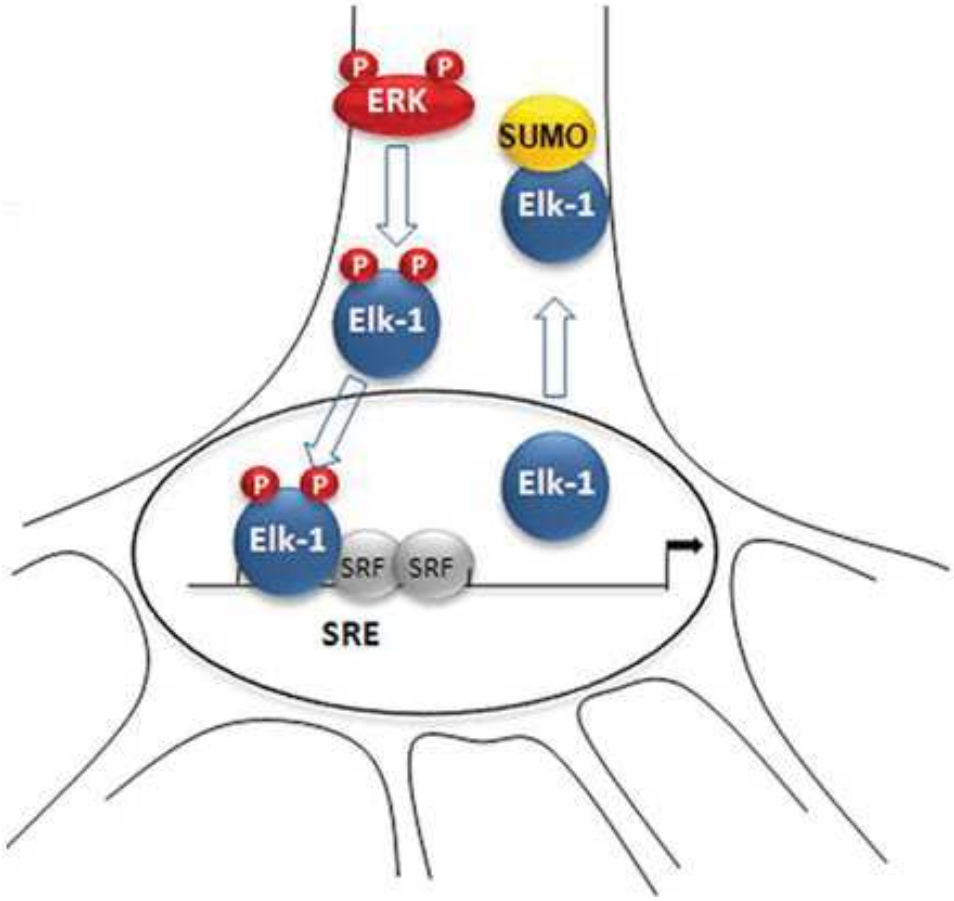

Figure 10: Cytoplasm to nucleus trafficking of Elk1

MAPK family (e.g. ERK) is crucial for Elk1 phosphorylation and activation, inducing its transport to the nucleus. Phosphor Elk1 interacts with two serum response factor (SRF) and bind to serum response element genomic sites to induce Elk1 dependent gene expression. The dephosphorylation and SUMOylation of Elk1 results in its trafficking from the nucleus back to the cytoplasm. Adapted from (Besnard et al., 2011).

Part 2: Histone posttranslational modifications and memory

I. General definition

Epigenetic is described as the heritable changes of a phenotype that happen without alteration of the DNA sequence (Waddington 1953). Regulation of DNA methylation, histone posttranslational modifications and non-coding RNA are the three main epigenetic processes. This manuscript is mainly focus on the histone posttranslational modifications.

In the nucleus, the basic structure of chromatin is the nucleosome. This structure is made of approximately 146 bp of DNA wrapped around a protein octamer composed of two copies of Histone 3 (H3), Histone 4 (H4) and Histone 2a (H2A) and 2b (H2B). Histones octamer are largely constituted of positively charged arginine and lysine residues, which ensure tight electrostatic interaction between histones (basic) and negatively charged DNA (acidic). Chromatin in the nucleus may adopt, in an interchangeable manner, an uncondensed or condensed state. The former known as euchromatin is transcriptionally active, and the latter known as heterochromatin is transcriptionally silent. Thus, signals that mediate rapid transcriptional responses need to first overcome nucleosome repression. As a solution, histone bound covalent modifications on their N-terminal part/tail. Histone proteins are indeed able to be naturally or chemically modified by the addition or the removal for example of acetylated, methylated, phosphorylated, ubiquitinated group, (Figure 11). The previously sited groups are the first discovered and the most studied. However, multiple other histone modification were found recently (e.g. serotonylation (Farrelly et al., 2019), dopaminylation (Lepack et al., 2020), acylation (Sabari et al., 2017)) revealing increase complexity of the chromatin. These histone posttranslational modifications are reversible and can affect chromatin compaction and 3D conformation (Gorkin et al., 2019), so that the cell can respond rapidly to changes in the environment. In this manuscript, we will discuss two of the most common histone modifications: acetylation and methylation.

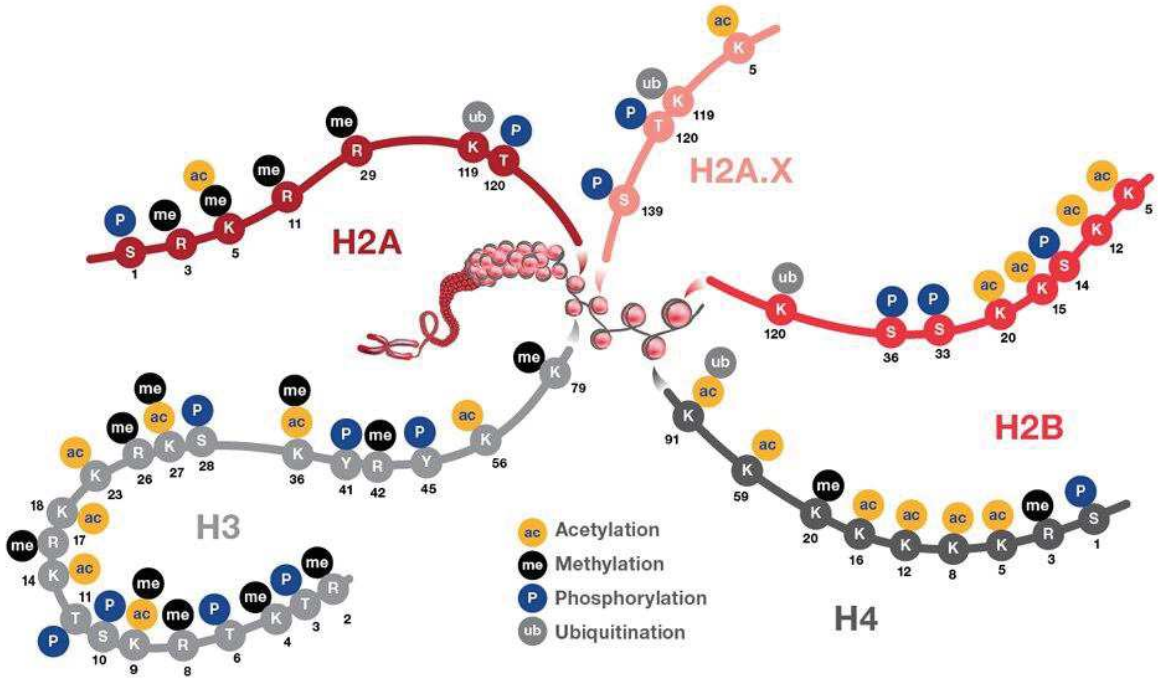

Figure 11: Epigenetic histone modification map

H2A, H2AX (variant of H2A), H2B, H3 and H4 post-translational modifications. Lysine (K) residues can be either acetylated, methylated or ubiquitinated, Arginine (R) residues can be methylated, and serine (S) and threonine (T) residues are possibly phosphorylated. (https://www.thermofisher.com).

These modifications are dynamic and depend on the environmental context. Methylation of histones in a genomic region may affect positively, or negatively, how a transcription factor interacts with the genome while acetylation of Lysine residues weakens the electrostatic interaction between DNA and histone, promoting transcription factor binding to DNA.

Histone modifications, methyl or acetyl groups are dynamically added or removed from histones cores by the action of specific enzymes. These enzymes can be seen as “writers” or “erasers” that give the opportunity to the genome to rapidly change conformation, making the DNA more or less accessible for gene transcription. Concerning acetylation, the Histone acetyl transferase (HAT) family is responsible for the addition of acetyl groups on histones (“writer”), and the Histone deacetylase (HDAC) family is responsible of its removal (“eraser”). Likewise, the addition or the removal of a methyl group on histone cores is modulated by two enzyme categories, respectively, histone methyl transferases (HMT) and histone demethylases (HDM).

Therefore, a tight balance between writers and erasers is essential to ensure proper histone modification, determine chromatin conformation and the way how transcription factors interact with the genome. Thus, epigenetic mechanisms are essential to respond properly to external stimulation and trigger proper gene transcription. These mechanisms are thus crucial for learning and memory consolidation processes, which will be discussed in the last part of this chapter.

II. Writers and erasers for acetyl- and methyl group

1. Acetylation: HAT & HDAC

Histone acetylase (HAT) and histone deacetylase (HDAC) family are a group of enzymes essential for the regulation of epigenetic and gene transcription. They are able to respectively add and remove acetyl groups on histone core proteins. Addition of an acetyl group create charge neutralization between DNA and histone of the nucleosome, thus modulating chromatin accessibility and transcription. Also, some transcription-associated proteins are directly able to recognize acetylated lysine as markers of transcription initiation.

A. Histone Acetyltransferase (HAT) family

The HAT family catalyzes the acetylation of histone through the addition of an acetyl group from acetyl coenzyme A (acetyl-CoA) to the lysine residue on the N-terminal part of histones (Figure 12). HAT proteins can be activated for example through autoacetylation of lysine residue, resulting in increased nuclear recruitment (Blanco-García et al., 2009) and catalytic activity (Thompson et al., 2004). The HAT family was initially classified in 1) cytoplasmic HAT, responsible of acetylation of newly synthetized histone prior nucleosome assembly and acetylation of non-histone protein and 2) in nuclear HAT, responsible of the acetylation of histones and regulating gene transcription (Schneider et al., 2013). Thus, hat1 was a part of the cytoplasmic HAT and the nuclear HAT were classified in different families: Gcn5-related N-acetyltransferases (GNAT) family, p300/CBP family, MOZ, yeast YBF2, SAS2, and TIP60 (MYST) family, transcription factor-related HATs, and nuclear receptor-associated HATs (Figure 13).

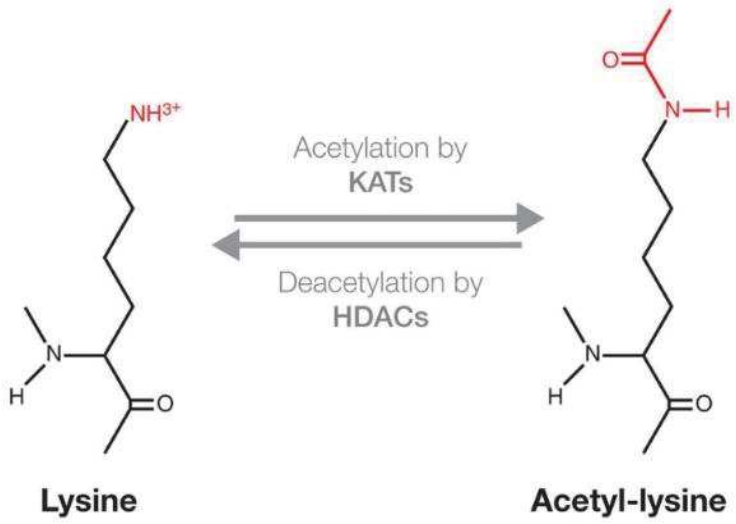

Figure 12: Acetylation and deacetylation of lysine residues

The acetylation and deacetylation of lysine residues is respectively mediated by lysine acetyl transferase (KAT) and histone deacetylase (HDAC) through the addiction or removal of an acetyl group on the last azote.

However, this nuclear and cytoplasmic classification is more historical and it is not adapted to all HATs since some of them can play a role in several cellular compartment thus, not entering into a particular group. Also, HATs were shown to target lysine of non-histone proteins and were then renamed as Lysine acetyltransferases (KAT). A more generic name and classification has been given to each HAT/KAT enzyme (1) that take into account their homology (capital letter as suffix) and (2) the order of discovery and published report (number as suffix). Thus, hat1 that was first discovered was renamed in KAT1, CBP and p300 from the same HAT family have been renamed respectively in KAT3A and KAT3B. For further information of HAT/KAT classification and functions see review (Allis et al., 2007).

B. Histone Deacetylase (HDAC) family

In contrast to HAT, HDAC family catalyzes deacetylation through the hydrolysis of acetyl group from the lysine residue and are known as repressor of the transcriptional program. In mammals we observed 18 members of the HDAC family. They are classified into different family, according to their similarity to yeast Hdac1, and separated into different groups, Class I, II, II and IV HDAC, according to their catalytic site, subcellular localization and other characteristics. Class I, II and IV HDAC are dependent of Zn2+ for enzymatic activity while class III HDAC, also named Sirtuins

(SIRT), are dependent of nicotinamide adenine dinucleotide (NAD+) for catalytic activity (Figure 13).

HDAC Class I family contains HDAC 1, 2, 3 and 8. They are all ubiquitously expressed and have a high deacetylase activity. They are responsible for the majority of deacetylation in the cell and are mostly localized in the nucleus. Class II HDAC is composed of HDAC 4,5,6,7,9 and 10 but is subdivided in Class IIa and Class IIb HDAC depending on their domain composition. Class HDAC IIa contains HDAC 4,5,7 and 9, and have the ability to shuttle between the nucleus and the cytoplasm in response to different environmental stimuli. This class of HDAC has low or no proper deacetylase activity and thus require other multiproteic complexes for enzymatic activity. HDAC II b is composed of HDAC 6 and 10 that are non-nuclear HDAC that deacetylate cytoplasmic substrates. Class III HDAC regroup all SIRT named from 1 to 7. While some Sirtuins are present in the nucleus (SIRT1, SIRT2, SIRT3, SIRT6, and SIRT7), other are predominantly present in the cytoplasm (SIRT1 and SIRT2), or even in the mitochondria (SIRT3, SIRT4, and SIRT5). Finally, class IV HDAC contain HDAC 11, the least studied nuclear HDAC that is predominantly expressed in brain and testis. For detailed information see review (Park and Kim, 2020).

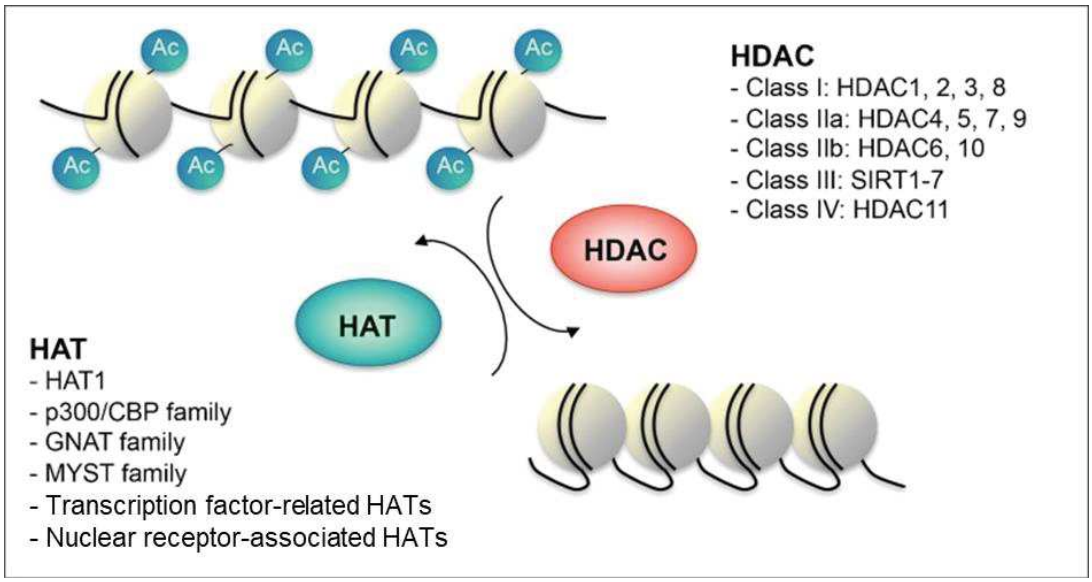

Figure 13: Histone acetyltransferase (HAT) and histone deacetylase (HDAC) families

The HAT family mediates histone acetylation, resulting in chromatin opening and accessibility. The balance is maintained due to the HDAC family that regulates the deacetylation and the chromatin condensation and inaccessibility. A tight balance between HAT and HDAC is required to maintain a correct chromatin conformation and accessibility. GNAT = Gcn5-related N-acetyltransferases, MYST = MOZ, yeast YBF2, SAS2, and TIP60 (MYST), SIRT = Sirtuins, Ac = acetylation. Adapted from (Schneider et al., 2013).

2. Methylation HMT & HDM

Histone methylation is important to regulate the access of transcription factors to specific DNA sites. The addition or removal of methyl residues on histones is catalyzed respectively by a specific group of enzymes named histone methyltransferase (HMT) and histone demethylase (HDM). The functional consequence of methylation is more complex than the acetylation one as it can be either linked to active euchromatin or to facultative and constitutive heterochromatin that can promote different degrees of gene transcription inhibition to silencing. Constitutive heterochromatin remains constantly closed in opposition to facultative heterochromatin that has the potential for gene expression at some point of the cell state.

A. Histone Methyltransferase (HMT) family

All known HMT transfer methyl group from S-adenosyl-methionine to Lysine or Arginine residues of the N-terminal tail of histones. The methylation state of lysine residue can either be mono- di- or trimethylated (Figure 14), while arginine can only be either mono- or dimethylated. In addition, arginine residues can be dimethylated in a symmetric (SDMA) or asymmetrical (ADMA) manner, meaning that the addition of methylation arrive either on the two different nitrogen atom of the last carbon (SDMA) or on the same nitrogen atom (ADMA).

Two major group of HMT exist depending on the type of residue they can methylate. We can distinguish the arginine specific methyltransferase and the lysine specific methyltransferase (KMT), which are studied in this project. Most of the KMT contain a catalytic core domain named SET, able to methylate lysine residues. The list of the different KMT and their new classification (1) that take into account their homology (capital letter as suffix) and (2) the order of discovery and published report (number as suffix) is detailed in a review from Allis and colleagues (Allis et al., 2007). Example of known histone methylase shown in Figure 15.

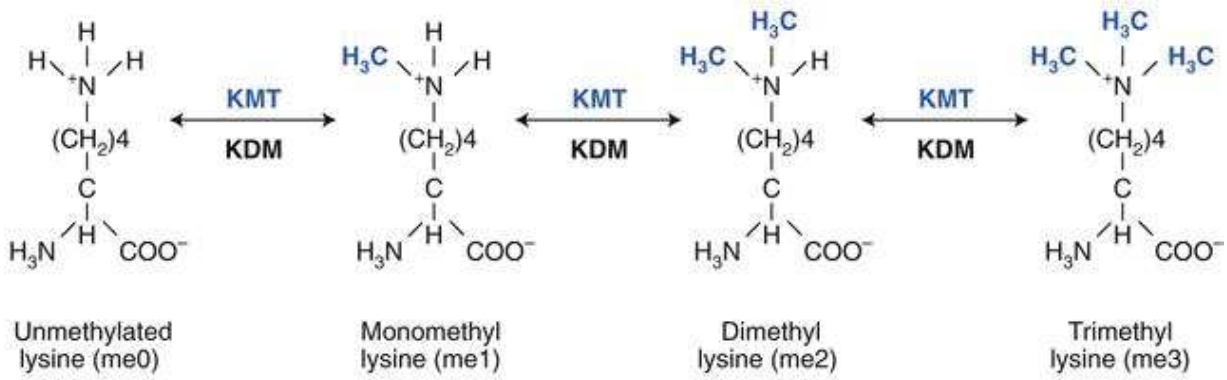

Figure 14: Methylation and demethylation of Lysine residue

The methylation and demethylation of lysine residues is respectively mediated by lysine methyl transferase (KMT) and lysine demethylase (KDM) through the successive addiction, or removal, of one, two or three methyl group to the last azote. (Husmann and Gozani, 2019).

B. Histone Demethylase (HDM) family

The presence of HDM allows the switch of transcriptional states by erasing pre-existing methyl-groups. In humans, only the JMJD6 enzyme is known to demethylate arginine. In contrast, a wide number of enzymes is recognized to be lysine demethylase (KDM). We can distinguish two main families of lysine HDM, depending on their catalytic domain: Lysine-specific demethylase (LSD or KDM) and Jumonji histone demethylase. Briefly, Lysine specific demethylase mediates the removal of methyl group dependent on FAD molecules, while Jumonji histone demethylase catalyzes demethylation via multiple steps using Iron (FeII). Similar to KAT and KMT classifications, the list of the different enzymes and their new classification is detailed in this review (Allis et al., 2007). Example of known histone demethylase shown in Figure 15.

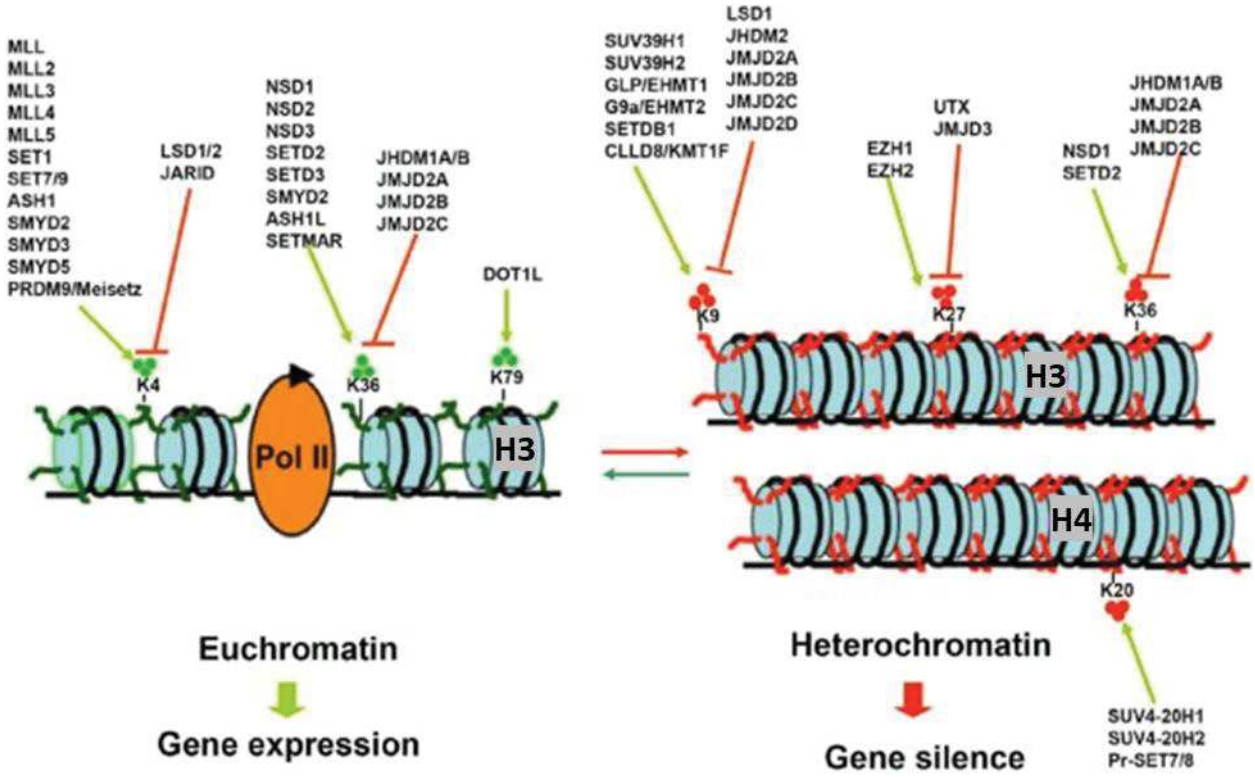

Figure 15: Histone methylation mechanisms and their writers and erasers

Representation of the different writers and erasers that play a role on methylation and demethylation processes of some histone marks. Writers and erasers are here represented with their name from the old classification. The green arrows represent the enzymes associated with methylation and the red one, shows the enzymes associated with demethylation. H3K4me3, H3K36me3 and HK79me3 are three examples of methylation associated with euchromatin and gene transcription, while H3K9me3, H3K27me3, H3K36me3 and H4K20me3 are examples of methylation associated with heterochromatin and gene silencing. PolII = RNA polII. Adapted from (Tian et al., 2013).

III. Regulation of Histone modification in learning and memory: normal and pathological conditions

Acetylation and methylation have different roles in the context of gene transcription. Indeed, acetylation is associated with transcriptional activation. For example, acetylation of histone 3 at the position lysine 27 (H3K27ac) as well as H3K9ac, H3K14ac, and H4K12ac are known as active marks that trigger transcription of genes (Wang et al., 2008b). In contrast, the functional role of the addition of methylation on lysine residues is more complex. While H3K4me3 and H3K36me3 are generally associated with transcriptional activity, H3K27me3, H3K9me3 are repressive marks and are associated with transcriptional inactivation (Barski et al., 2007). This chapter will describe how histone acetylation and methylation, as well as their writers and erasers, may impact on the

memory processes and how it can contribute to neurodegenerative diseases. Particular attention to H3K27ac, H4K12ac, H3K4me3 and H3K27me3, will be given.

1. Histone 3 Lysine 4 trimethylation (H3K4me3)

The H3K4me3 marks is localized around the TSS of actively transcribed genes (Guenther et al., 2005) (Barski et al., 2007). Interestingly, chromatin immunoprecipitation followed by genome wide sequencing (ChIP-seq) showed increased H3K4me3 in response to fear conditioning in mice (Collins et al., 2019b). In this study, the intensity, but also the broadness, of H3K4me3 peaks was found increased around the TSS of genes. Interestingly, genes showing broadening of H3K4me3 after fear conditioning were associated with synaptic plasticity and demonstrate increased expression.

The machinery responsible for H3K4 methylation includes: KMT2A (Mll1), KMT2B (Mll2), KMT2C (Mll3), KMT2D (Mll4), KMT2E (Setd1A) an KMT2F (Setd1B) (Collins et al., 2019a), Figure 16. All KMTs are strongly expressed in the nervous system and KMT2A-D is associated with impaired memory formation and intellectual disability (Kerimoglu et al., 2013) (Kleefstra et al., 2014) (Kerimoglu et al., 2017).

H3K4me3 demethylases include (1) all members of the KDM5 family: KDM5A (JARID1A), KDM5B (JARID1B), KDM5C (JARID1C) and KDM5D (JARID1D) and (2) member of the KDM1 family: KDM1A (LSD1) and KDM1B (LSD2) (Collins et al., 2019a), Figure 16. KDM5C (JARID1C) deletion is associated with memory impairment (Scandaglia et al., 2017) and mental retardation (Kleefstra et al., 2014), while little is known about the implication of the other KDM linked to H3K4me3. Decreased enrichment of H3K4me4 has been observed in relevant genes of cognitive impairment-related diseases, such as in a mouse model of Huntington's Disease (Vashishtha et al., 2013) and in postmortem brains of Alzheimer's disease patients (Smith et al., 2021).

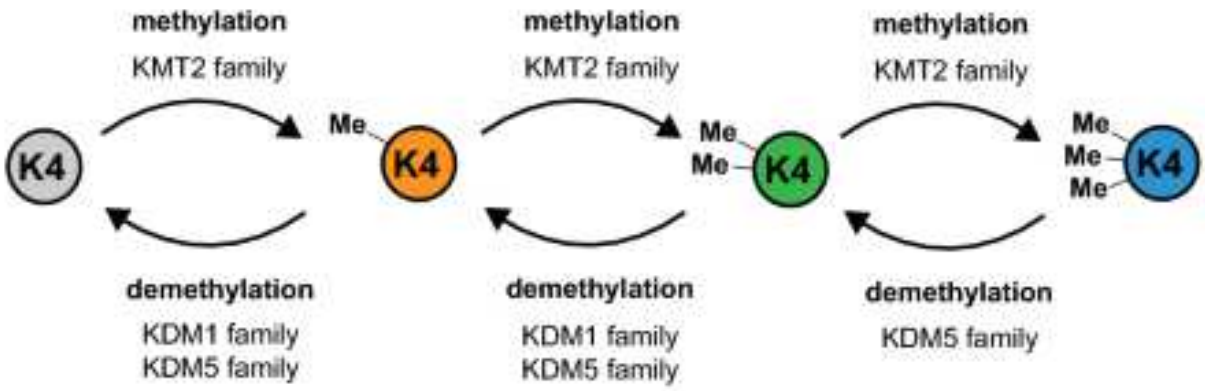

Figure 16: H3K4 writers and erasers

Histone 3 Lysine 4 can be mono- di- or trimethylated by the different members of the KMT2 family. Demethylation from tri- to di-methylation is mediated by KMT5 family. Further demethylation from tri- and dimethylation to monomethylation is mediated by both KDM5 and KDM1 family. E = methylation. (Collins et al., 2019a).

2. Histone 3 Lysine 27 trimethylation (H3K27me3)

H3K27me3 is found on genomic regions associated with gene silencing (Barski et al., 2007) and facultative heterochromatin. This facultative chromatin is found in a close conformation state at basal condition but may open in response to specific stimuli (Trojer and Reinberg, 2007). This action is possible due to the colocalization of H3K27me3 with H3K4me3. Both histone marks are required for opposite functions. If alone, H3K27me3 indicates silencing of genes. In contrary, if H3K4me3 is found on the same gene promotor, neuronal stimulation may induce removal of H3K27me3 repressive mark and rapid transcription of the gene. Those genes are called bivalent genes and are only activated upon specific conditions. (e.g. developmental state, neuronal stimulation…) (Bernstein et al., 2006).

H3K27me3 is mediated by the Polycomb Repression Complex 2 (PRC2) containing the KMT6A (EZH2) and KMT6B (EZH1) enzymes. KMT6A deletion is associated with hippocampal memory impairment and altered neurogenesis (Zhang et al., 2014).

The demethylation of H3K27me3 is induced by KDM6A (UTX) and KDM6B (JMJD3). KDM6A (UTX) deletion is linked to impairment of memory formation (Tang et al., 2017). H3K27me3 hypermethylation at C9ORF72 gene, whose mutations are associated with both Amyotrophic

lateral sclerosis and frontotemporal dementia, resulted in a decrease on its expression (Belzil et al., 2013).

3. Histone 3 Lysine 27 acetylation (H3K27ac)

Besides the methylated form, H3K27 is also found acetylated in euchromatin regions and is an active mark of transcription (Wang et al., 2008b). This mark is mostly found at promotor and TSS regions but is also found along the gene bodies and enhancer regions. Particularly, H3K27ac is also found covering gene bodies and proximal promoter TSS, therefore promoting a high expression of the associated genes, in specific cell types. These are so-called super enhancer genes (Hnisz et al., 2013). For example, H3K27ac in neurons is particularly localized on highly expressed neuronal genes (e.g. Gria2, Neurod2, Rbfox3), while in glial cells the mark is enriched on highly expressed glial genes (e.g. Olig1, Sox10, Mbp). Thus, H3K27ac distribution on super-enhancer genes defines the expression of genes regulating the molecular identity of each cell type.

We will discuss the link between the writers and erasers of H3K27ac with learning and memory below since they are common in H3K27ac and H4K12ac.

Concerning pathological conditions, H3K27ac changes are found in several neurodegenerative diseases such as in the cortical regions of post-mortem AD patients (Marzi et al., 2018) or in the striatum of Huntington Disease mouse models (Achour et al., 2015) (Merienne et al., 2019) (Alcalá-Vida et al., 2021). In accordance with the cell type specificity of H3K27ac, a study from one group in our lab in Huntington's disease mice demonstrated opposite dysregulation of H3K27ac in neuronal and glial cell (Alcalá-Vida et al., 2021). Thus, studying epigenetic at a cell-type specific level is incredibly important to better understand the pathological mechanisms involved in neurodegenerative diseases.

4. Histone 4 Lysine 12 acetylation (H4K12ac)

H4K12ac is another mark of active gene transcription localized predominantly around the promotor and the TSS of transcribed genes. Our lab previously demonstrate induction of

H4K12ac in the hippocampal region of in response to spatial MWM training in young rats (Bousiges et al., 2010). Other studies have shown that mice of 3 months of age demonstrate H4K12ac increase in response to fear conditioning (Peleg et al., 2010). However, they observed that aged mice demonstrate no change in of this histone mark in the same learning condition. The same group further observed a basal decreased of H4K12ac in the CA1 hippocampal region of aging mice compare to young control animal and in APP Alzheimer disease mice model compare to WT animal (Benito et al., 2015). Suggesting a high implication of H4K12ac in response to aging, learning and at least amyloid pathology.

The acetylation machinery specifically involved in each histone modification (H3K27ac or H4K12ac) is less investigated than the methylation one. However, the best-known HAT (also known Lysine acetyl transferase KAT) are CBP (KAT3A), p300 (KAT3B) and PCAF (KAT2B) and all of them are associated with learning and memory. Mice deficient for CBP (KAT3A) or P300 (KAT3B) demonstrated altered LTM (Alarcón et al., 2004) (Wood et al., 2005) (Oliveira et al., 2010) (Chatterjee et al., 2020). Also, PCAF (KAT2B) was found to be associated with memory formation (Maurice et al., 2008).

Concerning HDAC enzymes, most of their family members have also been found to be involved in learning and memory formation. Historically, the first demonstration of HDAC implication in learning and memory was published in 2009 by Guan and collaborators. They observed that, while overexpression of HDAC2, but not HDAC1, result in decreased memory formation and learning and synaptic number, HDAC2 deficient mice in contrast demonstrate memory facilitation and increased synaptic number in contextual the fear learning and spatial memory task (Guan et al., 2009). In contrast, Class I HDAC 1 is more essential for proper fear extinction learning (Bahari-Javan et al., 2012). HDAC Class II, is present in both the nucleus and the cytoplasm. For example, global deletion of HDAC 4 is able to ameliorate LTM in a *Caenorhabditis elegans model*. However, this LTM improvement is reversed by nuclear but not cytoplasmic restoration of HDAC4. This suggests that there are different roles for HDAC depending on their subcellular localization (Wang et al., 2011). Also, several HDACs have been found downregulated in post-mortem Alzheimer disease brain tissue (Schueller et al., 2020). Interestingly HDAC inhibitors and HAT activators have the ability to restore memory deficits in different Alzheimer's

disease mouse models (Alarcón et al., 2004) (Peleg et al., 2010) (Benito et al., 2015) (Chatterjee et al., 2018).

For more information on writers and erasers and their link with learning and memory see the chapter "*The Role of Dynamic Histone Modifications in Learning Behavior*" in Behavioral Neurogenomics (Fischer, 2019) .

Part3: Amyotrophic Lateral Sclerosis and Fronto-temporal dementia

Learning and memory are essential for the maintenance of information and the adaptation to new situations. Many diseases, in particular neurodegenerative diseases exhibit alterations of those two essential processes. In this manuscript we focus on the role of the *Fused in sarcoma* (FUS) protein in learning and memory. FUS is involved in two neurodegenerative diseases: Amyotrophic lateral sclerosis (ALS) and Frontotemporal dementia (FTD), that will then be described before a full introduction of FUS.

ALS and FTD are clinically quite different. Indeed, ALS is primarily associated with motor symptoms while FTD patients predominantly show with predominant behavioral and/or language impairment. However, both demonstrate alteration of brain regions associated with learning and memory and have common pathological causes. We will first describe both diseases and then detail that they belong to the same continuum.

I. Amyotrophic lateral sclerosis (ALS)

Amyotrophic lateral sclerosis (ALS) is also known as Charcot's disease, due to its first description in 1869 by the French neurologist Jean Martin Charcot. In the United states, ALS is usually called the Lou Gehrig's disease after the famous baseball player diagnosed as ALS patient in the 19s. ALS refer to no ("A-") muscle ("-myo-") nourishment ("-trophic"), with nerves ("lateral") degeneration that control the muscles and that leads to scarring or hardening ("sclerosis") in this region. ALS is the most frequent adult-onset neurodegenerative disease of the motor-neuron. This neurodegenerative disease is characterized by the progressive death of motor neurons and muscle weakness that leads in paralysis and death of patient 2 to 5 years after onset of symptoms, usually due to respiratory failure. Two types of neurons are typically degenerating in ALS: upper motor neurons (UMN), located in cortical areas, and projecting to lower motor neurons (LMN), in the spinal cord and brainstem (Figure 17).

ALS was first described as being a pure motor neuron disease. However, increased evidence points to at least half of ALS patients also developing either, mild behavior and/or cognitive

changes, or even meet criteria for dementia. Of note, among all ALS patients, cognitive impairment, or criteria for dementia, are usually associated with worsened disease progression and shorter lifespan. These patients are poorly characterized in the literature.

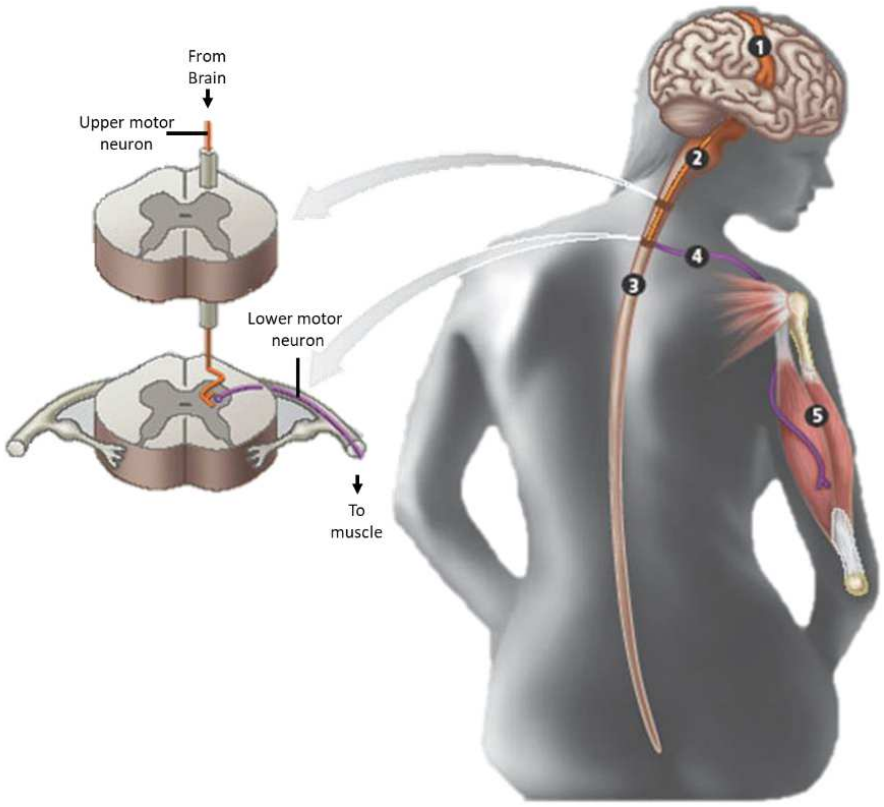

Figure 17: Upper and lower motor neurons affected in ALS.

Upper- (Purple) and Lower- (Orange) motor neurons degenerating in ALS. The soma of the upper motor neurons is localized in the motor cortex (1) and extended either to the brain stem (2) or to the spinal cord (3). Information is then relayed to the lower motor neurons (4) which have their cell bodies in the ventral horn of the spinal cord and their axons project directly to the muscles (5).

1. Epidemiology

Worldwide, ALS has an estimated prevalence around 2/100 000 person and an incidence of approximately 4/ 100 000 persons. However, the prevalence and incidence number of a disease may vary depending on the country and the ethnic population studied. For example, in a study analyzing European-American ALS patients the prevalence was found to be more than double the prevalence of African-American ALS patients (5.4 versus 2.3 per 100 000) (Mehta, 2018). The biggest European study concerning ALS incidence has been done on the 2-year period of 1998

and 1999, englobing all new cases of 18 years old and older in six population based in Ireland, UK, and Italy. Based on this study, we conclude that the predominant age of onset for ALS is above 60 years old with an estimation incidence of 2,16/100 000 person per year. The incidence is higher among men, 3.0 per 100 000 person per years, then among women, 2.4 per 100 000 person per years with a male to female incidence rates of 1.3. Also, the incidence rate increase with aging for both male and women, as observe in Figure 19 (Logroscino et al., 2010) (Logroscino et al., 2015).

2. Different forms and classification of ALS

ALS can be classified differently according to several criteria: whether it is familial or sporadic, the first region affected, the age of onset or the neuropathology.

A. Familial and sporadic forms of ALS

A majority of ALS cases, ~90%, are called sporadic (sALS) as occurring in patients without known family history, while the remain ~10% are classified as familial cases (fALS) due to recorded family history. Among fALS in Europe, 68% show occurrence of known causative mutations, while the rest of patients remained genetically unexplained. In sALS patients, 11% of patients are genetically explained, but 89% of sALS patients, cannot be linked to a known genetic cause (Mejzini et al., 2019) (Renton et al., 2014).

i. Genetic determinant of ALS

There is a high genetic heterogeneity in ALS. A majority of ALS cases, ~90%, are called sporadic (sALS) as not associated with a known family history of ALS. In contrast, ~10% of cases display family history and are termed familial ALS (fALS). Almost all of the fALS cases has been found to be inherited in an autosomal dominant manner. These last years, the discovery of new genes linked to ALS diseases has paced up thanks to next generation sequencing analyses of large population of ALS patients. Up to date, more than 50 potentially causative genes have been associated to ALS, with 4 major genes, *C9ORF72*, *SOD1, TARDBP*, and *FUS*.

The first ALS gene identified in 1993 is *SOD1,* encoding for copper/zinc superoxide dismutase 1 (SOD1) (Rosen et al., 1993). To date, more than 150 mutations have been identified in the *SOD1* gene, see review (Kaur et al., 2016). Mutations in this gene predominantly cause autosomal dominant disease and account for ∼14.8% of fALS cases and ∼1.2% of sALS cases in the European population (Zou et al., 2017), Figure19 A.

In 2006, the major pathological protein in *SOD1* negative ALS patients was proved to be the TAR-DNA-binding protein (TDP43), encoded by the *TARDBP* gene (Neumann et al., 2006). Subsequently, mutations in *TARDBP* were found in ALS patients (Kabashi et al., 2008) (Van Deerlin et al., 2008). TDP43 is an RNA/DNA binding protein, mostly localized in the nucleus involved in RNA metabolism, in particular transcription and splicing, RNA trafficking and processing. More than 50 different mutations were found in TDP-43 and altered its function in ribonucleoprotein binding and splicing. See Review (Prasad et al., 2019). *TARDBP* mutations in Europe account for approximately ∼4,2% of fALS cases and ∼0.8% of sALS cases (Zou et al., 2017), Figure 19 A.

We will develop the role of FUS in ALS and other associated neurodegenerative diseases in the next Chapter of the manuscript.

The most frequent ALS-associated gene mutation was discovered in 2011. It consists in an expansion of a noncoding GGGGCC hexanucleotide repeat in the gene called “Chromosome 9 open reading frame 72” (*C9ORF72*) (DeJesus-Hernandez et al., 2011) (Renton et al., 2011). *C9ORF72* mutation accounts for approximately ∼33.7% fALS and ∼5.1% sALS in Europe (Zou et al., 2017), Figure 19 A. Expansion in the GGGGCC repeats is transcribed into an RNA with the repeat expansions. This repeat expansion can exert toxic effects through different mechanisms, including haploinsufficiency, RNA toxicity and/or repeat associated non-ATG translation (RAN translation). See review (Balendra and Isaacs, 2018).

We can observe the repartition of the main ALS-causative genes in European familial and sporadic ALS population in Figure 19 A. Many other genes are associated with ALS, although less frequently than the four major ones and detailed in Figure 18 below. More information about genes and genetic variant linked to ALS can be found here: http://alsod.iop.kcl.ac.uk/. While

some of those genes might be responsible for almost half of fALS and for the majority of sALS cases, genetic contribution in ALS might not be the only explanation for disease susceptibility.

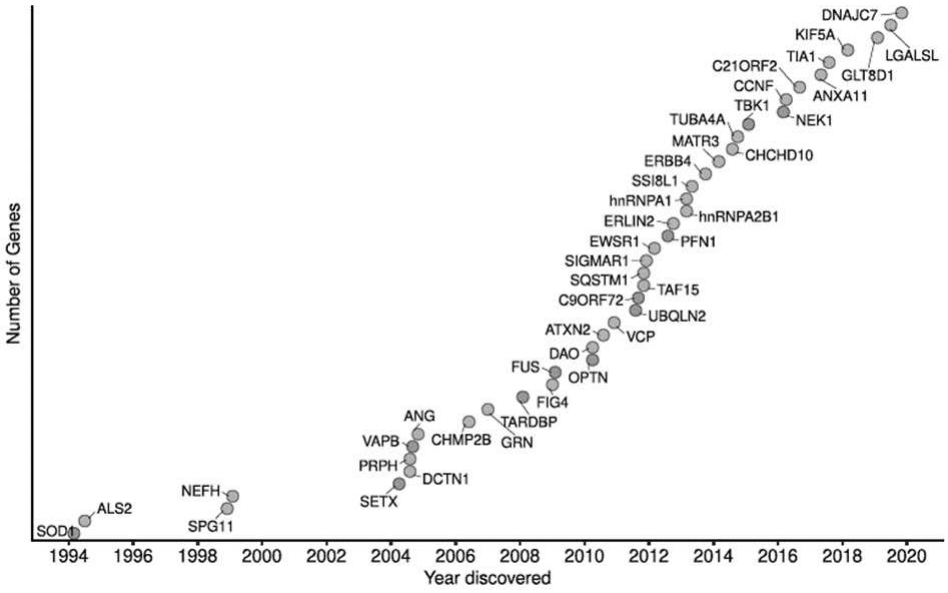

Figure 18: Genetic contribution in Amyotrophic lateral Sclerosis

Timeline of ALS-associated genes discovery. The four major genes causing ALS: SOD1 in 1993, TARDBP in 2006, FUS in 2009 and C9ORF72 in 2011, among others. Adapted from (Gregory et al., 2020).

ii. Non-genetic determinant and risk factor of ALS

Since ALS disease can not completely be explained due to gene mutation, either some genes involved in ALS are not yet discovered due to technical issues, either factor contributing to ALS are in part non-genetic. Among the few studies that tried to investigate the role of environmental contribution and the interaction between gene and environment in the context of ALS, smoking, diet, vigorous physical activities, exposure to chemicals, pesticides, metals, and electromagnetic fields (EMF) have been associated to ALS risk, although with minor contributions. Up to date, the only established risk factors are older age, male sex and family history of ALS (Ingre et al., 2015).

B. Clinical subtypes of ALS

Among ALS patients, location of symptoms onset is highly heterogeneous, and allows classification of various ALS subtypes. Most patients show “spinal onset” with primary weakness

in the arms or legs, while approximately 20% of patients demonstrate “bulbar onset” with first difficulty in speech or swallowing. Patients with bulbar onset show a worse prognosis and a much faster disease progression as compared to spinal onset cases. Finally, 3-5% of ALS patients face an even more serious outcome than spinal or bulbar onset as they developed a rare respiratory form with a survival time following diagnostic around 1.4 years (Swinnen and Robberecht, 2014). Interestingly, spinal onset is more frequent in men than women (Logroscino et al., 2010), while bulbar onset is equally distributed across genders, (Figure 19).

C. Heterogeneity of age at onset

Typical ALS disease is diagnosed around the age of 50-60 years old “adult-onset ALS”. However, a subset of patients develops ALS at much younger age. These patients are usually fALS patients, as sporadic cases tends to develop their first symptoms approximately at 58-63 years old, while the peak of disease onset is around 47 to 52 years old for fALS, (Logroscino et al., 2015) (Figure 19 B). Approximately 10% of patients displayed their first symptoms before 45 years of age, and are called “young onset ALS”. Young onset ALS cases are more likely to be males with a slower disease progression and are less likely to develop bulbar onset. Another 1% of ALS patients even demonstrate their first symptom before the age of 25 years old and are therefore characterized as “juvenile ALS”. Those juvenile cases are more likely familial cases of ALS and most of them live longer than those with adult onset. Juvenile and young onset ALS are frequently caused by *FUS* mutations, and, in this case, patients show rapid progression of the disease and short lifespan. This will be discussed later.

D. Neuropathological classification

One of the main pathological characterization of ALS is the presence of protein inclusions, with TDP43 the major component of those inclusion in almost 97% of all ALS cases (Neumann et al., 2006). In these patients, loss of nuclear TDP43 is associated with cytoplasmic accumulation and aggregation in neurons and glial cells. TDP-43 aggregates are found in motoneuron of the spinal cord but are also highly present in many cortical and subcortical regions of ALS patient’s brains, either sporadic or *C9ORF72* (Murray et al., 2011). The rest of ALS patients either present

pathological inclusions of SOD1 (2%) (Bruijn et al., 1998), or FUS (1%) (Bäumer et al., 2010). See Figure 19 C.

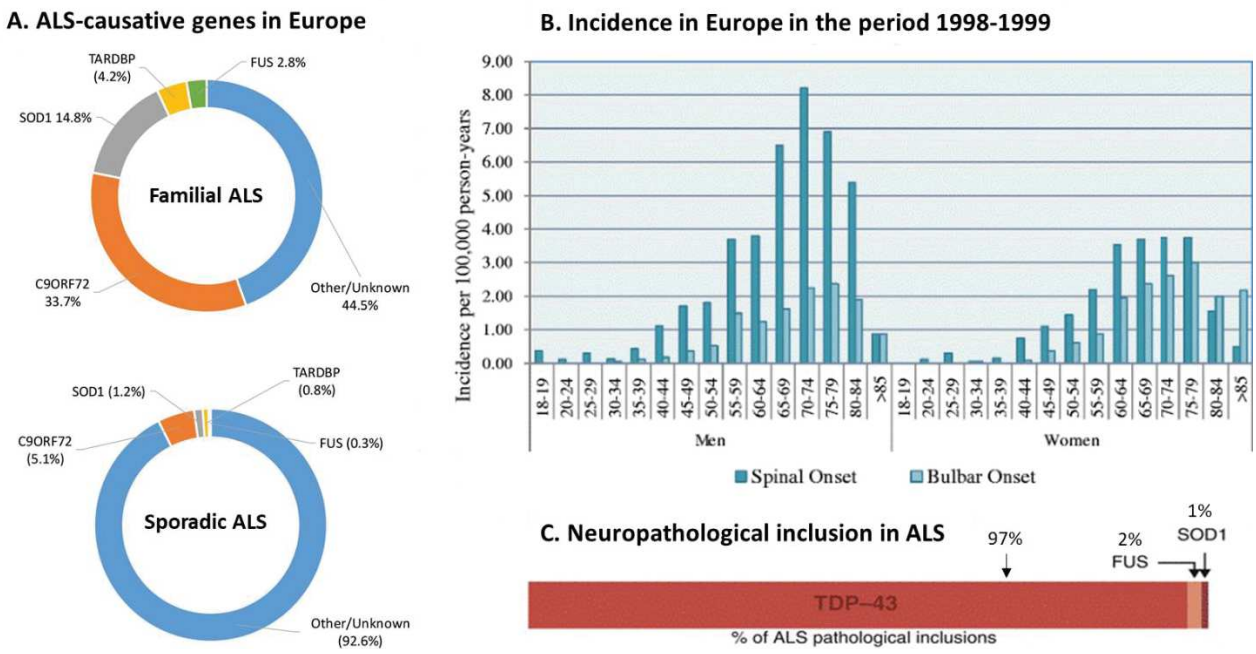

Figure 19: Repartition of the different form of ALS in Europe.

Distribution of the different ALS-causative genes in European familial and sporadic ALS populations **(A)**. Incidence of new ALS cases in the European population between 1998 and 1999. Results are classified by gender (Men and Women) and by age ranging from 18 to 85-years-old and older. Dark blue bar plots represent the amount of spinal onset cases and light blue bars plot the number of bulbar onset cases per 100 000 inhabitant per year **(B)**. Bar graph showing the distribution of proteins comprising the neuropathological inclusions in ALS, with TDP43 being the major component of them (97%), and FUS and SOD1 only representing 2% and 1% respectively **(C)**. Adapted from (Mejzini et al., 2019) and (Logroscino et al., 2015).

3. Extra-motor alterations: role of the Hippocampus and the frontal cortex in ALS

Even though ALS is a neurodegenerative disorder affecting primarily the motor system, extra-motor manifestations are increasingly recognized. Interestingly, ALS-linked neuropathological inclusions are observed in hippocampus and frontal cortex, two structures previously introduced as key brain regions involved in learning and memory. This is for example true for TDP-43 (Neumann et al., 2006). Consistent with the pathological observations, neuroimaging studies demonstrate frontal cortex and hippocampal alterations and atrophy in ALS, associated with cognitive alterations such as executive dysfunctions and memory deficits, critically involving the

frontal cortex and the hippocampus (Okamoto et al., 1992) (Mantovan et al., 2003) (Rippon et al., 2006) (Usman et al., 2011) (Kuruvilla et al., 2013) (Abdulla et al., 2014) (Stoppel et al., 2014) (Takeda et al., 2007) (Christidi et al., 2019). For more information of Hippocampal pathologies in ALS see review (Christidi et al., 2018).

Patients demonstrating motor deficit associated with either, cognitive impairment, or criteria for dementia, account for 30-50% of ALS patients and are usually associated with worsened disease progression and shorter lifespan (Olney et al., 2005) (Ishaque et al., 2018). Therefore, it is crucial to better understand extra-motor symptoms and the role of ALS-linked-protein in the different brain regions to better understand how it can influence the disease.

4. Treatment available for ALS patients

Treatment for ALS are mostly supportive. Physical therapy and nutritional support are prescribed to ameliorate the life quality of patient. Indeed, a recent study demonstrate a significant positive survival effect of high-caloric fatty det on ALS fast progression patients (Ludolph et al., 2020). At the end of the disease, when muscle can't support breathing by themselves, artificial ventilation can be used to allow a modest increase of survival time and maintain a certain life-quality (Bourke et al., 2006). At end stage, only support and palliation are available. Patients usually die from respiratory failure 3–5 years after diagnosis.

Up to date the USA Food and Drug Administration (FDA) have only approved two drugs to treat ALS patients: Riluzole leading to a modest 3 months increase in survival, and the recently accepted Edoravone. Riluzole, approved by the FDA in 1995, is an inhibitor of glutamatergic neurotransmission, it blocks the release of glutamate to decrease excitotoxicity. Riluzole is also acting on many other signaling pathways, and it remains unknwon whether the protection offered by riluzole is truly due to its anti-excitotoxic activity. Edaravone, is an antioxidant drug, approved in 2017, with effects restricted only to very early diagnosed ALS patients. Both drugs predominantly increase survival in the last stage of ALS, when mild weakness is already present and moderate assistance is needed. The difference between the two drugs also relies on the mode of administration. While Riluzole is made as a tablet to inject once a day, Edaravone is proposed as an injection required 10 days per months. See review (Jaiswal, 2019).

Due to the poor discovery of effective treatment against ALS, there is a crucial need of better understanding the mechanistic underlying each gene's mutation associated with the disease to identify new target for the development of new therapy.

II. Frontotemporal dementia (FTD)

Arnold Pick first identified and described clinical symptoms of Fronto-temporal dementia (FTD) in 1892 (Pick, 1892). A few years later, in 1911, Alois Alzheimer discovered protein aggregates in the frontal and temporal lobes of these patients, calling them "Pick bodies" in honor of Dr. Pick and naming the disorder Pick's disease (Alzheimer, 1911). However, Pick bodies were later identified as being Tau inclusions and the term "Pick's disease" is now reserved for one specific neuropathological subtype of FTD associated with Tau aggregates (Figure 20). FTD is the second most common young-onset dementia after Alzheimer's disease, appearing mostly before the age of 60 but with symptoms appearing from the early 20's until the late 90's.

FTD is characterized by the progressive loss of neurons in the frontal and temporal cortex. Symptoms include behavioral and personality changes and/or difficulties with speech and understanding of languages. FTD patient are described having a relatively preserved memory, although advanced FTD often causes memory loss in addition to the behavioral and language symptoms and dysfunctions.

1. Epidemiology

The worldwide estimated prevalence of FTD is 15–22/100,000, and incidence 2.7–4.1/100,000. Same as ALS, the prevalence and incidence of FTD is highly variable depending on the different region in the world. According to a study of Luukkainen and collaborators, comparing their study to previous ones, we observe a 1-year incidence ranging from approximately 1.9 to 11.3 cases per 100 000 persons in the European population in people aged from 45 to 65 years old. Concerning the European prevalence, we observe approximately 20.5 per 100 000 person in the same group of age (Luukkainen et al., 2015).

A. Genetic factor

FTD has a strong genetic contribution that is reflected by a high percentage (up to 50%) of patients with previous FTD or related dementia in the familial history. However a clear autosomal-dominant inheritance, associated to familial FTD (fFTD), is only observed in approximately 30% of patients (Turner et al., 2017). The remaining 70-90% FTD patients are described as sporadic cases (sFTD) with no clear inheritance and gene mutation. Most of FTD cases are explained by mutation in three genes: *C9ORF72* hexanucleotide repeat expansion, mutation in the progranuline/granuline (*PGRN*) gene and mutation in the microtubule associated binding protein Tau encoding gene (*MAPT*) (Turner et al., 2017).

MAPT was the first FTD-related gene discovered in 1998 (Hutton et al, 1998). It is located on the chromosome 17 and the encoded Tau protein is associated to microtubule binding and stabilization. Tau is excessively phosphorylated in FTD patients (Gasparini et al., 2007). MAPT mutation is present in 2-10% of all FTD and approximately 10% of fFTD (Ji et al., 2017).

PGRN, also located on chromosome 17, mutation is more common than *MAPT* in FTD, affecting about 20% of fFTD and 5% sFTD patients (Ji et al., 2017). *PGRN* is a secreted glycoprotein that is cleaved to form several granuline involved in multiple biological processes: cell-cycle regulation, development and survival of nerve cells, modulation of inflammation and so on. FTD associated mutation in *PGRN* causes decreased protein expression and haploinsufficiency in FTD patients. See review (Terryn et al., 2021).

The expansion of the noncoding GGGGCC hexanucleotide repeat in the previously described C9ORF72 gene, is the most common cause of familial FTD cases and account for 20-25% of fFTD and 6-8% of sFTD (Ji et al., 2017) (Marogianni et al., 2019).

Mutations in other genes account for less than 1 or 2% of fFTD. For example, mutations in *TARDBP* account for approximately 1% of FTD patients. Mutations in the Charged Multivesicular Body Protein 2B (*CHMP2B*) gene, on chromosome 3, encoding for a protein which is part of the component of the endosomal sorting required for transport complex III involved in cell surface

receptor degradation, account for less than 1% of fFTD. Mutations in the valosin containing protein gene (*VCP*), linked to the proteasome and trafficking of vesicles is found in less than 1% of fFTD. Mutation in Ubiquilin 1 gene (*UBQLN1*), a X-linked FTD mutation, and the Sequestosome 1/p62 (*SQSTM1*) gene, both involved in protein degradation, respectively account for less than 1% and 2% of fFTD. See review (Ji et al., 2017). Mutation in the coiled-coil-helix-coiled-coil-helix domain containing 10 (*CHCHD10*) gene, encoding for mitochondrial protein was also discovered in 2014 to be associated with 1-3% of fFTD. Mutation in the TANK-binding kinase 1 (*TBK1*) gene, coding for a serine-threonine-protein kinase that represent a bit more than 1% of fFTD was observed. See review (Abramzon et al., 2020). The most recently discovered FTD associated genes were found in the cyclin F (*CCNF*) gene (Williams et al., 2016) and in the T cell-restricted intracellular antigen-1 (*TIA1*) gene (Mackenzie et al., 2017), respectively in 2016 and 2017. To note, some other genes do not directly cause FTD but can modify the type of symptoms or age of onset of FTD.

B. Non-Genetic risk factors

The majority of FTD patients do not have a clear genetic explanation for their condition and a complex interaction between genetic factor and non-genetic environmental factors might contribute to FTD development. However, little is known about the non-genetic risk-factor associated with FTD. A history of stroke and transient ischemic attack (motor or speech impairment of more or equal to 5 min) is associated to increased risk of young onset dementia, as is a low number of year education and poor participation in cognitive activities (Cations et al., 2018). In the context of FTD, some studies demonstrate that diagnostic of head trauma or thyroid diseases increase risk factor for FTD, of respectively 3,3 and 2,5 fold (Rosso, 2003). Other studies suggest that obesity and smoking might increase the susceptibility to develop FTD (Rasmussen Eid et al., 2019)(Atkins et al., 2012). However, they might also be part of the prodromal stage of FTD, since changes in nutritional habits and increased compulsive behaviors are also characteristic of the disease. Cerebrovascular risk factors, such as type 2 diabetes in FTD, also show significant increased risk factor (Golimstok et al., 2014). Also, smocking, head injury, hypertension, depression, and autoimmune diseases might be associated with increased risk factor for FTD

2. FTD Classification

FTD patients are usually classified in different subgroup according to their clinical diagnostic or by the protein involved in the neuropathology. We will discuss the fact that clinical symptoms of FTD arise from diverse neuropathology and genetic causes and that the symptoms alone are not sufficient for a complete diagnostic.

A. Variant and clinical classification

FTD is classified into three different sub-groups based on the altered functions of the frontal and temporal lobes. See review (Liu et al., 2019).

Predominant alteration of the frontal cortex is associated to the most common form of FTD, the behavioral variant (bvFTD) that accounts for approximately 50% of FTD patients (Figure 21). bvFTD is characterized by changes in social behavior and conduct, with loss of social awareness and poor impulse control. Patients may present early disinhibition, stereotypic behavior, change in food preference and hyperorality, alteration in empathy, apathy and dysexecutive functions.

The two other forms of FTD are associated with predominant alteration of the temporal lobe and referred to as primary progressive aphasia (PPA), mostly affecting language skills, speaking, writing and comprehension (Neary et al., 1998), Figure 21. The Semantic variant of PPA (svPPA) is characterized by the loss of semantic understanding, resulting in impaired word comprehension, although the speech remains fluent and grammatically faultless. The progressive nonfluent variant of PPA (nfvPPA) is characterized by progressive difficulties in speech production, such as slower speech production and incorrect grammar and syntax, while the semantic knowledge remain well-preserved. svPPA and nfvPPA account each for 25 % of FTD cases.

B. Neuropathological classification

Beside the clinical and symptomatic classification, FTD patients can be classified according to neuropathological criteria. Indeed, the terminology frontotemporal lobar degeneration (FTLD)

refers to the neuropathology of FTD that is classified in subgroups according to the predominant type of abnormal protein aggregates in neuronal and glial cells. The identity of the pathological protein varies among cases and are classified in four subtypes. Almost half of FTD patients are immunoreactive for the hyperphosphorylated form of the microtubule associated binding protein Tau (MAPT), show Tau pathological inclusions and are termed FTLD-Tau (45% of FTD patients). The other half of FTLD patients are positive for ubiquitin inclusions (FTD-U) and negative for phosphorylated Tau. Most of the FTLD-U patients are also immunoreactive for TDP-43 and are referred to as typical FTLD-U or FTLD-TDP (45% of FTD patients). The remaining patients positive for ubiquitin aggregation but negative for TDP-43 inclusion are called atypical FTLD-U. Most of the atypical FTLD-U, are positive for both ubiquitin and fused in sarcoma (FUS) protein aggregation (FTLD-FUS) but negative for TDP-43 (9% of FTD patients). A small remaining proportion of atypical FTD-U cases are positive for ubiquitin inclusion but negative for both TDP43 and FUS and are classified as FTLD-UPS (for ubiquitin-proteasome system) (1% of FTD patients). The exact molecular pathology of patients classified as FTLD-UPS remain to be identified. See review (Boxer et al., 2013). See Figure 20.

However the neuropathology of FTLD is much more complex than those 4 subtypes and are subclassified according to other criteria such as the clinical features (e.g. differentiating Corticobasal Degeneration, CBD, and progressive supranuclear palsy, PSP, in FTLD-4RTau), predominance of hyperphosphorylated Tau variant in FTLD-Tau, the gene mutation in FTLD-TDP, inclusion component in FTLD-FUS but also the cell type affected and the anatomical distribution of the protein aggregation, Figure 21. More details on FTLD-FUS will be given in the next chapter when the other FTLD subgroups will not be further discussed here.

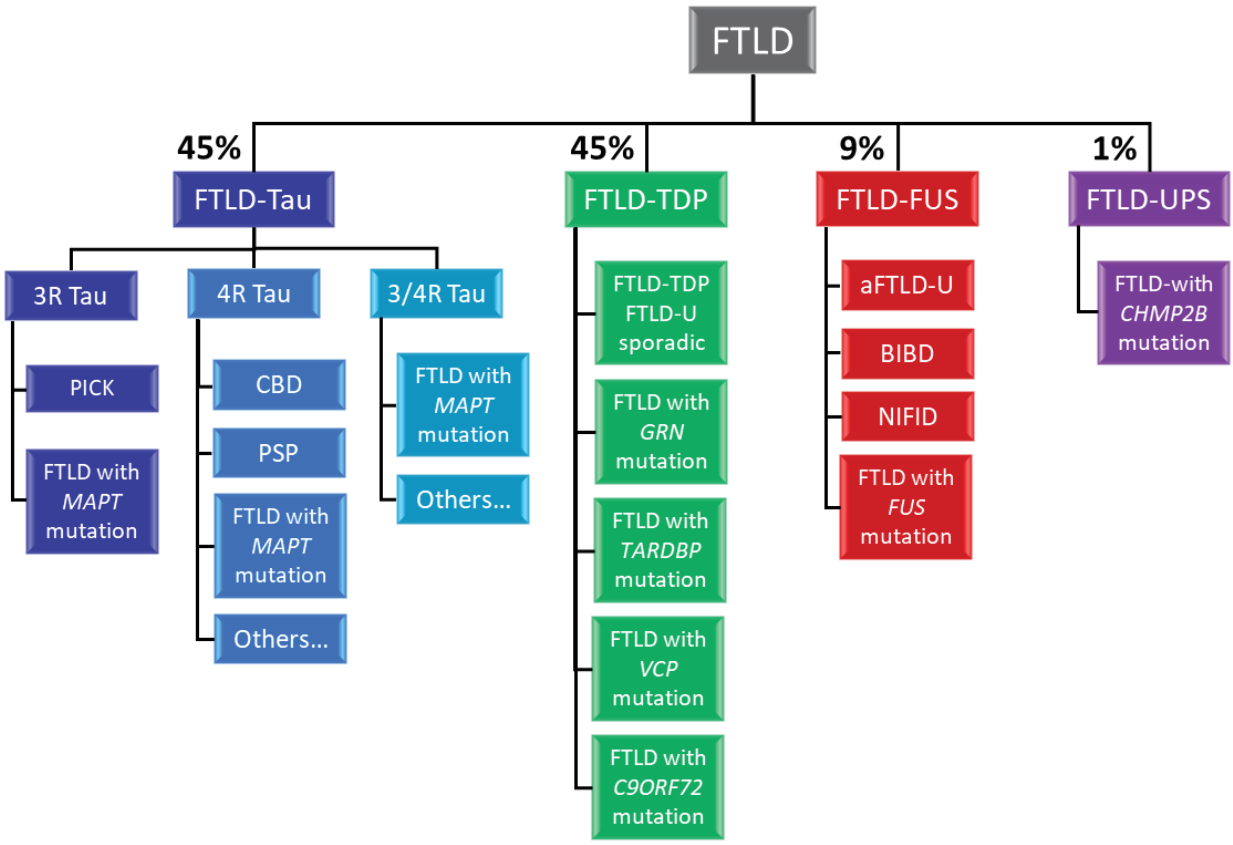

Figure 20: Neuropathological classification of FTD subtypes

FTD is classified in four main FTLD groups according to the different proteins present in the pathological inclusions and clinical symptoms (FTLD-Tau, FTLD-TDP, FTD-FUS and FTLD- UPS). Each group is further classified according to the variant of the pathological inclusions (e.g., FTLD-TAU), to the gene mutation (e.g. FTLD-TDP), or the inclusion component (e.g. FTLD-FUS). CBD = corticobasal degeneration, PSP = progressive supranuclear palsy, BIBD = basophilic inclusion body disease, NIFID = neuronal intermediate filament inclusion disease. Adapted from (Boxer et al., 2013).

C. Correlations between clinical and neuropathological classifications (135)

The correlation between genotype and phenotype, such as symptoms or neuropathology, is generally poor and not clear in FTD, even within the same family. The predominance of behavioral or language symptoms does not indicate unambiguously the proteinopathy or the underlying genetic mutation. Indeed, different mutations can lead to similar pathology. See review (Liu et al., 2019). For instance, TDP-43 pathology is associated with *TARDBP* mutations, but also *C9ORF72, GRN, VCP* or idiopathic FTD. Tau inclusions in FTD are found either in *MAPT* mutation carriers or sporadic cases, and FUS proteinopathy is only found in sporadic cases with unknown genetic inheritance. See Figure 21.

The majority of nfvPPA patients and a small proportion of svPPA patients are associated to Tau neuropathology. Indeed, most svPPA patients show TDP43 pathology. Almost half of the bvFTD patients display Tau proteinopathy, while the remainder are TDP-43 or FUS positive, Figure 21. In conclusion, the clinical symptoms of FTD arises from very diverse and complex neuropathology and genetic causes and symptoms are not sufficient to predict the exact diagnostic. See review (Liu et al., 2019).

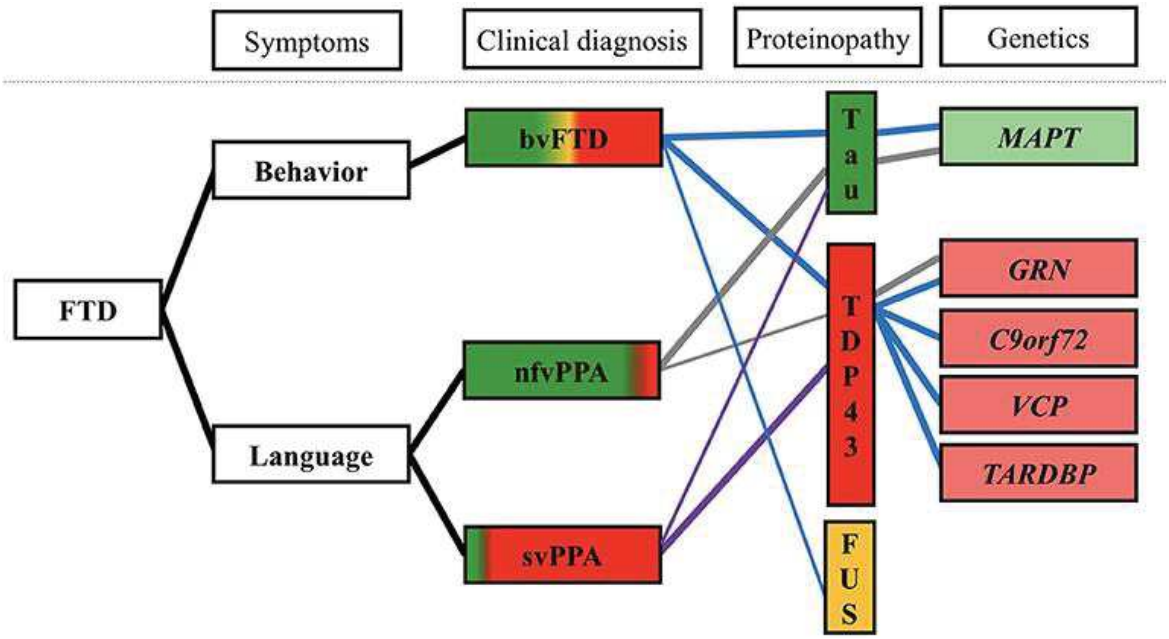

Figure 21: Correlations between genetic, pathology, clinical diagnosis, and symptoms in FTD

FTD disease is associate with behavioral (bvFTD) and language (nfvPPA and svPPA) clinical symptoms. The green, yellow and red colors of each clinical diagnosis represent the percentage of patients showing Tau (green), TDP43 (red) and FUS (yellow) proteinopathy. The blue lines represent the proteinopathy and genetic contribution in bvFTD, grey lines represent the proteinopathy and genetic aspect of nfvPPA and the purple lines demonstrate the different proteinopathy in svFTD. Neither proteinopathy and genetic contribution in FTD are associated with a specific clinical diagnosis, they rather show a more complex correlation. (Liu et al., 2019).

3. Altered neuronal structure and pathways in FTD

Neuroimaging is a powerful technique to image brain structure and indicate damaged brain regions, and is routinely used to determine and diagnose the different types of FTD. bvFTD is mostly characterized by predominant asymmetrical loss of grey matter in the orbitofrontal, prefrontal and anterior cortex, predominantly of the right hemisphere. Other subcortical

structures, such as the striatum and the thalamus also show significant atrophy, while the anterior cingulate cortex (ACC) and the insula are atrophied in correlation with disease severity. Alteration of the white matter connectivity is predominantly present between the frontal and temporal lobe (Figure 21. A). In the case of svPPA, the brain atrophy is mostly located in the temporal lobe, including the inferior temporal gyrus, the fusiform gyrus and para hippocampal gyrus and is predominantly visible on the left side of the brain hemisphere (Figure 21. B). Concerning the nfvPPA, region of the inferior frontal, insular, prefrontal, and temporal cortices and subcortical region of the caudate and putamen are particularly affected, mostly on the left hemisphere (Figure 21. C).

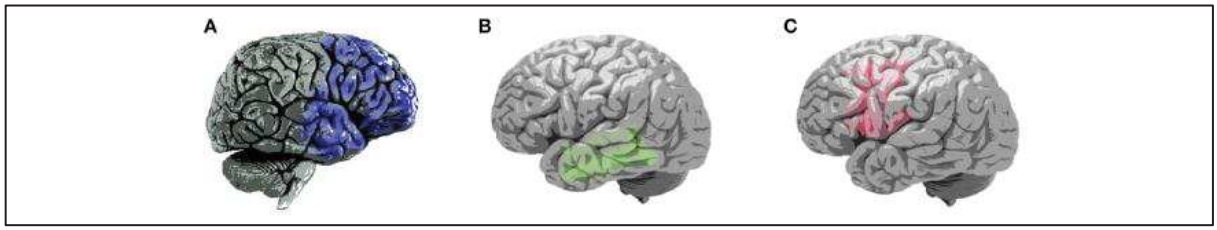

Figure 22: Neuroimaging representation of the three FTD clinical variants

The different FTD clinical diagnoses are associated with distinct brain atrophy. bvFTD demonstrates predominant brain atrophy in the prefrontal cortex, in blue **(A)**. svPPA is mainly associated with temporal cortical loss, in green **(B)** and nfvPPA shows predominant atrophy of the left fronto-temporal cortices, in pink **(C)**. (Liu et al., 2019).

Atrophy of the frontal and prefrontal cortex is associated with apathy, disinhibition and executive deficit observed more frequently in bvFTD. Degeneration of the right anterior temporal lobe is mainly associated with changes in behavior and personality as well as lack of empathy observed in bvFTD, while degeneration of the left anterior temporal lobe is associated with semantic loss observed in svPPA. The left anterior temporal lobe atrophy is also associated with visual compulsion, such as collecting colored and bright objects or jewelry. However, one third of patients with svPPA variant develop predominant alteration of the right temporal lobe, more frequently associated with verbal compulsion of word and symbols. Wide atrophy to the orbitofrontal cortex in FTD is associated with behavioral changes, including mood swing, emotional withdrawal, insomnia and change in food preference. Predominant alteration of the left inferior frontal cortex and insular cortex is associated to altered grammar and speech production as shown in nfvPPA. In conclusion, patients with predominant right-side atrophy are more likely to develop behavioral symptoms observed in bvFTD, while predominant left side

atrophy is rather associated with language impairment characterizing svPPA and nfvPPA. The ACC and insula, impacted in bvFTD, are associated with response to external stimuli to trigger appropriate behavior. In addition to cortical areas, several subcortical areas are also impacted in FTD. Text inspired by a review of Liu and collaborators (Liu et al., 2019).

4. Diagnostic & Treatment

A. Diagnostic

FTD can be misdiagnosed as Alzheimer disease or other neurodegenerative diseases. However early onset change personality may help to discriminate FTD from early AD symptoms, which is more associated with memory loss and impairment in orientation. FTD symptoms also frequently overlaps with other neurodegenerative diseases that exhibit motor deficit in particular ALS resulting in FTD with motor neuron diseases (FTD-MND), but also with Parkinsonism. FTD is also often mistaken with psychiatric disorders due to the presenting psychiatric symptoms which make FTD a difficult challenge to be diagnosed by clinicians.

B. Treatment

FTD is a fatal neurodegenerative disease with a short survival time of approximately 6 years after symptoms onset (Hodges et al., 2003). This short period of survival can be explained by the fact that FTD patient tend to develop ALS symptoms over time. Another explanation might be that their social withdrawal might trigger early institutionalization and decline. Currently no approved therapy and curative treatment exist to treat FTD patients. However, several drugs are used to treat symptoms, in particular, selective serotonin reuptake inhibitors to control compulsive behavior, mood swing and aggressive or agitated behavior (Lebert et al., 2004). Behavior modification, talk therapy, reality orientation may also help patients better control inappropriate and appropriate behavior and reduce disorientation. Help with personal hygiene and self-care may also be needed for everyday life.

III. FUS participates in both ALS and FTD

ALS and FTD share some common neuropathology and genetic defects, thus they are increasingly recognized as a continuum of the same disease spectrum with each ALS and FTD being the extreme of the spectrum, (Figure 24 A and Figure 24 B). In this chapters we will discuss the implication of the FUS protein in the behavioral and cognitive impairment linked to the ALS-FTD spectrum.

1. Germline mutations in *FUS* lead to ALS – FUS and possible other symptoms

In 2009, autosomal dominant mutations in the fused in sarcoma (*Fus*) gene were discovered (Vance et al., 2009) (Kwiatkowski et al., 2009). Approximately 60 mutations of *FUS* have been currently described, mostly localized in the NLS coding region, see review (Shang and Huang, 2016). In the Europe population, FUS account for ~2.8% fALS and to a small subset of sporadic cases, ~0,3% (Zou et al., 2017). Mutations of the gene *FUS* has been linked to juvenile ALS cases with rapid development of the disease (Bäumer et al., 2010) (Huang et al., 2010). ALS-FUS patients show FUS cytoplasmic aggregation in different regions and neuronal and glial cell populations, including the frontal cortex (Vance et al., 2009) (Kwiatkowski et al., 2009) (Bäumer et al., 2010). Interestingly, in ALS-FUS patients, cytoplasmic aggregates contain hypermethylated FUS. FUS can be methylated through arginine di-methylation either symmetric (symmetric di-methyl arginine), or asymmetrical (asymmetrical di-methyl arginine, ADMA). Extensive presence of ADMA FUS are observed in patient with FUS cytoplasmic aggregates (Dormann et al., 2012).

A possible cognitive deficit in ALS-FUS patients remain to be confirmed. Indeed, one 17-year old Japanese demonstrate severe mental retardation even before motor symptom onset (Yamashita et al., 2012), and one 19 years old Chinese girl had no mental retardation but learning difficulties (Zou et al., 2013), and several other studies identify ALS-FUS cases, around the age of 20, with same symptoms of mental retardation and learning difficulties (Bäumer et al., 2010) (Huang et al., 2010) (Yan et al., 2010) (Fecto and Siddique, 2011) (Belzil et al., 2012) (Onohara et al., 2015). A few subset of ALS patient with FUS mutation present FTD symptoms, and are classified as ALS-FTD FUS (Blair et al., 2010) (Broustal et al., 2010) (Yan et al., 2010).

2. FUS aggregates are found in a subset of FTD patients without *FUS* mutations

Contrary to ALS-FUS, *FUS* mutations are extremely rarely found in FTD patients. Only one familial case of pure FTD has been reported having mutation in the Fus gene (Van Langenhoven et al, 2010) and few patients demonstrate FUS variants and mutations (Snowden et al, 2011).

Even if in the absence of *FUS* mutation, FUS neuropathological inclusion are present in approximately 9% of FTD patients, usually with young onset disease (~35 years old) (Mackenzie et al., 2008). These patients are clinically referred as aFTLD-U or FTLD-FUS, as mentioned previously (Mackenzie et al., 2008). In FTLD-FUS patients, FUS cytoplasmic aggregates often colocalize with the other protein of the FET family (FUS EWS TAF15) (Neumann et al., 2011), the FUS nuclear transporter (transportine 1, TNPO1) (Suárez-Calvet et al., 2016) and is mostly found in its monomethylated or unmethylated states (Dormann et al., 2012). To note, FUS pathology can be subclassified in different groups according to the inclusion component. Thus, FUS inclusion associated to the presence of positive staining for intermediate filament is further classified as neuronal intermediate filament inclusion disease (NIFID) (Armstrong et al., 2011a) (Armstrong et al., 2011b) and inclusions positive for hematoxylin and eosin staining is classified as basophilic Inclusion Body Disease (BIBD) (Munoz et al., 2009) (Huang et al., 2010), Figure 21. FUS cytoplasmic inclusion are widespread in the central nervous system but prominent in the frontal and temporal lobes, thus affecting both the frontal cortex and the hippocampus (Mackenzie et al., 2008) (Neumann et al., 2009) (Neumann et al., 2011). To note, the striatum seems to be abnormally affected in FTLD-FUS patients (Snowden et al., 2011).

FTLD-FUS is usually associated with behavioral FTD (bvFTD) clinical form. To be classified as bvFTD patients need to meet at least three of the following criteria (Liu et al., 2019):

- Behavioral disinhibition (socially inappropriate behavior; Loss of manners or decorum; impulsive, rash, or careless actions) within the first 3 years.
- Apathy or inertia within the first 3 years
- Lack of empathy or sympathy (loss of response to other people's needs and feelings; loss of social interest, interrelatedness, or personal warmth) within the first 3 years

- Perseverations, stereotypies, or compulsions (simple repetitive movements; complex, compulsive or ritualistic behaviors; stereotypy of speech) within the first 3 years
- Dietary habit changes or hyperorality (altered food preferences; binge eating, increased consumption of alcohol or cigarettes; oral exploration or consumption of inedible objects)
- Executive-predominant deficits on neuropsychological profile with relative sparing of episodic memory and visuospatial skills

The clinical feature of FTD being very complex, bvFTD patients can be further classified in 3 different clinical forms (Snowden, 2001) (Neary et al., 2005).

- Disinhibited form: associate with affective disturbance, purposeless hyperactivity, social disinhibition and correlate with orbitofrontal-temporal lobe atrophy.
- Apathetic form: characterized by apathy, inertia, blunt emotion, lack of affect and economy of response usually associate with more wide-spread frontal atrophy.
- Stereotypic form: associate with markedly stereotyped, ritualistic behavior and muscular rigidity with significant striatal impairment.

In the literature, FTD-FUS is characterize by predominant atrophy of the orbitofrontal lob, anteromedial temporal lobe, anterior cingulate cortex, the insula and the caudate (Gordon et al., 2016), Figure 23.

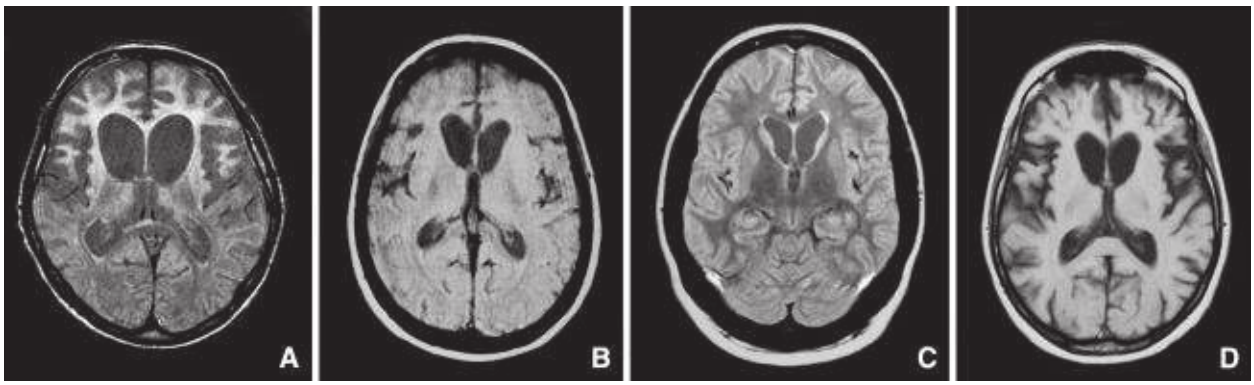

Figure 23: MRI scans of FTD-FUS patients

Representation of patients A, B and D with severe brain fronto-temporal atrophy and patients C with mild moderate-atrophy. We observe enlargement of the cerebral ventricles caused by the loss of different cortical areas. (Seelaar et al., 2010).

3. Other Fus-related diseases

FUS mutations and neuropathology have been observed outside the FTD-ALS clinical continuum. *FUS* mutations are also observed in essential tremor disease (Merner et al., 2012). Moreover, in the absence of mutation, cytoplasmic mislocalization or aggregation of FUS was observed to be widespread in polyglutamine diseases such as spino-cerebellar ataxia (Doi et al., 2010) and Huntington's disease (Doi et al., 2008).

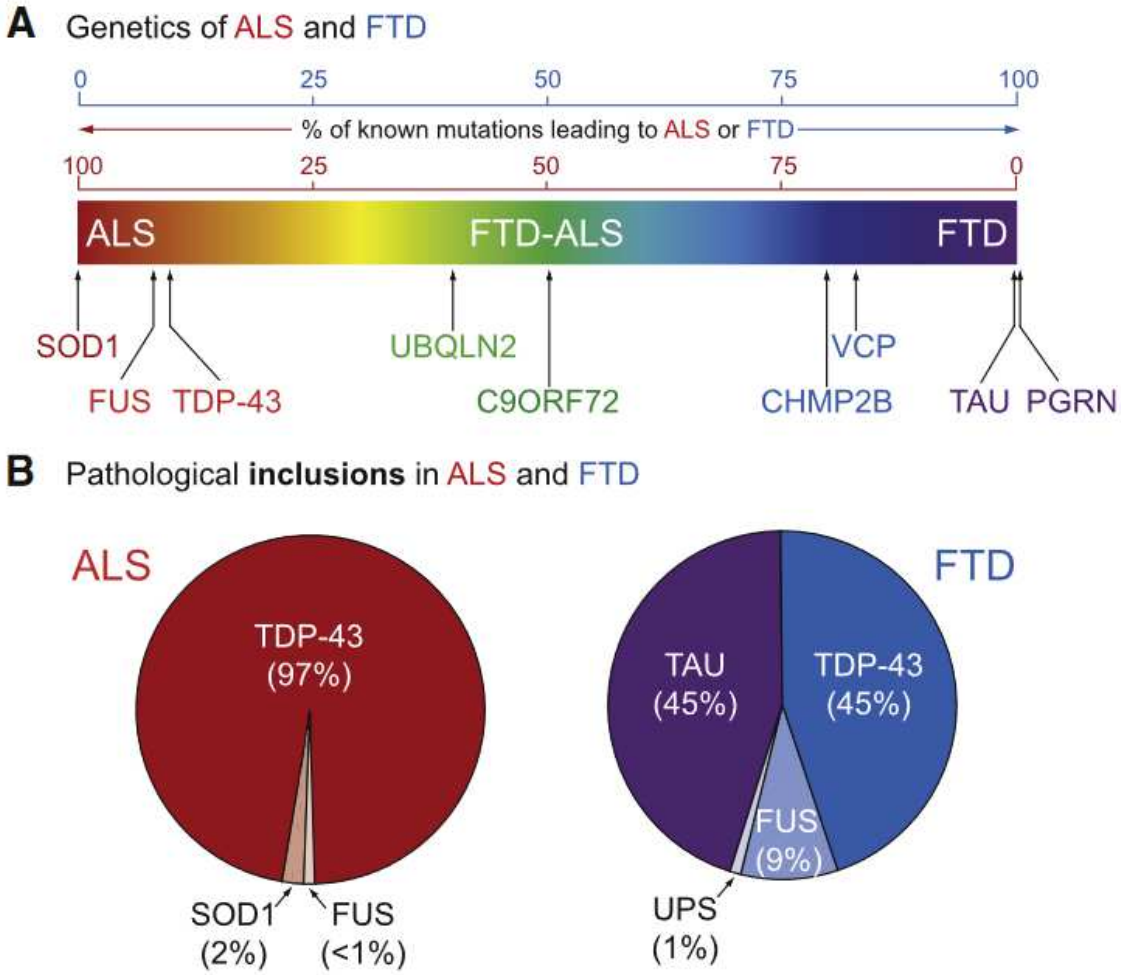

Figure 24: Genetic contribution and pathological inclusions in ALS & FTD

ALS and FTD are two diseases that represents the extremes of the same neurodegenerative continuum. ALS (red) extremity represents the ALS patients and the FTD, purple extremity represents the FTD patients. However, some patients develop ALS and FTD overlapping symptoms (middle). The main genes associated with ALS or FTD are represented on the bar graph **(A)**. Percentage of the different pathological inclusion in ALS and FTD **(B)**. (Ling et al., 2013).

Part 4: The Fused in Sarcoma (FUS) protein

As mentioned previously, mutations in the *FUS* gene have been linked to early onset and severe cases of familial ALS (~4-5%) and to a small subset of sporadic cases (~1%) (Deng et al., 2010) (Ikenaka et al., 2020) (Tyzack et al., 2019). In contrast, *FUS* mutations are rarely found in FTD patients and almost all FUS positive cases (~9%) are sporadic. However, both ALS and FTD demonstrate FUS neuropathological aggregates in widespread regions of the central nervous system. So far there is no clear explanation why *FUS* mutation predominantly triggers ALS, with predominant motor alteration, while FUS pathology in the absence of *FUS* mutation rather leads to FTD with cognitive alteration. The understanding of the different function of this protein is therefore of high interest to unravel altered mechanisms in both ALS and FTD pathophysiology.

I. FUS: Short story of discovery

Fused in Sarcoma / translocated in liposarcoma (FUS/TLS or FUS) was first identified as a chimeric oncoprotein in myxoid liposarcoma. In cancer, chromosomal translocation events can occur and result in the fusion of two endogenous transcription factors creating an aberrant transcription factor (e.g. fusion of the FUS protein with the CHOP transcription factor, FUS-CHOP) (Crozat et al., 1993) (Rabbitts et al., 1993).

In 2009, autosomal dominant mutation in the fused in sarcoma (FUS) gene were discovered (Vance et al., 2009) (Kwiatkowski et al., 2009). Those mutations are accompanied by increased cytoplasmic FUS protein and aggregates in different brain regions and spinal cord area of some patients with ALS symptoms. Shortly after, FUS has also been identified as a pathological protein in a subtype of FTD patients. This finding reinforced the idea that (1) ALS and FTD are belonging to the same spectrum of diseases and (2) that the study of FUS might be of high importance for the understanding of the two diseases.

II. Structure and localization

The FUS protein belong the FET family, a predominantly nuclear RNA-binding protein family. According to each letter, the FET family refer to FUS, EWS (Erwing sarcoma) and TAF15 (TATA box-binding protein-associated factor 68kD) proteins. These three proteins are closely linked, they contain several conserved domains, are ubiquitously expressed and are involved at all level of the DNA/RNA regulation. See review (Svetoni et al., 2016).

The *FUS* gene is located on chromosome 16p11.2 in humans and on chromosome 7 in the long arm q region in mice. However, *Fus* seems to be well conserved across species since orthologous genes have been identified in most species. *FUS* mRNA is composed of 15 exons that encode a 526 amino acid protein in human and 517-18 amino acid protein in mice. The FUS protein includes different well defined protein domains. The FUS N-terminal domain is composed of a glutamine-glycine-serine-tyrosine (QGSY)-rich region followed by a sequence rich in arginine and glycine (RGG). The C-terminal part of the protein contain an RNA recognition motif (RRM), a zinc finger domain (ZnF), an arginine-glycine-glycine (RGG)-rich domains, a nuclear export signal (E/NES) and a nuclear localization signal (NLS) composed of a well conserved proline-tyrosine (PY)-domain, Figure 25.

According to the e!Ensemble database, the *FUS* gene code for several splice variants. In human, *FUS* gene transcription is associated with 13 splice variants, with only FUS variant 1, 2 and 10 associate with the expression of a FUS coding protein. Full length protein and predominant variant, in human, is the FUS variant 1 composed of 526 amino acids. In mice, 16 different splice variants are observed and only 6 of them result in FUS protein translation (variant 1-4, 9 and 14). Full length protein and predominant variant, in mice, is the variant 3 of FUS that contain 518 amino acids. Since the implication of each variant is unknown, the manuscript will refer as FUS protein when speaking of any coding variant and the description of the protein will be focused on the full length and predominant variant.

The FUS protein is ubiquitously expressed in all different tissues and is thus widely expressed in different region of the central nervous system (Allen Brain Atlas). Its localization is mostly nuclear, but FUS is also present in the cytoplasm in lower quantity. In the manuscript, we will

focus on FUS implications and functions in cortical and hippocampal neurons and its relevance concerning cognitive alterations in the ALS-FTD pathology.

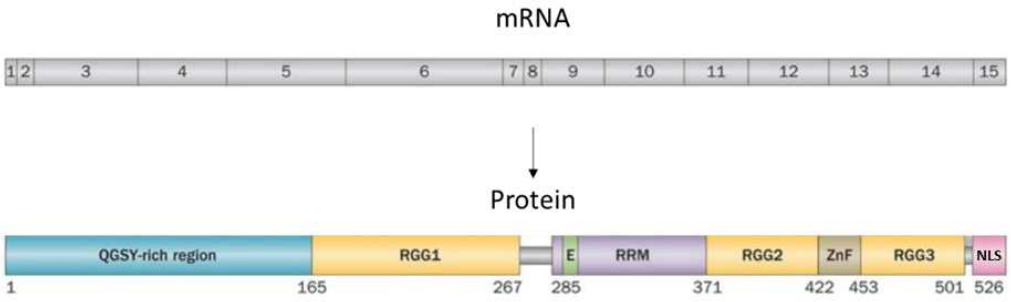

Figure 25: FUS mRNA and protein structure

FUS mRNA is composed of 15 exons, coding for a 526 amino acid protein. The FUS protein is composed of several functional domains: the Glutamine Glycine Serine Tyrosine (QGSY) -rich region, three Arginine Glycine rich domain (RGG1, RGG2 and RGG3), RNA recognition motif (RRM), Zinc finger motif (ZnF), a nuclear export signal (E) and a nuclear localization signal (NLS). Adapted from (Deng et al., 2010).

1. Role of FUS posttranslational modifications

The FUS protein can undergo a wide range of posttranslational modification. However only few of them have been precisely studied (Rhoads et al., 2018).

A. FUS arginine methylation

The most studied posttranslational modification is the methylation of arginine residues. The different RGG domains and the NLS domain of FUS contain numerous arginine that are extensively methylated. FUS interact with protein methyl transferases (PRMT1 & PRMT8), which are responsible for methylation of arginine residues (Scaramuzzino et al., 2013) on 22 sites of methylation on the FUS protein. Post translational methylation of FUS is, in part, responsible of the cellular localization of the protein, this will be detailed and discussed in the next part of this chapter. FUS post translational mono- or di-methylation R216, R234, R244, R407, R495, R503 and R514 are also associated with pathological states (Rhoads et al., 2018).

B. *FUS phosphorylation*

Another post-translational modification of FUS linked to nucleocytoplasmic localization of the protein is the phosphorylation of the Tyrosine residue Y526. The residue Y526 is one of the most important residues for a strong interaction of FUS with TNPO1 to induce FUS nuclear shuttling. Phosphorylation of Y526 occurs via the action of an src family kinase and is responsible of a higher amount of cytoplasmic FUS through decreased FUS/TNPO1 interaction (Darovic et al., 2015).

The N-terminal part of the FUS appears to be a prion-like amino acid sequence rich in serine, threonine, glutamine, asparagine and tyrosine. Prions are misfolded proteins with the ability to transmit their misfolded shape onto normal variants of the same protein. Mass spectrometry analyses revealed approximately 32 putative sites for FUS phosphorylation, either at serine or threonine residue of this prion-like domain. No tyrosine phosphorylation has been observed. N-terminal FUS phosphorylation is mediated by DNA protein kinase (DNA-PK) and is associated with cytoplasmic recruitment of FUS following DNA damage (Deng et al., 2014). Also, phosphorylation of the Prion like domain FUS appeared to decrease the aggregation property of FUS itself.

FUS phosphorylation is also associated with the ability to form Liquide Liquide Phase Separation (LLPS), which will be discussed in a next part of this cha. Treating FUS with DNA-PK to induce FUS phosphorylation disassembles FUS liquid droplets (Lin et al., 2017). This indicates that FUS post-translational phosphorylation has the ability to increase the soluble form of FUS and reduce aggregation.

FUS phosphorylated residues known to be associated with diseases states are : S57 S96, S115, S462 and Y526 (Rhoads et al., 2018).

C. *FUS Acetylation*

Mass spectrometry analyses also identify two sites for post-translational acetylation: K315-K316 and K510. Increase acetylation of the K315/K316 in the RRM domain is associated with decreased aggregation and decreased FUS/RNA interactions. On the other side, increase acetylation of the K510 found in the NLS affect FUS interaction with the TNPO1 and thus FUS nucleocytoplasmic

localization. FUS seems to be acetylated by CBP/p300 and deacetylated by SIRT and HDAC (Arenas et al., 2020). Other acetylation sites were also identified, A2, K332, K357, but more studies are required to determined their implication on FUS function (Rhoads et al., 2018).

D. Other Post-Translational modifications

Proteomic and in silico analyses of FUS reveal other post-translational modification putative sites. Ubiquitination of K264, K316, K334, K348, K357, K365 and K448 and N acetyl galactosamine - O - Glycosylation (addition of sugar molecule of the oxygen atom of serine or threonine) on T19 (Rhoads et al., 2018). All these modifications sites will require further investigations to determine their exact role in FUS function and if they are relevant in the context of Fus-opathies.

2. FUS nucleo-cytoplasmic shuttling

The FUS protein is predominantly localized in the nucleus, however constant nucleo-cytoplasmic shuttling is necessary to insure both cytoplasmic and nuclear function of FUS. Trafficking of protein between the cytoplasm and the protein is mediated by nuclear transport receptor (Importins, exportins, karyopherins).

A. FUS nuclear export

Only few information exists on the mechanisms involved in FUS export from the nucleus. Since FUS harbors a well conserved NES, it was initially thought that cargo proteins, such as exportin-1, could recognize the NES domain and induce FUS export to the cytoplasm. However, neither mutation nor silencing of exportin-1 have an impact on FUS nuclear export. Instead, it was proposed that FUS passively travel into the cytoplasm, since its small size is below the size limit for this passive diffusion through nuclear pores (Ederle et al., 2018). Recent study demonstrate that while no direct interaction is observed between FUS and exportin-1, direct binding of FUS with another exportin member, the exportin-4, is observed (Baade et al., 2021). Another proof that FUS might be exported in the cytoplasm in an independent manner of nuclear transport receptor result from the coimmunoprecipitation of FUS with CIP29, a component of the

messenger ribonucleoprotein and mRNA complex export (Sugiura et al., 2007). Thus, FUS might leave the nucleus in a way dependent of mRNA binding. Post-translational modification of FUS might also be required for its cytoplasmic export, since Phosphorylation leads to the cytoplasmic delocalization of FUS (Deng et al., 2014) (Darovic et al., 2015).

B. FUS nuclear import

Truncation of different regions of FUS highlighted that the C-terminal region harboring a Proline-Tyrosine nuclear localization signal (PY-NLS) is the only region required for normal nuclear location (Kino et al., 2011). Indeed, deletion of the last amino acid 514-526 demonstrate cytoplasmic delocalization of the protein. Interestingly this sequence is rich in Arginine residue frequently mutated in fALS cases (R521, R522 and R524), suggesting that arginine residues are essential for nuclear transport of FUS. In addition, direct interaction of FUS with several importin protein was observed (transportin 1, transportin 3, importinβ, importin 7, importin 13) (Baade et al., 2021). FUS import into the nucleus is mostly dependent upon to the C-terminal part of FUS (Both NLS and RGG domain) recognized by transportin 1 (Karyopherin β2 / TNPO1) (Dormann et al., 2010) (Dormann et al., 2012), Figure 26.

To note, mutations in the NLS domain of the FUS protein decrease binding of FUS to TNPO1 (Niu et al., 2012) (Dormann et al., 2012). Thus, mutant FUS are only able to interact with the TNPO1 via direct interaction with arginine residue of the RGG region (Dormann et al., 2012). However, arginine residues of the C-terminal region of FUS is susceptible to be highly methylated by protein methyl transferases PRMT1 and PRMT8 (Scaramuzzino et al., 2013) and extensive ADMA FUS are observed in cytoplasmic inclusion of patient with ALS-FUS (Dormann et al., 2012). Thus, in pathological states, methylation of the RGG region further disrupt the interaction between arginine residues and TNPO1 and impact FUS nuclear import (Dormann et al., 2012). In conclusion, nuclear import defect in ALS-FUS patients might be due to a combination of both genetic mutation and posttranslational modification, Figure 26.

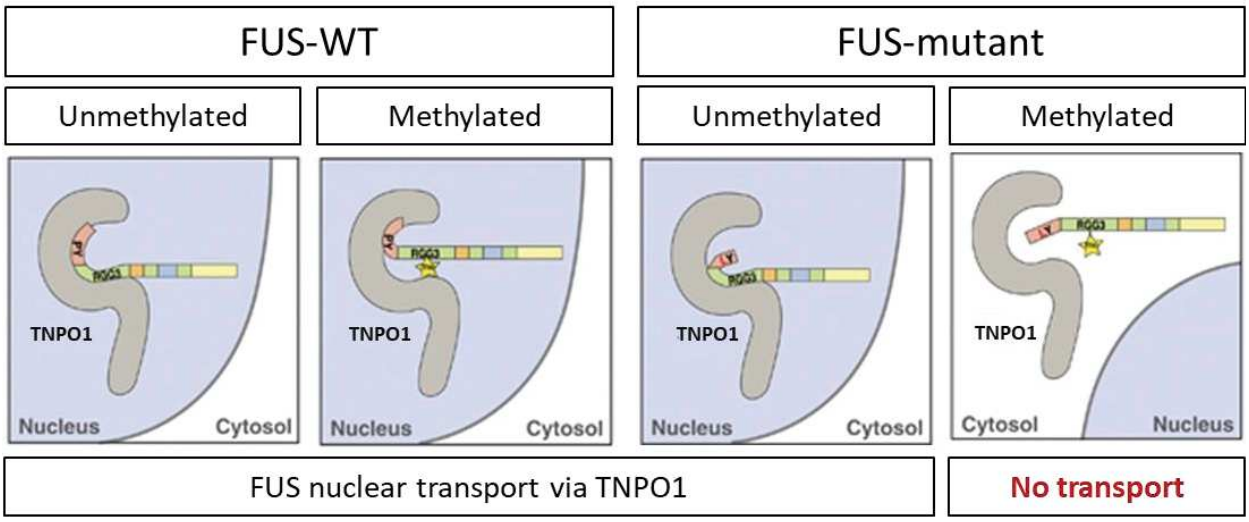

Figure 26: FUS import mechanism in the physiological and pathological conditions

Schematic representation of the proposed interaction of FUS with the transportin 1 (TNPO1). In physiological conditions, panel on the left, WT FUS interacts with TNPO1 *via* the PY (in red) and RGG (green) domain. The yellow stars represent asymmetric dymetylation of the RGG3 domain. Both the unmethylated and methylated WT FUS interact with TNPO1 and are transported to the nucleus. The right panel represents the FUS interaction with TNPO1 in the pathological conditions. The FUS mutation in the PY domain shows decreased interaction with TNPO1, while mutant asymmetric dymethylation totally disrupts interaction with TNPO1, thus abolishing FUS transport to the nucleus. Adapted from (Dormann et al., 2012).

III. FUS physiological functions

The FUS protein is ubiquitously expressed and predominantly nuclear in neurons. In the nucleus, FUS is binding to both DNA and RNA and participates in a wide range of functions associated with DNA and RNA metabolism and processing. This protein plays a role transcription and DNA repair but is also associated to RNA to regulate both coding and non-coding RNA as well as alternative splicing. FUS also plays a role in genomic stability and maintenance. In addition, the FUS protein is also present in lesser amounts in the cytoplasm of neurons and shuttles between the nucleus and the cytoplasm. Even if present in smaller cytoplasmic amounts, FUS displays critical functions, in particular at synaptic sites. Cytoplasmic FUS is involved in mRNA transport, in local translation and proper synaptic plasticity. FUS is also essential for the normal genesis of adult newborn neurons. All these functions are regulated by multiple post-translational modifications of FUS.

The multifunctional abilities of FUS in neuronal cells are recapitulated in the Figure 27 below.

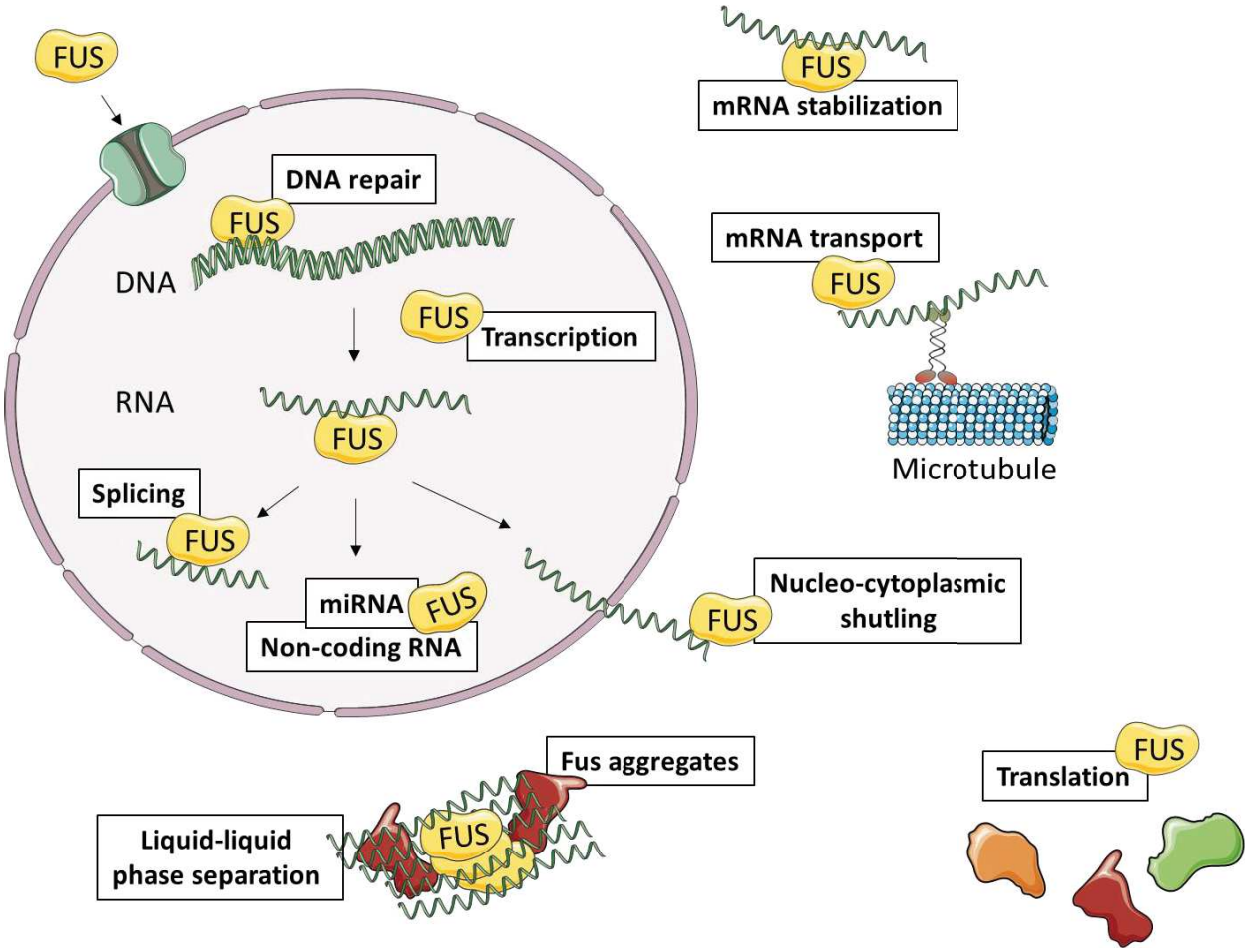

Figure 27: Nuclear and cytoplasmic function of FUS

The RNA/DNA FUS protein is associate with multiple functions in the nucleus and cytoplasmic compartment of neurons. In the nucleus, FUS is associate with a wide range of DNA and RNA processing (DNA damage, Transcription, splicing, regulation of miRNA and non-coding RNA). FUS is able to shuttle from the nucleus to the cytoplasm to insure several other cellular functions, such as, mRNA stabilization, mRNA transport, protein translation and liquid-liquid phase separation, which are altered in FUS pathological conditions. Designed with SMART - Servier medical ART.

1. Nuclear role of FUS

A. DNA binding

FUS protein is able to bind both single strand DNS (ssDNA) and double strand DNA (dsDNA), with a twofold higher affinity for ssDNA (Baechtold et al., 1999). The ability to bind DNA has been attributed to the RRM domain of FUS (aa 278-385). The RRM motif contains a unique “KK-loop” with three positively charges residues: K212, K315 and K316. Mutation of these Lysines to

Alanines to reduce electrostatic interaction with the phosphate residue of nucleic acids completely abolished the binding of FUS to DNA (Liu et al., 2013). Later on, FUS was even found to be mostly linked to active chromatin, and less FUS binding was observed on inactive chromatin regions. In contrast to the previous study, these authors suggested that the N-terminal QGSY-rich region (aa1-164) of FUS was responsible for binding to DNA and active transcription in an RNA dependent manner (Yang et al., 2014). There is thus no consensus on the mechanisms of FUS binding to DNA.

Precise genomic location of DNA-binding proteins can be monitored using Chromatin Immunoprecipitation (Chip). In 2011 it was shown that FUS bind about 1161 genes at the promoter region in Hela cells (Tan et al., 2012). ChIP followed by next generation sequencing (Chip-seq) in HEK cells, FUS was found to bind to 68% of transcription start site (TSS) regions of gene and colocalized with RNA pol II (Schwartz et al., 2012). However, results are not consistent in follow up studies, although performed in the same cell line. Indeed, Luo and collaborators found FUS binding only to 134 genes, mostly close to polyadenylation regions, while Fus knockdown did not potently modify transcription (Luo et al., 2015). Thus, here again, the exact binding regions of FUS on chromatin remain unclear.

B. Transcriptional activity of FUS

During the transcriptional process, FUS colocalizes with RNA pol II on gene promoter. It was proposed that FUS inhibits premature Ser2 phosphorylation on RNA pol II C-terminal domain to regulate elongation of gene transcription. Upon loss of FUS, increased uncontrolled transcription of genes is observed (Schwartz et al., 2012). FUS transcription is associated with both activation and repression of gene transcription (Tan et al., 2012). In vivo, most of the transcriptomic analyses have been done in the spinal cord and up to date only few studies focus on the implication of FUS deletion or mutation in the brain. Among those study, we can observe that FUS depletion is associate with dysregulation of several genes associated with synaptic functions (Scekic-Zahirovic et al., 2016), with a preference for the downregulating long-pre mRNA (Lagier-Tourenne et al., 2012). Also, FUSR514G mutation is associate with transcriptional alteration in the hippocampus of 12 months of age mice. Upregulated genes are associated with neuronal and chromatin organization, while downregulated genes are associated with transcription,

translation, and metabolic process. Importantly, FUS has also been found to be critical for the activity of several transcription factors including the ETS-transcription factor Erm / ETV5 (Picchiarelli et al., 2019).

C. DNA damage and genomic instability

i. DNA damage and repair

DNA damage is a process that accumulates with aging and can eventually lead to cell death. Intriguingly, DNA damage is also required for rapid expression of genes in specific context such as learning (Madabhushi et al., 2015). A balance between physiological and pathological DNA strand break is thus required for a normal functioning (Suberbielle et al., 2013). Neurons are particularly sensitive to DNA strand break, either single strand break (SSB) or double strand break (DSB) since they are unable to replicate DNA or divide. DNA DSB can be repaired, either by a process called homologous recombination (HR), or by non-homologous end joining (NHEJ). HR pathway uses an undamaged identical DNA sequence as template to maintain the fidelity of the previous DNA sequence, while NHEJ simply religates the two broken ends of DNA. Numerous studies demonstrate the implication of FUS in both DNA SSB and DSB. For more precise information see review (Kai, 2016) (Sukhanova et al., 2020).

Rapid recruitment of FUS is observed quickly after laser induced-DNA damage (Rulten et al., 2014) (Wang et al., 2013). FUS binds to ssDNA and dsDNA via its RRM domains (Baechtold et al., 1999) (Liu et al., 2013) despite recruitment to DNA damage site is not disrupted by mutations in these two regions. FUS is unlikely recruited to DNA damage sites through direct binding to nucleic acid (Mastrocola et al., 2013) but my depends upon poly ADP-ribose polymerase-1 (PARP1) protein (Naumann et al., 2018).

In the SSB repair pathways, FUS directly interacts with Poly (ADP-ribose) polymerase 1 (PARP-1), X-ray repair cross-complementing protein 1 (XRCC1) and DNA ligase IIIa (Lig III) to allow SSB repair (Rulten et al., 2014) (Wang et al., 2018). FUS interaction with PARP 1 is mediated by its RGG domain and is essential for further recruitment of XRCC1 and LigIII. Interaction with XRCC1 is mediated by the a.a.268 to 355 of FUS and the FUS/XRCC1/LigIII complex enhance DNA ligation

efficiency for DNA SSB repair, Figure 28. Defect in SSB is observed after the loss of FUS. In addition, mutation in the FUS protein (e.g., P525L) is responsible of the defective interaction and recruitment of the SSB machinery, which can leads, on the long term, to DNA DSB and possibly cell death. In accordance with these results, ALS-FUS patients also demonstrated defects in DNA SSB repair (Wang et al., 2018).

Concerning DSB, FUS was shown to be essential for both HR and NHEJ-mediated DNA DSB repair. Already in 1999, FUS was demonstrate to induce the formation of DNA D-loop withing duplex DNA of an homologous chromosome, an essential step for HR repair (Baechtold et al., 1999). FUS knockdown result in increased DNA DSB and induce DNA damage response signaling, such as reduced gamma H2AX (γH2AX) and 53 binding protein 1 (53BP1), on site of DNA damage (Wang et al., 2013). FUS interacts directly with HDAC1 through its G-rich (aa165-aa267) and C-terminal domain. Increased FUS/HDAC1 interaction and recruitment to DNA damage sites is observed following DNA damage. Knockdown of FUS results in decreased recruitment of p-ATM (Ser 1981 phosphorylated Ataxia-telangiectasia Mutated), repairing DNA DSB, but also decreases recruitment of Ku70, a NHEJ pathway protein and Nibrin (NBS1), an HR associated protein (Wang et al., 2013). Interestingly, FUS is even phosphorylated at its serine residue 42 by ATM itself (Gardiner et al., 2008), involved in HR, and at its N-terminal part by DNA-PK, required for NHEJ, after DNA strand break (Deng et al., 2014). See Figure 28. Mutation or knock down of the FUS protein impairs DSB repair, decrease interaction with HDAC 1 and altered recruitment of other DNA damage sensor, such as p-ATM, in culture cells (Rulten et al., 2014) (Wang et al., 2013). In line with these results, human induced pluripotent stem cells (iPSC) derived FUS-ALS motor neuron model (Naumann et al., 2018) as well as post-mortem cortex of fALS-FUS (Wang et al., 2013) and FTLD-FUS patients (Deng et al., 2014) demonstrate increase γH2AX. These data support that FUS is tightly linked to DNA damage responses and that these pathways are altered in FUS ALS or FTD.

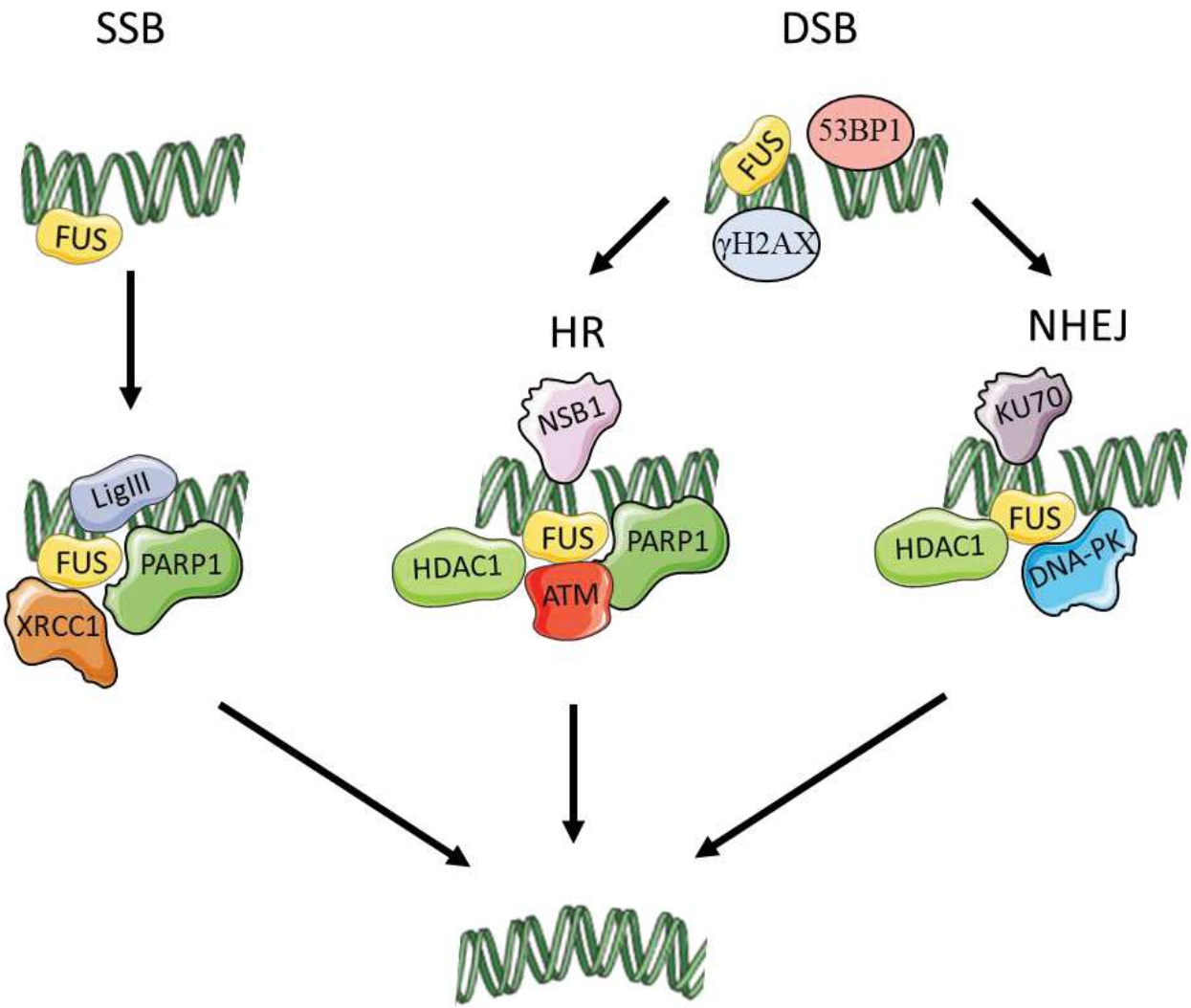

Figure 28: FUS functions and partners in DNA strand break repair

FUS is involved in both single strand breaks (SSB) and double strand breaks (DSB) and recruit and interact with different molecules depending on the repair pathway. FUS DNA SSB repair is mediated by poly (ADP-ribose) polymerase 1 (PAP1), X-ray repair cross-complementing protein 1 (XRCC1) and DNA Ligase II (Lig III). The presence of gamma H2AX and 53 binding protein 1 (53BP1) are markers of DNA DSB and dependent on FUS. DNA DSB is associated with two distinct mechanisms: homologous recombination (HR) or non-homologous end joining (NHEJ). FUS induces HR of DNA DSB through the recruitment of PARP1, Ataxia-telangiectasia Mutated (ATM), Histon deacetylase 1 (HDAC1) and Nibrin (NSB1), while NHEJ of DNA DSB arise through interaction with HDAC1, DNA protein kinase (DNA-PK) and Ku70. Designed with SMART – Servier medical ART and inspired from (Wang and Hegde, 2020) and (Sukhanova et al., 2020).

ii. FUS implication in development and in genomic instability

FUS is essential for neonatal viability. Mice with homozygous mutation of FUS, resulting in absent translation of the protein FUS, die few hours after birth (Hicks et al., 2000) (Scekic-Zahirovic et al., 2016). In a specific-pathogen-free animal facility it was observed that, while none of the FUS deficient inbred animal reach adulthood, partially outbred animals were able to survive. However, the partially outbred FUS deficient mice demonstrate complete sterility of male and reduced fertility of females. Male sterility in FUS-deficient mice was attributed to meiotic prophase alteration in testes (Kuroda et al., 2000). FUS-deficient cell analyses demonstrated karyotype aberration in the metaphase state (aneuploidy, chromosome breakage, centromeric fusion and presence of extrachromosomal DNA), thus, demonstrating a function of FUS in maintaining chromosomal stability (Hicks et al., 2000).

The balance between genome stability and instability is also regulated by retrotransposition events. Retrotransposons are a type of DNA mobile element that change their position within the genome. Interestingly, one study demonstrates that not Wild Type (WT) FUS but FUS mutation in the NLS domain (R514G and H517Q) is able to inhibit retrotransposition. Of note, mutant FUS also strongly colocalized in cytoplasmic aggregates with protein ORF1P, encoded by the long interspersed nuclear element 1 (LINE-1) retrotransposon (Pereira et al., 2018). Increased retrotransposition is associated to accelerated age dependent memory decline and decreased lifespan. However, retrotransposition events occurs actively in neurons, especially during neurogenesis and allows genomic diversity between neurons. We can then easily speculate that to decreased retrotransposition events could lead to alteration of the memory process in neurodegenerative diseases. Another retrotransposon element, the SVA, is located at the 5’ end of the FUS gene and act as transcriptional regulator. Interestingly, two polymorphic variants are found in this SVA region and result in differentially regulate expression of the FUS protein (Savage et al., 2014). All those transposition events and regulations are also highly synchronized by epigenetic mechanisms.

Finally, FUS is also essential in mechanistic involved in telomere protection. The RGG region of FUS is found to interact with a structure named G-quadruplex, a Guanin rich four stranded secondary structure found in telomeres. In parallel, FUS seems to bind to the SUV4-20H2 HMT

and regulate telomere end through histone methylation. Overexpression of FUS demonstrate increased methylation and telomere shortening (Takahama et al., 2013) (Kondo et al., 2018). Telomere shortening has already been associated with aging and different neurodegenerative disease. Reviewed in (Zhu et al., 2011).

D. RNA binding properties of FUS

FUS binds ssRNA with three-fold higher affinity than ssDNA of the same length and sequence, while FUS binding for dsDNA is weaker. FUS binding to dsRNA was also observed (Baechtold et al., 1999) (Wang et al., 2015). FUS shows increased affinity with increasing RNA-length (Lagier-Tourenne et al., 2012) (Wang et al., 2015) and displays enriched binding to GGUG- rich sequences *in vitro*, via the different RGG boxes, the ZnF and the RRM domain (Lerga et al., 2001) (Liu et al., 2013) (Wang et al., 2015). *in vivo* Croslinking Immuno Precipitation (CLIP) analyses followed by RNA sequencing, with an antibody recognizing FUS, demonstrates predominant binding to GUGGU region. FUS binding in mice is highly overlapping (69%) with FUS binding in human cortex (Lagier-Tourenne et al., 2012). However, the G/U rich region seems to be neither necessary nor sufficient for FUS binding (Lagier-Tourenne et al., 2012) (Wang et al., 2015). While the ZnF domain appears responsible for the GGU binding, the RRM domain of FUS might recognize other types of RNA with broader specificity (e.g., CG-, AUU-rich RNA and stem-loop/hairpin loop). The RGG domain was proposed to increase the binding affinity of FUS to RNA and promote destabilization of structured RNA conformation to allow additional binding (Loughlin et al., 2019).

FUS predominantly binds to intronic regions, but also to exons and both 5' and 3' untranslated region (UTR) regions (Lagier-Tourenne et al., 2012) (Nakaya et al., 2013) (Zou et al., 2013). FUS was proposed to bind at the beginning of long intronic regions (>100kb) to regulate transcriptional elongation (Lagier-Tourenne et al., 2012). Another CLIP-seq analyses demonstrate FUS binding around nascent RNA and proposed a role in activation/inactivation of transcription termination and polyadenylation, with enrichment in genes involved in synaptic activity (Masuda et al., 2015). Lagier-Tourenne et al, further identified over 5500 RNA target of FUS in mice and human cortex, mostly associated with gene transcription, synaptic transmission, glutamate signaling, metabolic process and cell-adhesion (Ishigaki et al., 2012) (Lagier-Tourenne et al., 2012) (Nakaya et al., 2013) (Zou et al., 2013). Some of these targets are even associated with ALS and/or

FTD pathologies: SOD1, Ubiquilin 1 and 2 (UBQLN1 & 2) and Mapt. Interestingly, a top candidate of FUS binding is the exon 7 and flanking intron 6 and 7 of *Fus* pre-mRNA itself (Lagier-Tourenne et al., 2012) (Zou et al., 2013) (Humphrey et al., 2020).

Besides FUS binding to pre-mRNA, binding to non-coding RNAs is observed, including long non coding RNA (Long ncRNA), pre-micro RNA (pre-miRNA), small nuclear RNA (snRNA), transfer RNA (tRNA) and ribosomal RNA (rRNA) (Lagier-Tourenne et al., 2012). The interaction of FUS with ncRNA can be involved in its regulation of gene expression, as exemplified with CCND1 expression in response to DNA-damage (Wang et al., 2008a).

E. miRNA-processing

FUS was shown to interact with pri-miRNA (miRNA precursor named primary miRNA) as well as with several proteins of the miRNA biogenesis complex, including Drosha (Gregory et al., 2004) (Morlando et al., 2012) (Sun et al., 2015). FUS Knock down indeed altered levels of several microRNA with relevance to neuronal functions (Morlando et al., 2012).

F. Alternative splicing

Another well-known function of FUS is modulation of splicing, consistent with its binding to intronic regions of pre-mRNAs (Lagier-Tourenne et al., 2012) (Nakaya et al., 2013) (Zou et al., 2013). Interestingly, FUS protein interacts with the spliceosome machinery. For example, with the uridine rich small nuclear RNA (U-snRNA) molecule U1 (Sun et al., 2015) (Jutzi et al., 2020) and U11 (Reber et al., 2016), and *FUS* mutations modified these interactions (Sun et al., 2015) (Jutzi et al., 2020). U1 and U11 ncRNAs involved in first steps of the spliceosome complex, suggesting a role of FUS in the initiation of the splicing machinery. Recently interaction of FUS with other component of the spliceosome machinery was also demonstrated (Jutzi et al., 2020). Consistent with this, *FUS* mutation, in culture cells and patient fibroblast, altered the expression of several U-snRNA and modified several splicing targets, predominantly encoding ribonucleoprotein, and protein involved in RNA metabolism (Sun et al., 2015) while causing cytoplasmic mislocalization and coaggregation of U1 (Gerbino et al., 2013) (Jutzi et al., 2020), U2 (Gerbino et al., 2013), U11 and U12 (Reber et al., 2016) snRNA spliceosome component. In FUS

depleted cells and mouse model, several genes, associated with vesicular transport and neuronal functions, showed differential splicing (Ishigaki et al., 2012) (Lagier-Tourenne et al., 2012) (Nakaya et al., 2013) (Reber et al., 2016), and, at least a significant proportion of these dysregulated splicing sites, are direct RNA targets of FUS (Nakaya et al., 2013). Typical examples of splicing controlled by FUS include Bdnf (Qiu et al., 2014), or MAPT (Orozco et al., 2012) (Scekic-Zahirovic et al., 2016) (Ishigaki et al., 2012), see review (Orozco and Edbauer, 2013). Even if the FUS domain 165-526 is essential for chromatin binding and transcription it is apparently not required for alternative splicing, while the N-terminal part containing the QGSY rich terminal site is necessary for these splicing events (Reber et al., 2016).

2. Role of FUS on cytoplasmic functions

A. Axonal transport

Transport of mRNA in neurons depends upon cytoskeleton (microtubules, actine, intermediate neurofilament) and motor proteins. The motor proteins responsible for the anterograde transport (toward the synapse) on microtubules are kinesin family members, while the motor protein responsible for retrograde transport (toward the soma) is dynein. ALS-linked mutant FUS robustly alters anterograde and modestly inhibits retrograde transport in neurons (Sama et al., 2017). In pathological states, FUS colocalized with kinesine-1 (KIF5a & KIF5c) in cytoplasmic aggregate leading to inability of microtubule to support transport and/or anchoring of cargoes (Yasuda et al., 2017). In iPSC-derived mature motoneurons from different ALS-FUS patients, there was decreased movement of mitochondrial and endoplasmic reticulum vesicle transport in axon. Interestingly, the decreased transport was associated to hypoacetylation of α-tubulin, a microtubule structural compound, and HDAC6 enzyme (Guo et al., 2017). This effect of FUS on axonal transport can either be direct through its binding to motors element such as KIF5A (Kanai et al., 2004) or cytoskeletal elements (Lin et al., 2016), but could also be indirect through transport of mRNAs required for axonal transport, including ND1-L, an mRNA encoding an actine stabilizing protein (Fujii and Takumi, 2005) (Jun et al., 2017) or other RNAs required for dendritic spine stabilization and receptor (Fujii et al., 2005) (Udagawa et al., 2015).

B local translation and synaptic morphology and function

One of the first demonstration of FUS being implicated in local translation was that FUS cytoplasmic aggregates are translationally active (Yasuda et al., 2017). Indeed, FUS transports and regulates local dendritic translation (Fujii et al., 2005) (Shiihashi et al., 2017), and is found at both pre- and post-synaptic spines, with a preference for presynaptic localization in both inhibitory and excitatory synapses (Belly et al., 2005) (Schoen et al., 2015) (Sahadevan et al., 2021). The expression of a mutant FUS neuron significantly decreased local axonal translation (López-Erauskin et al., 2018) and altered synaptic RNA stability (Sahadevan et al., 2021).

FUS protein regulates the subcellular localization, local translation, stabilization and/or degradation of several synaptic-related mRNA (Fujii et al., 2005) (Udagawa et al., 2015). In synaptoneurosomes extract, FUS bind more than 300 RNA (CLIP-seq), mostly associated with Glutamatergic and GABAergic but also transporters and calcium signaling proteins (Sahadevan et al., 2021). RNA-seq also demonstrate around 500 dysregulated genes in synaptoneurosomes extracts of FUS mutant mice (Sahadevan et al., 2021) (Scekic-Zahirovic et al., 2021) Up regulated genes are associated with genes related to synaptic function and transporters, and downregulated genes are associated with cytoskeleton and RNA-metabolism, all known functions of FUS. Only a modest overlap is observed between the CLIP- and the RNA-seq, suggesting that FUS binding to RNA alone is not sufficient to determine RNA fate (Sahadevan et al., 2021). Also, proteomic analyses even demonstrate interaction between FUS and NMDA receptor, essential for proper excitatory synapse functioning (Husi et al., 2000).

Deletion or overexpression of WT FUS, as well as mutation of the FUS protein, are associated with alteration of neuronal morphology and synaptic functions. Reduction or ablation of FUS in hippocampal neurons affect synaptic transmission, neuronal branching and spine morphology with increased numbers of filopodia immature dendritic spine (Fujii et al., 2005) (Udagawa et al., 2015). In addition, adult-induced loss of FUS leads to neuronal cell loss in the hippocampus upon aging (Ishigaki et al., 2017). Overexpression of WT FUS reduced neuronal branching (Machamer et al., 2018), and several synaptic marker are reduced upon ALS-FUS expression suggesting decrease synapses and altered inhibitory synapses (Shiihashi et al., 2017) (López-Erauskin et al., 2018) (Sahadevan et al., 2021) (Scekic-Zahirovic et al., 2021). Dendritic and synaptic defects are

also observed in spinal cord motor neurons of FUS mutant mice (Qiu et al., 2014) and deficit in long-term potentiation, dendritic length and spine formation and/or maturation are also visible in both hippocampal and cortical neurons when FUS is mutated (Huang et al., 2012) (Sephton et al., 2014) (Shiihashi et al., 2017) (Ho et al., 2021).

3. Role of FUS in adult neurogenesis

Adult neurogenesis is the process in which new neurons are generated in the adult brain. In aging and neurodegenerative diseases, altered neurogenesis correlates with cognitive decline. One main region responsible of adult newborn neurons in mammals is the DG of the hippocampus. FUS knock-down induces by RNA inhibition in the hippocampus significantly reduced adult new born cells and decreased neurogenesis markers (Ishigaki et al., 2017). Interestingly, adult neurogenesis in this model was rescued by the overexpression of WT FUS but not mutant FUS. Since these experiments have been done 2 weeks after injection, it is not clear if this decreased neurogenesis is due to inefficient cellular proliferation, altered neuronal differentiation or decreased cell survival during neurogenesis.

Knock down of FUS in cell culture is also associated with a significant decrease in cellular proliferation, due to fewer division events and increased phosphorylated H3, a marker of mitotic arrest (Ward et al., 2014). Interestingly, studies in FUS deficient mice demonstrated a potential role of FUS in meiotic prophase (Kuroda et al., 2000). Prophase is found in both meiosis and mitosis, supporting the suggestion that FUS is required for proper proliferation. Proteome analyses in FUS knock down cells highlight “chromatin organization” as the most common category for differentially expressed protein, with a transient decreased expression of several histone variants (H1, H2A, H2B, H3 and H4) (Ward et al., 2014).

During cell differentiation, analysis of FUS expression in isolated neuronal stem cells demonstrate primarily high expression followed by a significant reduction of FUS protein. Interestingly while FUS protein was indeed reduced during cell differentiation, FUS mRNA level only decrease later in the process. This suggest that FUS is involved in cell differentiation and that a potential posttranscriptional mechanism might regulate its expression during the all process (Svetoni et al., 2017).

4. FUS microenvironment and aggregation

FUS is a prototypical protein that undergoes liquid-liquid phase separation (LLPS). This process is responsible of the creation of two distinct phases from a single homogeneous mixture (such as oil and water). First, FUS protein meets all criteria for LLPS: 1) FUS proteins can form a membraneless compartment with assumed spherical shapes, named droplet, 2) FUS droplets have the ability to rearrange, and 3) if two FUS droplets are close to each other they can fuse to form a bigger droplet. In specific stress conditions (temperature, chemical agents…), FUS separate transiently from the bulk solvent and turn into a distinct liquid phase. In pathological condition this can lead to the formation of a more compact hydrogel form, or even form solid aggregates (Patel et al., 2015). The N-terminal part of FUS containing the QGSY-rich region is described as an intrinsically disordered region and low complexity region. Intrinsically disordered region refers to a protein sequence that lacks a fixed three-dimensional structure and may adopt different conformations depending on binding partners. Low complexity region refers to the fact that this sequence differ from the composition and complexity of most proteins (structure, function and evolution). This region, in FUS protein, is proposed to be responsible of FUS liquid separation (Lin et al., 2017), with the participation of RNA binding to FUS (Burke et al., 2015). Indeed, the QGSY-rich region induces FUS self-assembly which may favorize liquid separation of FUS (Yang et al., 2014). While FUS liquid separation is reversible, the presence of mutant FUS exacerbates its capacity to form liquid phase separation and result in the formation of FUS cytoplasmic solid aggregates (Murakami et al., 2015) (Patel et al., 2015), Figure 29.

Thus, one consequence of liquid phase separation is the assembly of cytoplasmic FUS aggregates in response to stress, in the so-called stress granule compartments. Stress granules are temporary cellular structures in which RNA and protein are regrouped together. RNA is indeed one component of FUS cytoplasmic aggregates (Fujii et al., 2005) (Murakami et al., 2015). Sequestration of RNA in FUS stress granules may be responsible for the decreased RNA transport and altered transcription described previously in FUS cell models. In normal conditions, the transient formation of stress granules promotes cell survival under stress condition. However, compromised stress granule response contributes to ALS-FTD FUS pathology and result in FUS neuronal aggregations (Kwiatkowski et al., 2009) (Neumann et al., 2009). Of note, FUS protein

aggregates are only reproduced in in vitro model, while murine knock in models do not lead to FUS aggregates (Scekic-Zahirovic et al., 2016) (Devoy et al., 2017).

The FUS QGSY- rich region is also proposed to be responsible for the prion-like property of FUS. This might explain first, why FUS become toxic and propagate in ALS and FTD sporadic cases without mutations and second, why WT FUS also become toxic and aggregate in the presence of mutant FUS in ALS disease.

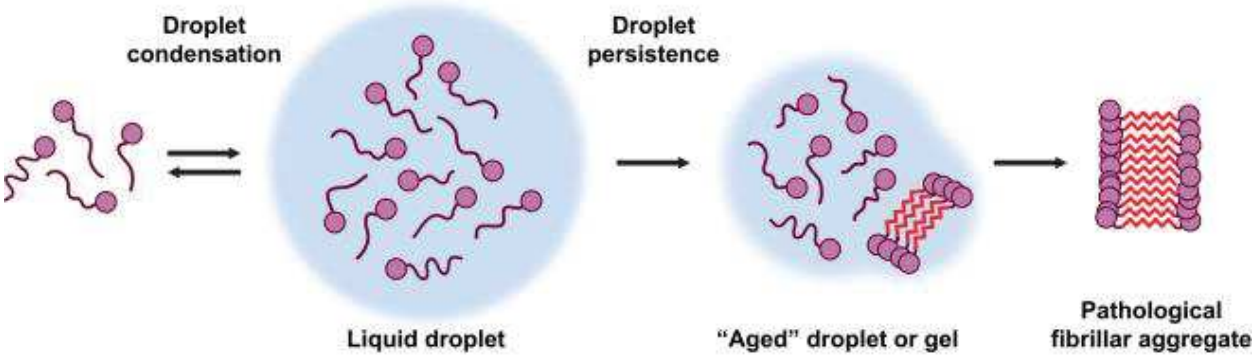

Figure 29: Liquid phase separation

The FUS protein is represented in purple with its prion like domain (purple line). FUS is able to form liquid-liquid phase separations, thus forming liquid droplets that can transiently separate from the bulk solvent. In aging, stressful conditions or in presence of a mutant protein, those droplets can become persistent and form a more jelly state. If this situation persists and aggravates these droplets can turn into pathological FUS fibrillar aggregates (in red). (March et al., 2016).

IV. FUS is a circadian gene

Several studies have demonstrated that *Fus* has a cyclic circadian expression in liver tissue (Kornmann et al., 2007), and in 14 different tissues in mice, including whole brain, prefrontal cortex and other tissues (Yan et al., 2008). Among the circadian proteins, brain, and muscle arnt-like 1 (Bmal1) and Circadian Locomotor Output Cycles Kaput (Clock) form a dimer complex positively stimulating gene expression of the Period (Per) and Cryptochrome Circadian Regulator (Cry) family. In turn, Per and Cry form a heterodimer preventing Bmal1 and Clock expression and complex formation. As a result, Per and Cry transcription are inhibited, and the Bmal1/Clock complex becomes active again. This loop regulates the opposite gene expression of Bmal1/Clock

and Per/Cry as well as several other circadian genes, and thus conduct essential functions and processes during our 24-hour circadian cycle.

Since *Fus* is itself a circadian gene, it was possible that FUS is part of this mechanism, which might underlie sleep disorders known to affect some ALS and FTD patients. In sleep-deprived mice, basal level of mRNA and oscillation amplitude were both diminish and *Fus* mutation in rats leads to abnormal circadian gene expression (Jiang et al., 2018). Indeed REV-ERBα, another circadian gene, directly bind to FUS promotor to regulate its expression. Knock down of FUS increased gene expression of Per2 and Cry1 while restoration of FUS rescued this action. Indeed, circadian transcription of FUS had an opposite pattern with Per2 expression (Kornmann et al., 2007). FUS is also able to bind Per2, Bmal1 and clock proteins and regulate Per genes in a manner that is dependent of the HDAC1 recruitment (Jiang et al., 2018). In all, FUS appears to be involved in circadian rhythm of transcription, with unknown consequences on whole body physiology.

V. Autoregulation of FUS

FUS autoregulation has first been highlighted in 2012, when Lagier-Tourenne, Polymenidou and colleagues decided to study mRNA binding landscape of FUS. For this purpose, they use FUS CLIP-seq in mouse brain. They found that one of the top candidate for FUS mRNA target is the exon 7 and flanking intron 6 and 7 of *Fus* pre-mRNA itself (Lagier-Tourenne et al., 2012). Thus, they proposed that FUS binds to its own pre-mRNA, to autoregulate its own protein levels. Three mechanisms of autoregulation have been proposed : skipping of the FUS exon 7 (Zhou et al., 2013), regulation through miRNA (Dini Modigliani et al., 2014) and retention of intron 6 and 7 of the FUS protein (Humphrey et al., 2020).

The recent study by Humphrey and collaborators highlighted that, among the three mechanisms identified in *FUS* autoregulation, the dominant mechanism was intron retention in the nucleus. In this study, they demonstrated that WT mice show high levels of retained introns 6 and 7 in the *Fus* mRNA. Pre-mRNA with retained introns accumulates in the nucleus but absent from the cytoplasm. In mice carrying *Fus* mutations and iPS neurons, retention of intron 6 and 7 is decreased. As a model, Humphrey et al, propose that when FUS levels increase, the protein binds to its own pre-mRNA and shift to another isoform that is either send for degradation or that the

isoform is retain in the nucleus to avoid translation. These results also explain the increased production of FUS protein in mutant mice, as decreased engagement of the autoregulatory loop leads to increased FUS protein, to compensate for nuclear loss of FUS, thus creating a vicious loop, Figure 30. Consistent with this study, Sanjuan-Ruiz et al showed that the expression of a wild type form of human FUS was able to elicit autoregulation of the mutant allele in *Fus* knock-in mice, leading to decreased levels of mutant FUS, and mitigated phenotype (Sanjuan-Ruiz et al., 2021). Both studies demonstrated that autoregulation of FUS is altered in different model of mutant and that this might be the reason of increase cytoplasmic FUS protein.

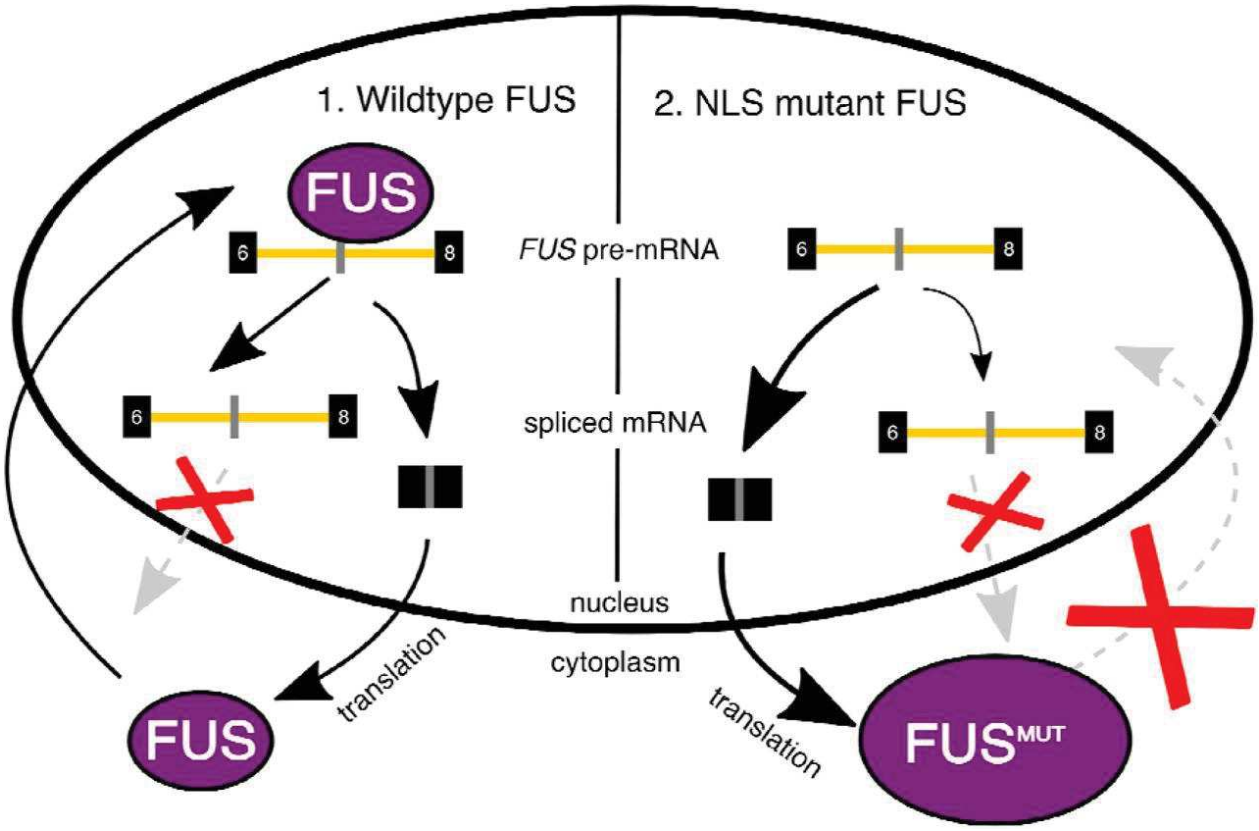

Figure 30: Proposed model for FUS autoregulation

In the wild type condition, FUS shuttles between the cytoplasm and the nucleus where it regulates its own expression (autoregulation). In the nucleus, FUS binds to its own pre-mRNA within intron 6 and 7. The intronic retention spliced variant of FUS is restricted to the nucleus and result in FUS mRNA degradation and regulation of cytoplasmic mRNA available for protein expression. In NLS mutant FUS condition, the mutant FUS is enable to be translocated in the nucleus, thus reducing the amount of intronic retention variant of FUS mRNA and increased cytoplasmic FUS. (Humphrey et al., 2020).

Part 5: Behavioral alteration in FUS rodent model

In the aim of better understanding the role of FUS in association with cognitive deficit, several mouse models have been developed trying to recapitulate ALS and FTD pathology.

I. FUS depleted model

In the literature, few studies show complete FUS deletion. Indeed, FUS deletion leads to perinatal lethality when raised in inbred colony, but is able to survive when raised in outbred colony (Hicks et al., 2000) (Scekic-Zahirovic et al., 2016). Outbred FUS-deleted mice present no ALS-like phenotypes but demonstrate increased activity and reduction in anxiety-like behavior (Kino et al., 2015). FUS silencing, induced by shRNA injection in the hippocampus, decreased anxiety and increased social interaction and novelty induced locomotor activity (Udagawa et al., 2015). Altered anxiety behavior and social interaction following silencing of FUS were rescued by overexpression of WT FUS but not mutant FUS (Ishigaki et al., 2017).

II. Expression of the WT and mutant human FUS

Mitchell and collaborators created a mouse model overexpressing WT human FUS. This study revealed that increased expression of the FUS WT form is toxic and leads to FUS cytoplasmic inclusion, motor neuron degeneration and early death in homozygous mice (Mitchell et al., 2013). In rats, overexpression of FUS impairs spatial acquisition in the Barnes Maze, a non-aquatic version of the MWM but did not lead to motor symptoms at the age of the cognitive deficits (Huang et al., 2011). In contrast, mouse model that only express human FUS similar to endogenous FUS level demonstrate no deficit in both acquisition and retention in the MWM. These mice however display other cognitive deficit since including altered freezing behavior during the acquisition of the fear conditioning test and significant decrease freezing during the short term and long term memory retention compare to WT mice (Ho et al., 2019). CAmKII promoter controlled expression of a human mutant FUS in the rat led to declined performance in the spatial Barnes maze until end stage (Huang et al., 2012). Several other mouse models based on the expression of the WT or the mutant human FUS paradigms showed altered memory in

fear conditioning test (Shiihashi et al., 2017) (López-Erauskin et al., 2018) (Ho et al., 2019) (Ho et al., 2021), changes in social behavior either decreased (Sephton et al., 2014) (Lysikova et al., 2019) or increased (López-Erauskin et al., 2018), decreased aggressive behavior (Sephton et al., 2014) (Munter et al., 2020) and altered recognition of either a new animal (Shiihashi et al., 2017) or object (López-Erauskin et al., 2018) (Munter et al., 2020) (Ho et al., 2021). Both the Acquisition and the memory retention (short term and long term memory) in the MWM spatial learning were affected in mice expressing human mutant FUS (Ho et al., 2021). Finally, mice expressing a human FUS mutation demonstrate increased locomotor activity (Shiihashi et al., 2017), reduced latency to immobility in the tail suspension test (sign of helplessness), decrease sucrose preference (anhedonia) and decrease score in the marble buried test (obsessive-compulsive behavior and autism spectrum disorder) (Munter et al., 2020).

III. FUS Knock-in mouse model

Our laboratory generated a new knock-in mice model to study the implication of FUS cytoplasmic delocalization in the ALS/FTD pathological context. While homozygous mice (*Fus*$^{\Delta NLS/\Delta NLS}$) die postnatal, heterozygous mice (*Fus*$^{\Delta NLS/+}$) survive until adulthood and recapitulate the genetic condition of some ALS-FUS patients (Scekic-Zahirovic et al., 2016). In one allele, a stop codon was inserted before exon 15 coding for the NLS signal, resulting in expression of a Fus protein harboring an NLS deletion. The construct also contains two LoxP sequences allowing for Cre reversal recombination to the WT locus, Figure 31. This mouse model recapitulate many pathological hallmarks observed in ALS-FUS patients, such as FUS cytoplasmic misslocalization, accompanied by motor deficit and moto neuron degeneration (Scekic-Zahirovic et al., 2016) (Scekic-Zahirovic et al., 2017). Importantly, these results found in *Fus*$^{\Delta NLS/+}$ mice have been fully reproduced by other groups using similar knock-in mice model (Devoy et al., 2017). FUS cytoplasmic misslocalization is an event observed in both ALS- and FTD-FUS patients. Therefore the *Fus*$^{\Delta NLS/+}$ mice have been further characterized to determined implication of the FUS mutation regarding FTD-linked phenotypes with particular attention to the frontal cortex (Scekic-Zahirovic et al., 2021). As soon as 4 months, these mice present a significant increase in locomotor activity compared to their WT littermates. 10 months of age *Fus*$^{\Delta NLS/+}$ mice trained in the Morris Water Maze, followed by a 22-days long term memory retrieval, to challenge the frontal cortex, demonstrate significant decreased in memory retention. Also, these mice demonstrate a weaker

memory consolidation, as the memory of the platform location extinguish faster in the *Fus*$^{\Delta NLS/+}$ mice compare to control WT mice. In both, the resident-intruder test and the 3-chamber test *Fus*$^{\Delta NLS/+}$ mice demonstrate an increase time of interaction with other mice, closely reflecting social disinhibition observed in FTD-FUS patients.

Thus, alterations of FUS observed in mice with depleted or overexpressed FUS as well as in transgenic knock-in mouse model, all lead to an array of symptoms and phenotypes characteristic of FTD disease.

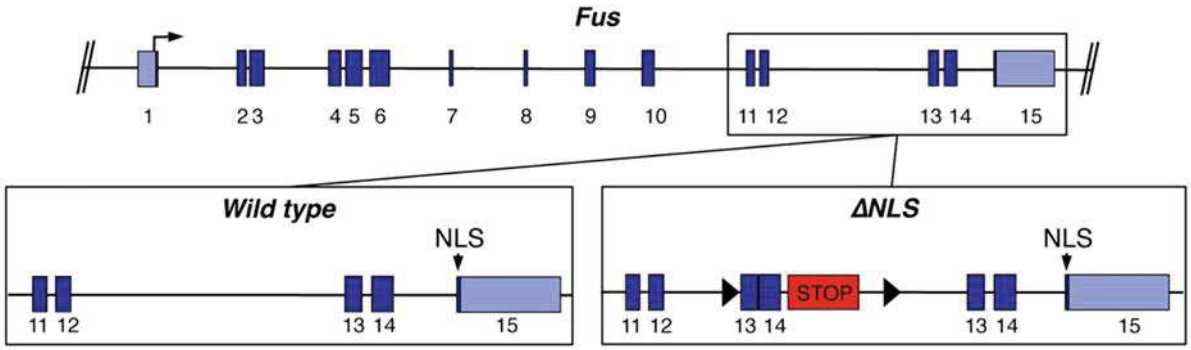

Figure 31: Schematic genomic representation of our proposed ALS/FTD – FUS mouse model

WT FUS (left) is composed of 15 exons with exon 15 coding for the nuclear localization signal (NLS). In our construct (right) a stop codon was inserted before the exon 15 in one FUS allele, resulting in expression of a FUS protein harboring an NLS deletion. The construct also contains two LoxP sequences allowing the Cre reversal recombination to the WT locus. Adapted from (Scekic-Zahirovic et al., 2016).

Part 6: Epigenetic alterations associate to FUS dysfunction

The first indication that FUS might have a role in epigenetic regulation arise from the fact that FUS either interact, regulate or co-aggregate with several histone posttranslational writers and erasers. see review (Bennett et al., 2019).

FUS binds to and modulates HAT CBP, p300 and TIP60. FUS appears to inhibit both CBP and p300 activity (Wang et al., 2008b) via its N-terminal region (a.a. 1-211). FUS also cooperates with HDAC1 to regulate either DNA damage response (Wang et al., 2013) or circadian gene regulation (Jiang et al., 2018). HDAC1 mislocalize in the cytoplasm in a FUS transgenic model (Scekic-Zahirovic et al., 2016), possibly due to induction of HDAC1 serin phosphorylation know to induce cytoplasmic delocalization of the protein under neurotoxic conditions (Zhu et al., 2017). HDAC3 and SIRT7 coprecipitates with FUS to induce its deacetylation (Arenas et al., 2020). FUS also colocalize with HDAC2 (Wang et al., 2013). Thus, FUS pathological condition might lead to a wide range of epigenetic marks.

Consistent with this hypothesis, yeast overexpressing WT FUS demonstrate significant decreased of H3S10ph and H2BT129ph, hypoacetylation of H3K14ac and H3K56ac and decrease H4R3me2 (Chen et al., 2018). H3S10ph is associate with both transcriptional repression and activation, while H2BT129ph is a mark of active transcription. In another study, Overexpression of WT FUS leads to hyperacetylation of H3K9K14 on the CCND1 promotor gene, while knock down of FUS decreased acetylation of H3K9K14 (Wang et al., 2008b). Both H3K14ac and H3K56ac marks are associated to DNA damage repair. Interestingly, H4R3me2, associate with active euchromatin, is methylated by Hmt1, a yeast homologue of PRMT1. mutant FUS or overexpression of WT FUS result in decreased nuclear PRMT1 reducing ADMA of H4R3me2. This decrease was observed in parallel with hypoacetylation of H3K9K14 and decreased transcription (Tibshirani et al., 2015) (Chen et al., 2018), suggesting a crosstalk and coregulation between different epigenetic marks. Transgenic mice overexpressing WT FUS also demonstrate hypoacetylation of the H3K9K14 mark at late stage in the spinal cord (Rossaert et al., 2019). In Hela Cells, overexpression WT FUS induce increase trimethylation of both H3K9 and H4K20 at telomers, two marks of transcriptional repression (Takahama et al., 2013). In response to DNA DSB damage, FUS recruits and colocalizes

with a variant of the H2A isoform (γH2AX phosphorylated on serine 139) (Wang et al., 2013). When FUS is depleted, through RNA interference, H3 phosphorylation is increased resulting in slower proliferation (Ward et al., 2014). Further suggesting a relationship between epigenetic marks and FUS pathology, HDAC inhibition in a WT FUS overexpressing mouse model rescued H3K9K14ac, increase lifespan and delayed symptoms (Rossaert et al., 2019). Sea review (Cobos et al., 2019). All histone dysregulations described in the different FUS pathological models are represented in Figure 32.

However, almost all this experiment has been performed upon overexpression of WT FUS, which has dramatic effects on cellular viability. Furthermore, most of the epigenomic experiments have been performed in cell cultures, with limited relevance to the actual affected cell type (adult neurons). Last, these studies were limited to global analysis of histone marks with Western Blot but did not investigate genome wide modifications of the epigenome.

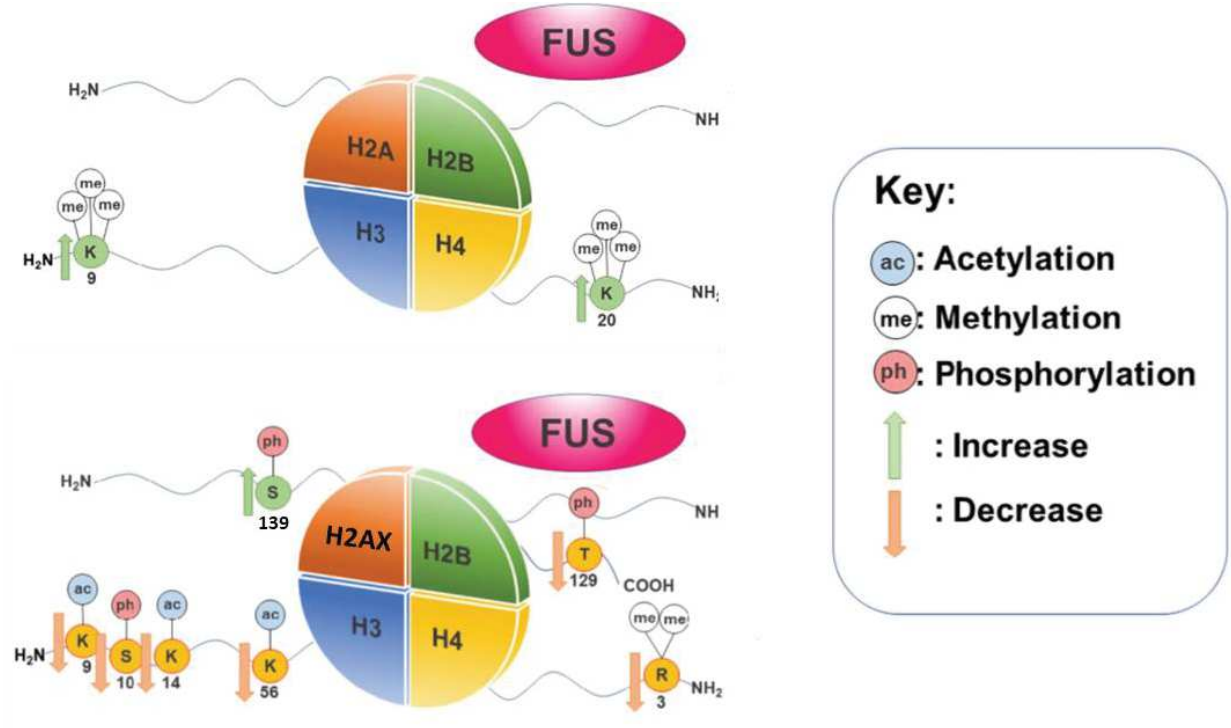

Figure 32: Histone modification dysregulation in FUS model

FUS pathological conditions are linked to several histone modification of H2B, H3, H4 and histone H2AX variant of H2A. The different modifications are associated with increased trimethylation of H3K9 and H4K20 and increased phosphorylation of H2AX S139. Other marks are found decreased in the different FUS pathological models, such as phosphorylation of H3BT129 and H3S10, demethylation of H4R3 and acetylation of H3K9, H3K14 and H3K56. Adapted from (Cobos et al., 2019).

OBJECTIVES OF THE THESIS

OBJECTIVE OF THE THESIS

FUS cytoplasmic mislocalization is linked to Amyotrphic lateral sclerosis (ALS) and Frontotemporal dementia (FTD). Among its multiple physiological roles, FUS is involved in gene expression, epigenetic modifications and synaptic functions. We hypothesized that FUS mislocalization in ALS/FTD will influence epigenetic regulations and associated transcription, ultimately impacting neuronal functions and cognitive abilities. During the 4th years of my thesis, we particularly addressed these questions in the hippocampus, a key brain region involved in memory.

We performed our studies in *Fus*$^{\Delta NLS/+}$ mice, a knock-in mouse model carrying a FUS relevant truncating mutation developed in Dupuis Lab. The use of a single copy mouse model is highly analogous to the genetic situation of FUS-ALS patients. In addition, *Fus*$^{\Delta NLS/+}$ mice demonstrate cytoplasmic mislocalization of the FUS protein, as observed in both ALS and FTD patients.

To understand FUS-associated pathological changes in the hippocampus and its relation to memory processes, the PhD studies were declined in four objectives:

1) What is the extent of cognitive deficits in *Fus*$^{\Delta NLS/+}$ mice?

2) Are the transcriptomic (basal conditions or during memory formation) and epigenomic landscapes (basal conditions) altered in *Fus*$^{\Delta NLS/+}$ hippocampus?

3) Where does FUS bind on the genome? Does FUS mutation have an impact of FUS chromatin binding in *Fus*$^{\Delta NLS/+}$ mice?

4) Are epigenomic alterations associated with changes in chromatin accessibility?

My scientific contributions are detailed in two major result sections that are presented in the next pages as two papers in preparation. Our main study, presented hereafter as the scientific contribution 1 in preparation, aims to characterize hippocampal alterations and the associated epigenetic and transcriptomic changes observed in *Fus*$^{\Delta NLS/+}$ mice. To do so, we used several next-generation sequencing techniques (RNA-seq, ChIP-seq and ATAC-seq) and we performed epigenomic and open chromatin regions analyses specifically in FACS-isolated hippocampal neuronal nuclei. My second scientific contribution aims to perform a comprehensive analysis of

the behavioral/cognitive alterations present in *Fus*$^{\Delta NLS/+}$ mice and better characterize the model. In this paper, we tested the locomotor activity, the anxiety, the cognitive flexibility but also different aspects of the memory (e.g., spatial memory and procedural memory), as well as different components of episodic-like memory (What? Where? When?).

SCIENTIFIC CONTRIBUTIONS

Scientific contribution 1:

Memory dysfunctions and associated epigenetic and transcriptomic changes in an ALS/FTD mouse model linked to a FUS mutation

Tzeplaeff, L.[1,2], Seguin, J.[1], Cosquer, B.[1], Le Gras, S.[3], Plassard, D.[3], Megat, S.[2], Dieterlé, S.[2], Alcala Vida R.[1], Cassel, J.-C.[1], Merienne, K.[1], Dupuis, L[2]*. and Boutillier, A.-L[1]*.

[1] Université de Strasbourg, Laboratoire de Neuroscience Cognitives et Adaptatives (LNCA), Strasbourg, France

[2] Université de Strasbourg, INSERM, UMR-S1118, Strasbourg, France

[3] Université de Strasbourg, Institut de Génétique et de Biologie Moléculaire et Cellulaire (IGBMC), Plateforme GenomEast, Illkirch

* Equal contribution

In preparation for *Neuron*.

INTRODUCTION

FUS is a ubiquitously expressed RNA binding protein that has pleiotropic roles in RNA metabolism, including transcription, splicing, mRNA transport, microRNA and circRNA biogenesis and mRNA translation (Lagier-Tourenne et al., 2010, 2012). As a protein involved in gene expression, FUS is highly enriched in the nucleus, yet shuttles between nucleus and cytoplasm. FUS carries a C-terminal PY-NLS allowing nuclear entry and is subject to post-translational modifications regulating nuclear import and function. Abnormalities in FUS subcellular localization are found in multiple neurodegenerative diseases. First, germline mutations in FUS are a cause of young onset amyotrophic lateral sclerosis, with rapid disease progression. FUS mutations lead to FUS pathological aggregates, mostly located in the cytoplasm, and are usually located in or close to the PY-NLS, causing defective import of FUS in the nucleus. FUS aggregates are also found in a large subset of patients with FTD, along with other proteins of the FET family (Urwin et al., 2010). In addition, FUS is mislocalized in the cytoplasm, but not aggregated, in most ALS cases, but also in other neurodegenerative diseases in the absence of germline *FUS* mutations. FUS mislocalization has broad effects on neuronal functions as heterozygous mice with a knock-in deletion of *Fus* PY-NLS, causing cytoplasmic mislocalization of FUS in the absence of aggregates, developed cognitive deficits and defects in memory consolidation (Scekic-Zahirovic et al., 2021).

Several independent lines of evidence suggest an important role for FUS in the hippocampus. First, FUS pathology is prominent in the hippocampus of FTD patients with FUS pathology (Armstrong et al., 2011b, 2011a; Baborie et al., 2011; Mackenzie et al., 2011). Further, ablation of *Fus* in outbred mice leads to prominent hippocampal alterations (Kino et al., 2015), and Fus knockdown in the hippocampus leads to neuronal death and behavioral phenotypes (Udagawa et al., 2015). In addition, human wild type FUS expression leads to defects in fear conditioning, decreased LTP and abnormal dendritic spine morphology in the hippocampus (Ho et al., 2019). Last, FUS appears required for spine formation and maturation (Fujii et al., 2005; Udagawa et al., 2015), AMPA receptors expression (Udagawa et al., 2015) or adult neurogenesis (Ishigaki et al., 2017), all critically involved in hippocampal function. However, despite this evidence, the mechanisms linking FUS mislocalization and/or aggregation, to hippocampal function and memory formation are still not characterized.

FUS is involved in multiple steps of gene expression including transcription, alternative splicing, and interacts and modulates activity of a number of chromatin remodeling enzymes, including HDAC1 (Wang et al., 2013), SWI/SNF (Lindén et al., 2019) or CBP/p300 (Wang et al., 2008). In addition, several studies observed that manipulation of FUS levels in cellular models was able to alter histone post-translational modifications (Cobos et al., 2019; Tibshirani et al., 2015; Ward et al., 2014). Here, we hypothesize that cytoplasmic FUS mislocalization altered nuclear FUS function in chromatin remodeling during memory formation (Campbell and Wood, 2019; Yap and Greenberg, 2018; Marco et al., 2020). We observed defects in hippocampal dependent memory in mice with cytoplasmic FUS mislocalization, accompanied by prominent alterations in learning induced transcriptional changes. We further found large scale chromatin remodeling at transcription start sites of highly expressed genes and established that FUS binds the chromatin especially at the TSS of genes carrying ETS-transcription factor binding sites. Our results suggest that in the hippocampus, FUS mutation leads to a local alteration of FUS function at FUS target chromatin sites, which directly or indirectly (via ELK factors) leads to activity-induced transcriptional alterations and memory defects.

MATERIEL AND METHODS

Animals

Experimental protocols and animal care were in compliance with the institutional guidelines (Council directive 87/848, October 19, 1987, Ministère de l'agriculture et de la Forêt, Service vétérinaire de la Santé et de la Protection Animale) and international laws (directive 2010/63/UE, February 13, 2013, European Community) and policies. APAFIS: 11229 (RôledeFUSdanslarégul_2017091118178028_v4)

Wild type and heterozygous *Fus*$^{\Delta NLS/+}$ mice from B57/BL6 genetic background were generated as described previously (Scekic-Zahirovic et al., 2016) and bred and housed in the animal facility of the Laboratory of Cognitive and Adaptative Neuroscience (LNCA) of Strasbourg. Mice were housed in group under a 12 light/dark cycle (light on at 7:00 a.m.), in a temperature and humidity-controlled room (22 ± 2 °C; 50% ± 5 humidity) with *ad libitum* access to food and water. For behavioral test, mice were single housed one week prior the test and habituate to handling 5 min a day for 3 days.

Morris water maze

Wild type and heterozygous *Fus*$^{\Delta NLS/+}$ mice of 4 months of age were trained to perform the hidden-platform version of the spatial Morris Water Maze for 5 consecutive days (n=11 animal per genotype). In a room, a circular pool (diameter 160 cm and height 60 cm) is in the center and is surrounded by distal visual cues made of different shapes and colors on the walls. To habituate the mice to the pool and the platform rule, the pool is first field with water (21°C) and a visible platformed is located in the NW quadrant (diameter 10 cm, 1cm above the surface). Starting from the middle of the pool, mice have 60s to find the platform, if not, they are gently brought there. After 10s on the platform, mice are brought back to their home cage. Then, the pool is field with water up to 20 cm below the border so that mice can see the visual cues on the walls and the water is opacified with medon white to avoid mice seeing the platform. Before acquisition, mice performed a 2 min forced swim (no platform), starting from the middle of the pool, to make sure they can all swim and complete the test. On the next days, mice were trained for 5 consecutive acquisition days to find the spatial position of the hidden platform located in the SE quadrant. Mice were trained with 4 trials a day, in group of 3, with an intertrial interval of

2-5 min, maximum duration of the test 60s. If not completed on time, mice were guided to the platform. Mice remain 10s there before brought back in the home cage. Animals were starting each trial from each of the 4 cardinal points (North (N), Est (E), South (S), and West (W)) from the edge of the pool, facing the wall. The sequence of the starting point was randomized each day. Mice were tested for memory retention on day 5, 24h after last training to test recent memory, and 30 days after last training to test remote memory (duration of the test 60s. The platform was removed, and the pool was virtually separated in 4 quadrants (SE, NE, NW, SW). At the end of the 24h memory retention, the platform was electrically brought to its original position to avoid extinction, and day 5 acquisition take place as described previously. Data and heat maps were collected by the ANY-maze (Ugo Basile) video tracking system. Average speed and distance travelled to reach the SE target platformed were analyzed during acquisition. Time spends in the different quadrants, average distance from the target platform and the crossing annulus were analyzed during memory retention tests.

Analyses of MWM data

Data collected during the acquisition and during the different probe trials are presented as mean ± standard error of the mean (SEM). Values of $p < 0.05$ were considered significant and are noted in the text. Graphics and statistical analyses were performed using GraphPad Prism 8 (GraphPad, CA). Performances recorded during acquisition (distance and mean speed) were evaluated using repeated two-way ANOVA considering the factors of “genotype” (WT vs FUS) and “day” (1–5) and followed by Šidák correction for multiple comparisons. Mean time spent in the different quadrants, were analyzed using two-way ANOVA with Šidák correction for multiple comparisons. Mean distance to platform was analyzed with the unpaired t test and the number of crossing annulus with the non-parametric unpaired Man-Whitney rank test. The time spent in quadrant was also compared to chance (i.e., 15 s) with the one sample t test.

Western blot of subcellular fractionations

Nuclear and cytoplasmic fractions were prepared from frozen dorsal hippocampi (n=6 animal per genotype) using the NE-PER® Nuclear and Cytoplasmic Extraction reagents (Thermo Scientific) according to the manufacturer. Protein concentration was quantitated using the BCA protein assay kit (Pierce). Western blots were performed as described above, using following primary antibodies: goat anti-FUS against the N-terminal part of protein (ProteinTech 11570; 1:1000) and

rabbit anti-FUS against the C-terminal part of protein (Bethyl A300-294A, 1:10000) all diluted in 3% non-fat milk in PBS, followed by incubation with horseradish peroxidase (HRP)-labeled secondary antibodies anti-goat (Sigma A5420), anti-rabbit (P.A.R.I.S. BI2407) diluted 1:5000 in PBS. Antibodies rabbit anti-HDAC1 (Bethyl A300-713A, 1:1000) was used as loading control for nuclear fraction and mouse anti sheep SOD1 (Merk 574597, 1:1000) was used as loading control for cytoplasmic fraction. Blots were analyzed with chemiluminescence (ECL; Luminata Forte Kit, Millipore WBLUF0500) using the Molecular Imager Chemidoc XRS (Biorad) as detection system and total protein as loading controls.

Quantification of protein on Western blot

Stain-free imaging allowed for the normalization of each protein bands to the total amount of protein with the ImageLab software (Biorad). Results were compared to the relative amount of proteins in WT mice. Data are presented as mean ± standard error of the mean (SEM). Values of $p < 0.05$ were considered significant and are noted in the text. Graphics and statistical analyses were performed using GraphPad Prism 8 (GraphPad, CA). Genotypes were compares using the unpaired two tailed *t-test.*

Brain perfusion for immunohistochemistry

Mice were deeply anesthetized with 0.1ml/10g Ketamine (Imalgène 1000) and Xylazine (Rompun 2%) (respectively 20% and 15% in NaCl 0,9%) and transcardiacly perfused with PB (0.1 M phosphate buffer) followed by cold 4% paraformaldehyde (PFA) in PB. Brains were removed and fixed overnight in 4% PFA and subsequently merged in 30% sucrose solution at 4°C until the brain sank. Brains were cut with the cryostat into 30um thick coronal sections in the whole hippocampus. Sections were kept at 20°C in cryoprotectant (0.1 M PB, 0.15 M NaCl, 30% (v/v) ethylene glycol, 30% (v/v) glycerol) until immunostaining.

Immunohistochemistry

Free floating brain sections were rinsed three times in PBS (0.25% Triton X-100 in PBS, 137 mM NaCl, 2.7 mM KCl, 10 mM Na2HPO4, 1.8 mM KH2PO4). For heat-induced epitope retrieval, floating sections were kept in sodium citrate (pH 6, 10 mM, 80°C, 30 min) and washed three times in 1XPBS. Sections were blocked in blocking solution 1XPBS with 0.5% Triton and 5% Horse serum for 30 minutes and then incubated overnight in the following primary antibodies at 4°C: rabbit

anti-FUS (ProteinTech, 1:1,000) and mouse anti-NeuN (Millipore, 1:500) in PBS with Triton 0.1%. The next day, brain sections were rinsed and incubated at RT for 1h30 respectively with, donkey anti-rabbit Alexa 488-conjugated (Jackson 1:500 in 1XPBS) and donkey anti-mouse Alexa 594-conjugated (Molecular Probes, 10ug/ml) in PBS with Triton 0.1%. After three washes in 1XPBS, brain sections were incubated in Dapi diluted 1:1000 in 1XPBS for nuclei staining, washed two times in 1XPBS before drying and mounting sections in Mowiol (Life Technologies; 1:10,000), coverslipped, and kept at 4°C for long storage.

Acquisitions were performed using a fluorescence microscope coupled with an ApoTome module (Zeiss).

Golgi staining

Mice that had underwent a 4-days training in the MWM were killed 4 days later. Total brains were collected from MWM-trained mice and home cage (HC) control mice (n=5 per group and conditions). The Rapid Golgi stain kit (FD Neurotechnologies, Inc.) was used according to the manufacturer's instructions. Brain coronal section of 100 µm thickness of the dorsal hippocampal region were made using a Vibratome (VT1000M; Leica). Images of basal and apical dendrites of the CA1 pyramidal neurons were acquired using a brightfield microscope (Explora Nova, La Rochelle, France) using a 100 times magnification for each genotype and conditions. We obtained 8–10 hippocampal sections for the dendritic spine analyses.

Quantification and analyses of dendritic spines

Dendritic spines were identified based on their morphological appearance. Spines were classified into four different types: Muschroom spines (protrusion with large neck and big head), stubby (big protrusion with no obvious separation between neck or head), thin (protrusion with long neck and small head) and filopodia (protrusion with long neck and no head). For each animal, 6 neurons per animal were analyzed, counting the total number of each different types of spine shapes on 20mm long segments. A total of 6 segments per neurons were counting comprising 3 basal segments and three apical segments. Thus, a total of 36 sections (basal and apical together) per animal were counting in total. The spine density was presented as the number of spines per 20 µm of dendritic length.

Data are presented as mean ± standard error of the mean (SEM). Values of $p < 0.05$ were considered significant and are noted in the text. Graphics and statistical analyses were performed using GraphPad Prism 8 (GraphPad, CA). Genotypes and conditions were compares using the repeated two-way ANOVA with Šidák correction for multiple comparisons.

RNA extraction

Mice that had underwent a 3-days training in the MWM were killed 1h after the last training. Half dorsal hippocampus of trained mice and their home cage (HC) control were chopped on ice with a razor blade before extraction of total RNA using the RNeasy Lipid Tissue Mini Kit (Qiagen).

RNA sequencing and analyses

Quality control, libraries and sequencing were proceeded by the GenomEst platform (IGBMC, Strasbourg). RNA quality was measured using the Agilent Bioanalyzer system and all RNA integrity number (RIN) were all above 9.5. The library was sequenced on Illumina Hiseq 4000 sequencer as Single-Read 50 base reads following Illumina's instructions, with 3 biological replicates sequenced per condition. We obtained approximately 40 million reads per samples with a minimum of 85% uniquely mapped read per sample. Reads were mapped onto the mm10 assembly of Mus musculus genome (UCSC Genome Browser) using STAR (v2.5.3a). Read counts have been normalized across samples with the median-of-ratios method proposed by Anders and Huber. Comparisons of groups were performed using the test for differential expression implemented in the Bioconductor package DESeq2 (v1.16.1). P-values were adjusted for multiple testing using the Benjamini and Hochberg method. Clustering analysis and heat maps between groups were generated using R (Bioconductor). Representation of the Q1 to Q4 gene expression groups were also represented on the R-software. Cross-comparison of RNA-seq data were represented with a proportional Venn diagram and performed using eulerr in the R software. Gene ontology (GO) associated with the differential expressed genes were analyzed using the DAVID software. The top 10 biological process, cellular component, molecular function and KEGG pathways with FDR adjusted p-value <0.05 were represented on the graphics. Further GO term analyses were performed with the GREAT software, representing enriched term with statistical significance of FRD p-adjusted value<0.05. Gene expression in the different genotypes and conditions are presented as mean ± standard error of the mean (SEM). Values of $p < 0.05$ were

considered significant and are noted in the text. Graphics representing of relative gene expression were performed using GraphPad Prism 8 (GraphPad, CA). And results showing a

Nuclear extraction for ChIP-seq

A total of two (ChIP-seq FUS) or of four (ChIP-seq of histone modifications) hippocampi were chopped on ice with a razor blade (n = 2 biological replicate per group), then homogenize in PBS with Protein Inhibitor Cocktail (Roche, cOmplete ref#11836145001). Tissues were mechanically dissociated with pipettes and with the dounce B (loose) and then transfer in microcentrifuge tubes for fixation with 1% PFA at RT for 10 min. Cross-linking was stopped by adding 1.67M of glycine at RT for 5 min. Tissues were centrifuge at 4°C, 3600g for 5 min and then incubate in PBS with PIC at 4°C for 5 min, this step was repeated two times. After centrifugation tissues were incubated in cell lysis buffer (10mM HEPES pH8, 85mM KCL, 0,5% NP-40 in ddH2O) with PIC at 4°C for 7 min. Pellet were collected by centrifugation at 4°C, 5000 rpm for 20 min, resuspend in nuclei extraction buffer (0,1% SDS, 10 mM EDTA pH8, 50 mM Tris in ddH20) with PIC at 4°C for 7 min and nuclei were collected after centrifugation at 4°C, 5000 rpm for 10 min. Nuclei were resuspended in PBS with PIC at 4°C for 5 min and centrifuge one last time at 4°C, 5000 rpm for 5 min to obtain a clean pellet of nuclei. For the ChIP-seq FUS, nuclei pellets were frozen at -80 °C until the day of the experimentation. For ChIP-seq of histone modifications, samples were resuspended in cold PBTB (5% BSA, 0.1% Tween-20 in PBS) for filtration with the CellTrics® 50 µm filters (Sysmex, 04-004-2327) neuronal nuclei staining and further used for neuronal staining.

An additional step of fixation was added for the protocol of ChIP-seq experiment against the FUS protein. After tissue dissociation in the dounce B (loose), the sample was transfer in microcentrifuge tubes for fixation with 1:250 of Crosslink gold at RT for 30 min. Crosslink gold allow better protein-protein crosslinking. Then sample was centrifuge at 4°C 3600g for 5min and wash two time in PBS with PIC before to continue with the fixation of 1%PFA and the next steps of the protocol above.

Nuclear extraction for ATAC-seq

The protocol for nuclear extraction was adapted from the Encode ATAC-seq protocol for frozen tissue. A total of two frozen hippocampi was crushed directly in the dounce B (loose) into fine powder while cold on dry ice (n=2 biological replicate per group). On ice resuspend pulverized

tissue in 1 ml ice-cold 1x PBS with Protein Inhibitor cocktail (Roche, cOmplete ref#11836145001). Sample were transferred in microcentrifuge tube and centrifuge at 2000g at 4ºC for 3 min. Pellet was resuspended in in LB1 buffer (50mM HEPES pH 7.5, 150mM NACL, 1M EDTA pH 8.0, 0.25% Triton x 100, 10% Glyrerol, 0.5% PN-40 and PIC in ddH2O) ad rotate tubes at 4ºC for 10 min. Sample were transfer back in the douncer for further mechanical dissociation and then transfer to a new tube for centrifugation at 2000g at 4ºC for 5 min. Sample was resuspended in cold PBTB (5% BSA, 0.1% Tween-20 in PBS) for filtration with the CellTrics® 50 µm filters (Sysmex, 04-004-2327) neuronal nuclei staining.

Neuronal staining for ChIP-seq of histone modification

Nuclei preparation for ChIP-seq of histone modification were further prepared for neuronal staining of hippocampal nuclei. Neuronal nuclei were stained using mouse anti-NeuN, 1:1000 (Millipore, Ref: MAB377, Lot: 2967854) in the PBTB (5% BSA, 0.1% Tween-20 in PBS) with addition of 3% normal horse serum. Nuclei were incubated at 4°C during 30 min. For control of no Ab and 2nd Ab, a few microliters of resuspended nuclei were not incubated with anti-NeuN. sample were centrifuged at 4°C, 5000 rpm during 5 min and wash in 1 ml PBTB with 3% NHS before centrifugation. Nuclei were incubation with the secondary Alexa 488 donkey anti mouse, 1:1500, (Invitrogen, Ref: A21202, Lot: 1022448) in PBTB with 3% NHS at 4°C during 15 min. Nuclei were centrifuged at 4°c, 5000 rpm for 5 min, then wash in PBST (PBS, 0.5% Tween-20), centrifuged and resuspended in PBS for nuclei sorting.

Neuronal staining for ATAC-seq

Neuronal staining was preceded same as above but using a mouse anti NeuN conjugate Alexa Fluor 405 nm antibody 1:200 (Novus, Ref: NBP1-92693AF405, Lot: 02071-112519-AF405) for 30 min of incubation at 4°C.

Neuronal staining for ChIP-seq of histone modification and ATAC-seq

Neuronal and non-neuronal nuclei were collected using the Fluorescent Activated Nuclei Sorting technic (FANS, Aria Fusion), equipped with a 70 µm nozzle at the IGBMC (Strasbourg, France). We collected the neuronal nuclei with the 488-nm laser. We were able to collect between 1 and 2 million neurons following this protocol. Nuclei were collected in 1.5 ml low binding tubes, then

were centrifuge at 4°C, 5000 rpm for 5 min to remove supernatant and the pellet were frozen at -80°C until ChIP-seq experiment for histone modification.

ChIP-sequencing of histone modification

ChIP experiments were always done in two biological replicate per condition. On ice, between 1 and 1.2 million frozen neuronal nuclei were resuspended in 500-600uL Nuclei lysis buffer (10 mM EDTA, 50mM Tris-HCL pH8.1, 1mM NaBu and 1% SDS for H3K4me3, H4K12ac, H3K36me3 and H3K27ac or 0,4%SDS for H3K27me3, in ddH2O) with PIC in a 15 ml TPX tube (Diagenode). Nuclei were sonicated using the sonicator (Bioruptor Plus sonication divice, Diagenode) with 17 cycles of 30sec ON / 30sec OFF on High Power with breaks to vortex tubes every 5 min. 4uL of the supernatant was checked on 1,5% agarose gel to confirm DNA fragment of approximately bellow 500bp after sonication and between 500bp and 100bp after a protocol for rapid decrosslinking. Sonicated chromatin was centrifuged at 4°C, 14000g for 10 min to get read of debris. Supernatant was diluted in Chip Dilution buffer (1.1% Triton X-100, 1.2 mM EDTA, 16.7 mM Tris-Cl, pH 8.1, 167 mM NaCl in ddH2O) to obtain a final concentration of 0,1%SDS. Approximately 40 000 nuclei were saved before IP for total input chromatin and the rest of the sample were split in minimum 400 000 nuclei per Chip. Samples were incubated ON at 4°C with the following primary Ab: rabbit anti H4K12ac, 9μg/Chip (Diagenode, Ref: C15410331, Lot: A2439P), rabbit anti H3K4me3, 4,25μg/Chip (Diagenode, Ref: C15410003-10, Lot: A1052D), rabbit anti H3K27ac, 3,1μg/Chip (Abcam, Ref: ab4729, Lot: GR3216173-1), rabbit anti H3K36me3, 3,4μg/Chip (Diagenode, Ref: C154101192, Lot: A1845P), rabbit anti H3K27me3, 5μg/Chip (Diagenode, Ref: C15410195, Lot: A0821D). On the next day samples were incubated with 50μl/Chip magnetic beads (Diagenode protein A, Ref: C03010020-150) at 4°C during 2h. Beads were previously washed three times in Chip dilution buffer with 0,1% SDS and blocked ON at 4°C with BSA. Chip-DNA were then washed 5 min in several buffers, using a magnetic rack: Low salt, High Salt, LiCL and TE buffer. Chip-DNA was then incubated in 300 μl elution buffer (1% SDS, 0.1 M NaHCO3 in ddH2O) at RT for 5 min and at 65°C for 10 min. The crosslinking was reversed by addition of 0,2M NaCL, ON at 65°C. Then DNA was purified with RNAse (Abcam, Ref: ab52579, Lot: GR314429-2) at 37°C for 30 min, and in Proteinase K buffer (Invitrogen, Ref: 100005393, Lot :1834876) at 45°C for 1h. Finally, the DNA was extracted with the MicroChip Diapure columns (Diagenode, Ref: C03040001) and quantification of DNA concentration was calculated using the Qubit. All samples reached the minimum of 2μg required for sequencing.

Chip-sequencing of the FUS protein

Chip experiment targeting the FUS protein was performed in two biological replicates per condition. The protocol is similar to the one just described before, except the following steps: the nuclei pellet of total tissue was resuspended in 700uL Nuclei lysis buffer with this time only 0.2% SDS, and then, sonicated with 15 cycles of 30sec ON / 30sec OFF. We used a primary rabbit antibody anti FUS 15μg/Chip (Bethyl, Ref: A300-293A, Lot: A300-293A-5).

Quality control, libraries, sequencing, and analyses of Chip-sequencing

Quality control, libraries and sequencing were proceeded by the GenomEst platform (IGBMC, Strasbourg). Each sample have a minimum of 95% read positions with a base quality score over 30. The library was sequenced on Illumina Hiseq 4000 sequencer as Single-End of 50 base reads following Illumina's instructions. We obtained approximately 50 million reads (ChIP-seq of histone modifications) and 30 million reads (ChIP-seq of FUS) per samples with 75% to 92% uniquely mapped read per sample. Sequenced reads were mapped to the Mus musculus genome assembly mm10 (UCSC Genome Browser) using Bowtie. Data were normalized to 20 million reads.

Mapped reads aligned along the repeated elements within the mouse genome were removed by using RepeatSoaker tools (Dozmorov et al., 2015) for ChIP-seq on histone modifications. Biological duplicates were performed for all marks. They were analyzed independently in the same pipeline, and only differential peaks replicating were further analyzed. Inputs were used as controls. Peak detection of histone markers was performed using SICER v1.1 (Xu et al., 2014) with the following parameters: window size: 200; evalue: 0.003. Gap size parameters were selected according to the score value estimated by statistical method implemented in SICER: selected values of gap size are 600, 400, 1000 and 1600 for H4K12ac, H3K4me3, H3K27ac and H3K27me3 respectively. Peak detection for the ChIP-FUS was performed using Macs2 v2.1.1.20160309. Peaks were annotated relative to genomic features using Homer AnnotatePeaks v4.9.167 (ChIP-seq of histone modifications) and v.11.1 (ChIP-seq of FUS) (Heinz et al., 2010) with annotation from Ensembl v87. As reference coordinates, we used RefSeq genes for Mouse mm10 genome. The differential analyses of the ChIP-seq against the FUS protein was done on the union of peaks detected in each genotype. Increased and decreased regions were selected if their p-adjusted value < 0.05.

Read coverage of peaks was calculated for each sample using bedtools multicov, from BEDTools (Quinlan and Hall, 2010), and differential enrichment analysis was performed using DESeq2 (Love et al., 2014) with default parameters providing as input normalized reads for each peak and biological sample.

Quality control, libraries, sequencing, and analyses of ATAC-sequencing

Quality control, libraries and sequencing were proceeded by the GenomEst platform (IGBMC, Strasbourg). Each sample have a minimum of 88% read positions with a base quality score over 30. The library was sequenced on Illumina Hiseq 4000 sequencer as Paired-End of 100 base reads following Illumina's instructions. We obtained approximately 76 million reads per samples. Sequenced reads were mapped to the Mus musculus genome assembly mm10 (UCSC Genome Browser) using Bowtie v.2.3.4.3. Data were normalized to 30 million reads. Peak calling was performed using Macs2 v2.2.4. Peaks were annotated relative to genomic features using Homer v.11.1 (Heinz et al., 2010). As reference coordinates, we used RefSeq genes for Mouse mm10 genome. For the differential opening analysis we took the union of open chromatin region (OCR) detected. Increased and decreased regions were identified with p-adjusted value < 0.05.

Analyses of ChIP-seq and ATAc-seq data

Proportional Venn diagram showing the colocalization of histone marks were represented with R using eulerr. PCA analyses, dendrogram, heatmap, MA-plot, Z-score expression and Volcano plot for ChIP-seq or ATAC-seq data were created with the R software.

For the ChIP-seq analyses, the genomic distribution of the different ChIP-seq was collected with seqMINER v1.2.168,69 (Ye et al., 2011, 2014) by using Refseq genes. Mouse mm10 genome is used as reference coordinates for the genebody and TSS representation and the total read obtained in each experiment was used as reference coordinates for the peak center representation. Graphics were represented with the R software. The distribution of peaks along genic and intergenic region was performed using homer annotation. The gene ontology associated with the differential enriched peaks were analyzed using the GREAT software v.4.0.4. The Top 15 biological process pathways with FDR adjusted p-value <0.05 were represented on the graphics. Predicted promotor motif associated with the differentially enriched peaks were analyzed using GREAT v.3.0.0. and results showing FDR adjusted p-value <0.05 were represented on the

graphics. Peaks colocalization was identify with bedtools. The different tracks showing peaks distribution on the genome was visualized with the UCSC genome Browser software. Graphic Representing the histone marks enriched genes (HMEG) in the Q1 to Q4 gene expression group was performed on Excel.

For ATAC-seq, Footprint analyses were performed with Tobias.

RESULTS

I. structural and functional hippocampal impairment in *Fus*$^{\Delta NLS/+}$ mice

We previously showed that 10 months old *Fus*$^{\Delta NLS/+}$ mice displayed memory alterations in the spatial reference memory, a task that is highly dependent on proper hippocampus function. We asked whether this could be affected earlier and performed the Morris Water Maze (MWM) test at 5 months of age. To evaluate both recent and remote spatial memory, we used a protocol involving 5 days of acquisition trial followed by two probe trials at 24h and 30 days after the last acquisition (Figure 1D). Both wild type (WT) and *Fus*$^{\Delta NLS/+}$ mice showed diminished distance to reach the platform over the 5 days of acquisition training, suggesting ability of learning in both genotypes. However, *Fus*$^{\Delta NLS/+}$ mice did not further improve performance after 3 days of training, showing a significant decreased performance at day 5 as compared to WT mice (interaction DayXGenotype $p<0.0116$, performance at day 5: $p=0.0393$) (Figure 1E). Importantly, this phenotype was not due to motor problems in *Fus*$^{\Delta NLS/+}$ mice as we did not observe differences in swim speed across genotypes (Figure S1A). In the retention trial, WT mice spent significantly more time in the target quadrant. *Fus*$^{\Delta NLS/+}$ mice tended to show decreased performance as compared to wild type mice at 24 hours, and this difference was significant when remote memory was tested, 30 days after the last training session (Figure 1F). *Fus*$^{\Delta NLS/+}$ mice crossed significantly less the annulus region than wild type littermates and did not distinguish efficiently the target quadrant from the adjacent quadrant (Figure 1G-J & Figure S1B-D). Synaptic rearrangement during the first 4 days after a spatial memory task represents a major mechanism in learning and memory. Using Golgi staining, we quantified dendritic spine morphology in the CA1 region of the dorsal hippocampus 4 days after the last training. *Fus*$^{\Delta NLS/+}$ mice demonstrate significantly less mushroom spines in basal condition and after learning (Genotype $p=0.0194$, Figure 1K, and Figure S2). Thus, *Fus*$^{\Delta NLS/+}$ mice display impaired spatial long-term memory as early as 5 months of age, that manifests in a lack of precision for both recent and remote memories and is associated with abnormal structural plasticity (i.e., global decrease in mature dendritic spine number).

FUS expression levels were evaluated in the hippocampus of *Fus*$^{\Delta NLS/+}$ mice and control WT littermates. FUS was highly expressed in dorsal hippocampal neurons of the CA1 region of both genotypes, as shown by double NeuN/FUS immunostaining (Figure 1A). Interestingly, the overall

FUS staining appeared increased in *Fus*$^{\Delta NLS/+}$ CA1 neurons, and this was confirmed by increased total FUS protein levels (p=0.0004) (Figure 1B) and increased *Fus* mRNA levels in bulk tissues (p=0.0102) (Figure 1C).

II. The Fus$^{\Delta NLS}$ mutation impairs hippocampal learning-induced transcriptome

The establishment of long-term memory as well as learning-induced synaptic rearrangement is dependent upon *de novo* gene transcription (Dubue et al., 2015; Remaud et al., 2014). Since FUS has been involved in transcription and splicing, we hypothesized that the memory defects of *Fus*$^{\Delta NLS/+}$ mice could be caused by alterations in the learning-induced transcriptome. We therefore performed RNA sequencing of the dorsal hippocampus at basal state (Home cage, HC) or after 3 days of MWM training (Learning conditions) in *Fus*$^{\Delta NLS/+}$ mice and WT littermates. DESeq2 analyses revealed that differentially expressed genes (adjusted p-value <0.1, minimum 100 reads) were clearly separated between the HC and learning conditions for both genotypes (Figure 2A and Figure S3A). These differential analyses further showed that the alterations in gene expression between *Fus*$^{\Delta NLS/+}$ mice and WT occur mainly upon learning (Figure 2A, B), as only 6 differentially expressed genes (DEG), including *Fus* itself were observed between WT and *Fus*$^{\Delta NLS/+}$ mice in HC conditions. However, learning led to 590 DEG in WT mice including 264 downregulated and 326 upregulated genes, while 573 (446 up, 127 down) genes were differentially expressed in *Fus*$^{\Delta NLS/+}$ mice upon learning (Figure 2B, Figure S3B). Strikingly, learning DEGs were only partially overlapping between WT and *Fus*$^{\Delta NLS/+}$ mice (Figure 2B). Gene ontology (GO) analyses confirmed the different transcriptional response to 3 days of training in *Fus*$^{\Delta NLS/+}$ and WT mice: while in WT mice, upregulated genes were mainly associated with transcription (e.g., transcription factor activity, negative and positive regulation of transcription, transcription factor binding) (Figure 2C), this group of genes was significantly less expressed in *Fus*$^{\Delta NLS/+}$ upon the same training (Figure 2D left). As an example, WT mice significantly upregulated several immediate early genes (e.g., Junb), as well as several transcription factors (e.g., Ets2, Etv1 and Etv5 from the ETS transcription factor family, but also, Atf4, Foxo3, Max, Rorb and Nfkbia, an inhibitor of the Nfkb transcription factor), and these genes exhibited a dampened transcriptional induction in *Fus*$^{\Delta NLS/+}$ mice (Figure 2E). Contrastingly, *Fus*$^{\Delta NLS/+}$ mice upregulated genes primarily associated with neuronal and synaptic related functions (Figure 2C), whereas these did not show significant upregulation in WT mice (Figure 2D right). Some of these genes are associated with

glutamatergic (e.g., Gria2, Gria3, Grin2a, Grin3a and Grm5) as well as GABAergic- (e.g., Gabra2 and Gabrb2) related functions (Figure 2F). Downregulated genes were enriched in similar GO terms between *Fus*$^{\Delta NLS/+}$ and WT mice, mainly related to extracellular matrix/region/space terms (FigureS4A, B). Thus, the ΔNLS mutation leads to little change in the basal hippocampal transcriptome, but pronounced alterations, notably on upregulated genes, in the response to spatial memory training.

III. The FusΔNLS mutation remodels chromatin at transcription starts sites in hippocampal neurons

To evaluate if altered gene transcription in *Fus*$^{\Delta NLS/+}$ mice can be due to alterations in basal epigenetic marks in neurons, we performed chromatin immunoprecipitation followed by deep sequencing (ChIP-seq) on neuronal nuclei sorted by Fluorescent activated cell sorting (FACS) from hippocampal tissue of HC WT and *Fus*$^{\Delta NLS/+}$ mice. In both genotypes, the total number of neuronal sorted nuclei were comparable, suggesting that the downstream analyses are not biased by neuronal loss. We focused on H3K4me3, H4K12ac and H3K27ac histone marks, as markers of transcriptionally active chromatin, and H3K27me3 as a marker of inactive transcription. Principal component analyses (PCA) and dendrograms using the Simple Error Ratio Estimate (SERE) score of the different ChIP-seq samples demonstrated a clear genotype effect (Figure S5A, B). Indeed, in hippocampal neurons of *Fus*$^{\Delta NLS/+}$ mice, we observed that specific genomic loci were generally enriched in active histone marks: H3K4me3 (2855 increased peaks), H4K12ac (4155 increased peaks) and H3K27ac (367 increased peaks) (Figure 3A). The ChIP-seq experiment for the repressive H3K27me3 histone mark was performed in different experiments and after batch correction of the replicates (Fig S6A), we found that 251 peaks were depleted in histone mark (Fig S6B). Together, these results are indicative of prominent chromatin remodeling in hippocampal cells of *Fus*$^{\Delta NLS/+}$ mice. We will refer to genes presenting with increased active histone marks as histone mark enriched genes (HMEG). Analysis of the peak center demonstrated a global increase of active histone mark and decrease of the H3K27me3 repressive mark in *Fus*$^{\Delta NLS/+}$ mice (Figure 3B, S6C). We then analyzed the distribution of the different marks on the genome and more particularly in HMEG. Most of the detected peaks for the three active marks were located in the genic regions, and this enrichment was more pronounced for HMEGs with 88% to 96% of differentially enriched peaks located on genic region (Figure 3C). Indeed, increased

active marks predominantly located at the transcription start site (TSS) of HMEGs (Figure 3D, E). The H3K27me3 repressive mark showed a global decrease on the genome and as well as in the TSS of genes, while we noted an increase at the TTS (Fig S6C). We then analyzed the functional categories of HMEGs using GREAT and the top 15 significant hits are represented for biological processes for each mark (Figure 3F). Gene affected by H3K4me3 enrichment were mainly associated with histone modification and post-translational modifications of proteins, while H4K12ac increased peaks were observed on genes associated with mRNA processing and mRNA metabolic and catabolic processes. Significant enrichment of H3K27ac was associated to dendritic and synaptic-related genes (Figure 3F). Depleted H3K27me3-genes were significantly associated to transcription and RNA metabolic processes (Figure S6D). Although GO terms substantially differed between the different active histone marks, there was a high overlap between genes showing H3K4me3 and H4K12ac increase enrichment (1764 common peaks), with GO term associated with chromatin modification and peptidyl acetylation and methylation (Figure S7A and Figure S7B). Among those genes we observed methyltransferase (e.g., Kmt2a, Kmt2c), demethylases (e.g., Kdm1b, Kdm2a, Kdm2b, Kdm5b, Kdm6b, Kdm7a), acetyltransferases (e.g., Kat6b, Kat2b, Ep300, Clock) and lysine deacetylases (e.g. Hdac2, Hdac3, Hdac5, Sirt3, Sirt5), suggesting major impacts on chromatin organization. More interestingly we found that 205 peaks demonstrated increased enrichment for the three active histone marks on genes associated with neuronal/synaptic functions (e.g., Bdnf, Grin2a, Grin2b, Grin2d Ntrk2, Nr4a3, Mapt, Mef2c, Mef2d, Ache, Crebbp) (Figure S7A and Figure S7C). An example for the genomic distribution of H3K4me3, H4K12ac and H3K27ac on the Kmt2a gene, a lysine methyltransferase regulating the methylation of H3K4me3, and on the Grin2a gene, the glutamate ionotropic receptor NMDA type subunit 2A, is shown in Figure S7D and Figure S7E. In all, the ΔNLS mutation profoundly modified the epigenetic landscape at TSS of genes involved in particular in chromatin remodeling, RNA metabolism, and neuronal/synaptic genes.

IV. Altered histone chromatin marks are associated with increased basal and learning-induced mRNA expression levels on highly expressed genes in ***Fus*$^{\Delta NLS/+}$** mice

To determine if a correlation exist between HMEGs and mRNA expression in *Fus*$^{\Delta NLS/+}$ mice, we integrated both analyses. Interestingly, HMEGs showed significantly increased expression (calculated as z-score) in HC *Fus*$^{\Delta NLS/+}$ mice (Figure 4A & Figure SA, B), whatever the histone mark

considered, while this was not observed in groups of randomly chosen genes containing the same number of genes (FigureS8C). This increased expression of HMEGs was maintained in learning conditions (Figure4A & Figure SA, B). We then asked whether HMEGs were related to the level of gene expression and clustered genes from our HC RNA-seq data in four quartiles of expression named Q1 to Q4 (Q1 = not expressed or lowly expressed (0-25%), Q2 = middle low expressed (25-50%), Q3 = middle high expressed (50-75%) and Q4 = highly expressed (75-100%)) (Figure 4B). This is of particular interest since the level of active histone marks correlate well with the level of transcription, as observed in FigureS8D. Interestingly, more than half of HMEGs are present in the Q4 highly expressed group of genes (Figure 4C). Thus, epigenomic alterations in *Fus*$^{\Delta NLS/+}$ mice are found on already highly expressed genes in the hippocampus and correlate with discrete increase of gene expression.

V. FUS binds at discrete genomic sites related to ETS transcription factors

Our next goal was to decipher how the *Fus* ΔNLS mutation can alter chromatin structure and gene expression and we first checked whether overall FUS protein quantities were affected in the nuclear compartment. Subcellular fractionation followed by western blotting using an antibody recognizing the N-Ter of FUS (i.e., all forms of FUS) indicated that, as expected, *Fus*$^{\Delta NLS/+}$ hippocampi displayed increased cytoplasmic FUS protein while the same amount was found in the nucleus of both genotypes (Figure 5A, B). Nevertheless, using an antibody targeting the C-terminal part of FUS (i.e., recognizing full length WT FUS only), we found that levels of WT FUS were decreased in both cytoplasmic and nuclear compartments (Fig 5A, C). This suggests that truncated FUS is indeed delocalized in the cytoplasm, but that a significant fraction is capable of entering the nucleus despite the absence of NLS. Thus, the *Fus* ΔNLS mutation might interfere with normal nuclear FUS functions. To address the possible alterations in FUS nuclear functions, we performed ChIP-seq of FUS in hippocampal nuclei, using an antibody recognizing all forms of FUS. We observed 386 genomic regions significantly bound to FUS. GO analysis showed that FUS-bound genes were mostly related to RNA metabolism, ribosome/translation and mitochondria (Figure 5D, E). These analyses were also performed in FUS mice and PCA analyses demonstrated that sample primarily separated according to the genotype (Figure 5F), but DESeq2 analyses did not reveal a significant differential FUS binding between FUS and WT mice (Figure S9A). However, we observed a predominant localization of FUS protein at the TSS of its target genes (Figure 5H)

and FUS binding showed a (nonsignificant) trend to increased binding in FUS versus WT mice (Figure 5G, H). Interestingly, FUS -target genes could be separated into three clusters presenting with either high, moderate, or low binding as shown in Figure 5H by representative genes, respectively *Mrpl44*, *Mrpl13* and *Mrpl1*. Functional analyses revealed an enrichment in GOTERM related to mitochondrial ribosome in each cluster, including *Mrpl* genes and genes encoding mitochondrial complex I enzymes (NADH dehydrogenases), but cluster 2 (moderate FUS binding) showed additional enrichment in ncRNA, rRNA and RNA metabolic processes related genes and cluster 3 (low FUS binding), in genes related to RNA polymerase I and RNA polymerase II/TFIIH complex (Figure S9B, C). Strikingly, predicted promoter motif revealed predominant binding of FUS on a single DNA motif family, that associated with the different members of the ETS family (GGAA), among which ELK1 showed the highest significance (Figure 5I). Of note, transcription of FUS-target genes might be altered as FUS bound genes showed a global higher (z-scores) expression level in basal conditions (HC) in *Fus*$^{\Delta NLS/+}$ mice (Figure 5J.). In all, our results show that FUS binds preferentially to the TSS region of a limited set of genes, characterized by the presence of an ETS-binding motif.

VI. FusΔNLS mutation results in altered transcription factor binding on open chromatin regions

In view of the extent of histone alterations in the *Fus*$^{\Delta NLS/+}$ mice, we then wondered if the overall chromatin conformation, as well as the chromatin accessibility, would be impacted in our model. To answer this, we performed an Assay for Transposase-Accessible Chromatin (ATAC) followed by genome-wide sequencing (ATAC-seq). This technique is used to study open chromatin regions (OCR). PCA analyses and dendrograms using the SERE score demonstrated that sample were separated according to their genotypes, except for one sample (Figure S10 A, B). However, chromatin opening was not significantly changed in *Fus*$^{\Delta NLS/+}$ mice compared to WT (Figure S10 C). Nevertheless, footprint analyses performed with TOBIAS (Bentsen et al., 2020) revealed altered binding accessibility of several transcription factors, including decreased binding of two ETS family members : Elk1 and Elk3 (Figure 6 A). Both of these ETS member bind to highly similar GGAA motif, as that observed in the promoter motif analyses of the FUS ChIP-seq (Figure 6B). We then analyzed expression level of genes in OCR containing the GGAA motif in their TSS and observed that, despite decreased binding of transcription factors, they presented an increased

expression level (z-scores) in basal and learning condition in *Fus*$^{\Delta NLS/+}$ mice (Figure 6C). In conclusion, our data show that the *Fus* ΔNLS mutation leads to altered binding of several transcription factors and point to the ETS family members (e.g., ELK1/3) as interesting targets as they appear repeatedly in our ATAC-seq and ChIP-seq FUS data.

CONCLUSION

In sum, we demonstrated in this study that Fus is able to bind specific loci on DNA, likely ETS/ELK promoter responsive elements present at the TSS of highly expressed genes and that the truncated FusΔNLS mutation then possibly exerts transcriptional alterations that are significantly measurable on the hippocampal transcriptome of trained mice. Such alterations may underlie the deficits in hippocampo-dependent spatial memory we evaluated in *Fus*$^{\Delta NLS/+}$ mice and the possible mechanisms associated to these processes will be presented in the discussion section of the manuscript.

Figure 1

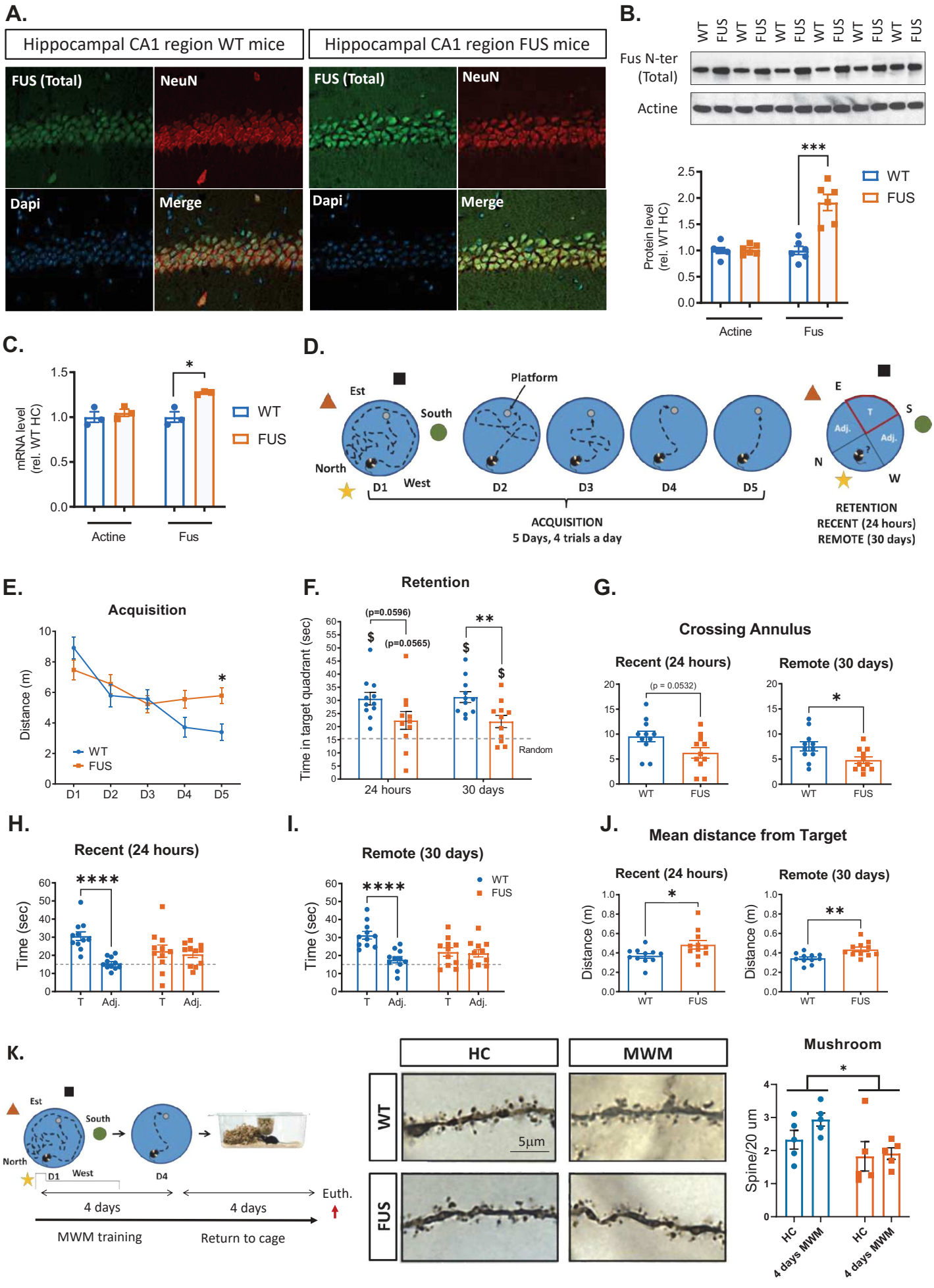
A.
Hippocampal CA1 region WT mice
Hippocampal CA1 region FUS mice
FUS (Total)
NeuN
Dapi
Merge
B.
WT FUS WT FUS WT FUS WT FUS WT FUS WT FUS
Fus N-ter (Total)
Actine
***
Protein level (rel. WT HC)
WT
FUS
Actine
Fus
C.
*
mRNA level (rel. WT HC)
WT
FUS
Actine
Fus
D.
Est
South
North
West
Platform
D1
D2
D3
D4
D5
ACQUISITION
5 Days, 4 trials a day
E
S
N
W
T
Adj.
RETENTION
RECENT (24 hours)
REMOTE (30 days)
E.
Acquisition
Distance (m)
WT
FUS
D1 D2 D3 D4 D5
F.
Retention
(p=0.0596)
(p=0.0565)
**
$
Time in target quadrant (sec)
Random
24 hours
30 days
G.
Crossing Annulus
Recent (24 hours)
Remote (30 days)
(p = 0.0532)
*
WT
FUS
H.
Recent (24 hours)
****
Time (sec)
T
Adj.
I.
Remote (30 days)
****
WT
FUS
Time (sec)
T
Adj.
J.
Mean distance from Target
Recent (24 hours)
Remote (30 days)
*
**
Distance (m)
WT
FUS
K.
Est
South
North
West
D1
D4
4 days
4 days
Euth.
MWM training
Return to cage
HC
MWM
WT
FUS
5µm
Mushroom
*
Spine/20 um
HC
4 days MWM
HC
4 days MWM

Figure 1. FUS mutation induce spatial memory deficit and synaptic dysfunction in the hippocampus of *Fus*$^{\Delta NLS/+}$mice.

(A) Hippocampal brain section from 5-month-old WT and *Fus*$^{\Delta NLS/+}$ mice immunostained for Total FUS (green), NeuN (red) and DAPI (blue) in the CA1 brain region.

(B) Protein level analyses showing FUS overexpression in the hippocampus of *Fus*$^{\Delta NLS/+}$mice at the age of 5 months. Actine is used for control protein expression. Data are represented as mean ± SEM (n = 6 per group). ***p<0.0001 using the unpaired t-test.

(C) RNA-seq data showing *Fus* mRNA levels in the hippocampus of 5-month-old WT and *Fus*$^{\Delta NLS/+}$ mice. Actin is used as control. Data are represented as mean ± SEM (n = 3 per group). *p<0.05 using unpaired t-test.

(D) Experimental design of the 5-days spatial learning in the MWM**.**

(E) Totaldistance travelled to reach the target platform in the MWM during the 5 consecutive days of aquisition. Data are represented as mean ± SEM (n = 11 per group). *p<0.05 using repeated two-way ANOVA with Šidák correction for multiple comparisons.

(F) Mean time spent in the Targetquadrant during the recent (24 hours) and remote (30 days) retention tests. Dashed line (grey) represent the value for "chance" (15s). Data are represented as mean ± SEM (n = 11 per group). *p<0.05 using repeated two-way ANOVA with Šidák correction for multiple comparisons. $p<0,05 vs Random value using One sample t test.

(G) Number of time crossing the annulus area during the recent and remote retention tests. Data are represented as mean ± SEM (n = 11 per group). *p<0.05 using non parametric unpaired Man-whitney rank test.

(H) Time spent in the Targetquadrant (T) vs. time spent in the favorite adjacent quadrant (Adj.) during the recent retention test. Data are represented as mean ± SEM (n = 11 per group). ****p<0.0001 using two-way ANOVA with Šidák correction for multiple comparisons.

(I) Time spent in the Targetquadrant (T) vs. time spent in the favorite adjacent quadrant (A) during the remote retention test. Data are represented as mean ± SEM (n = 11 per group). ****p<0.0001 using two-way ANOVA with Šidák correction for multiple comparisons.

(J) Mean distance from the Target quadrant during the recent and remote retention test. Data are represented as mean ± SEM (n = 11 per group). *p<0.05, **p<0.01 using unpaired t test.

(K) Experimental scheme of the spine analyses in the CA1 region of the hippocampus (upper part), typical examples of a dendritic fragment (left) and number of mushroom spine in the hippocampal CA1 region in WT and *Fus*$^{\Delta NLS/+}$ mice either trained 4 days in the MWM or left in their home cage (HC) (right). Data are represented as mean ± SEM, (n = 5 per group). *p<0.05 using repeated two-way ANOVA with Šidák correction for multiple comparisons. Euth = Euthanasia. Scale bar 5μm.

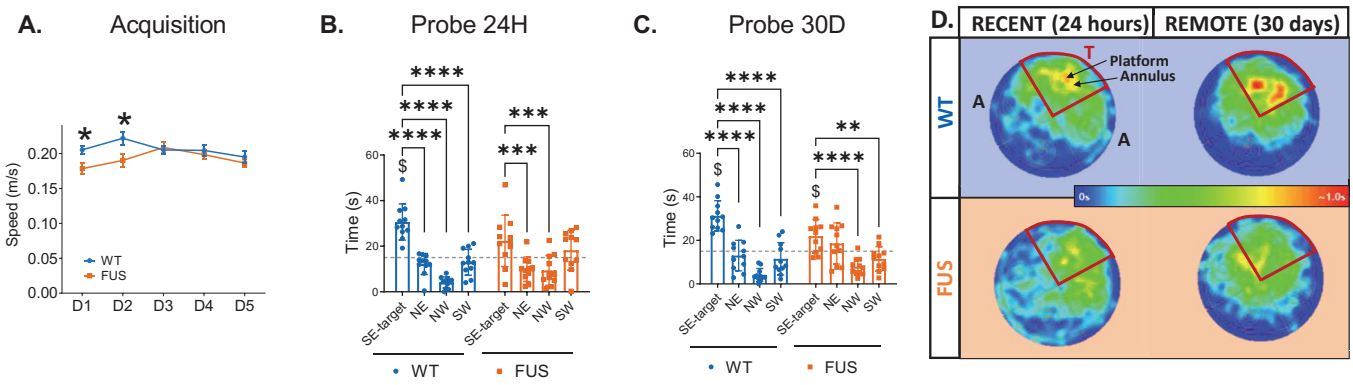

Figure S1. Details of acquisition and retention in the MWM for Figure 1.

A. Mean swimm speed in the MWM during each trial of the 5 acquisition days. *p<0.05 using repeated two-way ANOVA with Šidák correction for multiple comparisons.

B. Time spent in each quadrant. Data are represented as mean ± SEM (n = 11 per group). *p<0.05, **p<0.01, ***p<0.001, ****p<0.0001 using repeated two-way ANOVA with Šidák correction for multiple comparisons.

C. Heat map representing time spent in the spatial MWM during the recent and remote memory test. The target quadrant "T" is highlighted in red and "A" mean Adjacent quadrant. **D.** Time spent in the 4 quadrants. The gray dotted line represents the random time in a quadrant (15sec). Results are represented by the mean of each group ± standard error of the mean, n=11 per group.

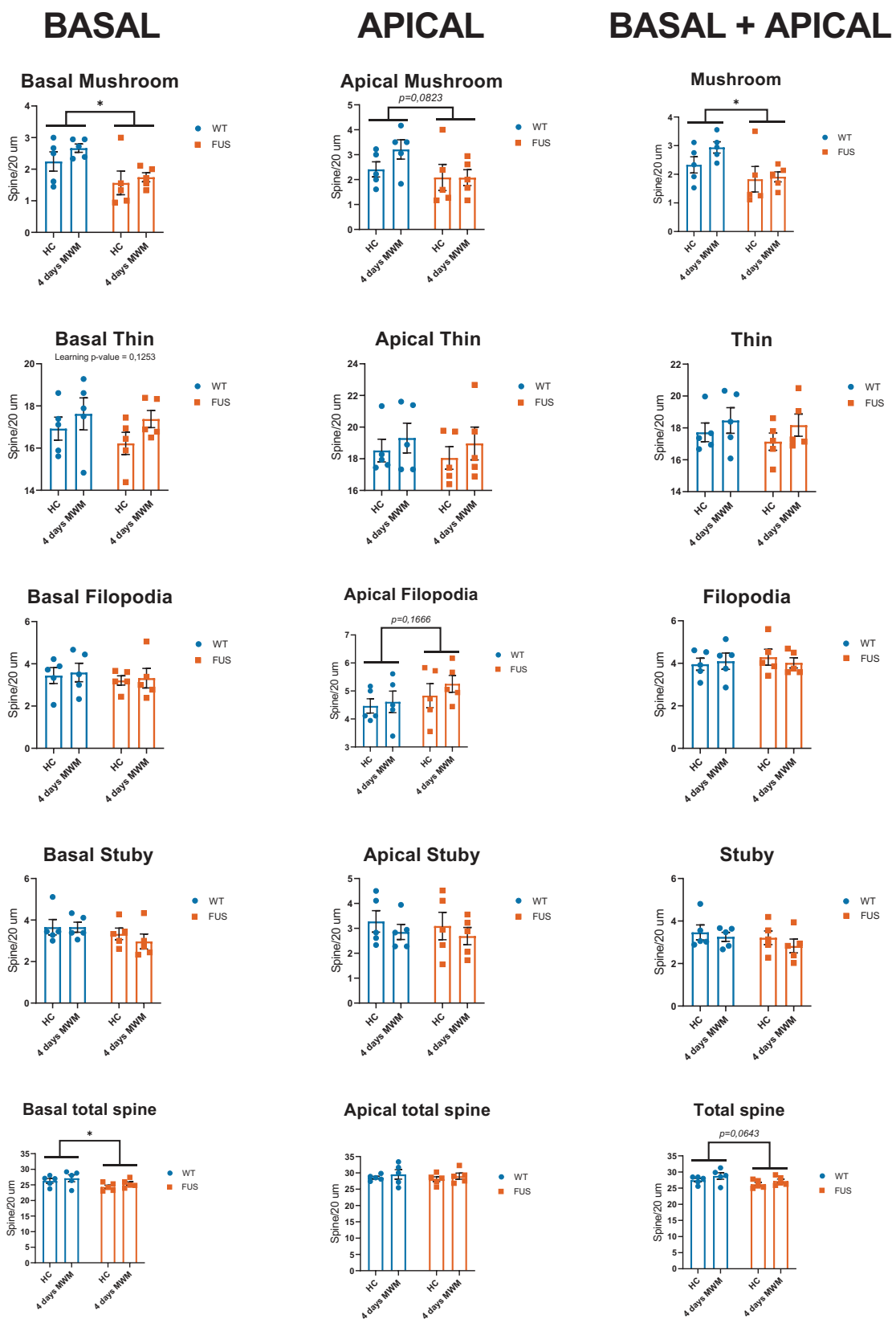

Figure S2. Spine counting details. Number of spines in each cluster (mushroom, thin, filopodia, stubby or all) on basal or apical dendrites as well as the sum of both in the hippocampal CA1 region for WT and *Fus*$^{\Delta NLS/+}$ mice either trained 4 days in the MWM or HC conditions. Data are represented as mean ± SEM, (n = 5 per group). *p<0.05 using repeated two-way ANOVA with Šidák correction for multiple comparisons.

Figure 2


A.
WT_HC
FUS_HC
FUS_HC
FUS_HC
WT_HC
WT_HC
WT_MWM
WT_MWM
WT_MWM
FUS_MWM
FUS_MWM
FUS_MWM
-3 -2 -1 0 1 2 3
B. DIFFERENTIALLY EXPRESSED GENES
HC:
Down
Up
FUS vs. WT
5
1
200 0 200 400
Learning vs. HC:
WT
FUS
264
326
127
446
200 0 200 400
FUS
FUS
210
54
73
168
158
288
WT
WT
C. DEG UP in Learning vs. HC mice
WT (326 genes)
FUS (446 genes)
Transcription
Neuron / Synapse
rhythmic process
transcription, DNA-templated
regulation of transcription
nucleus
transcription factor activity,
DNA binding
nucleoplasm
negative regulation of transcription
positive regulation of transcription
transcription factor binding
dendritic spine
protein binding
cytoplasm
metal ion binding
postsynaptic density
dendrite
neuronal cell body
postsynaptic membrane
nervous system development
neuron projection
0 2 4 6
p-value < 0,05
-log10(FDR p-value)
D. GO Term:
Transcription (61 genes)
Neuron / Synapse (59 genes)
Learning
****
****
Z-score values
1.0 0.5 0.0 -0.5 -1.0
WT FUS
WT FUS
E. GO Term : Transcription
WT HC
FUS HC
WT MWM
FUS MWM
mRNA level (rel. WT HC)
0 1 2 3
Ets2 Etv1 Etv5 Junb Atf4 Foxo3 Max Nfkbia Rorb
F. GO Term : Neuron / Synapse
mRNA level (rel. WT HC)
0.0 0.5 1.0 1.5
Gria2 Gria3 Grin2a Grin2b Grin3a Grm5 Gabra2 Gabrb1
Glutamate related genes
GABA related genes

<u>Figure 2.</u> Dysregulated expression of transcription- and synaptic-related genes and synaptic alterations in the hippocampus of *Fus*$^{\Delta NLS/+}$ mice during spatial memory formation.

(A) Heat map representing the expression z-score of all significant dysregulated genes of the RNA-seq analyses in the dorsal hippocampal region, shown per animal (n=3 per group). Adjusted p_value <0.1 using the FDR value with no Fold change selection.

(B) Number of significant differientially expressed genes in the dorsal hippocampus between FUS and WT in the HC condition (bar graphe on the top), MWM condition compared to HC condition for both WT and FUS group (bar graph on the bottom), adjusted p< 0.1 using the FDR value with a Cut off of 100 reads for gene expression and no Fold change selection. The two quantitative Venn diagrammes represent the common or uniquelly differentially expressed genes. In green the down regulated genes and in red the upregulated genes. (n=3 per group).

(C) DAVID analyses of the Top 10 Bilogical process, molecular function, cellular component and KEGG pathways associated with the upregulated genes in the dorsal hippocampus of the MWM group compared to the HC groupe for WT (blue) and FUS mice (orange), with x-axis representing the -log10(FDR p-value) and the dashline delimiting the FDR p-value of 0,05. (n=3 per group).

(D) Z-score expression of genes included in GO term « transcription » (left) and « neuron/synapses » (right) in the MWM condition from the RNA-seq analyses. (n=3 per group). ****p<0,0001 with the non-parametric Mann Whitney rank test.

(E) RNA-seq data showing the expression of genes in the dorsal hippocampus related to « Neuron and Synapse » annotation terms in DAVID. Data are represented as mean ± SEM and normalized to WT HC, (n = 3 per group). *adjusted p<0.1 using FDR.

(F) RNA-seq data showing the expression of genes in th edorsal hippocampus related to « Transription » annotation terms in DAVID. Data are represented as mean ± SEM and normalized to WT HC, (n = 3 per group). *adjusted p<0.1 using FDR.

(G) Experimental sheme of the spine analyses in the CA1 region of the hippocampus (upper part), typical examples of a dendritic fragment (left) and number of mushroom spine in the hippocampal CA1 region in WT and *Fus*$^{\Delta NLS/+}$ mice either trained 4 days in the MWM or left in their home cage (HC) (right). Data are represented as mean ± SEM, (n = 5 per group). *p<0.05 using repeated two-way ANOVA with Šidák correction for multiple comparisons. Euth = Euthanasia.

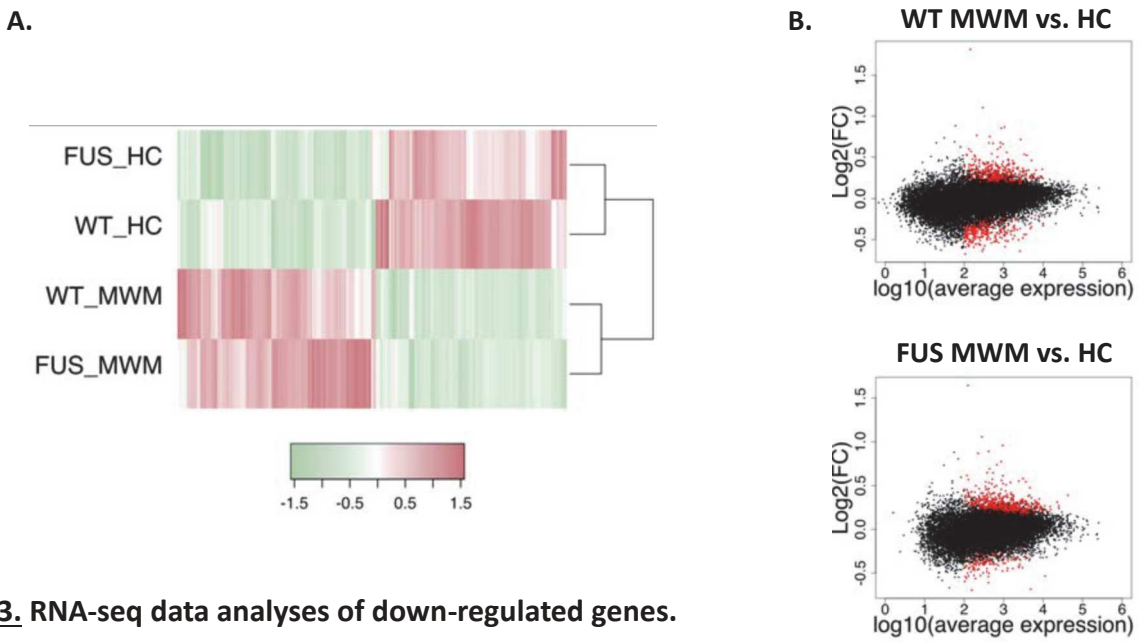

Figure S3. RNA-seq data analyses of down-regulated genes.

(A) Heat map representing the expression z-score of all significant dysregulated genes of the RNA-seq analyses in the dorsal hippocampal region, comparing the average of samples from WT and *Fus*$^{\Delta NLS/+}$ mice in both HC and MWM condition. (n=3 per group). Adjusted p_value<0.1 using the FDR value with no Fold change selection.

(B) MA-plot representing differential expression of genes in the dorsal hippocampus between MWM and WT condition in WT mice (top graph) and in *Fus*$^{\Delta NLS/+}$ mice (bottom graph), with x-axis representing the log10(average expression) and the y-axis the log2(Fold change) of each gene. Significantly dysregulated genes are represented by red dots. (n=3 per group). Adjusted p<0.1 using the FDR value with a Cut off of 100 reads for gene expression and no Fold change selection.

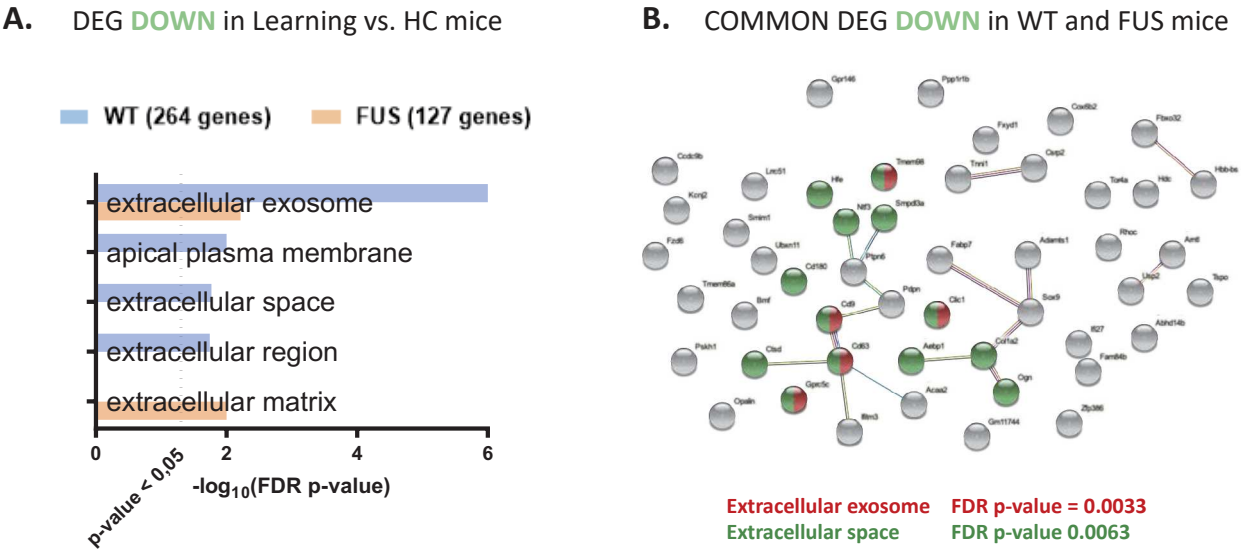

Figure S4. RNA-seq data analyses of down-regulated genes.

(A) DAVID analyses of the biological processes associated with the downregulated genes in the dorsal hippocampus of the MWM group compare to the HC groupe for WT (blue) and FUS mice (orange), with x-axis representing the -log10(FDR p-value) and the dashline delimiting the FDR p-value of 0,05. (n=3 per group).

(B) STRING gene expression analyses of commonly down-regulated genes in Fus and WT mice, delineating the significant functional GO-TERMS associated to the extracellular exosome and space (Cellular Component).

Figure 3

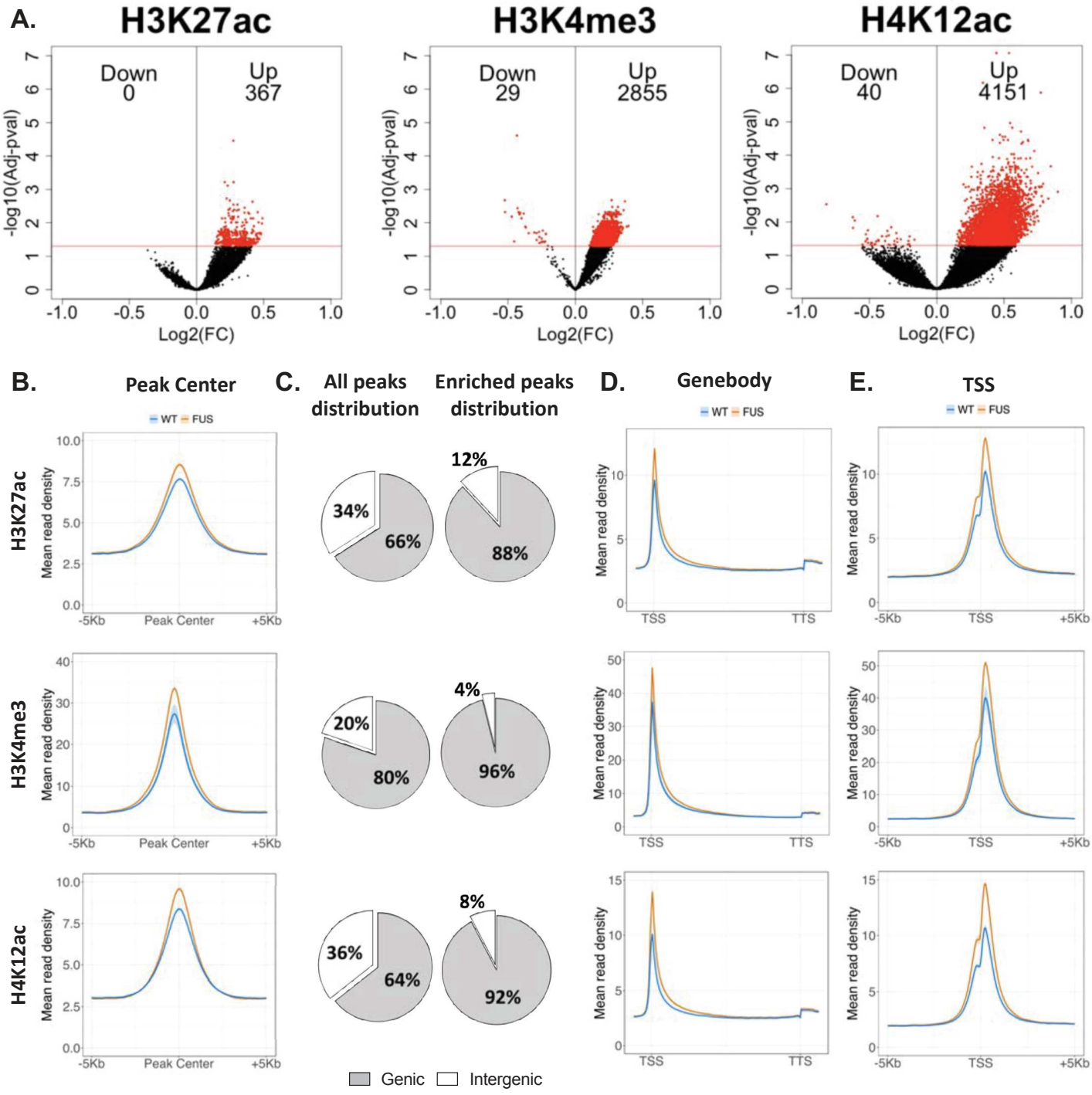
A.
H3K27ac
H3K4me3
H4K12ac
Down
Up
0
367
29
2855
40
4151
-log10(Adj-pval)
Log2(FC)
B.
Peak Center
C.
All peaks distribution
Enriched peaks distribution
D.
Genebody
E.
TSS
WT FUS
H3K27ac
H3K4me3
H4K12ac
Mean read density
-5Kb
Peak Center
+5Kb
TSS
TTS
34%
66%
12%
88%
20%
80%
4%
96%
36%
64%
8%
92%
Genic
Intergenic

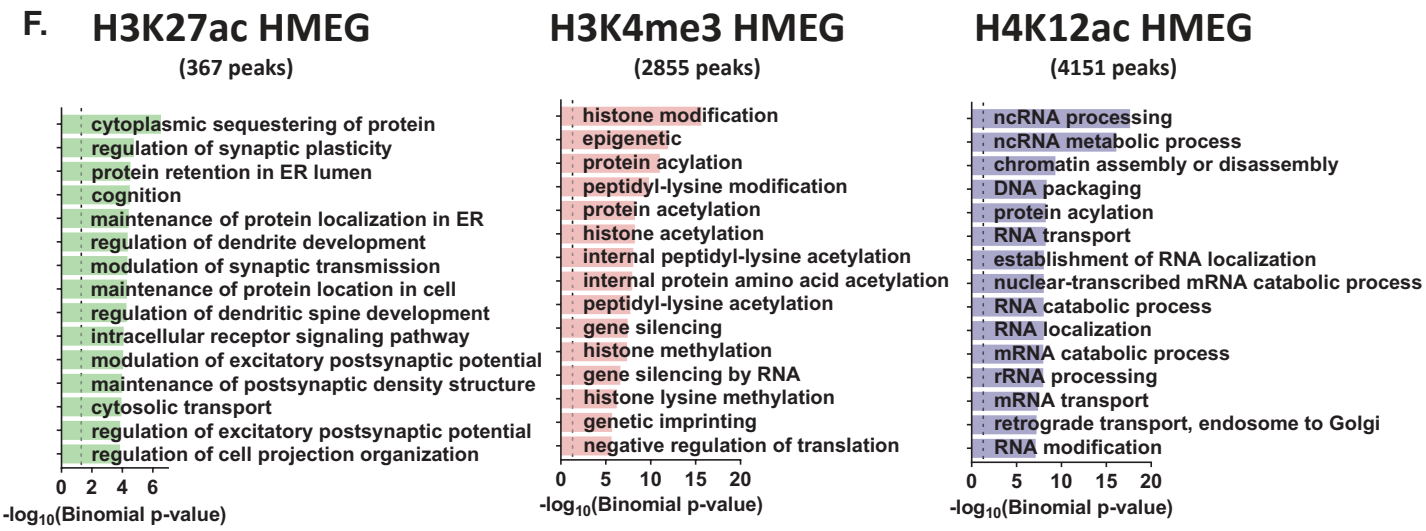
F.
H3K27ac HMEG
(367 peaks)
cytoplasmic sequestering of protein
regulation of synaptic plasticity
protein retention in ER lumen
cognition
maintenance of protein localization in ER
regulation of dendrite development
modulation of synaptic transmission
maintenance of protein location in cell
regulation of dendritic spine development
intracellular receptor signaling pathway
modulation of excitatory postsynaptic potential
maintenance of postsynaptic density structure
cytosolic transport
regulation of excitatory postsynaptic potential
regulation of cell projection organization
-log10(Binomial p-value)
H3K4me3 HMEG
(2855 peaks)
histone modification
epigenetic
protein acylation
peptidyl-lysine modification
protein acetylation
histone acetylation
internal peptidyl-lysine acetylation
internal protein amino acid acetylation
peptidyl-lysine acetylation
gene silencing
histone methylation
gene silencing by RNA
histone lysine methylation
genetic imprinting
negative regulation of translation
-log10(Binomial p-value)
H4K12ac HMEG
(4151 peaks)
ncRNA processing
ncRNA metabolic process
chromatin assembly or disassembly
DNA packaging
protein acylation
RNA transport
establishment of RNA localization
nuclear-transcribed mRNA catabolic process
RNA catabolic process
RNA localization
mRNA catabolic process
rRNA processing
mRNA transport
retrograde transport, endosome to Golgi
RNA modification
-log10(Binomial p-value)

Figure 3. FUS mutation induce an increase in active histone marks at the TSS of genes related to synapses, chromatine modification and RNA processing in hippocampal neurons.

(A) Volcano plots representing the differential analyses of H3K27ac (left), H3K4me3 (middle) and H4K12ac (right) in the hippocampus. Peak calling was performed using SICER p<0,003. The red line represents the cut-off of significance (Adjusted p-value < 0,05 using FDR with no Fold change selection), red dots show all peaks with significant differential enrichment of histone marks in *Fus*$^{\Delta NLS/+}$mice compare to WT. Two biological replicates per histone mark with n = 2 FANS sorted neurons of a mix of 4 hippocampi per replicate.

(B) Mean gene profiles established with SeqMiner at the peak center for H3K27ac, H3K4me3 and H4K12ac (from top to bottom) for the two biological replicates. Mean profiles for WT in blue and *Fus*$^{\Delta NLS/+}$ in orange. Data are represented as mean ± SEM in blue (WT) or orange (*Fus*$^{\Delta NLS/+}$) shadow.

(C) Pie charts representing the percentage of H3K27ac, H3K4me3 and H4K12ac (from top to bottom) peaks present on genic and intergenic regions in the WT genome for control (left) and for significant enriched peak in *Fus*$^{\Delta NLS/+}$ (right).

(D) Mean gene profiles established with SeqMiner on the gene bodies for H3K27ac, H3K4me3 and H4K12ac (from top to bottom) for the two biological replicates. Mean profiles for WT in blue and *Fus*$^{\Delta NLS/+}$ in orange. Data are represented as mean ± SEM in blue (WT) or orange (*Fus*$^{\Delta NLS/+}$) shadow. TSS= transcription start site, TTS = transcription terminal site.

(E) Same analyses as in (D) but for TSS.

(F) GREAT analyses of the top 15 biological processes of genes associated with H3K27ac, H3K4me3 and H4K12ac (from left to to right) significantly enriched peaks (Peaks Up, histone mark enriched genes (HMEG)) in the hippocampus of *Fus*$^{\Delta NLS/+}$mice. Dash line represents Binomial adjusted p-value < 0.05.

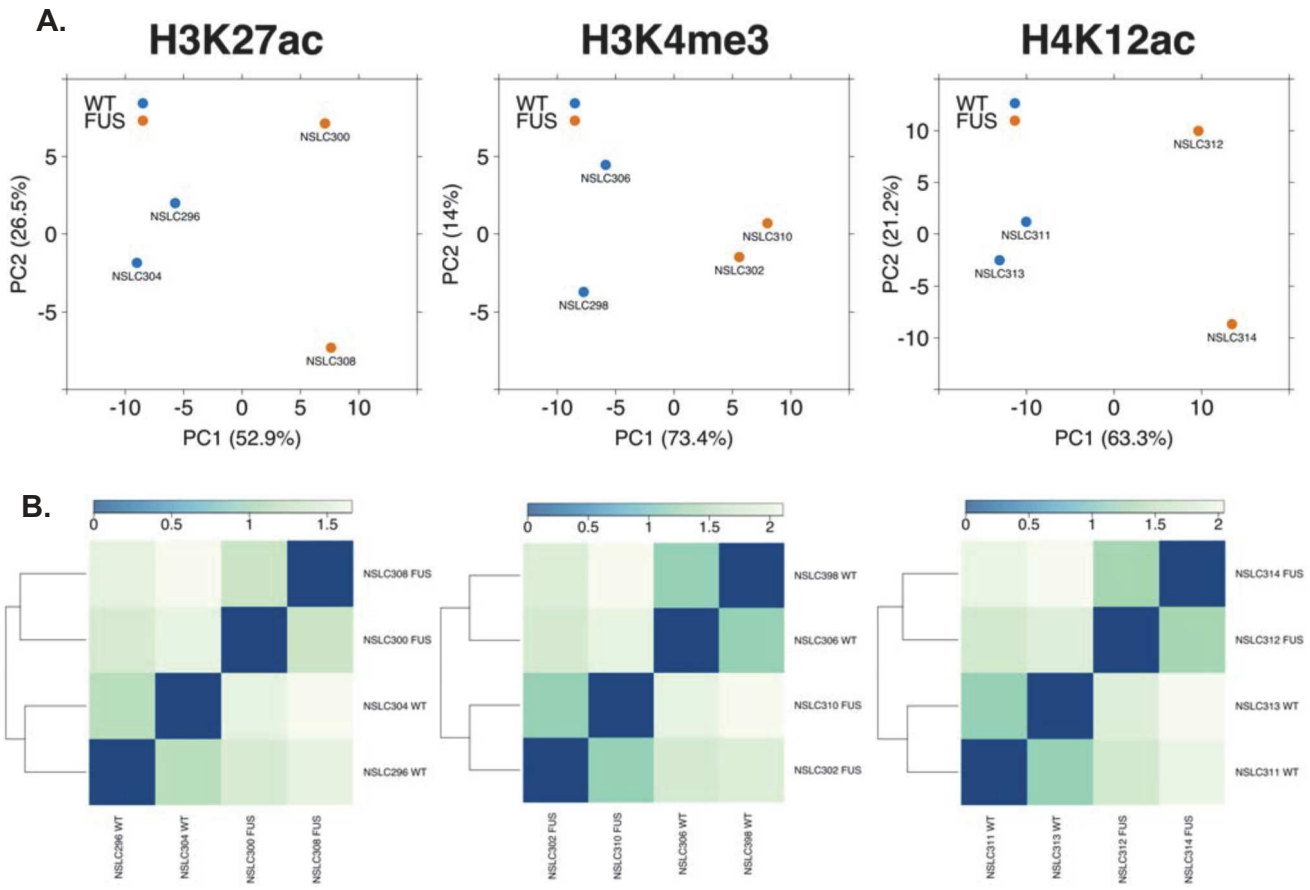

Figure S5. Chip-seq PCA and heatmap analyses of H3K27ac, H3K4me3 and H4K12ac.

(A) PCA analyses of H3K27ac, H3K4me3 and H4K12ac., WT (blue) and *Fus*$^{\Delta NLS/+}$ (orange). Two biological replicates with n = FANS sorted neurons of a mix of 4 hippocampi per replicate.

(B) Heatmap and dendrogram of H3K27ac, H3K4me3 and H4K12ac, using the Simple Error Ratio Estimate (SERE) score. Two biological replicates with n = FANS sorted neurons of a mix of 4 hippocampi per replicate.

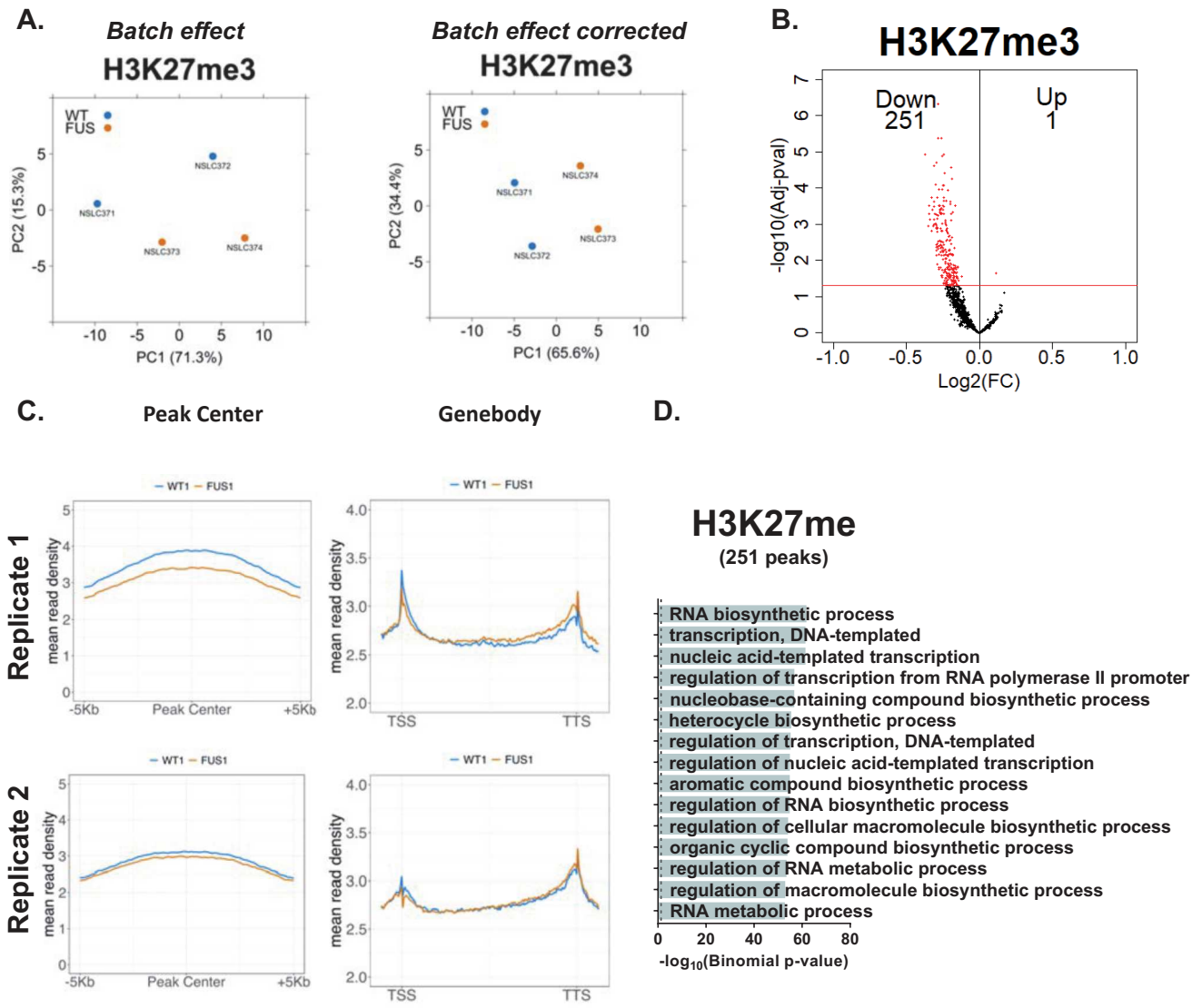

<u>Figure S6:</u> Analyses of the ChIP-seq H3K27me3 repressive mark in two different batches.

(A) PCA analyses of the two replicates of ChIP-seq H3K27me3 before the Deseq2 batch correction. Two biological replicates with n = FANS sorted neurons of a mix of 4 hippocampi per replicat. PCA analyses of the duplicates of ChIP-seq H3K27me3 after the DESeq2 batch correction. Two replicates with n = mix of 4 hippocampi per replicate.

(B) Volcano plot of the differentially-enriched H3K27me3 peaks. Peak calling was performed using SICER p<0,0003. The red line represents the cut off of significance (Adjusted p-value < 0,05 using FDR with no Fold change selection), red dots show all peaks with significant diference in H3K27me3 enrichment in *Fus*$^{\Delta NLS/+}$ mice compare to WT. Two biological replicats with n = FANS sorted neurons of a mix of 4 hippocampi per replicat.

(C) Peak center (left) and Gene profile (right) of replicate 1 (top) and 2 (bottom) done in two different batches demonstrate depletion of H3K27me3 in *Fus*$^{\Delta NLS/+}$ mice compare to WT. n = FANS sorted neurons of a mix of 4 hippocampi per replicat.

(D) GREAT analyses of the top 15 biological processes of genes associated with H3K27me3 significantly depleted peaks (Peaks down) in the hippocampus of *Fus*$^{\Delta NLS/+}$mice. Two biological replicates with n = FANS sorted neurons of a mix of 4 hippocampi per replicate. Dotted line represents Binomial adjusted p-value < 0.05.

A.

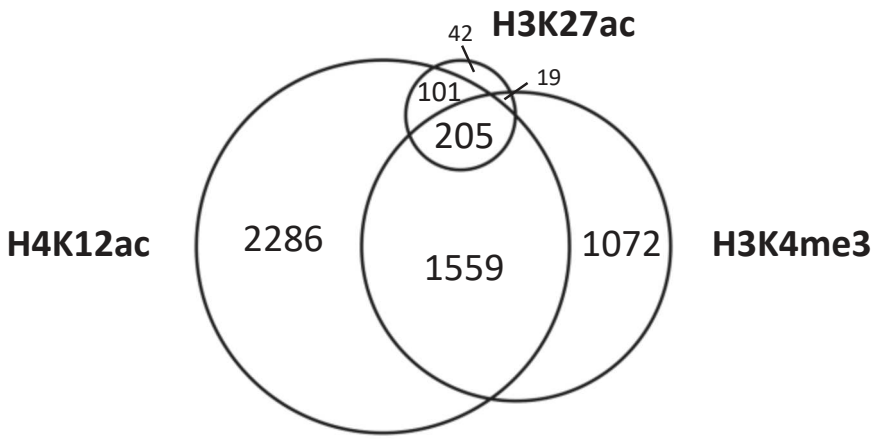

B. H3K4me3 & H4K12ac

(1764 peaks)

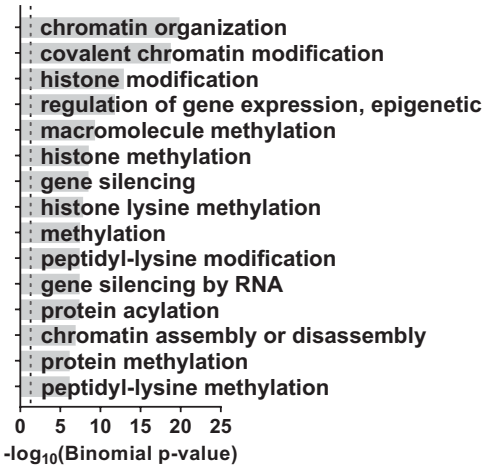

C. H3K27ac & H3K4me3 & H4K12ac

(205 peaks)

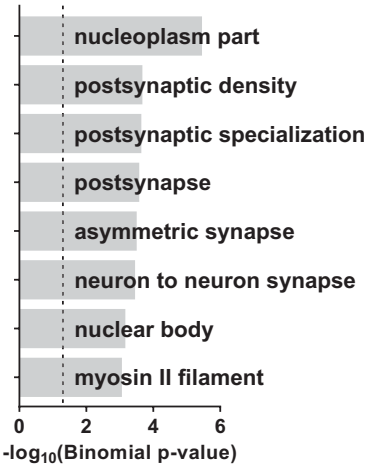

D.

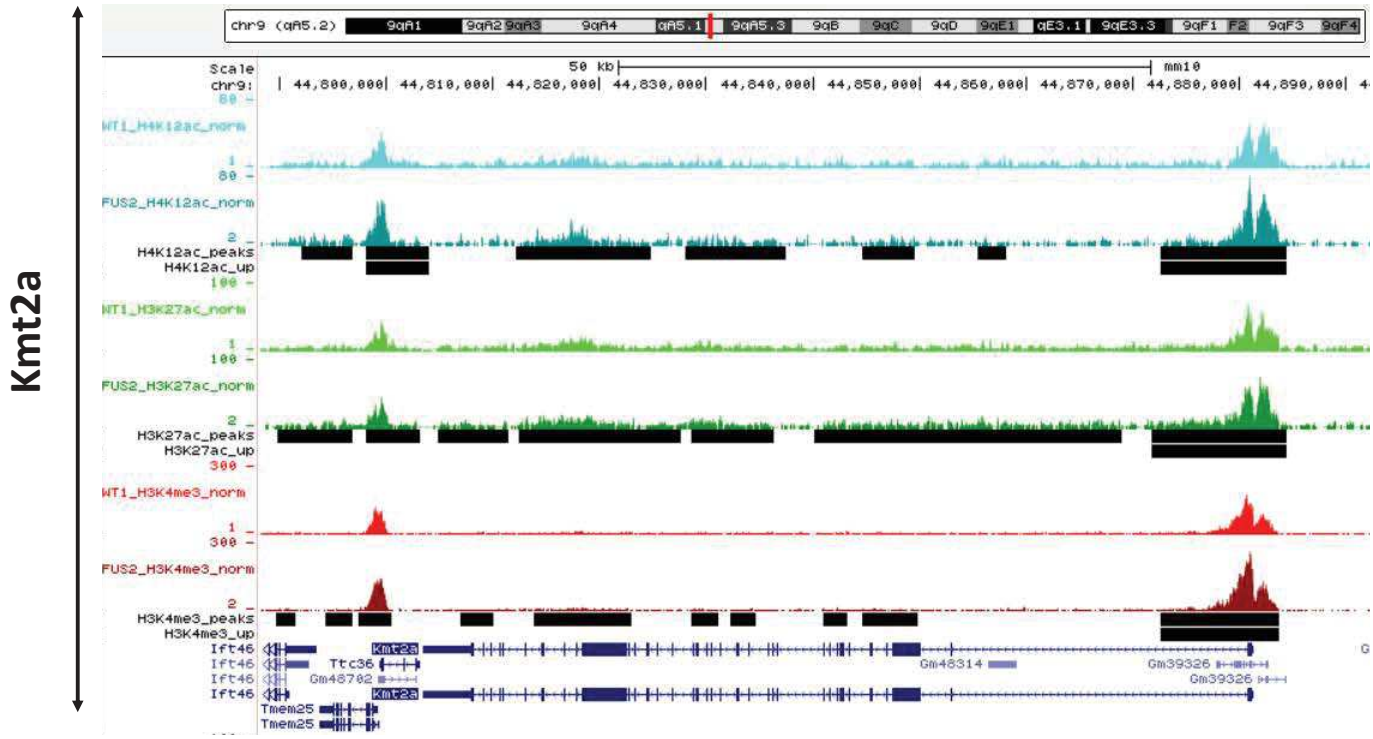

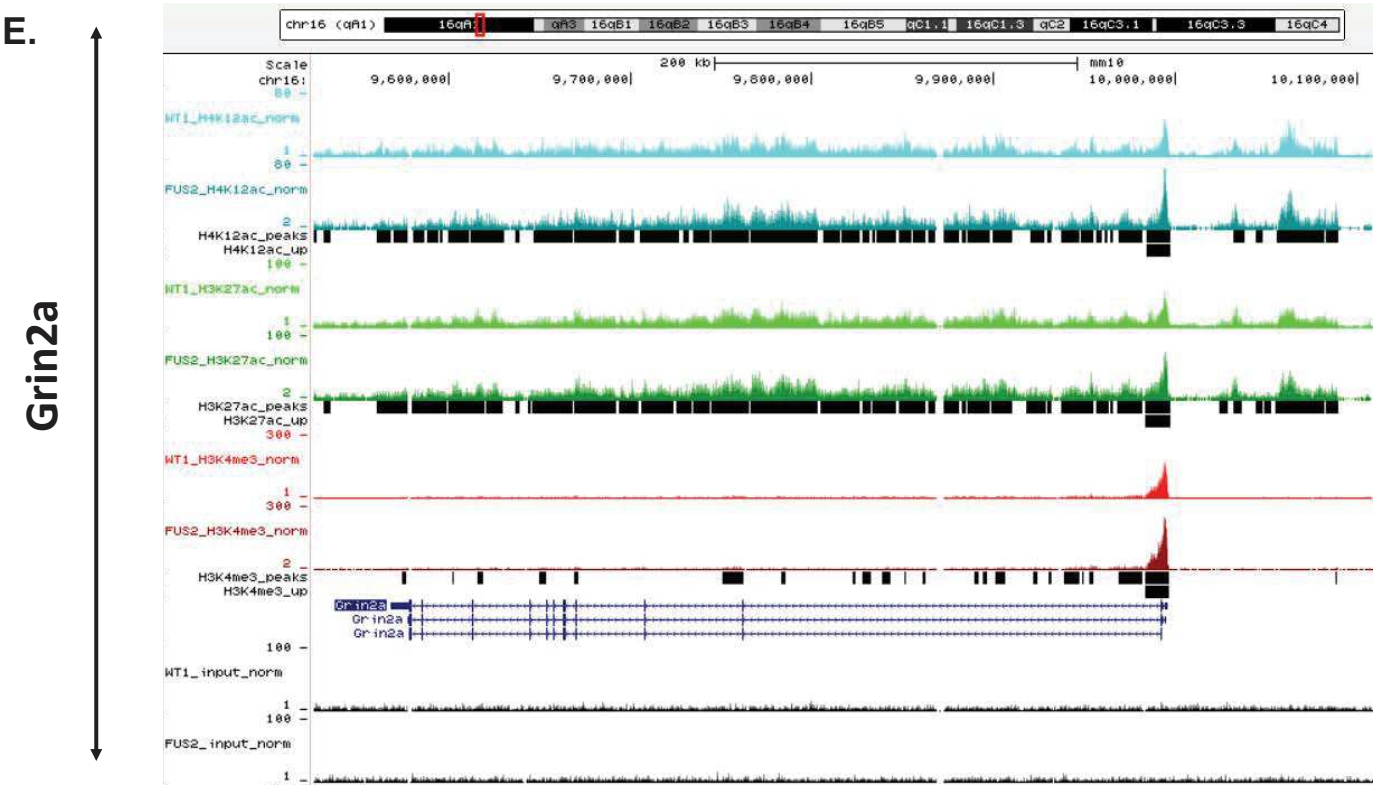

Figure S7: Common dysregulation of active histone marks on chromatin remodling and synaptic-related genes

(A) Venn diagrams representing the overlap of *Fus*$^{\Delta NLS/+}$ enriched peaks for H3K27ac, H3K4me3 and H4K12ac.

(B) GREAT analyses of the top 15 biological processes of genes associated with H3K4me3 and H4K12ac significantly enriched peaks (Peaks Up) in the hippocampus of *Fus*$^{\Delta NLS/+}$mice. Two biological replicates with n = FANS sorted neurons of a mix of 4 hippocampi per replicate. Dotted line represents Binomial adjusted p-value < 0.05.

(C) GREAT analyses of the cellular component of genes associated with H3K4me3, H4K12ac and H3K27ac significantly enriched peaks (Peaks Up) in the hippocampus of *Fus*$^{\Delta NLS/+}$mice. Two biological replicats with n = FANS sorted neurons of a mix of 4 hippocampi per replicate. Dotted line represents Binomial adjusted p-value < 0.05.

(D) Genome browser visualisation of H3K4me3, H4K12ac and H3K27ac on the Kmt2a gene and significant increased peak on the TSS in *Fus*$^{\Delta NLS/+}$ mice compared to WT. Example of one WT and *Fus*$^{\Delta NLS/+}$ replicate, n = FANS sorted neurons of a mix of 4 hippocampi per replicate. Peak calling was performed using SICER p<0,003 and differential analyses was performed using DESeq2 FRD adjusted p-value <0,05.

(E) Genome browser visualisation of H3K4me3, H4K12ac and H3K27ac on the Grin2a gene and significant increased peak on the TSS in *Fus*$^{\Delta NLS/+}$ mice compared to WT. Example of one WT and *Fus*$^{\Delta NLS/+}$ replicate, n = FANS sorted neurons of a mix of 4 hippocampi per replicate. Peak calling was performed using SICER p<0,003 and differential analyses was performed using Deseq2 FRD adjusted p-value <0,05.

Figure 4

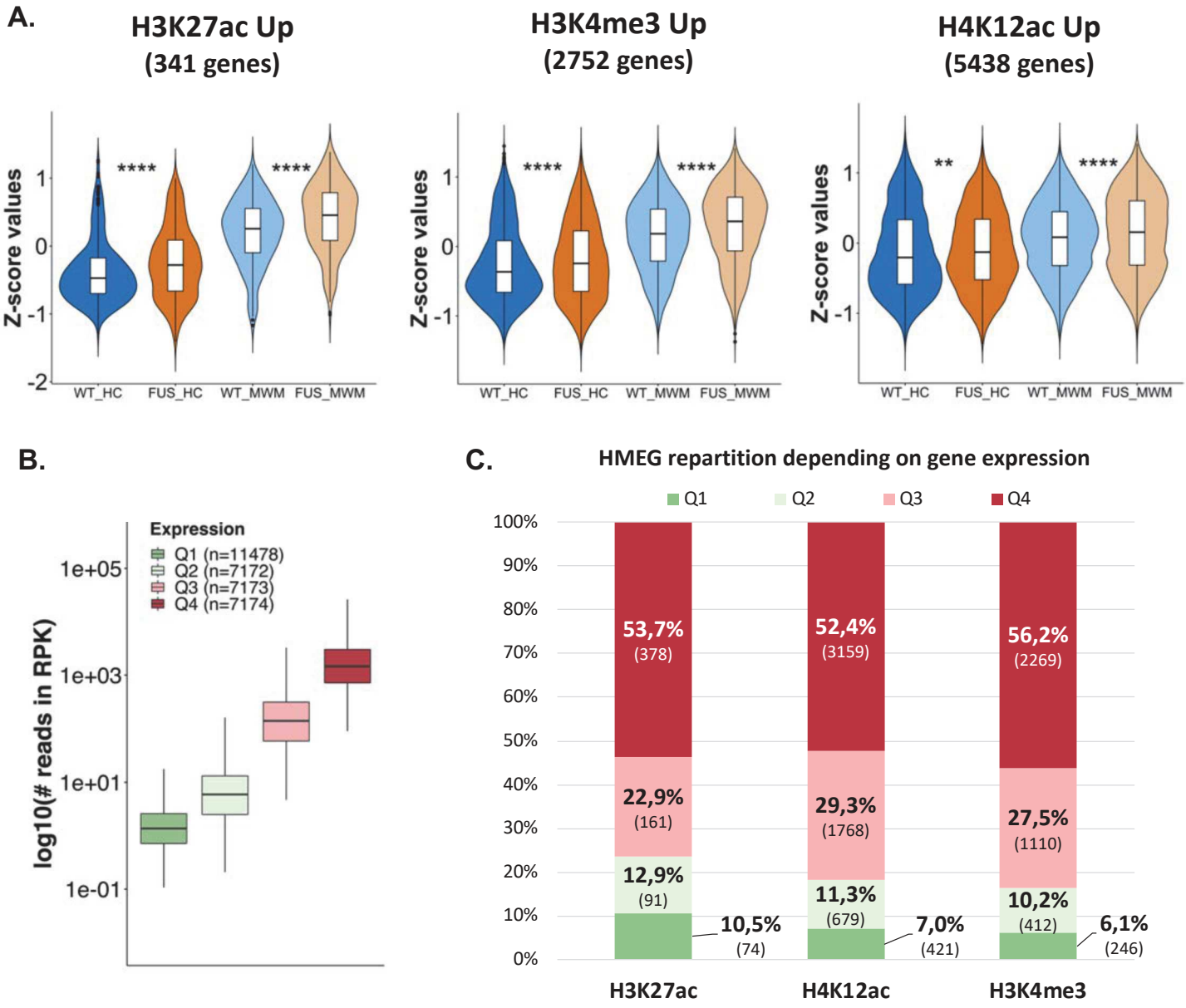

<u>Figure 4.</u> Histone Mark Enriched Genes (HMEG) display increased gene expression in FUS mice and are highly expressed genes.

(A) Z-score expression of all significant HMEG in the hippocampus, comparing WT (blue) and *Fus*$^{\Delta NLS/+}$ (orange) mice in both HC (dark color) and MWM (light color) conditions. (n=3 per group for RNA-seq). **p<0.01, ****p<0,0001 with the non-parametric Mann Whitney rank test.

(B) RNA-seq date separated into four groups (Q1 to Q4), Q1 = not expressed or lowly expressed (0-25%), Q2 = middle low expressed (25-50%), Q3 = middle high expressed (50-75%) and Q4 = highly expressed (75-100%). (n=3 per group).

(C) HMEG répartition (in percentage) within Q1-Q2-Q3 and Q4 groups. (n=3 per group for RNA-seq & for Chip-seq two replicates per histone mark).

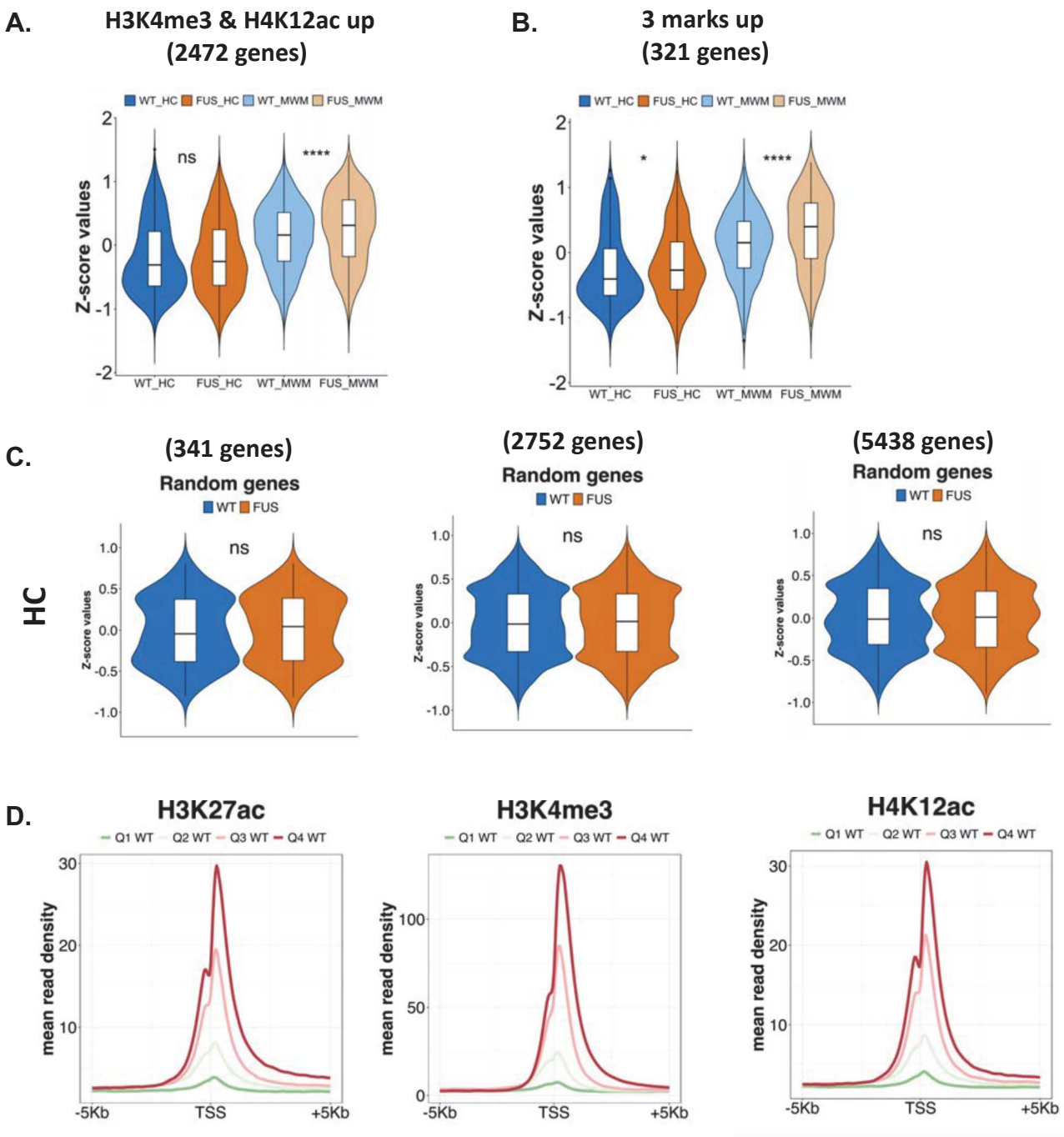

<u>Figure S8:</u> Histone mark profiles on Q1-Q2-Q3 or Q4 group and expression of random genes.

(A,B) Z-score expression of all significant co-localized H3K4me3 and H4K12ac HMEG (left) or all significant HMEH for the co-localization of the three marks (right) in the hippocampus, comparing WT (blue) and *Fus*$^{\Delta NLS/+}$ (orange) mice in both HC (dark color) and MWM (light color) conditions. (n=3 per group for RNA-seq). *p<0.05, ****p<0,0001 with the non-parametric Mann Whitney rank test.
(C) Z-score expression of random genes from the RNA-seq analyses. The same number of random genes than H3K27ac, H3K4me3 and H4K12ac (left to right) HMEGs in HC (top) and MWM (bottom) condition were used (n=3 per group). This analyses on random genes was performed 5 times with the same results.
(D) Mean H3K27, H3K4me3 and H4K12ac (from left to right) profiles at TSS relative to gene expression obtained from RNA-seq data. Expressed genes were separated into four groups (Q1 to Q4), Q1 = not expressed or lowly expressed (0-25%), Q2 = middle low expressed (25-50%), Q3 = middle high expressed (50-75%) and Q4 = highly expressed (75-100%). (n=3 per group for RNA-seq & for Chip-seq two replicates per histone mark).

Figure 5

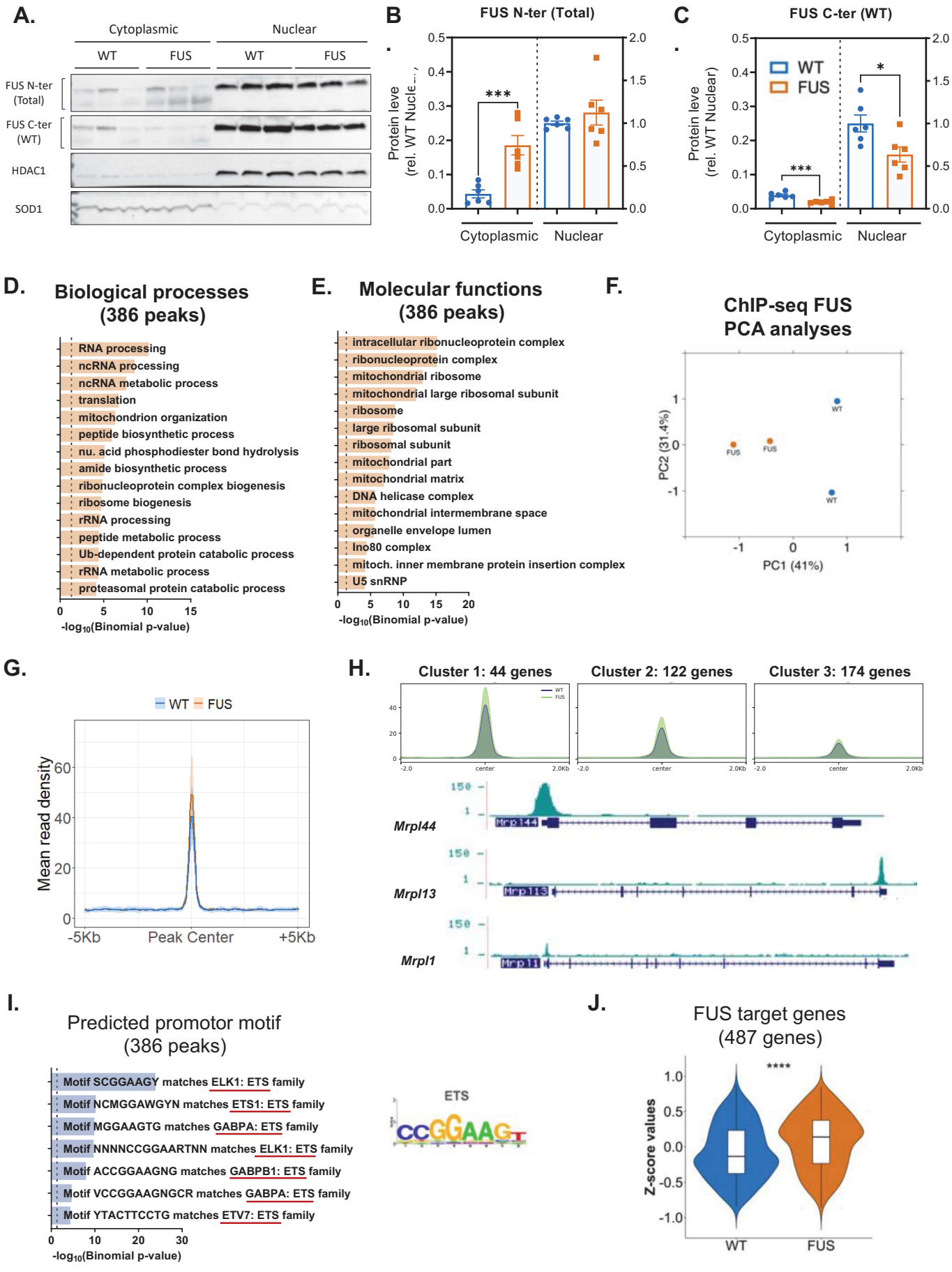
A.
Cytoplasmic
Nuclear
WT
FUS
WT
FUS
FUS N-ter (Total)
FUS C-ter (WT)
HDAC1
SOD1
B
FUS N-ter (Total)
Protein leve
(rel. WT Nucle
***
Cytoplasmic
Nuclear
C
FUS C-ter (WT)
Protein leve
(rel. WT Nuclear)
WT
FUS
*
***
Cytoplasmic
Nuclear
D.
Biological processes
(386 peaks)
RNA processing
ncRNA processing
ncRNA metabolic process
translation
mitochondrion organization
peptide biosynthetic process
nu. acid phosphodiester bond hydrolysis
amide biosynthetic process
ribonucleoprotein complex biogenesis
ribosome biogenesis
rRNA processing
peptide metabolic process
Ub-dependent protein catabolic process
rRNA metabolic process
proteasomal protein catabolic process
-log10(Binomial p-value)
E.
Molecular functions
(386 peaks)
intracellular ribonucleoprotein complex
ribonucleoprotein complex
mitochondrial ribosome
mitochondrial large ribosomal subunit
ribosome
large ribosomal subunit
ribosomal subunit
mitochondrial part
mitochondrial matrix
DNA helicase complex
mitochondrial intermembrane space
organelle envelope lumen
Ino80 complex
mitoch. inner membrane protein insertion complex
U5 snRNP
-log10(Binomial p-value)
F.
ChIP-seq FUS
PCA analyses
PC2 (31.4%)
PC1 (41%)
WT
FUS
G.
WT
FUS
Mean read density
-5Kb
Peak Center
+5Kb
H.
Cluster 1: 44 genes
Cluster 2: 122 genes
Cluster 3: 174 genes
Mrpl44
Mrpl13
Mrpl1
I.
Predicted promotor motif
(386 peaks)
Motif SCGGAAGY matches ELK1: ETS family
Motif NCMGGAWGYN matches ETS1: ETS family
Motif MGGAAGTG matches GABPA: ETS family
Motif NNNNCCGGAARTNN matches ELK1: ETS family
Motif ACCGGAAGNG matches GABPB1: ETS family
Motif VCCGGAAGNGCR matches GABPA: ETS family
Motif YTACTTCCTG matches ETV7: ETS family
-log10(Binomial p-value)
ETS
J.
FUS target genes
(487 genes)
****
Z-score values
WT
FUS

Figure 5. FUS ChIP-seq analyses in *Fus*$^{\Delta NLS/+}$ hippocampi showing that FUS is bound at the TSS of ETS-target genes associated with RNA-processing, ribosomal and mitochondrial functions.

(A-C) Western Blot analyses of the nucleo-cytoplasmic location of total (N-ter) FUS (A and B) and WT (C-ter) FUS (A and C) in both WT and *Fus*$^{\Delta NLS/+}$ mice at the age of 5 months. HDAC1 and SOD1 are respectively used for nuclear and cytopasmic protein control. Data are represented as mean ± SEM relative to WT HC nuclear expression (n = 6 per group). *p<0.05 , ***p<0.0001 using the unpaired t-test.
(D) PCA analyses of the FUS ChIP-seq, WT (blue) and *Fus*$^{\Delta NLS/+}$ (orange). Two biological replicates with n = mix of 2 hippocampi per replicate.
(E, F) GREAT analyses of the top 15 biological processes (E) and molecular functions (F) of FUS-bound genes in the hippocampus. Dash line represents Binomial adjusted p-value < 0.05.
(G) Mean gene profiles established with SeqMiner at the peak center for FUS. Mean profiles for WT in blue and *Fus*$^{\Delta NLS/+}$ in orange. Data are represented as mean ± SEM in blue (WT) or orange (*Fus*$^{\Delta NLS/+}$) shadow.
(H) Genome browser visualization of FUS binding on the TSS of mitochondrial ribosome genes : *Mrpl44*, *Mrpl13* and *Mrpl1* gene (from top to bottom). Example of one WT replicate.
(I) GREAT analyses of the top 15 predicted promotor motifs of FUS-bound genes in the hippocampus. Dash line represents Binomial adjusted p-value < 0.05. Predicted Promoter sequence of ETS (right).
(J) z-score expression of all FUS target genes in the hippocampus, comparing WT (blue) and *Fus*$^{\Delta NLS/+}$ (orange) mice in HC condition. (n=3 per group for RNA-seq). ****p<0.0001, with the non-parametric Mann Whitney rank test.

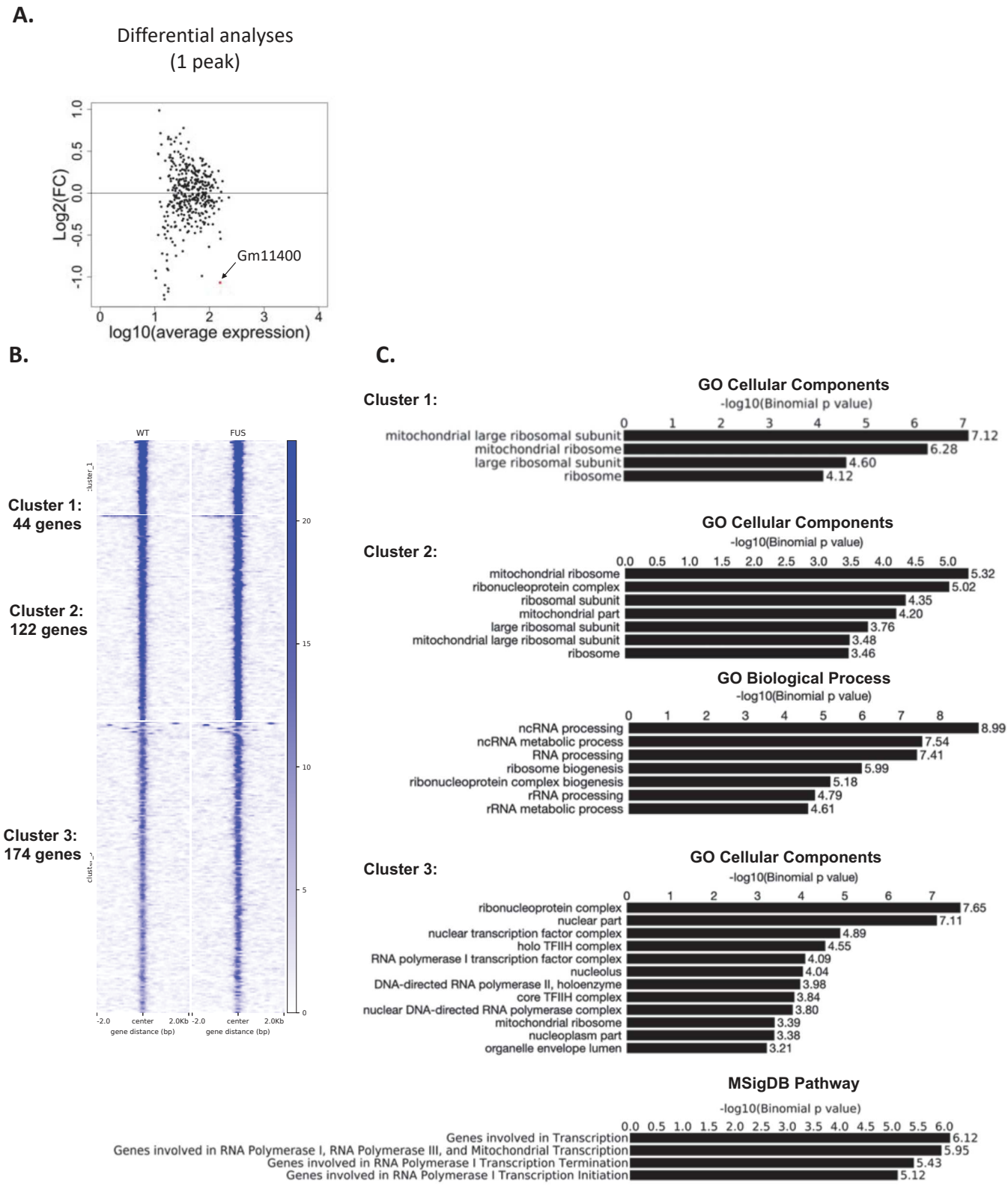

<u>Figure S9</u>: Differential analyses and clustering of FUS ChIP-seq data.

(A) Differential analyses of chromatin-bound FUS in the hippocampus using DESeq2 (Adj_p value<0.05). Peak calling was performed using MACS2. No differential binding of FUS is observed in *Fus*$^{\Delta NLS/+}$ compared to WT mice. Two biological replicates with n = mix of 2 hippocampi per replicate.
(B) Heatmaps and mean profile plots generated using plotHeatmap and plotProfile tools show FUS enrichment at the peak center. Three clusters were generated.
(C) GREAT 3.0.0. analyses of the 3 different clusters showing GOTERMS for cellular components and Biological Process, and MsigDB Pathways when significant.

Figure 6

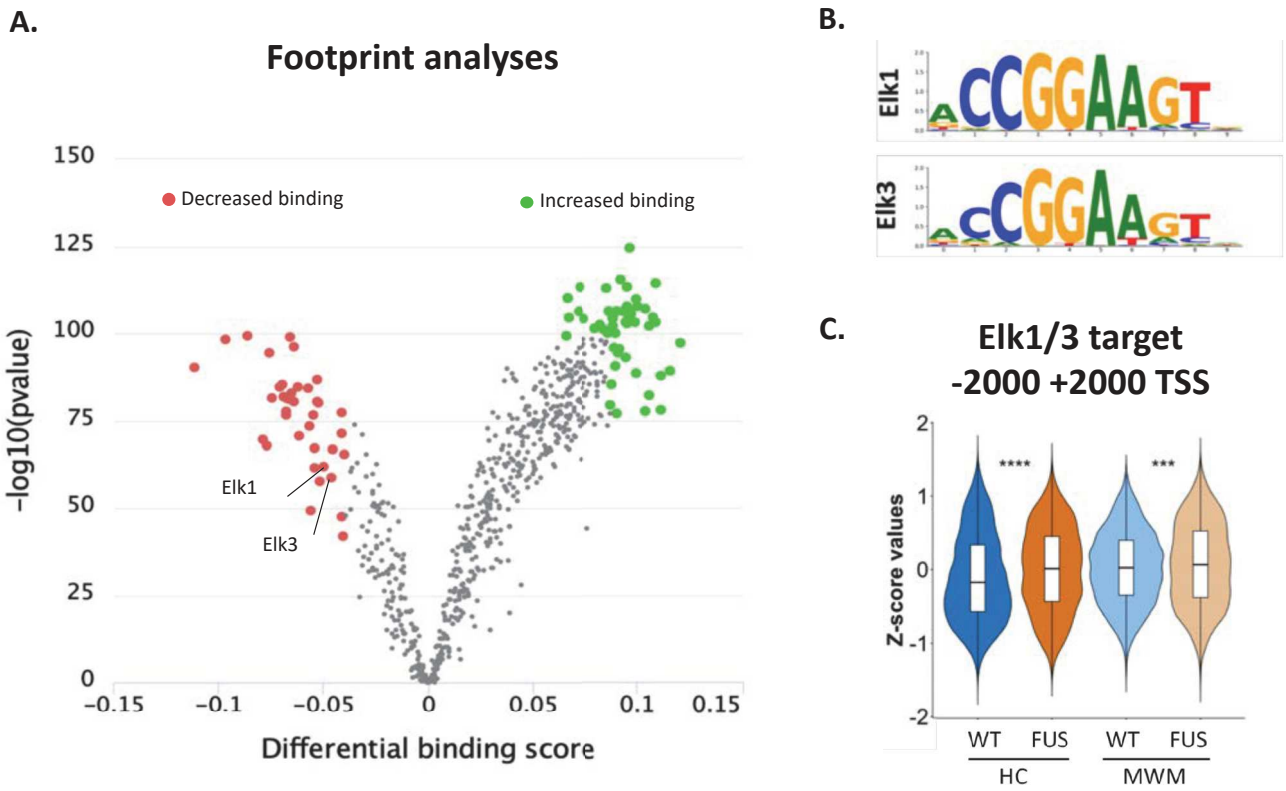

Figure 6: Altered transcription factor binding on the chromatin of *Fus*$^{\Delta NLS/+}$ mice.

(A) Footprint analyses performed with Tobias reveal decreased binding of Elk and increased binding of Mef transcription factors on the chromatine of *Fus*$^{\Delta NLS/+}$ mice. Four biological replicates with n = FANS sorted neurons of a mix of 4 hippocampi per replicate.

(B) Predicted promoter sequence of Elk1 (upper part), Elk3 (bottom part).

(C) Z-score expression of all Elk1-Elk2 target-genes in the hippocampus, comparing WT (blue) and *Fus*$^{\Delta NLS/+}$ (orange) mice in HC condition. (n=3 per group for RNA-seq). ***p<0.001, ****p<0.0001 with the non-parametric Mann Whitney rank test.

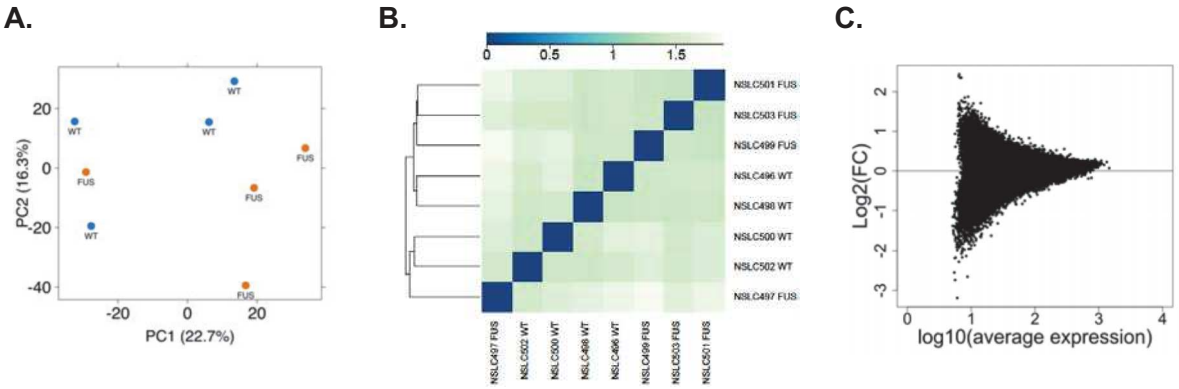

Figure S10: Open Chromatin region (OCR) analyses.

(A) PCA analyses of the ATAC-seq, WT (blue) and *Fus*$^{\Delta NLS/+}$ (orange). Four biological replicates with n = FANS sorted neurons of a mix of 2 hippocampi per replicate.

(B) Heatmap and dendrogram of ATAC-seq analyses. Using the Simple Error Ratio Estimate (SERE) score. Four biological replicates with n = FANS sorted neurons of a mix of 2 hippocampi per replicate.

(C) differential analyses of OCR in the hippocampus. Peak calling was performed using SICER p<0,003. No differences in OCR is observed in *Fus*$^{\Delta NLS/+}$ compared to WT mice. Four biological replicates with n = FANS sorted neurons of a mix of 2 hippocampi per replicate.

Scientific contribution 2:

Behavioral characterization of *Fus*$^{\Delta NLS/+}$ mice

(In preparation)

Tzeplaeff, L. et al,

MATERIEL AND METHODS

Animals

Experimental protocols and animal care followed the institutional guidelines (council directive 87/848, October 19, 1987, Ministere de l'agriculture et de la Forêt, Service Vétérinaire de la Santé et de la Protection Animale) and international laws (directive 2010/63/UE, February 13, 2013, European Community) and policies. APAFIS: 11229 (RôledeFUSdanslarégul_2017091118178028_v4)

Wild type and heterozygous *Fus*$^{\Delta NLS/+}$ male mice from C57BL/6 genetic background were generated in the animal facility of the Laboratory of Cognitive and Adaptative Neuroscience (LNCA, Strasbourg) as described previously (Scekic-Zahirovic et al. 2016). Mice were group-housed under a 12 light/dark cycle (light on at 7:00 a.m.), in a temperature and humidity-controlled room (22 ± 2 °C; 50% ± 5 humidity) with *ad libitum* access to food and water. Mice were single housed one week prior the test and habituated to handling a few min per day for 3 days. Handling was done with a tube for object tasks and with the experimenter's hand for water-based tasks. Five different cohorts of mice (cohort 1 to 5) were used for the behavioral characterization of the FUSΔNLS mutation, and each cohort was systematically weighed at the age of 5 months.

Locomotor activity

Mice, both genotype were tested for locomotor activity at 3 months of age (cohort 1, n = 11 FUS and n = 12 WT). Mice were not handled prior the test to study spontaneous locomotor activity during two consecutive days.

Actigraphy, the day of the test, mice are single housed in individual cages (29,5 x 11,5 x 13 cm). Each cage is place on a rack with infrared photocells on each extremity of the cage (front and back part). The number of infrared beams breaks due to the mouse is summed every 10 min

(homemade apparatus and software, LNCA). Mice were recorded for 52h? with the first 3 hours dedicated the analysis of locomotor habituation.

Analyses, the locomotor activity of mice was analyzed in terms of average number of beam breaks per hour or per period (Night or Day). Data were represented as mean ± standard error of the mean (SEM). Values of $p < 0.05$ were considered significant. Graphics and statistical analyses were performed using GraphPad Prism 8 (GraphPad, CA). The normality was tested with the Shapiro-Wilk test. The mean movement per hour between genotypes was analyzed using repeated two-way ANOVA considering the factors of "genotype" (WT vs FUS) and "hour" followed by a Šidák correction for multiple comparisons. Mean beam breaks per period (Night or day) was analyzed between genotype with the unpaired t-test.

Anxiety test

Mice, At the age of 5 months *Fus*$^{\Delta NLS/+}$ mice and their WT littermates were tested for anxiety like behavior, either in the elevated plus maze (cohort 3, n = 7 FUS and n = 12 WT), or in the Light/Dark box (cohort 2, n = 10 animal per genotype). To study spontaneous anxiety behavior, mice were not handling prior testing. Mice were place in the behavioral room 30 min before the beginning of the test.

Elevated plus maze, The apparatus is a plus shape device composed of two open arms (lit compartments) and two closed arms (dark compartment) raised 53 cm above the floor. Each arm is 35 cm long and 5 cm large and the close arms are surrounded by 14.?5 cm high black and opaque walls. A central platform (5 x 5 cm) connects both the open and closed arms arranged in a plus shape. The entire apparatus is placed in the empty MWM tank. Mice were allowed to move freely in the apparatus for 10 min.

Light/Dark box, the apparatus is composed of two compartments connected by a tunnel. One compartment is completely closed, opaque and dark, while the other compartment with transparent walls and cover was exposed to light (1000 Lux at floor level). Mice were first introduced in the dark room and were able to move freely between both compartments for 5 min.

Analyses, Data were collected by the ANY-maze (Ugo Basile) video tracking system. For the Plus maze, the duration, and the number of entries in each arm was analyzed. For the Light/dark box, the latency to first enter the light area, as well as the duration and the number of entries in each compartment was analyzed. Data were represented as mean ± standard error of the mean (SEM). Values of $p < 0.05$ were considered significant. Graphics and statistical analyses were performed using GraphPad Prism 8 (GraphPad, CA). The normality was tested with the Shapiro-Wilk test. The difference between time spent in the different zone were analyze with the unpaired t-test, and differences between the number of entries in the different areas was analyzed using the unpaired Man-Whitney rank test.

Object tests

Mice, two cohorts (cohort 2 and 4) of 5 month of age mice were used for the different object tests. Cohort 4 (n = 12 per genotype) was used in the novel object recognition (NOR) task with a 3h probe test, the new object location (OL), the object in place (OiP) and the temporal order memory (TOM) task. Cohort 2 was used to test novel object recognition (NOR) with a 24h probe test (cohort 2, n= 10 per genotype). Mice were maintained in a room next to the behavioral room 3 days before and for the duration of the experiment. The NOR test for cohort 2 and cohort 4 were done on different days. The open field and the objects were cleaned with 30% ethanol and rinsed with water between each animal to ensure the absence of olfactory cues. For each test, new sets of objects (size, color, shape, texture…) were presented to the mice. Only one test per day were assess.

Habituation, before exposition to any object each cohort were familiarized for 15 min to an open field (52 x 52 x 40 cm) with a visual cue placed on one of the four walls.

Novel object recognition (NOR), two identical objects (A1 and A2) were placed symmetrically, face to face, at the same distance of the center, in the open field for the acquisition phase. Mice were allowed to explore the two objects during 10 min before returning to their home cage for either 3 hours (cohort 4), or 24 hours (cohort 2). For the retention phase, mice were re-introduced for another

10 min in the box where they were exposed to one familiar (A) and one new (B) object placed at the same locations as the previous objects.

Object location (OL), for the acquisition phase, three different objects were placed at 10 cm from three of the four corners of the open field. Mice were allowed to visit the objects during 10 min before returning to their home cage. The retention phase was performed 3 hours later. Mice were re-introduced for 10 min in the open field where one of the three objects has been moved to the opposite available corner.

Object in place (OiP), On day four, during the acquisition phase, two different objects (A and B) were placed symmetrically, face to face, at the same distance from the center of the open field. Mice were allowed to explore each object during 15 min and were brought back in their home cage for 5 min. During the retention phase, two identical objects were presented to the mice (B1 and B2) at the exact same position as the previous ones. For 15 min mice were allowed to interact with both objects.

Temporal order memory (TOM), On day five, mice were exposed to two different acquisition phase of 10 min followed by a retention phase of 10 min. During the first acquisition phase, two identical objects (A) were placed symmetrically, face to face, at 10 cm from two opposite corners of the open field. Mice spent 1 hour in their home cage between the two acquisition phases. For the second acquisition phase, the objects were replaced by two other objects, both identical (B). After a period of 1 hour, mice were re-introduced into the open field for the retention phase. This time, mice were exposed to one of each object (A and B) presented during the two acquisition phases. Objects were always placed at the same position during each phase of the test.

Analyses, Data were collected by the ANY-maze (Ugo Basile) video tracking system. The experimenter manually recorded time exploring object during the video recording and later analyze result while being blind to the genotype. During habituation, time spent in each of the center or border zone, as well as total distance travel were quantified. The time exploring each object was recorded during all acquisition and retention phases and results were represented in total % of time exploring the novelty-associated object. Data were represented as mean ± standard error of the mean (SEM). Values of $p < 0.05$ were considered significant. Graphics and statistical analyses were performed using GraphPad Prism 8 (GraphPad, CA). The normality was tested with the Shapiro-Wilk test. Differences between genotypes concerning the % of time

exploring the novelty-associated object was analyzed using the unpaired t-test. The % of time exploring the novelty-associated object was also compared to chance level (i.e., 50% for NOR, OiP and TOM and 33% for OL) with the one sample t-test. Time exploring each object in the OL retention task was analyzed using the two-way ANOVA, using genotype and object as factor, followed by a post-hoc Tukey correction for multiple comparisons. Differences in time exploring the old and new object for the 3h and 24h NOR recognition test were also analyzed with the linear mixed model to identify slop differences for each genotype and between genotypes.

Morris water maze test

Mice, Wild type and heterozygous *Fus*$^{\Delta NLS/+}$ mice of 5 months of age were used for the Morris Water Maze experiment (cohort 4, n=12 animal per genotype). Each day, mice were place in the room 30 min before the start of the experimentation. Between each trial, mice were placed under a heat lamp to prevent hypothermia and to dry properly.

Habituation, A circular pool of 160 cm of diameter and 60 cm of height is located in the center of the room. The pool is virtually divided in four equal quadrants (SE, NE, NW, and SW) and is surrounded by differentially shaped and colored distal visual cues on the walls. The pool is first filled with only 5 cm water (21°C). A visible platformed is located in the NW quadrant (diameter 10 cm, 1cm above the surface). Starting from the middle of the pool, mice have 60s to find the platform. If the mice failed to locate the platform, they are gently brought/guided? on it. Mice must remain 10s on the platform before to returning to their home cage.

Forced swim, The pool was filled with up to 20 cm water below the border so that mice are able to see the visual cues on the walls. The platform was removed, and mice performed a 2-min swimming trial, starting from the middle of the pool. This step ensures that all mice are able to swim and that there is no quadrant preference.

Acquisition, the next day, mice were trained to perford the hidden-platform version of the spatial Morris Water Maze for 6 consecutive days. The platform was place 1 cm below the water surface and the water was opacified with Medon white to avoid visualization of the hidden platform. The hidden platform was first located in the SE quadrant. Mice were trained 4 trials a day for 6 days,

with an intertrial interval of 2-5 min between 60s-cut off trials. after 60s, mice were guided to the platform. After 10s on the platform, mice returned in their home cage. For each 4-trial session, the mice started the test from one of the 4 cardinal points (North (N), Est (E), South (S), and West (W)) at the edge of the pool, facing the wall. The sequence of the starting points was randomized each day.

Reversal, after 6 days of training with the hidden platform in the SE quadrant, the platform was moved to the opposite NW quadrant and mice were further trained to find the hidden platform for 3 consecutive days. Mice were trained the same way as explained above.

Probe trial, the platform was removed, and mice were tested for memory retention with a 60-s probe test at two different time points. The first probe test was performed during acquisition phase, on day 4, 24h after the last training of day 3. The second test for memory retention was performed after the reversal, 24h after the last training of day 3. At the end of the first probe test, the platform was automatically brought to its original position after 60s (Platform connected to an Anymaze software, Ugo Basile) so that mice are able to naturally find it and thus avoid extinction of the platform position.

Analyses, Data were collected by the ANY-maze (Ugo Basile) video tracking system. Average speed and distance travelled to reach the SE target platformed were analyzed for the acquisition phase. Time spent in the different quadrants, average distance from the target platform and annulus crossings were analyzed for memory retention tests. Data are represented as mean ± standard error of the mean (SEM). Values of $p < 0.05$ were considered significant. Graphics and statistical analyses were performed using GraphPad Prism 8 (GraphPad, CA). Data normality distribution was tested with the Shapiro-Wilk test. Performances recorded during acquisition (distance and mean speed) were analyzed using repeated two-way ANOVA (“genotype” (WT vs FUS) and “day” factors) followed by Šidák correction for multiple comparisons. Mean time spent in the different quadrants was analyzed using two-way ANOVA with Šidák correction for multiple comparisons. Mean distance to platform was analyzed with the unpaired t test and the number of crossing annulus with the non-parametric unpaired Mann-Whitney rank test. Time spent in quadrant was also compared to chance (i.e., 15 s) with the one sample t test.

Double H test

Mice, At the age of 5 months, *Fus*$^{\Delta NLS/+}$ mice and their WT littermates were tested for procedural memory (cohort 5, n = 7 FUS and n = 9 WT). Each day, 30 min before starting the experiment, mice were place in the testing room for habituation. Between each trial, mice were allowed placed under a heat lamp to prevent hypothermia.

Habituation, the double-H apparatus is made of transparent plexiglass and composed of three parallel arms (55 x 10 x 25) all connected by a central zone (100 x 10 x 25). The two extremities of the middle arm are by convention called North (N) and South (S) arm. The extremities of the two other arms are called NW, SW and NE, SE. The double H apparatus is place into the MWM tank so that mice have access to the different visual cues place on the walls. The first day, the apparatus was filled with fresh water (21°C). Access to the NW-SW arm was blocked with a movable transparent plexiglass door and a visible platform was placed at the end of the NW arm. During 4 consecutive trials, mice were trained to swim to the NW target platform, starting from the SW arm. The trials lasted maximum 60s and mice were returned to their home cage after a 10s-stay on the target platform.

Acquisition, the water of the double H was opacified with Medon white. The platform was moved to the extremity of the NE arm and placed 1cm below the surface. The movable transparent plexiglass door was relocated to block the access to the N central arm. During the 2 first days, mice had 1 session of 4 trials per day (2-5 min intertrial interval). However, on day 3 and 4 mice had one session of 4 trials in the morning and another session of 4 trials in the afternoon to ensure proper procedural learning. During each session of 4 trials, mice started from the S arm and were able to swim freely in the water for a maximum of 60s. If mice failed to find the NE target platform, they were gently guided to the platform and after 10s, they were returned to their home cage.

Probe trial, Memory retention of the procedural information was tested on day 5, 24 hours after the last training. The platform was removed from the apparatus and the movable transparent plexiglass door was relocated to block the access to the NW arm. Mice were place in the SW arm to start the test. Thus, if mice remembered the procedural information, they would directly swim

to the N arm (Procedural arm), whereas if they remember the spatial location of the platform, they would directly swim to the NE arm (Spatial arm).

Analyses, Data were collected by the ANY-maze (Ugo Basile) video tracking system. The distance travelled to reach the NE target platformed and the number of errors were analyzed for the acquisition phase. Since mice were trained in a procedural task, the correct path was "turn right then left in the N arm". An error was counted if the mouse first turned on the left, and another error was counted if the mouse entered the NW, SW and/or the SE arm. Thus, we could count a maximum of 4 errors since each type of error was only counted once. During the probe test, time spent in each of the Procedural (N) and Spatial (NE) arms and latency to first enter the Spatial arm (NE) was analyzed. The first and second arm entered was also noted for each mouse. Data are presented as mean ± standard error of the mean (SEM). Values of $p < 0.05$ were considered significant. Graphics and statistical analyses were performed using GraphPad Prism 8 (GraphPad, CA). Normality distribution of the data was tested with the Shapiro-Wilk test. Time in each arm and latency of the first entry into the Spatial (NE) arm was analyzed by the unpaired t-test. Time spent in both the Procedural (N) and Spatial (NE) arms were also compared to chance level of 8.5 s (i.e., defined as the total time of the probe (60s) divided by the number of arm available for a visit (NE, SE, Center E, N, S, Center W, and SW)) with the one-sample t-test.

RESULTS

I. Body weight reduction and early hyperactivity behavior in *Fus*$^{\Delta NLS/+}$ mice

For the purpose of our study we used the *Fus*$^{\Delta NLS/+}$ mouse line previously described our previous studies (Scekic-Zahirovic et al., 2016) (Scekic-Zahirovic et al., 2017) (Scekic-Zahirovic et al., 2021) (Sanjuan-Ruiz et al., 2021). Each of the five cohorts of mice we used was weighed at the age of 5 months and one cohort (cohort 5) was weighed on a monthly basis to follow weight gain across time (Figure 1A). Each cohort of *Fus*$^{\Delta NLS/+}$ mice showed reduced body weight at the age of 5 months compared to their WT mice (Cohort 1: $p = 0.0895$, Cohort 2: $p = 0.0019$, Cohort 3: $p = 0.0372$, Cohort 4: $p = 0.0144$ and Cohort 5: $p = 0.0008$). *Fus*$^{\Delta NLS/+}$ mice weighed on a monthly basis indeed demonstrated a significant decrease in body weight gain (cohort 5: *Fus*$^{\Delta NLS/+}$ vs WT: $p = 0.0123$), already visible at the age of 2 months (cohort 5, 2 months: *Fus*$^{\Delta NLS/+}$ vs WT: $p = 0.0290$) (Figure S2).

At 3 months of age mice were tested for spontaneous locomotor activity (cohort 1, see Figure S1). The 3 first hours served as habituation in the new environment. We observed that *Fus*$^{\Delta NLS/+}$ mice have increased locomotor activity compared to WT during the first hour of habituation ($p=0.0395$), while both genotype calm down and significantly reduced their movement after 3 hours of habituation (Time $p < 0.0001$), Figure S3. Locomotor activity was further recorded for 48 consecutive hours. Our result shows an almost two time increase in mean movement per hour between *Fus*$^{\Delta NLS/+}$ mice and their WT littermates (*Fus*$^{\Delta NLS/+}$ vs WT: $p < 0.0001$) (Figure 1C). This effect was observed during both the nocturnal active period ($p < 0.0001$) and the diurnal inactive period ($p = 0.0244$) of mice (Figure 1B). These results are in accordance with previously published data showing increase locomotor activity in *Fus*$^{\Delta NLS/+}$ mice at the ages of 4 and 10 months (Scekic-Zahirovic et al., 2021), suggesting that both low weight and hyperactivity might be the first symptoms in *Fus*$^{\Delta NLS/+}$ mice.

II. FusΔNLS mutation has no effect on anxiety

Mice were also tested for anxiety-like behavior in both the elevated plus maze (Cohort 3, Figure S1) and the light dark box (Cohort 2, Figure S1). No behavioral difference was observed in the elevated plus maze (Figure 2B) and in the light/dark box (Figure 2C).

III. *Fus*$^{\Delta NLS/+}$ mice have difficulties in discriminating the "what", "where" and "when" components of memory

In our previous data we demonstrated memory dysfunctions associate with cortical and hippocampal alterations in *Fus*$^{\Delta NLS/+}$ mice (Scekic-Zahirovic et al., 2021) (Tzeplaeff et al., in preparation). Also, different mouse model harboring human FUS mutations demonstrate a decreased discrimination ability in the novel object recognition (NOR) test (López-Erauskin et al., 2018) (Munter et al., 2020) (Ho et al., 2021). Object-related tests indeed allow investigation of various aspects of learning and memory in mice. In our study we tested the What Where and When components of memory. Before exposition to test object, mice were allowed to habituate in the open field. We observed that *Fus*$^{\Delta NLS/+}$ mice spent a longer time in the center zone of the open field compared to WT mice ($p = 0.0115$), (Figure 2A), while no difference concerning the distance traveled was observed between groups (result shown for the cohort 4).

Mice were then tested for object recognition memory (What?) in the NOR task (Figure 3A). Long term memory (LTM) was tested at two time points. Recent LTM was tested 3 hours after initial exposure (cohort 4, Figure S1 & Figure 3B), and remote LTM was tested 24 hours after initial exposure (cohort 2, Figure S1 & Figure 3C). There was no specific novel object LTM alteration in *Fus*$^{\Delta NLS/+}$ mice whatever the time point. Both genotypes spend significantly more than half of the time exploring the novel object (Probe 3H *vs* chance level: WT $p < 0.0001$ & *Fus*$^{\Delta NLS/+}$ $p = 0.0040$) (Probe 24H *vs* chance level: WT $p < 0.0001$ & *Fus*$^{\Delta NLS/+}$ $p = 0.0004$). However, analyses of the time exploring the new and the familiar object with the linear mixed model demonstrated significant differences in how *Fus*$^{\Delta NLS/+}$ mice explore the new object (Probe 3H: slop WT vs *Fus*$^{\Delta NLS/+}$ $p = 0.0015$) (Probe 24H: slop WT vs *Fus*$^{\Delta NLS/+}$ $p = 0.0278$).

Then, to study if *Fus*$^{\Delta NLS/+}$ mice can detect a change in object position (Where?) we assessed the object location (OL) test (cohort 4, Figure S1) and tested memory retention after a delay of 3 hours (Figure 3D). Even if *Fus*$^{\Delta NLS/+}$ mice and their WT littermates demonstrated significant

preference for the moved object when compared to chance level (WT vs chance p = 0.0104 & *Fus*$^{\Delta NLS/+}$ *vs* chance p = 0.0001), *Fus*$^{\Delta NLS/+}$ mice explored equally the new object and object 2 (Figure 3E). Thus, while WT displayed an exclusive preference for the moved object, *Fus*$^{\Delta NLS/+}$ mice did not discriminate between the moved object and the unmoved object 2.

The object in place (OIP) test evaluate object place associative memory (cohort 4, Figure S1) testing the "what" and "where" associative component of memory (Figure 3F). After a 5 min retention delay, *Fus*$^{\Delta NLS/+}$ mice were unable to detect a change in object place association (WT vs chance p = 0.0107 & *Fus*$^{\Delta NLS/+}$ *vs* p = 0.3300; *Fus*$^{\Delta NLS/+}$ *vs* WT: p < 0.0111), (Figure 3G).

Finally, we investigated the ability of *Fus*$^{\Delta NLS/+}$ mice in detecting which object was presented first (What & When?), in the Temporal order memory (TOM) (cohort 4, Figure S1 & Figure 3H). While WT mice showed a preference for the first presented object (WT vs random p = 0.0312), *Fus*$^{\Delta NLS/+}$ mice explored equally the two objects which suggest that *Fus*$^{\Delta NLS/+}$ mice were unable to identify which one was presented first (*Fus*$^{\Delta NLS/+}$ *vs* random p = 0.4383), (Figure 3I). Time exploring each object during acquisition I represented in Figure S4A-E.

IV. *Fus*$^{\Delta NLS/+}$ mice demonstrate delayed spatial learning in the MWM

Fus$^{\Delta NLS/+}$ mice show reduced spatial memory acquisition and retention in the Morris Water maze (MWM) (Scekic-Zahirovic et al., 2021) (Tzeplaeff et al., in preparation). Thus, we further decided to characterize different aspects of spatial memory (cohort 4, Figure S1). Same as previously described, we observed reduced acquisition performances in the MWM (*Fus*$^{\Delta NLS/+}$ *vs* WT: p = 0.0126), (Figure 4A). During the acquisition phase, recent LTM retention was tested 24h after the 3rd day of MWM (Probe 1). While WT mice showed a clear preference for the target quadrant after only three days of training (WT vs random p = 0.0080), *Fus*$^{\Delta NLS/+}$ mice were unable to do so (*Fus*$^{\Delta NLS/+}$ *vs* random p = 0.1657; *Fus*$^{\Delta NLS/+}$ *vs* WT: p < 0.0111), (Figure 4B).

Then, to analyze memory flexibility and strategy switching, more dependent on the frontal cortex, we changed the position of the platform from the SE to the opposite NW quadrant after 6 days of learning and further trained the mice to find the platform for three more days. Although WT mice seemed to learn faster the new position of the platform, there was no significant differences across genotypes (*Fus*$^{\Delta NLS/+}$ *vs* WT: p = 0.2152, day effect and interaction?). Recent LTM was also tested 24 hours after the 3rd day of reversal learning. Both genotypes were able to discriminate the target NW-reversal quadrant (Figure 4C). However, *Fus*$^{\Delta NLS/+}$ were less accurate

in their search for the platform as demonstrated by a reduced number of annulus (*Fus*$^{\Delta NLS/+}$ *vs* WT: p = 0.0328) and platform crossing (*Fus*$^{\Delta NLS/+}$ *vs* WT: p = 0.0511), (Figure 4D, E).

V. *Fus*$^{\Delta NLS/+}$ mice demonstrate delayed procedural learning in the double H

Besides neurodegeneration of the frontal and temporal cortex, FTD-FUS patients demonstrate predominant atrophy of the striatum (Snowden et al., 2011). Since the striatum is necessary for procedural learning (knowing how ?), we decided to test *Fus*$^{\Delta NLS/+}$ mice in the double H maze (cohort 5, Figure S1), designed in our laboratory for rats and adapted here for mice (Kirch et al., 2015), (Figure 5A). Mice were trained 4 days to start from the S arm and first turn right then left to find the hidden platform in the NE arm. During the acquisition phase, we observed a significant genotype difference (*Fus*$^{\Delta NLS/+}$ *vs* WT: p = 0.0378), (Figure 5B). While WT mice already demonstrated a decreased number of errors on the 2nd day of acquisition, *Fus*$^{\Delta NLS/+}$ mice still made the same number of error as the first day (Day 2: *Fus*$^{\Delta NLS/+}$ *vs* WT: p = 0.0066) and only showed reduced errors on the 3rd day of acquisition (Figure 5C). Thus, *Fus*$^{\Delta NLS/+}$ mice demonstrate delayed learning compared to their WT littermates. We then tested recent LTM retention 24 hours after the last day of training. For this purpose, the starting point switched from the S to the SW arm. Normal mice preferentially rely on a procedural learning-based strategy (turn right then left in the N arm, named here procedural arm). If procedural learning is affected, mice may adopt a spatial learning-based strategy (go straight to the NE arm, named here spatial arm) to find the platform. We observed no differences in memory retention between the two genotypes. Both *Fus*$^{\Delta NLS/+}$ mice and WT littermate directly swam into the procedural arm (N), (Figure 5F), and spent significantly more time in this arm compared to chance (8.5s) (WT *vs*: p < 0.0124 *Fus*$^{\Delta NLS/+}$ vs p = 0.0220), (Figure 5D). After a short delay (~20-25sec), mice left the procedural (N) arm for the spatial (NE) arm where the platform was previously located (Figure 5E, F). Thus, both genotypes demonstrated good flexibility and adaptation to the new situation.

Figure 1

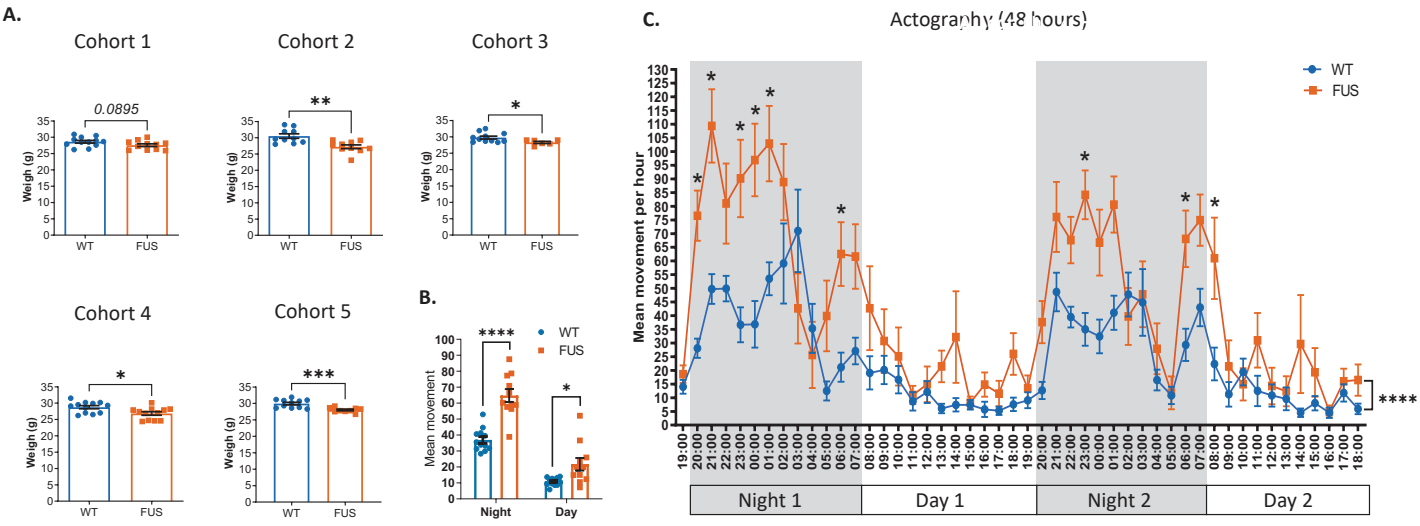

Figure 1. FUSΔNLS mutation results in decreased body weight and increased global locomotor activity

(A) Bargraphs representing the weight of WT and $FUS^{\Delta NLS/+}$ mice at 5 months of age for each cohort used in this study. Data are represented as mean ± SEM. Cohort 1 , n = 12 WT & 11 $FUS^{\Delta NLS/+}$; Cohort 2, n = 10 per group; Cohort 3 , n = 12 WT & 7 $FUS^{\Delta NLS/+}$; Cohort 4, n = 12 per group; Cohort 5, n = 11 WT & 9 $FUS^{\Delta NLS/+}$. *p<0.05, **p<0.01, ***p<0.001 using the unpaired t test.

(B) Mean movement per hour, calculated by the actigraphy, during the dark phase (Night) and the light phase (Day) at 3 months of age. Data are represented as mean ± SEM (n = 12 WT & 11 $FUS^{\Delta NLS/+}$). *p<0.05, ****p<0.0001 using the repeated two-way ANOVA with Šidák correction for multiple comparisons.

(C) Actography representing the mean movement per hour for both $FUS^{\Delta NLS/+}$ and WT littermates on 48 consecutive hours. The dark phase is represented with grey shadow and the light phase is left without any shadow. Data are represented as mean ± SEM (n = 12 WT & 11 $FUS^{\Delta NLS/+}$). *p<0.05, ****p<0.0001 using the repeated two-way ANOVA with Šidák correction for multiple comparisons.

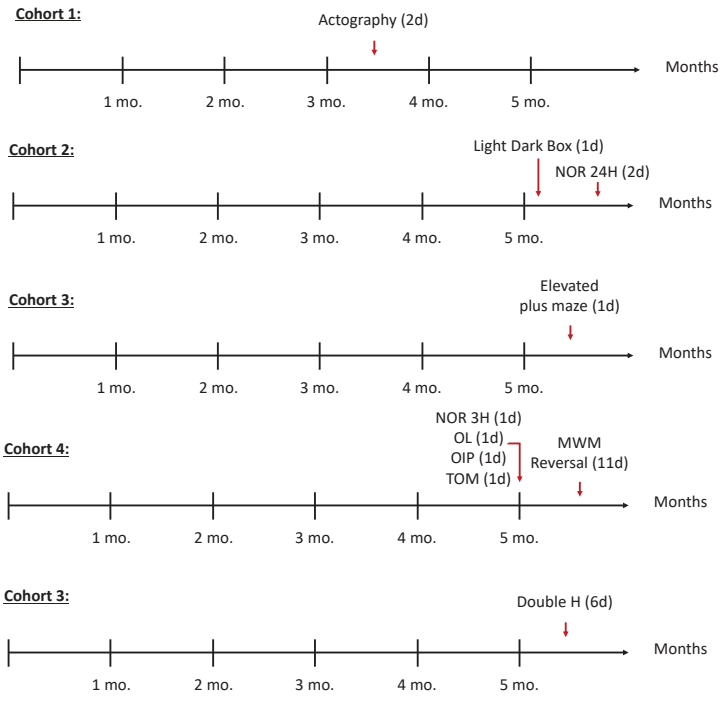

Figure S1. Experimental design of the different cohorts

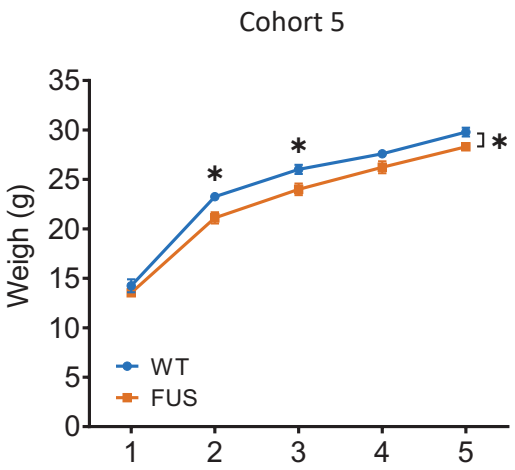

Figure S2. reduce weigh gain in FUS$^{\Delta NLS/+}$ mice

Weight gain per month from weaning to 5 months of age in WT and *Fus*$^{\Delta NLS/+}$mice. Data are represented as mean ± SEM (n = 12 WT & 7 FUS$^{\Delta NLS/+}$). *p<0.05 using repeated two-way ANOVA with Šidák correction for multiple comparisons.

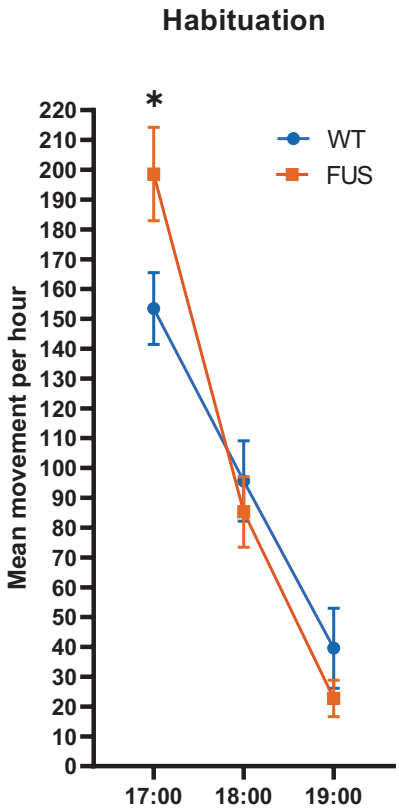

Figure S3. 3-hour habituation before actography recording

Graphic showing the 3 first hours (habituation) of mean movement in the actography rack for WT and *Fus*$^{\Delta NLS/+}$mice at the age of 3 months. Data are represented as mean ± SEM (n = 12 WT & 11 FUS$^{\Delta NLS/+}$). *p<0.05 using repeated two-way ANOVA with Šidák correction for multiple comparisons.

Figure 2

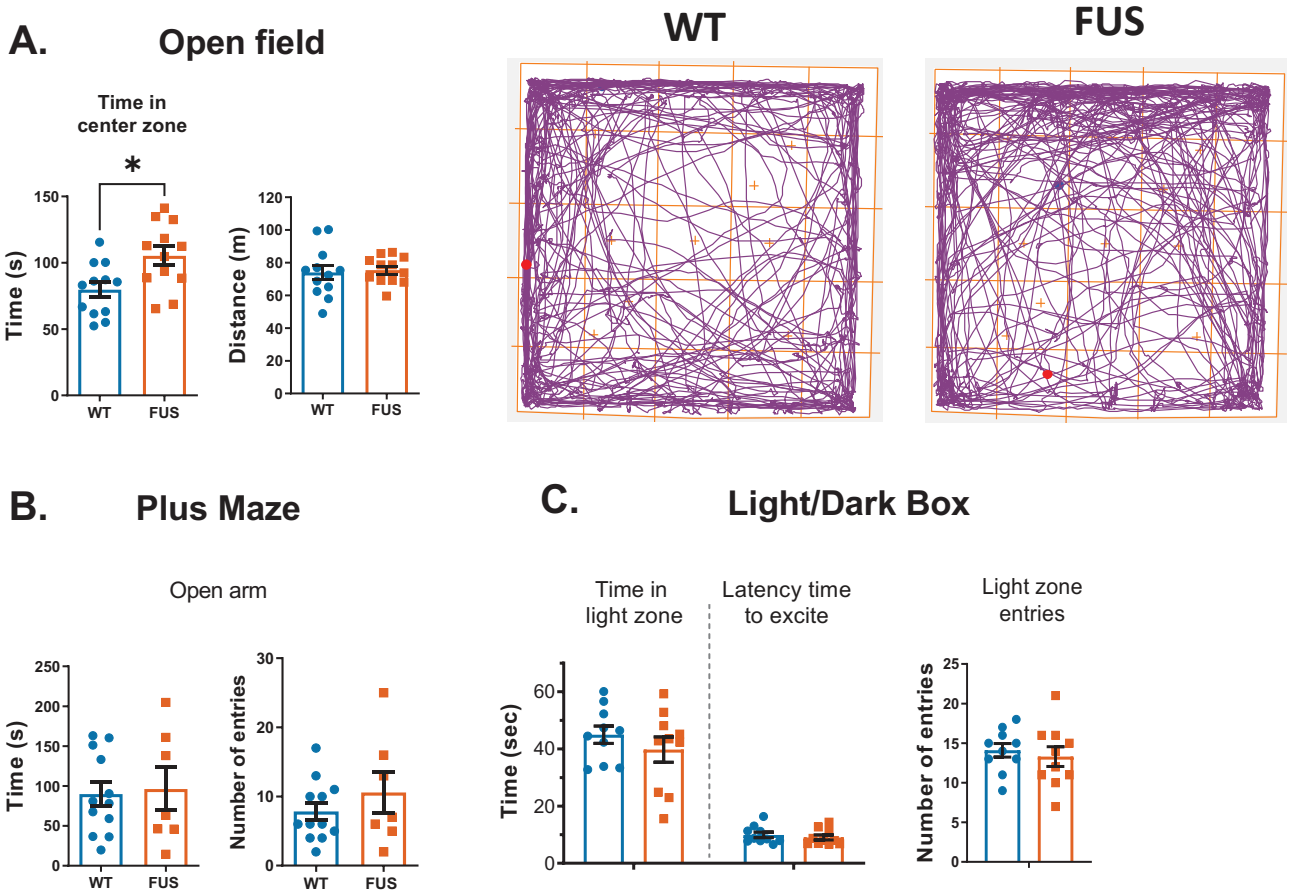

Figure 2. FUS mutation does no affect anxiety.

(A) Total distance travelled and time in the center zone of the Open field (left). Representative behavior of WT and $FUS^{\Delta NLS/+}$ mice in the open field. Bargraph data are represented as mean ± SEM (n = 12 per group). *p<0.05 using unpaired t test.

(B) Time and number of entries in the open arm of the elevated Plus maze. Data are represented as mean ± SEM (n = 12 WT & 7 $FUS^{\Delta NLS/+}$). Tested using unpaired t test.

(C) Light dark box : time in the light zone, latency to first exit and number of entries in the lit area. Data are represented as mean ± SEM (n = 10 per group). Tested using unpaired t test.

Figure 3

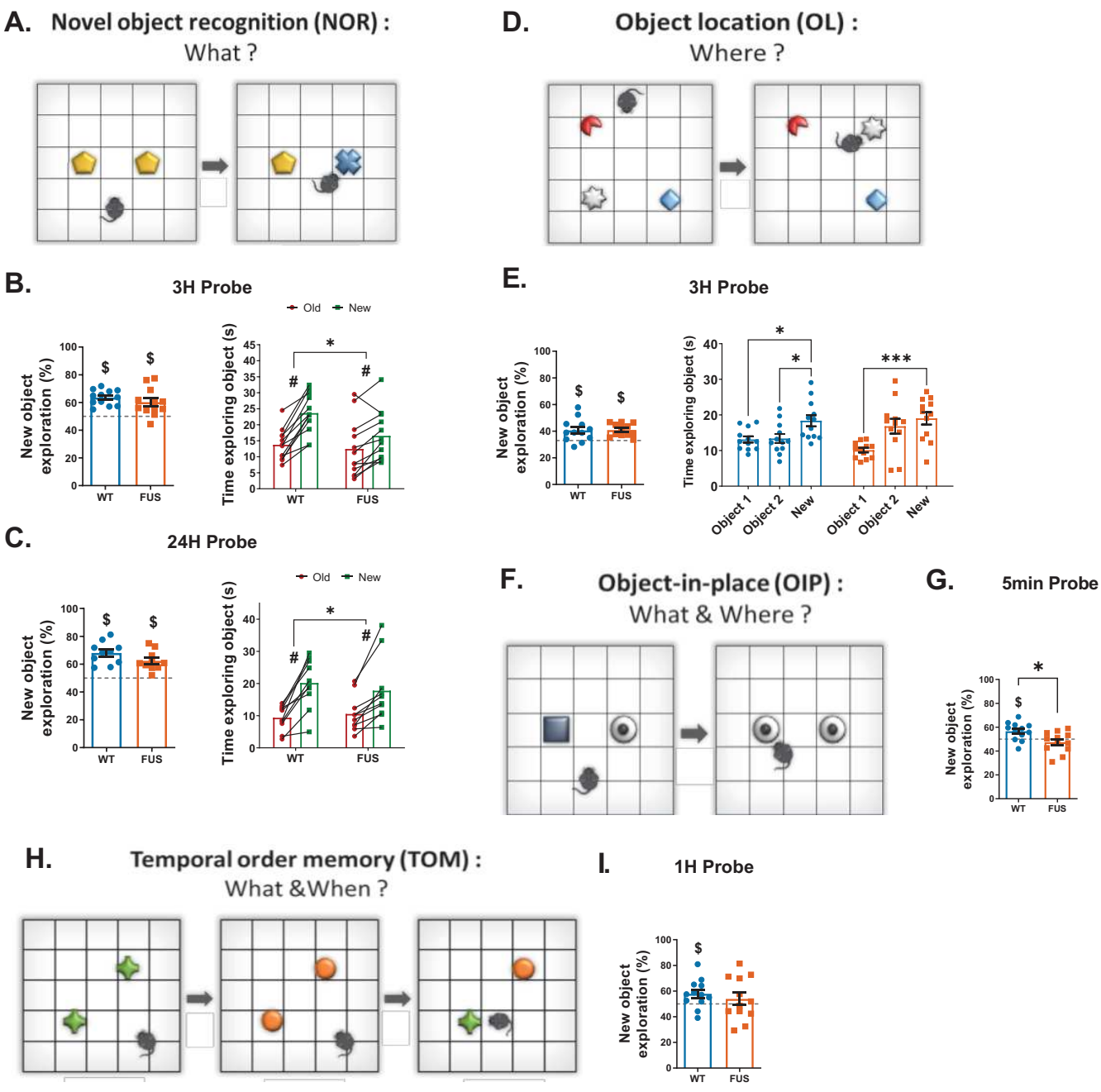
A.
Novel object recognition (NOR) :
What ?
D.
Object location (OL) :
Where ?
B.
3H Probe
Old
New
New object exploration (%)
Time exploring object (s)
WT
FUS
E.
3H Probe
Object 1
Object 2
New
C.
24H Probe
F.
Object-in-place (OIP) :
What & Where ?
G.
5min Probe
H.
Temporal order memory (TOM) :
What &When ?
I.
1H Probe

<u>Figure 3.</u> FUS mutation induce What Where and When « episodic like » memory alterations.

(A) Design of the novel object recognition test.

(B) Percentage (%) of novel object exploration and time exploring each object during the 3H Probe test. Data are represented as mean ± SEM (n = 12 per group for 3H Probe, and n = 10 per group for 24H Probe). $ $p<0.05$ vs Random value using One sample t test. # $p<0,05$ slop ≠ 0 and * $p<0,05$ slop FUS vs. slop WT using the linear mixed model.

(C) Percentage (%) of novel object exploration and time exploring each object during the 24H Probe test. Data are represented as mean ± SEM (n = 10 per group for 24h Probe). $ $p<0.05$ vs Random value using One sample t test. # $p<0,05$ slop ≠ 0 and * $p<0,05$ slop FUS vs. slop WT using the linear mixed model.

(D) Design of the object location test.

(E) Percentage (%) of novel object exploration and time exploring each object during the 3h Probe test. Data are represented as mean ± SEM (n = 12 per group). *$p<0.05$, ***$p<0.0001$ using the two-way ANOVA with Tukey correction for multiple comparisons. $ $p<0.05$ vs Random value using One sample t test.

(F) Design of the object in place task.

(G) Percentage (%) of novel object exploration during the 5min Probe test. Data are represented as mean ± SEM (n = 12 per group). * $p<0.05$ using unpaired t test. $ $p<0.05$ vs Random value using One sample t test.

(H) Design of the temporal order memory task.

(I) Percentage (%) of novel object exploration during the 1H Probe test. Data are represented as mean ± SEM (n = 12 per group). $$p<0.05$ vs Random value using One sample t test.

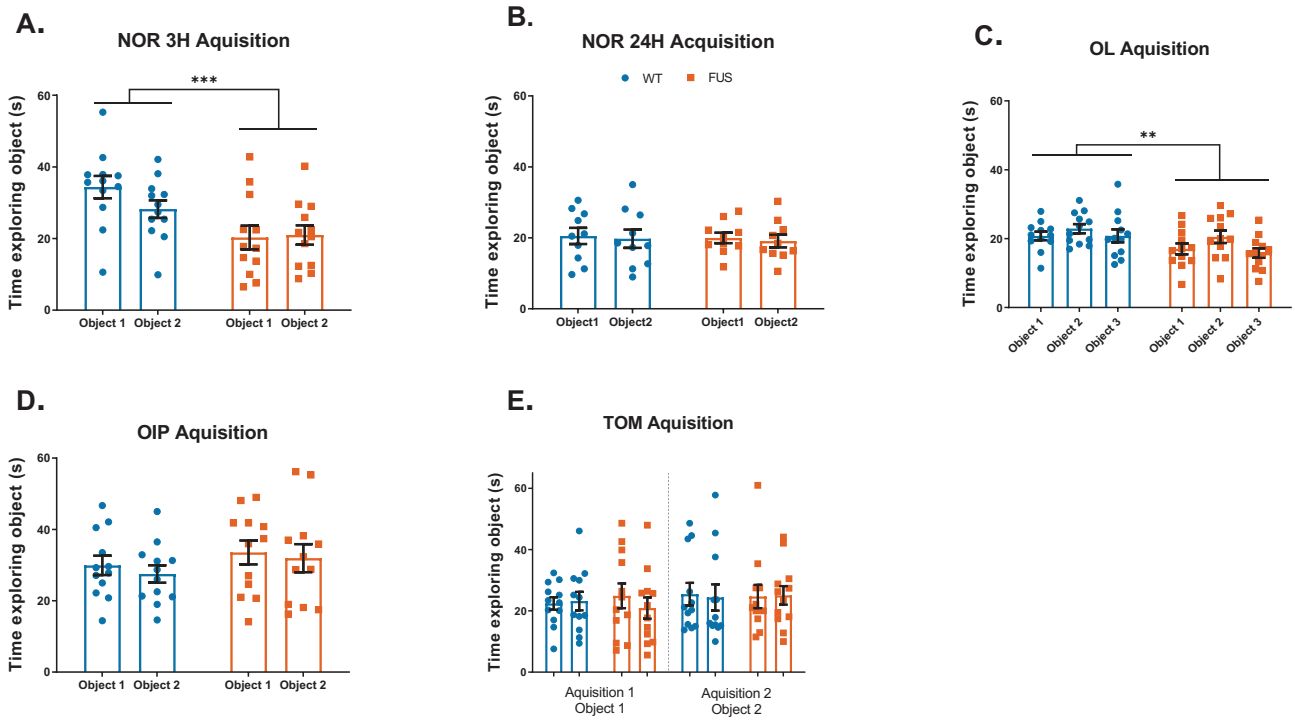

<u>Figure S4.</u> Time exploring each object during acquisition.

(A) Time exploring object 1 and 2 during acquisition of the NOR, cohort 4. Data are represented as mean ± SEM (n = 12 per group). ***p<0.0001 using the two-way ANOVA with Tukey correction for multiple comparisons.

(B) Time exploring object 1 and 2 during acquisition of the NOR, cohort 2. Data are represented as mean ± SEM (n = 10 per group). Tested with the two-way ANOVA with Tukey correction for multiple comparisons.

(C) Time exploring object 1 and 2 during acquisition of the OL, cohort 4. Data are represented as mean ± SEM (n = 12 per group). **p<0.001 using the two-way ANOVA with Tukey correction for multiple comparisons.

(D) Time exploring object 1 and 2 during acquisition of the OIP, cohort 4. Data are represented as mean ± SEM (n = 12 per group). Tested with the two-way ANOVA with Tukey correction for multiple comparisons.

(E) Time exploring object 1 and 2 during acquisition of the TOM, cohort 4. Data are represented as mean ± SEM (n = 12 per group). Tested with the two-way ANOVA with Tukey correction for multiple comparisons.

Figure 4

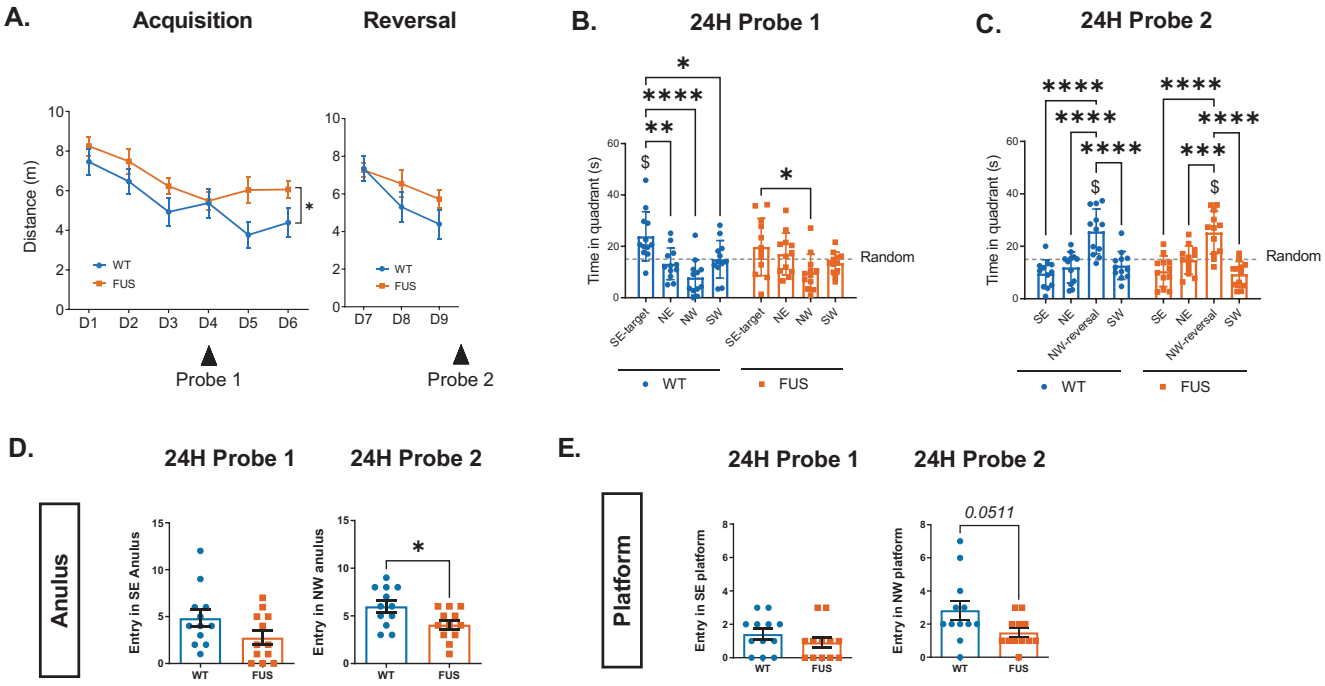

Figure 4. ***Fus*$^{\Delta NLS/+}$ mice demonstrate decreased ability to learn and locate the platform in the MWM spatial task.**

(A) Total distance travelled to reach the target platform in the MWM during the 6 consecutive days of acquisition (left) and the 3 consecutive days of reversal (right). Black arrow highlights the days of probe test. Data are represented as mean ± SEM (n = n = 12 per group). *p<0.05 using repeated two-way ANOVA with Šidák correction for multiple comparisons.
(B) Mean time spent in each quadrant during the recent (24 hours Probe test 1) retention test. Dash line (grey) represent the random value of 15s. Data are represented as mean ± SEM (n = 12 per group). *p<0.05, **p<0.01, ****p<0.0001 using repeated two-way ANOVA with Šidák correction for multiple comparisons. $p<0,05 vs Random value using One sample t test.
(C) Mean time spent in each quadrant during the recent (24 hours Probe test 2) retention test. Dash line (grey) represent the random value of 15s. Data are represented as mean ± SEM (n = 12 per group). ***p<0.001, ****p<0.0001 using repeated two-way ANOVA with Šidák correction for multiple comparisons. $p<0,05 vs Random value using One sample t test.
(D,E) Number of crossings of the annulus and the platform area during the 24-hour Probe test 1 (left panel) and the 24-hour Probe test 2 (right panel). Data are represented as mean ± SEM (n = 12 per group). *p<0.05 using non parametric unpaired Man-whitney rank test.

Figure 5

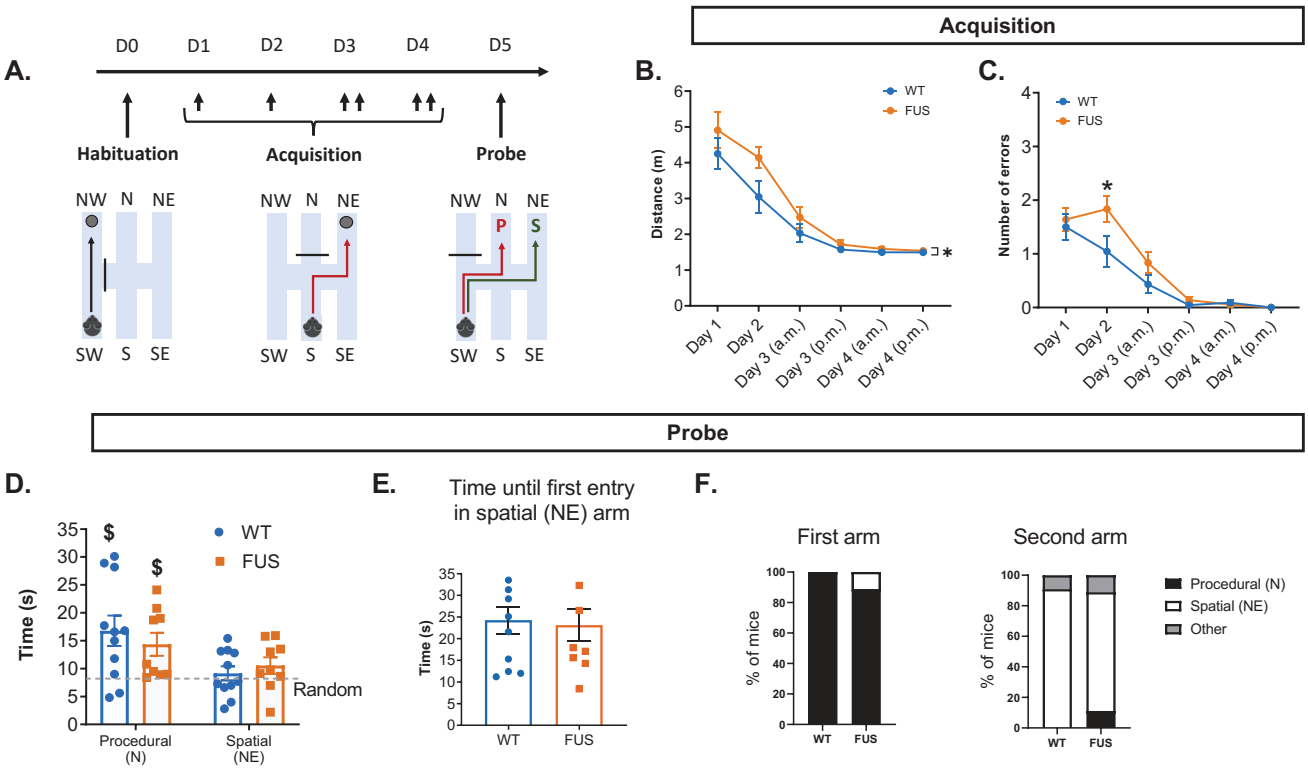

<u>Figure 5.</u> *Fus*$^{\Delta NLS/+}$mice demonstrate delayed learning in the double H with no apparent problem in flexibility.

(A) Design of the 5-day acquisition protocol in the double H.

(B) Total distance travelled to reach the target platform in the NE arm of the double H during the 4 consecutive days of acquisition. Data are represented as mean ± SEM (n = 11 WT & 9 FUS$^{\Delta NLS/+}$). * p<0.05 using repeated two-way ANOVA with Šidák correction for multiple comparisons.

(C) Total number of errors to reach the target platform in the NE arm during the 4 consecutive days of acquisition. Data are represented as mean ± SEM (n = 11 WT & 9 FUS$^{\Delta NLS/+}$). * p<0.05 using repeated two-way ANOVA with Šidák correction for multiple comparisons.

(D) Mean time spent in the procedural (N) and spatial (NE) arms during the recent 24 hours retention test (Probe). Dotted line (grey) represents the random value of 8.5s. Data are represented as mean ± SEM (n = 11 WT & 9 FUS$^{\Delta NLS/+}$). Test using repeated two-way ANOVA with Šidák correction for multiple comparisons. $ p<0,05 vs Random value using One sample t test.

(E) Mean latency to switch from the procedural (N) to the spatial (NE) arm during the recent 24 hours retention test (Probe). Data are represented as mean ± SEM (n = 11 WT & 9 FUS$^{\Delta NLS/+}$). Tested using unpaired t test.

(F) Proportion (%) of mice choosing the procedural (N, black), spatial (NE, white) or other (grey) arm as first (left panel) and second arm (right panel), (n = 11 WT & 9 FUS$^{\Delta NLS/+}$).

GENERAL DISCUSSION

I. Behavioral analyses of *Fus*$^{\Delta NLS/+}$ mice reveal an overall decrease in learning and memory that reflects alterations in different brain regions and cell-types.

The paper from Scekic-Zahirovic and collaborators in which I participated (see Scekic-Zahirovic et al., 2021 in "Annexes"), focused on behavioral alterations associated to cortical dysfunctions. They demonstrated hyperactivity as well as social and executive dysfunctions. Those alterations where mainly linked to inhibitory neurons default in the frontal cortex. In the studies presented herein, we have performed a comprehensive characterization of cognitive functions in the ALS/FTD *Fus*$^{\Delta NLS/+}$ mice at an early stage (4-5 months of age). Focused on hippocampal alterations in the *Fus*$^{\Delta NLS/+}$ mouse model, we first observed that mice displayed delayed acquisition performance and altered memory retention in the spatial MWM task, which was associated to decreased mature spines and altered learning-induced gene expression in the hippocampus (Glutamatergic and GABAergic alterations) (see experimental contribution 1). Then, in a second study (see experimental contribution 2), we explored several other aspects linked to the FUSΔNLS mutation, including anxiety and spatial and procedural memory. We also assessed object related tests that allow investigation of various aspects of the What Where and When memory components. Thus, we confirmed hippocampal alterations and further proposed widespread alterations of different parahippocampal regions and of the striatum. In conclusion, even if *Fus*$^{\Delta NLS/+}$ mice are able to succeed in most of the tasks, they demonstrate a global decrease of learning and memory and are even unable to associate the "what" and "where" component of memory and which item has been experienced first. Thus, our mouse model highlights a widespread dysfunction in several brain regions, suggesting that more focus should be given to these brain regions in ALS/FTD patients.

1) Hyperactivity, an early FTD symptom in *Fus*$^{\Delta NLS/+}$ mice

Our studies demonstrate hyperactivity in *Fus*$^{\Delta NLS/+}$ mice at the age of 3, 4 and 10 months. These symptoms seem even more marked at the early age of 3 months. In the literature, transgenic overexpression of mutant FUS also causes hyperactivity (Shiihashi et al., 2017). Hyperactivity symptoms are also observed in other FTD mouse model such as Tau (Jul et al., 2016) and C9ORF72 (Chew et al., 2015) mouse model, and might reflect purposeless hyperactivity observed in the disinhibited form of behavioral FTD patients (Neary et al., 2005; Snowden et al., 2011).

Ritualistic/repetitive behavior is also a common characteristic of FTD-FUS patients displaying predominantly the behavioral variant of FTD (Snowden et al., 2011). The increased locomotor activity behavior may also be a consequence of the early cortical hyperexcitability observed in ALS patients (Geevasinga et al., 2016). Therefore, current studies in Dupuis Lab are led to analyze electrocorticography in *Fus*$^{\Delta NLS/+}$ mice. Interestingly, the increased locomotor phenotype is also observed when FUS is silenced *via* shRNA injection in the hippocampus (Udagawa et al., 2015) pointing out a specific involvement of the hippocampus in FUS mediated hyperactivity. Hyperactivity could be triggered by FUS dysfunction in specific cell types, for example oligodendrocytes (Guzman et al., 2020). This is of particular importance regarding the emerging role of glial cells in ALS and FTD (Radford et al., 2015) and the dysregulation of oligodendrocytes in the spinal cord of our *Fus*$^{\Delta NLS/+}$ mouse model (Scekic-Zahirovic et al., 2017).

In our study, we also demonstrated that *Fus*$^{\Delta NLS/+}$ mice exhibited significant decreased body weight compared to their WT littermates, and this may be in line with increased locomotor activity. Another hypothesis would be decreased food intake and/or metabolic alterations in *Fus*$^{\Delta NLS/+}$ mice. Indeed, ALS patients demonstrate metabolic abnormality (Joardar et al., 2017) and dietary support is associated with increased survival in fast progression ALS patients (Ludolph et al., 2020).

2) Hippocampal dysfunction in *Fus*$^{\Delta NLS/+}$ mice.

In the literature, FTD patients are characterized having a relative spared episodic memory and visuospatial skills (Liu et al., 2019). However, our study demonstrated that *Fus*$^{\Delta NLS/+}$ mice present hippocampal alteration. We observed diminished acquisition in the spatial MWM in two independent cohorts of mice at the age of 5 months. We also confirmed memory impairment at two different ages (5 and 10 months), two different timepoints of the learning acquisition (3 or 4 days) and of the consolidation steps (recent and remote LTM). We thus demonstrated that both the acquisition and the recent and remote LTM were reduced in *Fus*$^{\Delta NLS/+}$ mice. Other ALS/FTD mouse models, for example mimicking TDP43 pathology, demonstrate spatial alterations (Swarup et al., 2011; Tsai et al., 2010). Also, a model expressing human mutant FUS demonstrates spatial alterations in the Barnes maze and MWM (Ho et al., 2021; Huang et al., 2012). Hippocampal alterations are further supported by several studies in mice expressing human

mutant FUS (Shiihashi et al., 2017; López-Erauskin et al., 2018; Ho et al., 2019; Sahadevan et al., 2021). Additionally, our analyses in the previous study demonstrated decreased mature spine morphology in the CA1 hippocampal region of *Fus*$^{\Delta NLS/+}$ mice and abnormal glutamatergic and GABAergic learning-induced gene expression. Interestingly, in the MWM, regardless of memory recall time (probe test), we observed a decrease in capacity of *Fus*$^{\Delta NLS/+}$ mice to precisely localize the platform. In the literature, altered neurogenesis has been described as relevant for lack of precision (Clelland et al., 2009; Garthe et al., 2009). In the literature, altered neurogenesis was only described in mice harboring FUS downregulation (Ishigaki et al., 2017). Since it is not clear what would be the implication of FUS mutation in this process. To answer this question, we are currently analyzing neuronal proliferation and survival in *Fus*$^{\Delta NLS/+}$ mice following BrdU injection.

While the temporal atrophy is a determined aspect of FTD patients, only few study focused on hippocampal alteration in ALS patients (Christidi et al., 2019; Stoppel et al., 2014; Takeda et al., 2008). Considering our results, we propose that the analyses of the hippocampus might be critical in the context of ALS-FTD disease, especially in the particular context of FUS where literature is even more absent.

3) And what about the para hippocampal network in *Fus*$^{\Delta NLS/+}$ mice?

Our studies also assessed object related tests to investigate various aspects of the What Where and When memory components. Most of the previous mouse models expressing human FUS demonstrated alteration in recognizing a new object (Ho et al., 2021; López-Erauskin et al., 2018; Munter et al., 2020). Similar results were observed in other ALS and/or FTD mice model, such as in TDP43 (Alfieri et al., 2016; Rodriguez-Ortiz et al., 2013; Tsai et al., 2010) mouse models. Here we demonstrated that expression of the murine mutant FUSΔNLS is associated with slight diminution in novel object recognition as well as in object location. However, even with decreased performance, FUS$^{\Delta NLS}$ mice are perfectly able to discriminate a new or a moved object. In contrast, we demonstrated the inability of FUS mice to associate object and place information or to determine which item was experienced first, thus revealing slight alteration of the “what” and “where” brain networks and predominant impairment of the “What Where” and “What When” brain networks. In the literature, each memory component can be associate with interactions between different brain regions and brain networks.

The success of the NOR, testing the "what" component is associated with the perirhinal cortex (object identity), the lateral entorhinal cortex and the mPFC for the 24H memory recall (Akirav and Maroun, 2006). Brain regions associated with the ability to localize objects in the OL task are in part the hippocampus (Barker and Warburton, 2011; Oliveira et al., 2010), the subiculum and the medial entorhinal cortex (context related). The OIP task testing object place associative memory, testing the association of the identity ("what") and the location ("where") of an object, relies on the entorhinal cortex. The TOM task, testing the order in which items has been presented, was proven to be dependent of the hippocampus (Barker and Warburton, 2011), the perirhinal cortex and mPFC cortex (Barker and Warburton, 2011). For more information see Chapter "The Value of the Object Recognition Paradigm in Investigating Animal Models of Alzheimer's Disease: Advances and Future Directions" in Handbook of Behavioral Neuroscience (Mathis, 2018).

Thus, our research demonstrates further support for hippocampal alterations in *Fus*$^{\Delta NLS/+}$ mice. However, here we proposed that FUS mutation might also have a more widespread impact on parahippocampal regions.

4) **Cortical alterations** in *Fus*$^{\Delta NLS/+}$ mice**.**

Cortical modules, and particularly the mPFC is tightly linked to Long term memory (LTM), (Bicks et al., 2015; Frankland and Bontempi, 2005; Tonegawa et al., 2018). In the MWM, our mouse model demonstrates diminished LTM retention for both the recent (24 hours) and remote (30 days) time point. Also, even if *Fus*$^{\Delta NLS/+}$ mice are able to discriminate a new object in the NOR, they demonstrate a slight decrease compared to their WT littermates, including in the 24 hours recent LTM. Interestingly, previous study of Scekic-Zahirovic and collaborator from 2021, in which I participated, highlighted social behavior abnormality at 4, 10 and 22 months and diminished remote LTM consolidation at the age of 10 months in *Fus*$^{\Delta NLS/+}$ mice, both reflecting frontal cortex alterations (Scekic-Zahirovic et al., 2021).

Changes in social behavior were also observed in other mice model expressing human mutant FUS (López-Erauskin et al., 2018; Lysikova et al., 2019; Sephton et al., 2014) or in C9ORF72 (Jiang et al., 2016) and CHMP2B ALS and/or FTD mice model (Gascon et al., 2014). These results are in

accordance with the social disinhibition present in the disinhibited form of behavioral FTD patients where predominant orbitofrontal-temporal lobe atrophy is observed (Snowden, 2001; Neary et al., 2005). In the particular case of FTD-FUS we also observe early decline in social conduct (Roeber et al., 2008).

Concerning altered consolidation memory, several other studies on mice expressing human FUS demonstrate altered fear conditioning memory (Shiihashi et al., 2017; López-Erauskin et al., 2018; Ho et al., 2019, 2021) and altered recognition of either a new animal (Shiihashi et al., 2017)(Shiihashi et al, 2017) or object (López-Erauskin et al., 2018; Munter et al., 2020; Ho et al., 2021). Such memory alteration are also observed in other FTD mice model for example overexpressing WT TDP-43 (Alfieri et al., 2016), overexpressing human mutant tau protein (Chatterjee et al., 2018) or expressing human mutant VCP (Rodriguez-Ortiz et al., 2013). In the literature, FTD patients demonstrate executive dysfunction with difficulty for planification, maintain a sustain attention, remember instructions and manage multiple task, dependent of the frontal cortex with relative sparing of episodic memory and visuospatial skills (Liu et al., 2019). Altered attention and memory dysfunction is also observed in patients harboring FTD-FUS neuropathology (Roeber et al., 2008). This is in accordance with our model since *Fus*$^{\Delta NLS/+}$ mice are able to remember the platform location in the MWM but demonstrate significant reduction of this memory compared to WT mice. Cortical alterations and cognitive impairment are also described in pure ALS and overlapping ALS-FTD patients (Mantovan et al., 2003; Rippon et al., 2006; Usman et al., 2011). Thus, cortical alterations are observed in both ALS and FTD patients and are present in *Fus*$^{\Delta NLS/+}$ mice.

Altered LTM retention and social alteration in in *Fus*$^{\Delta NLS/+}$ mice, were proposed to be the result of synaptic defect, in part due to inhibitory synapses (Sahadevan et al., 2021; Scekic-Zahirovic et al., 2021). Human mutant FUS expression in mice model is indeed associated with decreased dendritic branching and spines in the cortex (Sephton et al., 2014; Shiihashi et al., 2017). However, there is no study concerning the specific alteration of inhibitory neurons in ALS-FTD FUS model.

5) *Fus*$^{\Delta NLS/+}$ mice demonstrate striatal alterations in accordance with FTD-FUS disease.

Lastly, we focused on the role of FUS in procedural memory (knowing how / Habits learning) using the double-H paradigm (Kirch et al., 2015). We demonstrated that *Fus*$^{\Delta NLS/+}$ mice have a delayed acquisition in the double H. However, after 5 days *Fus*$^{\Delta NLS/+}$ mice performed similarly to their WT littermates, and they did not present procedural memory alteration. Thus, we concluded that FUS mutation may induce slower procedural learning that can be compensated by overtraining mice. Procedural learning is mainly dependent of the striatum (Packard and Knowlton, 2002). This structure is poorly characterized in the different ALS/FTD mice model. Nevertheless, disturbed striatal gene expression is observed in a FUS knockout mouse model (Kino et al., 2015), suggesting that FUS expression has also a role in the striatum. As further indication of striatal alteration in ALS/FTD disease, mice expressing a human truncated FUS protein demonstrated an altered EEG spectrum in the striatum as early as 2 and 5 months (Vorobyov et al., 2021). Interestingly, striatal atrophy is one characteristic of FTD-FUS patients (Josephs et al., 2010) mainly associated with the stereotypic form of bvFTD (Snowden et al., 2011).

Altogether, our different studies proposed a more widespread brain alteration in the ALS-FTD spectrum than previously described. We observed cortical, hippocampal, parahippocampal and striatal dysfunctions possibly due to altered function of the different neuronal and glial cell types. Furthermore, cognitive alterations are present at an early age in our *Fus*$^{\Delta NLS/+}$ mouse model and are present way before the ALS-motor symptoms (Scekic-Zahirovic et al., 2017, 2021). Dupuis lab is currently working on a new conditional mouse model expressing FUSΔNLS mutation only in the adulthood. This model will help to better understand the implication of FUS dysfunction in neurons of patients harboring genetic mutation (with developmental implication of FUS) vs. patients developing sporadic FUSopathies presenting no mutation of the FUS gene. We expect that further characterization and study of the implication of mutant FUS in the different brain regions and cell-types may help to identify early changes and molecular marks in the context of ALS-FTD disease.

II. Potential mechanisms underlying molecular and behavioral alterations in *Fus*$^{\Delta NLS/+}$ mice.

In the present study, we demonstrated delayed acquisition performance and altered hippocampal-dependent memory retention in mice harboring the heterozygous FUSΔNLS mutation. We further showed that these behavioral alterations were accompanied by structural (mushroom spines) and transcriptional dysregulations in the hippocampal brain region. *Fus*$^{\Delta NLS/+}$ mice and WT littermates indeed demonstrate differential gene expression during the memory consolidation process. Despite few changes of gene expression in the HC condition, we observed that the chromatin already shows many epigenomic alterations. We observed increased enrichment of active marks (H3K4me3, H4K12ac and H3K27ac) and decreased enrichment of the H3K27me3 repressive mark in isolated hippocampal neurons. The different groups of HMEG (Histone mark-enriched genes) show a discrete increase of their expression, suggesting that FUSΔNLS mutation has an impact on both the conformation of the chromatin and on new gene expression. Importantly, we also identified potential FUS-target genes by ChIP-seq analyses, mainly related to mitochondrial ribosome genes, and revealed a preferential FUS binding to ETS family motifs (GGAA). In parallel, we demonstrated that the DNA binding of several transcription factors was altered in the hippocampus of *Fus*$^{\Delta NLS/+}$ mice, among which Elk1 and Elk3 ETS members were affected. Thus, our data show that FUSΔNLS mutation influences the organization of the chromatin, particularly that of the active chromatin, with a significant impact on the learning induced transcriptome and further behavioral alterations though a mechanistic that could be dependent of the ETS family of transcription factors.

1) Do the effects of the FUS mutation occur through a direct mechanism of FUS in the nucleus?

Our study demonstrates that despite NLS truncation, FUSΔNLS proteins can be found in the nucleus and even represent 40-50% of the total nuclear FUS fraction, with no significant change in the total amount of nuclear FUS (Figure 5A-C). Entry of the FUSΔNLS mutant was already described previously (Sanjuan-Ruiz et al., 2021) and proposed to be mediated by two different mechanisms. First, mutant FUS nuclear import can be mediated by the WT FUS protein itself, since WT and mutant FUS interact together (Vance et al., 2013; Qiu et al., 2014). Second, even if

nuclear import of FUS is predominantly mediated by the NLS region, the RGG region alone is also able to interact with the transportin 1 (Dormann et al., 2010) and other nuclear import receptors (Baade et al., 2021; Gonzalez et al., 2021). Given that in cell cultures, FUS binds to DNA (Yang et al., 2014) and interacts with RNApol II to regulate gene transcription (Schwartz et al., 2012), we thus suspected that FUS-DNA interactions might be impaired if FUS mutants were present into the nucleus. Our ChIP-seq study performed with an antibody able to recognize all FUS proteins at their C-terminus domain shows that, whatever the presence of WT and/or ΔNLS FUS proteins, they could bind identical genomic regions (Figure S9). Of note, to our knowledge, our ChIP-seq study is the first to decipher the precise genomic distribution of FUS in brain cells, more precisely in the hippocampus. We found that FUS was predominantly localized at the TSS of genes, similarly to results obtained by Schwartz and collaborators in HEK293 cells (Schwartz et al., 2012). However, while they described a widespread binding of FUS on the HEK293 cells genome (9731 genes, representing 68% of expressed genes), we observed significant binding of FUS to 386 genomic regions. These differences might be due to different function of FUS in different tissues/developmental and postnatal stages (Blechingberg et al., 2012; Schoen et al., 2015). The starting material which was cell cultures for Schwartz et al. (2012) and hippocampal tissues in our study, may also have been differently influenced by the protein-DNA fixation step and/or antibody used, and it is then possible that our chromatin immunoprecipitation only captured DNA fragments with the highest amount of bound FUS. However, we observed that more than 90% of the FUS bound-target genes in hippocampal cells were similar to that observed in muscle cell cultures (C2C12), using the same technique/antibody (Picchiarelli et al, unpublished). This suggests a common role of FUS in the different tissues.

In terms of functional annotation, these FUS-target genes were associated to RNA metabolism, translation/ribosome, and mitochondria -related genes. These terms are in accordance with the different FUS functions. The role of FUS in RNA metabolism, including transcription, splicing, polyadenylation, miRNA processing and RNA transport is well described in the introduction and in several excellent reviews (Lagier-Tourenne et al., 2010; Ling et al., 2013; Birsa et al., 2020).

Several hypotheses can account for genomic alterations induced by the FUS mutation and impacting on learning and memory processes.

The mitochondria hypothesis. Interestingly, we observed that FUS binds to a large number of mitochondrial ribosomal proteins (Mrpl and Mrps) proteins (Fig 5H). These proteins are encoded by the nuclear genome, synthetized in the cytoplasm, and transported into the mitochondria to be assembled into mitochondrial ribosomes. Mrp proteins translate 13 proteins encoded by the mitochondrial gene that all play a role in the mitochondrial respiratory chain. Abnormal expression of Mrpl is associated with mitochondrial metabolic disorder and cellular dysfunctions (Huang et al., 2020). More interestingly, FUS target Mrpl3 gene, that is related to neurodegenerative diseases and memory impairment in a spontaneous mutation mouse model (Cahill et al., 2020). Thus, we propose that altered expression of FUS target genes such as *Mrpl* genes, as well as genes encoding mitochondrial complex I enzymes, could directly lead to altered mitochondrial functions and underlie FUSΔNLS mice memory deficits. Indeed, mitochondrial functions represent crucial factors for proper formation of dendritic spines of newly formed hippocampal neurons during adult neurogenesis (Arrázola et al., 2019; Richetin et al., 2017). Adult neurogenesis is associated to hippocampal precision memory (Clelland et al., 2009; Garthe et al., 2009), which is impacted in our FUSΔNLS mice.

In line with this hypothesis, Dupuis lab observed altered mitochondrial morphology in C2C12 expressing the same FUSΔNLS mutation (Picchiarelli et al, unpublished). Another FUS Knock In mouse model demonstrate altered gene expression mostly of mitochondrial genes at late age (12 months), while no altered expression was observed at young age (3 months)(Devoy et al., 2017). To note, 48 of our FUS target genes colocalized with the dysregulated genes in old mice, including some Mrp genes (Devoy et al., 2017). In the literature, abnormal mitochondrial shapes, shortening, fragmentations and damage were observed when expressing human mutant FUS in neuronal cell culture (Deng et al., 2015; Tradewell et al., 2012), in pre- and postsynaptic neuro muscular junctions of human FUS mice model (Sharma et al., 2016) and in FTLD-FUS brain sample (Deng et al., 2015). Deng and collaborators further proposed that mitochondrial abnormality could be multifactorial and that one mechanistic might involve the molecular chaperone HSP60 and result in increased FUS translocation into the mitochondria. Interestingly, our Chip-seq FUS data in the hippocampus demonstrate FUS binding on the *Hsp90* gene, another heat chock protein involved in protein translocation to the mitochondria (Young et al., 2003). In addition, *Hsp90* mRNAs also interact with human mutant FUS protein (Tsai et al., 2020). Thus, we can speculate that mutant FUS might modify its own entry into the mitochondria, as well as the entry of other proteins, through direct regulation of the *Hsp90* gene and mRNA. Further implications

of mutant FUS regarding mitochondrial dysfunctions in the context of ALS are described in these reviews (Smith et al., 2019; Birsa et al., 2020). Altogether, our Chip-seq FUS shows increased evidence of a direct role of mutant FUS in RNA processing and mitochondrial dysfunctions in the ALS-FTD spectrum.

The "transcriptional partner" hypothesis Surprisingly, no significant change of FUS binding to DNA was identify on the *Fus*$^{\Delta NLS/+}$ genome. Thus, if FUS is correctly localized on the genome of *Fus*$^{\Delta NLS/+}$ mice, how can we explain the transcriptomic and behavioral alterations in our model? We found that FUS-bound genes were globally more expressed in *Fus*$^{\Delta NLS/+}$ than in WT hippocampi (Figure 5J). However, one by one, none of these target genes showed significant up-regulation. We can thus only speculate about a possible scenario involved in FUS-induced dysregulations. FUS was shown to directly bind the C-term domain of RNAPol2 and modulate the amount of Ser2 phosphorylation present near the gene TSSs (Schwartz et al., 2012). The effect of the FUSΔNLS mutation on these interactions is not known in our model, but a loss of function could lead to Ser2 hyperphosphorylation at TSSs of bound genes and change their transcription rate. What happens in our model is not clear and should be complemented by targeted ChIP-seq performed with the different forms of Phospho-RNApol2. Of note, the cluster 3 of FUS-bound genes (low binding) were enriched in genes related to RNA polymerase II/ TFIIH complex, emphasizing the relationship of FUS regulation of genes form the core transcriptional machinery. Such alterations may be in line with the lower levels of transcription (particularly that of IEGs) measured after training in our transcriptomic study (Figure 2). Another hypothesis is that FUS is a protein able to mediate liquid-liquid phase separation (described in the introduction) and create microenvironment in a reversible manner. Some FUS mutants are unable to easily reverse this situation, resulting in a less dynamic environment (Murakami et al., 2015; Patel et al., 2015). Thereby, if microenvironment formation is altered in our model, this might influence the way that FUS recruits and interacts with the transcriptional apparatus during transcription initiation, further altering gene transcription (Yang et al., 2014).

The Elk1/3 hypothesis. Strikingly, promoter motif analyses of our FUS ChIP-seq data demonstrated an almost exclusive binding of FUS on ETS family motifs (GGAA) (Figure 5I). Further, our ATAC-seq data highlighted altered binding of several transcription factor among which the binding of Elk1 and Elk3, members of the ETS family, was significantly reduced. Elk1, is

highly involved in learning and memory processes, see review (Besnard et al., 2011). A study reported that the specific inhibition of Elk-1 phosphorylation, and subsequent nuclear translocation, was associated with a defect in the glutamate-induced expression of IEGs bearing SRE site(s) on their promoters, such as c-fos or junB (Lavaur et al., 2007). Interestingly, upon learning conditions, our RNA-seq data demonstrated a reduced expression of a group of genes including such immediate early genes in *Fus*$^{\Delta NLS/+}$ mice compared to their WT littermates (see for example Junb expression on Figure 2E). A decrease of nuclear Elk family members in FUS hippocampal neurons is also in line with our ATAC-seq data showing decreased binding at Elk1/Elk3 genomic loci (Figure 6A). Indeed, if the ΔNLS mutated FUS could bind Elk1/3 either in cytoplasm or in the nucleus, it may directly prevent proper Elk1/3 binding to its responsive elements in learning and memory related genes. Thus, compromising interactions between FUS and Elk1/Elk3 or other ETS family member (and other transcription factors) could stand as a potential mechanism underlying altered transcriptomic and behavioral changes in the *Fus*$^{\Delta NLS/+}$ mouse model.

Our study demonstrated that the presence of the FUSΔNLS mutation is associated with a wide range of epigenetic changes. Important questions are to understand how these epigenetic modifications occur and how they affect the learning process. In our model, we observed increased enrichment of histone marks associated with open chromatin regions and gene transcription (H4K12ac, H3K4me3 & H3K27) and decreased enrichment of histone marks associated to chromatin compaction and gene silencing (H3K27me3). The group of HMEG associated with active marks were highly expressed genes and further demonstrated significant increased expression in *Fus*$^{\Delta NLS/+}$ mice (Figure 4A & Figure S8A, B). FUS is known to bind the histone acetyltransferases CBP and p300 (Wang et al., 2008) and some HDACs isoforms (Wang et al., 2013; Arenas et al., 2020) and such binding may be compromised by the FUS mutation on the N-term NLS domain. This could contribute to alterations of the chromatin landscape (acetylation/methylation status of histones) at the specific sites we deciphered. Integration of epigenetic modifications and transcriptomic alteration interestingly pointed to dysfunctions of the glutamatergic synapse during the process of learning (Figure D1). Indeed, after 3 days of training sessions in the Morris water maze, among the 288 DEG uniquely up regulated in the hippocampus of FUS mice (Figure 2D), 121 overlapped with H3K4me3 HMEG, 138 with H4K12ac HMEG and 24 with H3K27ac HMEG (Figure D1). Representative genes commonly affected by the 3 histone marks were Grin2a, Grin2b, Gria2 or Lrrc7. These results suggest that FUS-induced

changes of chromatin are sufficient to inappropriately promote the transcription of these highly expressed genes in the hippocampus when animals are challenged (here by spatial training), as their expression levels were not modified in learning WT mice. It is noteworthy that among the uniquely up-regulated DEG in response to learning in WT mice, some of them were also overlapping with HMEG (52 with H3K4me3 HMEG, 63 with H4K12ac HMEG and 8 with H3K27ac HMEG) found in FUS mice, but their expression was not significantly changed in basal conditions (RNA-seq data, HC). These genes did not display a "neuronal/synaptic" but rather a "transcriptional" signature, as for example, four members of the ETS family (Ets2, Etv1, Etv3, Etv5) that displayed increased TSS H4K12ac levels (and H3K4me3 for Ets2). This indicates the co-existence of different mechanisms, leading to a dysfunction in gene transcription and more particularly on the ETS members in FUS mice.

Others… Lastly, integration of FUS-target genes with active HMEG revealed 9 genes in common for H3K27ac, 59 genes in common for H3K4me3, 133 genes in common with H4K12ac, among which 5 were common to the three marks (Figure D2). Interestingly, functional analyses of these genes revealed that more than half of them encode nuclear proteins, among which a strong linkage could be found using STRING gene expression analyses on a core node associated to gene transcription/expression and DNA-binding. This node comprises on the one hand Kmt2a/Kdm2b enzymes and, on the other hand, the transcriptional repressor YY1 and the transcription factor Myc.

Kmt2a/Kdm2b specifically methylate/demethylate H3K4 and are thereby directly relevant of the dysregulations we observe at the epigenomic level in FUS mice. Additionally, Kmt2a gene expression was significantly induced in *Fus*$^{\Delta NLS/+}$ mice after MWM training, pointing to a new putative link between DNA binding of FUS, epigenomic dysregulation and transcriptomic alteration in *Fus*$^{\Delta NLS/+}$ mice. This mechanism might even be dependent of ETS member, since EWS, another protein of the FET family is proposed to act in collaboration with ETS and p300 HAT to bind to H3K4me3 and H3K27ac and regulate the expression of other histone modifier, in Erwin Sarcoma cell lines (Sand et al., 2015). Lastly, Kmt2a conditional KO mice were recently reported to present memory dysfunctions (Kerimoglu et al., 2017). Interestingly, Kmt2a knocked down hippocampal neurons presented decreased H3K4me3 levels on the TSS of genes that were specifically enriched for the consensus ETS sequence (Kerimoglu et al., 2017).

Intriguingly, FUS, YY1 and Myc have been associated to DNA guanine quadruplexes (G4) (Li et al., 2021; Mishra et al., 2016; Spiegel et al., 2021), a Guanine rich four stranded secondary structure. The formation of G4 structures were originally described in human cells (Biffi et al., 2013) and further mapped in promoters of highly expressed/active genes in mammalian cells (Kouzine et al., 2017). Interestingly, the RGG region of FUS is found to interact with G4 structure, found in telomeres. Recently, TDP-43 has also been described as a G4 binding protein interacting with GGGGCC rich transcript of the C9ORF72 gene involved in ALS (Ishiguro et al., 2016). Whether or not FUS mutation could directly impair G4 quadruplex formation, or indirectly via altering the promoter conformation of specific G4 interacting proteins such as YY1 and Myc in the hippocampus, is an exciting (and speculative) hypothesis that remains to be tested in *Fus*$^{\Delta NLS/+}$ mice.

Together, these results emphasize that FUS may regulate the transcriptional environment at the TSS of highly expressed genes (co-partners, histone marks, 3D chromatin structure) rather than the transcription, but that will be able to promote inappropriate gene transcription upon activation (here learning).

2) Do the effects of the FUS mutation occur through an indirect mechanism of FUS in the cytoplasm?

In addition to the import of mutant FUS in the nucleus, our study demonstrated an increase of cytoplasmic FUS, mainly composed of the mutant FUSΔNLS (Figure 5A-C). This observation was already described in our previous studies (Scekic-Zahirovic et al., 2017, 2021; Sanjuan-Ruiz et al., 2021) as in other FUS Knock In mouse model (Devoy et al., 2017; Zhang et al., 2020). FUS is tightly controlled by autoregulation mechanisms (Zhou et al., 2013; Dini Modigliani et al., 2014; Humphrey et al., 2020). However, the presence of FUS mutation is associated with disrupted FUS autoregulation and FUS increase expression in the cytoplasm. This was also demonstrated in *Fus*$^{\Delta NLS/+}$ mouse model (Sanjuan-Ruiz et al., 2021). In the cytoplasmic compartment, FUS is associated with several functions such as axonal transport (Sama et al., 2014) and subcellular localization, local translation, stabilization and/or degradation of several synaptic-related mRNA (Fujii et al., 2005; Udagawa et al., 2015). Thus, FUS interacts with numerous proteins in the cytoplasm. Interestingly, several altered mechanistic were attributed to cytoplasmic

sequestration of proteins due to increased interaction with the mutant FUS. For example, FUS R521C mutant expression in HEK293 cells demonstrates a two-time increase in its half-life and increased interaction stability compared to WT FUS (Qiu et al., 2014). Thus, in the presence of different mutation of FUS, we observe sequestration of kinesine-1 (Yasuda et al., 2017), several mRNAs (Tsai et al., 2020), but also sequestration and cytoplasmic mislocalization of several spliceosome components (Gerbino et al., 2013; Jutzi et al., 2020; Reber et al., 2016) and HDAC1 (Scekic-Zahirovic et al., 2016). This information leads to two hypotheses. A first hypothesis could be that mutant FUS promotes an interaction with a cytoplasmic protein that would alter its recruitment and localization in the cytoplasm (loss of function). In our model we can hypothesize that mutant FUS may alters the localization of other histone modifier enzymes such as that described for e.g. HDAC1 (Scekic-Zahirovic et al., 2016) , thus resulting in changes in the different histone marks associated with open chromatin and transcription and ultimately impacting gene expression. Another hypothesis could be that in our model, mutant FUS might interact with the different member of the ETS family or other transcriptional partners (also discussed above). This idea is supported by recent finding showing direct interaction between FUS and ETV5 member of the ETS family (Picchiarelli et al., 2019). Interestingly, sequestration of SRF, an Elk1 partner, is sufficient to disrupt long-term spatial memory in the MWM (Dash et al., 2005).

Lastly, increased mRNA interaction with mutant FUS might explain why structural and behavioral alterations are observed in *Fus*$^{\Delta NLS/+}$ mice without major changes in gene expression. Consequently, mRNA might be present in a satisfactory quantity in the cell without being at the right place for transcription. Indeed, a mutant FUS model demonstrated a significant decrease in intra-axonal protein synthesis (López-Erauskin et al., 2018) and FUS CLIP-seq performed in the cortex of the *Fus*$^{\Delta NLS/+}$ mouse model demonstrated that FUS interacts with several glutamatergic and GABAergic mRNA target at the synapse location (Sahadevan et al., 2021). In our RNA-seq data, these RNAs were unchanged in HC condition. However, Sahadevan and collaborators only find a poor correlation between gene expression changes and CLIP-seq target genes, suggesting that FUS-mRNA interaction could be altered in our model without visible changes at the transcriptomic level. Upon learning condition, we interestingly observed an overlap of 12 genes that were clearly associated with the glutamatergic synapse between genes uniquely up-regulated in FUS mice and FUS CLIP-seq (e.g., Gri2, Gria3) (Figure D3). Thus, the specific increase of neuronal/synaptic gene expression only observed in learning FUS mice may come from

increased-dependent FUS stabilization of their mRNAs in the cytoplasmic compartment. As previously mentioned, FUS is part of the spliceosome machinery and is involved in alternative splicing (Lagier-Tourenne et al., 2012). Therefore, total mRNA level might be unchanged in our model, but this does not exclude differences in splicing variant that could result in morphological and behavioral alteration in *Fus*$^{\Delta NLS/+}$ mice model. As an example, FUS binds to Tau pre-mRNA in mice brain and regulate alternative splicing of exon 10 (Orozco et al., 2012). Increased inclusion of exon 10 is associated with predominant expression of the 4R Tau isoform and FTD disease (McCarthy et al., 2015). Thus, deeper analyses on splice variants should be led in the hippocampus of *Fus*$^{\Delta NLS/+}$ mice to answer this question.

Also, to be able to properly conclude on altered gene expression in *Fus*$^{\Delta NLS/+}$ mice, we need to take in consideration that mRNA quantity in the cell relies on the dynamic between mRNA synthesis and mRNA degradation. Thus, if both mechanisms were altered in the same direction in our model, this would result in unchanged total RNA but would possibly have an impact on neuronal activation and behavioral response of mice.

The different hypothesis in which FUS may regulate transcriptional alterations are recapitulated in the Figure D4.

Figure D1

Integration of training-induced genes (RNA-seq) with FUS ChIP-seq

• *H3K4me3*

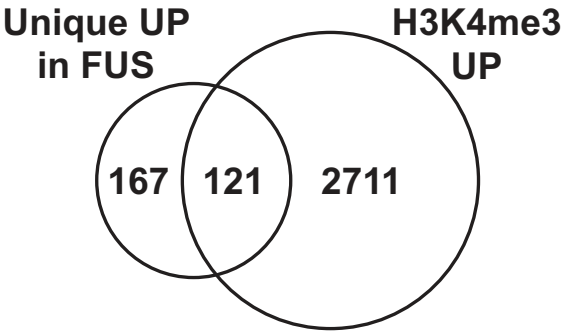

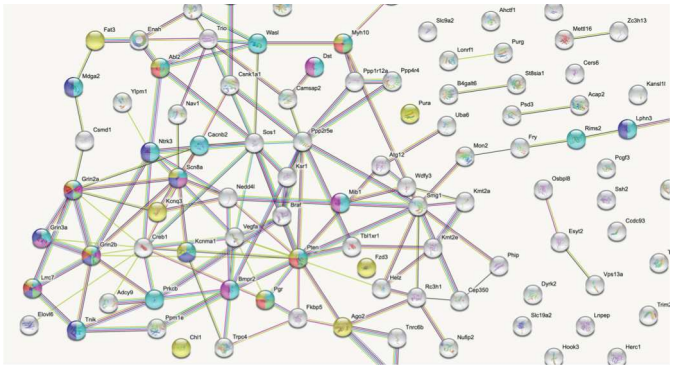

Glutamatergic synapse	FDR 4,2^{E}-04
Dendritic spine	FDR 0,0087
Synapse	FDR 2,2^{E}-05
Dendrite	FDR 8,8^{E}-05
PSD	FDR 0,023
Neuron spine	FDR 0,0098

• *H4K12ac*

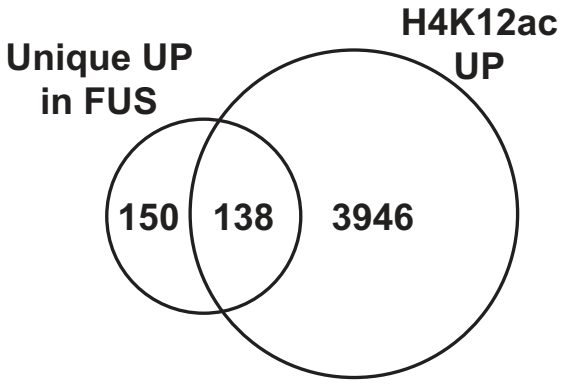

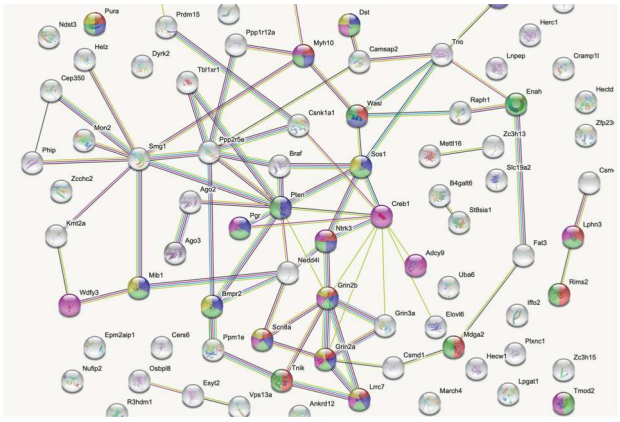

Glutamatergic synapse	FDR 2,6^{E}-04
Post-synapse	FDR 3,5^{E}-04
Synapse	FDR 3,5^{E}-04
Axon	FDR 0,0041
PSD	FDR 0,0088

• *H3K27ac*

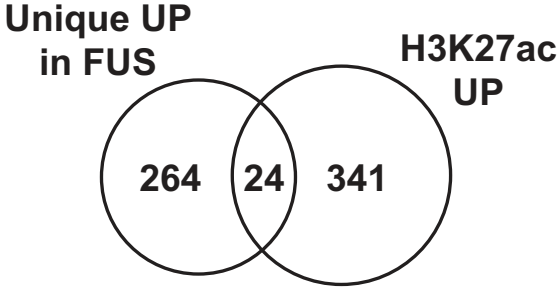

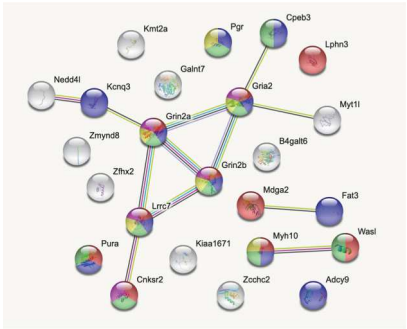

Glutamatergic synapse	FDR 1,4^{E}-07
Dendrite	FDR 1,6^{E}-07
Post-synapse	FDR 1,3^{E}-06
Dendritic spine	FDR 2,2^{E}-05
PSD membrane	FDR 2,9^{E}-05

Figure D2

Integration of FUS-targets (ChIP-seq FUS) with histone modifications (ChIP-seq)

• *H3K4me3*

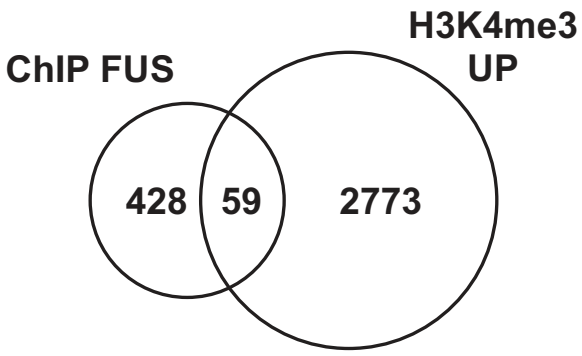

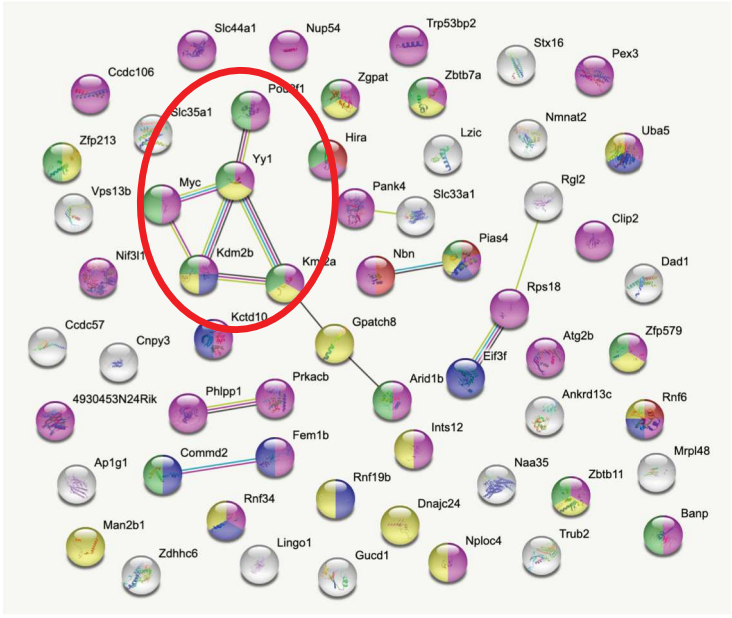

PML Body	FDR 0,0433
Nucleus	FDR 0,0026
Ubi conjugation pathway	FDR 0,0053
Zinc	FDR 0,0053
Transcription	FDR 0,0206

59 FUS-target genes were found H3K4me3 hypermethylated in FUS vs WT, among which 34/59 (57%) genes encoded for nuclear proteins.
The red node enlights Kmt2a, Kdm2b, Myc, YY1 and Pou2f1.

• *H3K27ac*

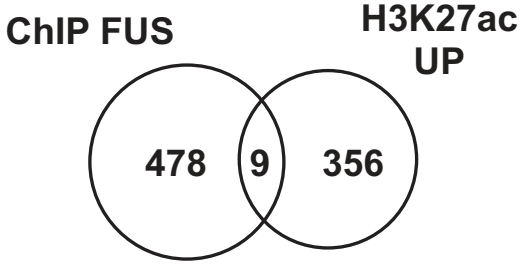

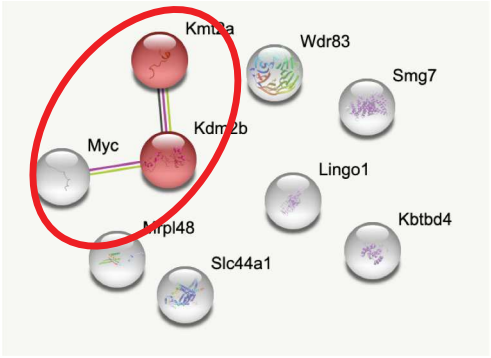

MF_Unmeth CpG bdg	FDR 0,0433

9 FUS-target genes were found H3K27 hyper-acetylated in FUS vs WT, among which Kmt2a, Kdm2b and Myc.

• *H4K12ac*

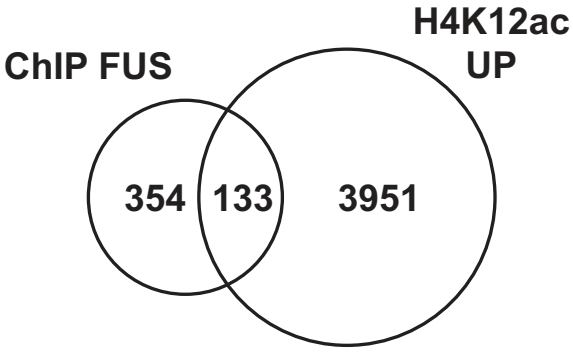

- Translation initiation FDR 0,0233
- Gene expression FDR 9,5E-06
- Ubi dpdt catab. process FDR 0,0074
- RNA metab. process FDR 0,0053
- ncRNA processing FDR 0,0245

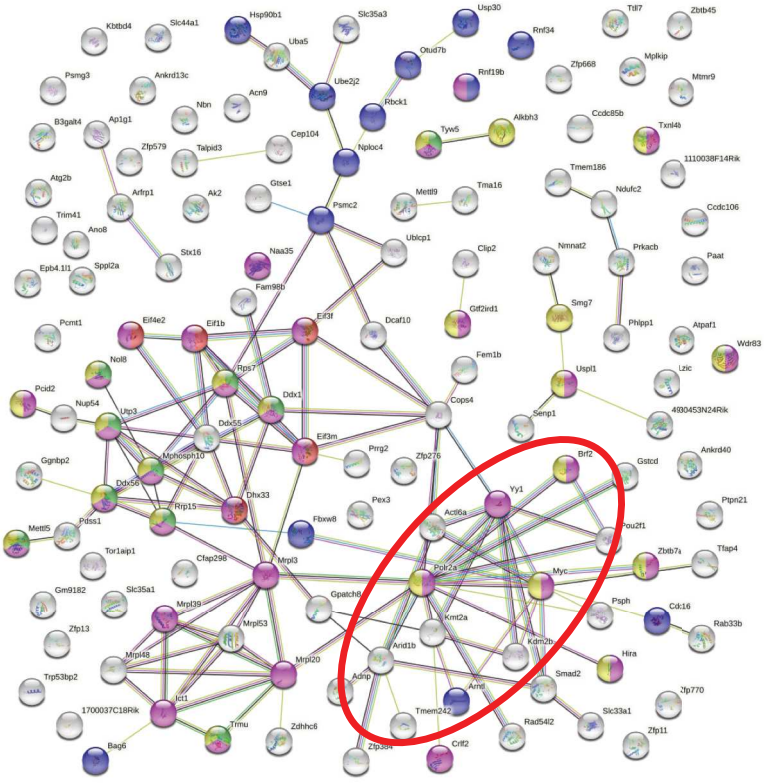

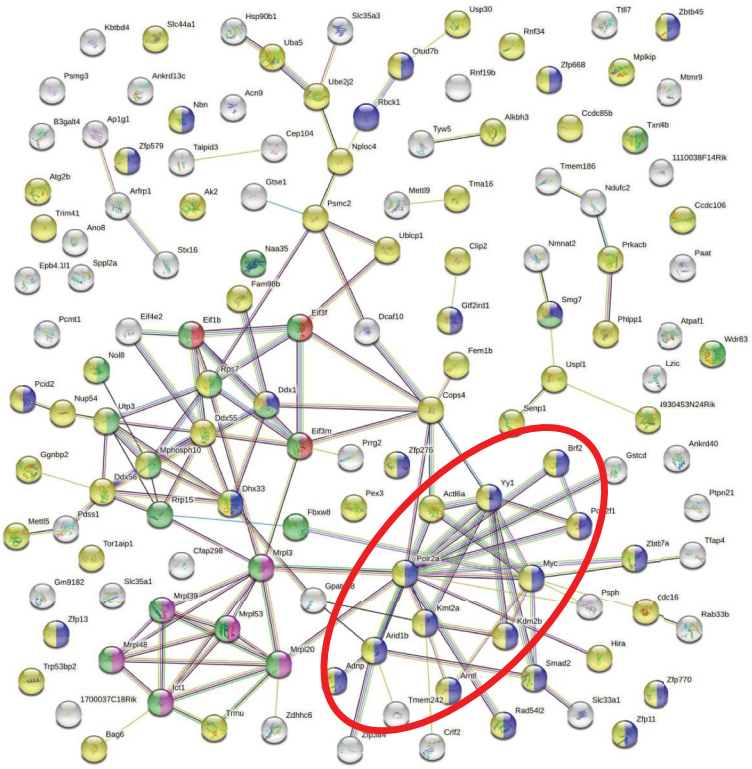

- Euk 43S pre-init. cplx FDR 0,0219
- Mitoch large ribo subunit FDR 0,00041
- DNA binding FDR 0,0122
- Nucleus FDR 1E-06
- Ribonucleoprot cplx FDR 1,6E-06

133 FUS-target genes were found H4K12 hyper-acetylated in FUS vs WT, among which a highly significant enrichment in gene expression related GOTERMS and again Kmt2a, Kdm2b, Myc, YY1, Pou2f1, Polr2a,…
71/133 (53%) genes encode for nuclear proteins.

Figure D3

Integration of training-induced genes (RNA-seq) with FUS CLIP-seq

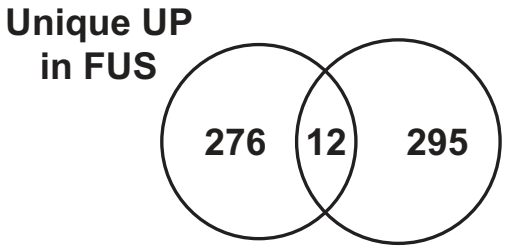

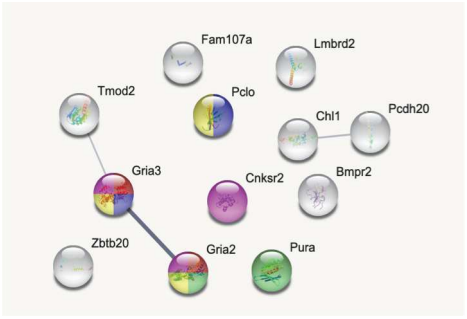

AMPA glu recept complex	FDR 0,0140
Post-synapt density mbne	FDR 0,0031
Fiber to Purk. cell synapse	FDR 0,0142
Terminal bouton	FDR 0,0024
Dendrite cytoplasm	FDR 0,0198

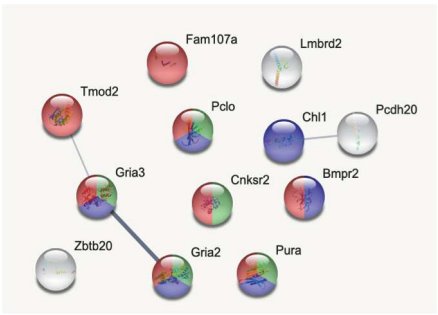

Synapse	FDR 7E-05
Glutamatergic synapse	FDR 0,00066
Dendrite	FDR 0,00029

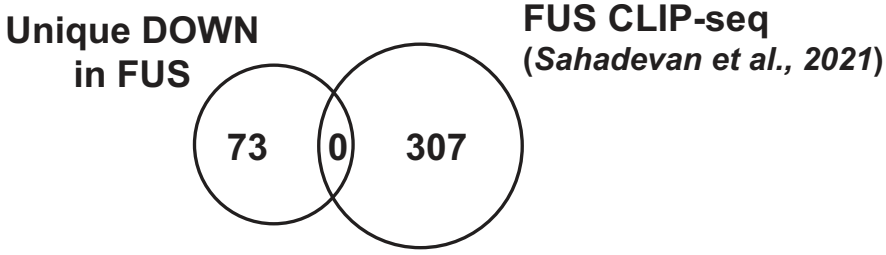

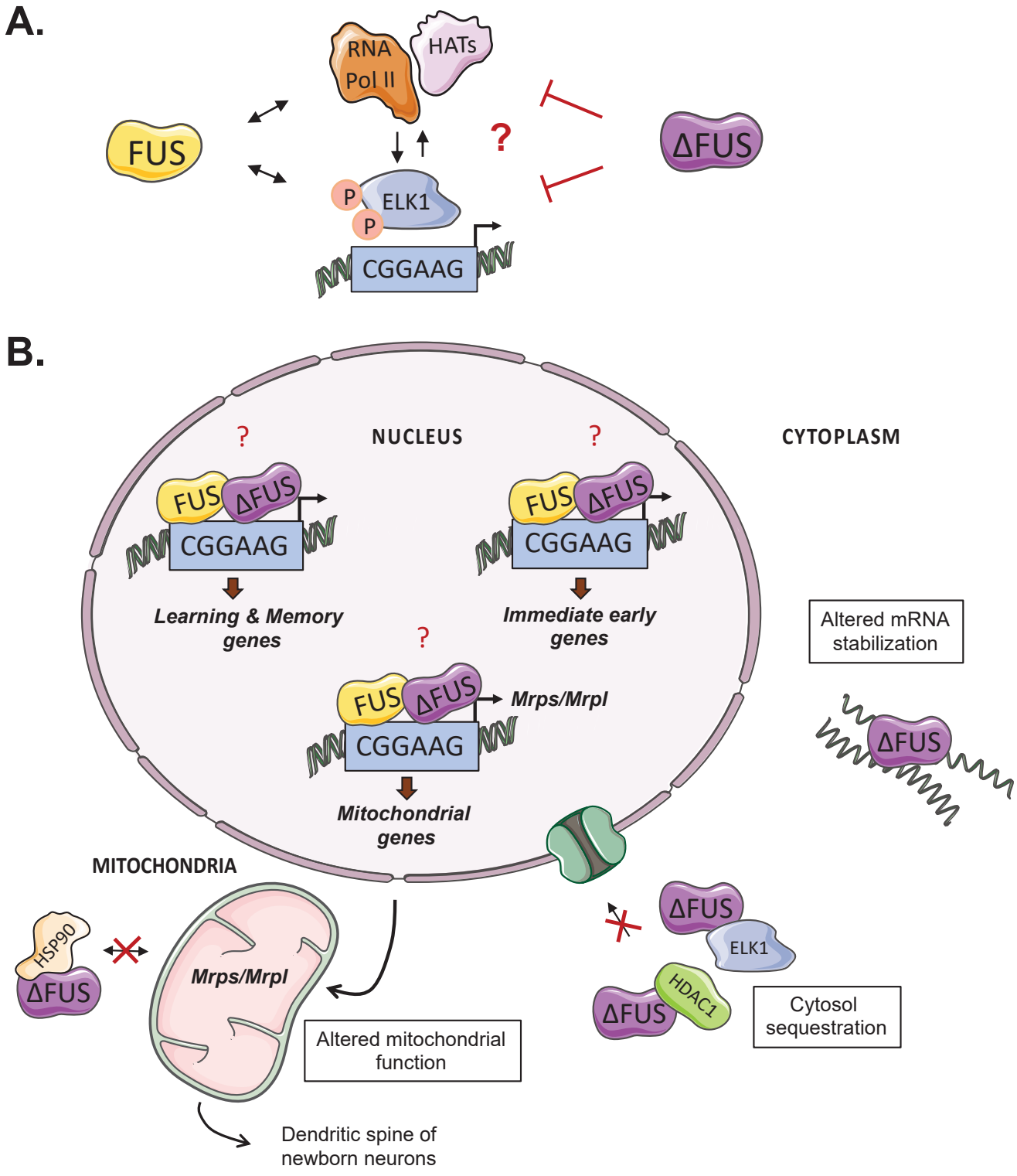

<u>Figure D4.</u> Hypothetical scheme of potential FUS-induced mechanisms leading to memory dysfunction. A. We hypothesize that members of the ELK1/ETS family could be a FUS binding partner. Several of our data converge to ETS/ELK1 promoter motifs (« CGGAAG ») and the competition of WT FUS and FISΔNLS (ΔFUS) mutation on these sites may induce a subsequent

dysregulation of FUS regulated genes, e.g. lack of co-activator recruitment, improper 3D conformation, as FUS is also known to bind partners acting on transcription (e.g. RNApol2, CBP). ΔFUS mutation could thus block these interactions (or recruits others?) at these sites. **B.** Many ETS/ELK-responsive genes are linked to learning and memory functions and, in the nuclear compartment, ΔFUS may impact the training-induced transcriptome and the early gene response as observed in our data sets, as well as the mitochondrial function through dysregulation of mitochondrial ribosomes (Mrps/Mrpl). Increased levels of ΔFUS mutated protein in the cytoplasm may impact mRNA stabilization, HSP90 trafficking and/or sequester major transcriptional actors (e.g. ELK1, HDAC1).

III. Model validity, consequences for ALS-FTD patients and therapeutical perspectives.

To be considered a validated animal model of the ALS-FTD spectrum our *Fus*$^{\Delta NLS/+}$ mice need to meet three criteria : homology or etiological similarity (i.e. construct validity), isomorphism or similarities of the symptoms (i.e. face validity); predictivity or identical pharmacological reactivity (i.e. predictive validity) (Willner, 1984).

The use of a single copy mouse model is highly analogous to the genetic situation of FUS-ALS patients, with most of the mutation present in the C-terminal region of the FUS protein, including the NLS domain (Shang and Huang, 2016). FUS mutations lead to FUS cytoplasmic delocalization and pathological aggregates, mostly located in the cytoplasm in fALS (Kwiatkowski et al., 2009; Vance et al., 2009) and sALS (Bäumer et al., 2010; Zou et al., 2013). FUS cytoplasmic mislocalization, in the absence of germline *FUS* mutations, is observed in several fALS and sALS cases (Tyzack et al., 2019; Ikenaka et al., 2020). FUS cytoplasmic aggregates are also found in a large subset of patients with FTD (Urwin et al., 2010). Altogether, our mouse model recapitulates the heterozygous mutation present in FUS fALS patients and the cytoplasmic delocalization observed in both ALS and FTD patients. Of note, this model might also be of high importance to understand other FUS-related diseases, sometimes termed FUSopathies. Indeed, *FUS* mutations are also observed in essential tremor disease (Merner et al., 2012) and in the absence of mutation, cytoplasmic mislocalization or aggregation of FUS is observed in polyglutamine diseases such as spino-cerebellar ataxia (Doi et al., 2010) and Huntington's disease (Doi et al., 2008). Therefore, we think that our model offers a good homology, since it reflects several causes (1) the mutation state, (2) the cytoplasmic mislocalization, observed in ALS-FTD and other FUSopathies.

Our studies demonstrate that FUS mutation is responsible for several behavioral changes accompanied by physiological and molecular changes in the hippocampus, in particular large changes in histone chromatin marks and gene dysregulation in response to learning. In the literature, it is clearly established that FTD patients demonstrate frontal and temporal alterations, and one might think that behavioral changes in *Fus*$^{\Delta NLS/+}$ mice primarily reflect FTD pathology. However, increasing evidence demonstrates mental retardation and learning

difficulties (Bäumer et al., 2010; Belzil et al., 2012; Fecto and Siddique, 2011; Huang et al., 2010; Onohara et al., 2015; Yamashita et al., 2012; Yan et al., 2010; Zou et al., 2013) as well as concomitant FTD disease (Blair et al., 2010; Broustal et al., 2010; Yan et al., 2010) in ALS patients. Cytoplasmic FUS aggregates are indeed not only present in motoneurons of the spinal cord but also present in the frontal cortex (Kwiatkowski et al., 2009). However, most studies focus on FUS aggregation in motoneurons of the spinal cord or in the motor cortex, and to the best of our knowledge, there is no study concerning FUS aggregation in other brain regions. In non-FUS ALS patients, the hippocampus is known to be affected and atrophied (Neumann et al., 2006; Takeda et al., 2007, 2008; Abdulla et al., 2014; Christidi et al., 2018; Machts et al., 2018; Christidi et al., 2019). These last years, particular attention has been raised to developed sensitive cognitive screening tools, to highlight cognitive dysfunction in ALS patients (Gosselt et al., 2020). However, the fact that ALS-FUS is mainly associated with severe and rapidly progressing juvenile ALS cases (Yamashita et al., 2012; Zou et al., 2013) may explain why we have so little information concerning behavioral and hippocampal alterations in this context: disease-progression is so fast that it does not allow for precise characterization beyond motor dysfunction. Altogether, our *Fus*$^{\Delta NLS/+}$ mouse model demonstrates good isomorphism to study the similarity of symptoms in FTD and could help to better characterize the potentially presymptomatic hippocampal ALS pathology.

Do our results have consequences concerning future therapeutical strategies? We demonstrated that several histone marks were altered in *Fus*$^{\Delta NLS/+}$ mice. We observed an enrichment of histone marks associated with active chromatin (acetylation, methylation). The goal of my thesis was mainly to better understand FUS function in the brain rather than the discovery of new therapeutical targets. However, epigenomic alterations are widely described in the literature in the context of neurodegenerative diseases, and several studies focus on normalizing the epigenome with the use of specific drugs. These drugs, mainly based on HDAC inhibitors and HAT activators, have the ability to rescue the memory deficits in different Alzheimer's disease mouse models (Alarcón et al., 2004; Peleg et al., 2010; Benito et al., 2015; Chatterjee et al., 2018) or restore metabolic and lipid functions in the spinal cord of another ALS-FTD mouse model expressing human FUS (Guo et al., 2017; Burg et al., 2021). However, this type of strategy may not be suitable to address hippocampal dysfunctions in our mouse model since HDAC inhibitors and HAT activators could result in even more increased acetylation levels. Mutant FUS is

associated with decreased acetylation levels in murine spinal cord (Burg et al., 2021) and in motor neurons of primary spinal cord cultures (Tibshirani et al., 2015), while we observed increased acetylation in the hippocampus in this study. It is therefore likely that HDAC inhibitors/ HAT activators might positively affect some cells while negatively influence other cell types involved in ALS and FTD pathophysiology. Furthermore, while HDAC2 deficient mice demonstrate memory facilitation and an increased number of synapses in contextual fear learning and spatial memory tasks (Guan et al., 2009), neuron- specific loss of HDAC4 leads to defects in motor coordination and learning as well as increased anxiety-like behaviors (Kim et al., 2012). We discussed the potential negative effect of HDAC inhibitors in more details in a commentary appended to this thesis in the annex section (Boutillier et al., 2019).

Altogether, it is still too early to conclude about predictivity and identical pharmacological reactivity in the *Fus*$^{\Delta NLS/+}$ mouse model since no treatment are currently available to treat epigenetic alterations in ALS-FTS disease. Targeting acetylation might be a promising approach in certain circumstances, however drugs that interact with more precise targets, or the development of a local treatment specifically in motoneurons or cortical regions might be required to treat epigenetic alterations in the context of ALS-FTD diseases.

ANNEX

Publication 3: In the same mouse model developed in Dupuis Lab, the paper of first co-authors Jelena SCEKIC-ZAHIROVIC and Inmaculada SANJUAN RUIZ demonstrated that FUS mislocalization is sufficient to induce cortical synaptic defects that could lead to FTD-like symptoms (Scekic-Zahirovic et al., 2021). In this publication, I assessed and analyzed the locomotor activity *Fus*$^{\Delta NLS/+}$ mice at 4 months of age and performed the RNA-extraction/RNAseq study from the pre-frontal cortex of 6 months of age *Fus*$^{\Delta NLS/+}$ mice. **(Attached)**

> *Scekic-Zahirovic, J., Sanjuan-Ruiz, I., Kan, V., Megat, S., De Rossi, P., Dieterlé, S., Cassel, R., Jamet, M., Kessler, P., Wiesner, D., et al. (2021). Cytoplasmic FUS triggers early behavioral alterations linked to cortical neuronal hyperactivity and inhibitory synaptic defects. Nat Commun 12, 3028.*

Publication 4: In an article of EBioMedicine, Viviana MORESI and colleagues provided genetic evidence that skeletal muscle HDAC4 exerts a protective role for neuromuscular junction and muscle innervation in amyotrophic lateral sclerosis (ALS) (Pigna et al., 2019). With the collaboration of Anne-Laurence BOUTILLIER and Luc DUPUIS, I participated to the literature search and the writing of a comment that discussed the potential negative effect of HDAC inhibitors in the context of ALS (Boutillier et al., 2019). **(Attached)**

> *Boutillier, A.-L., Tzeplaeff, L., and Dupuis, L. (2019). The dark side of HDAC inhibition in ALS. EBioMedicine 41, 38–39.*

Publication 5: Boutillier Lab is interested in epigenetic alterations in the context of neurodegenerative diseases. When I arrived in the laboratory, the paper of Snehajyoti CHATTERJEE and collaborators investigating the effect of CSP-TTK21 treatment on THY-Tau22 Alzheimer mouse model, was in revision (Chatterjee et al., 2018). Thus, I had the chance to participate to some complementary experiments, including western blot and RT-qPCR quantifications and analyses.

> *Chatterjee, S., Cassel, R., Schneider-Anthony, A., Merienne, K., Cosquer, B., Tzeplaeff, L., Halder Sinha, S., Kumar, M., Chaturbedy, P., Eswaramoorthy, M., et al. (2018). Reinstating plasticity and memory in a tauopathy mouse model with an acetyltransferase activator. EMBO Molecular Medicine 10, e8587.*

Publication 6: During my thesis, a colleague from Boutillier Lab was working on transgenic mice harboring a microglia-specific knock-down of Bmal1 (Wang et al., 2021). For the purpose of the study involving the circadian clock, we needed to work at two people to allow for several timed perfusion/dissection that aim to isolate microglia during the light and dark phase of mice. I also contributed to the MWM analyses.

Wang, X.-L., Kooijman, S., Gao, Y., Tzeplaeff, L., Cosquer, B., Milanova, I., Wolff, S.E.C., Korpel, N., Champy, M.-F., Petit-Demoulière, B., et al. (2021). Microglia-specific knock-down of Bmal1 improves memory and protects mice from high fat diet-induced obesity. Mol Psychiatry.

nature COMMUNICATIONS

ARTICLE

https://doi.org/10.1038/s41467-021-23187-9 OPEN

Cytoplasmic FUS triggers early behavioral alterations linked to cortical neuronal hyperactivity and inhibitory synaptic defects

Jelena Scekic-Zahirovic[1,14], Inmaculada Sanjuan-Ruiz[1,14], Vanessa Kan[2,3], Salim Megat[1], Pierre De Rossi[4], Stéphane Dieterlé[1], Raphaelle Cassel[1,5], Marguerite Jamet[1], Pascal Kessler[6], Diana Wiesner[7,8], Laura Tzeplaeff[5], Valérie Demais[9], Sonu Sahadevan[4], Katharina M. Hembach[4], Hans-Peter Muller[7], Gina Picchiarelli[1], Nibha Mishra[10,11], Stefano Antonucci[7,8], Sylvie Dirrig-Grosch[1], Jan Kassubek[7], Volker Rasche[12], Albert Ludolph[7,8], Anne-Laurence Boutillier[5], Francesco Roselli[7,8], Magdalini Polymenidou[4], Clotilde Lagier-Tourenne[10,11], Sabine Liebscher[2,3,13,15]✉ & Luc Dupuis[1,15]✉

Gene mutations causing cytoplasmic mislocalization of the RNA-binding protein FUS lead to severe forms of amyotrophic lateral sclerosis (ALS). Cytoplasmic accumulation of FUS is also observed in other diseases, with unknown consequences. Here, we show that cytoplasmic mislocalization of FUS drives behavioral abnormalities in knock-in mice, including locomotor hyperactivity and alterations in social interactions, in the absence of widespread neuronal loss. Mechanistically, we identified a progressive increase in neuronal activity in the frontal cortex of *Fus* knock-in mice in vivo, associated with altered synaptic gene expression. Synaptic ultrastructural and morphological defects were more pronounced in inhibitory than excitatory synapses and associated with increased synaptosomal levels of FUS and its RNA targets. Thus, cytoplasmic FUS triggers synaptic deficits, which is leading to increased neuronal activity in frontal cortex and causing related behavioral phenotypes. These results indicate that FUS mislocalization may trigger deleterious phenotypes beyond motor neuron impairment in ALS, likely relevant also for other neurodegenerative diseases characterized by FUS mislocalization.

[1] Université de Strasbourg, Inserm, Mécanismes centraux et périphériques de la neurodégénérescence, Strasbourg, France. [2] Institute of Clinical Neuroimmunology, Klinikum der Universität München, Ludwig-Maximilians-University Munich, Munich, Germany. [3] BioMedical Center, Medical Faculty, Ludwig-Maximilians-University Munich, Munich, Germany. [4] Department of Quantitative Biomedicine, University of Zurich, Zürich, Switzerland. [5] Université de Strasbourg, UMR 7364 CNRS, Laboratoire de Neurosciences Cognitives et Adaptatives (LNCA), Strasbourg, France. [6] Université de Strasbourg, Inserm, Unité mixte de service du CRBS, UMS 038, Strasbourg, France. [7] Department of Neurology, Ulm University, Ulm, Germany. [8] Deutsches Zentrum für Neurodegenerative Erkrankungen (DZNE), Ulm, Germany. [9] Plateforme Imagerie In Vitro, CNRS UPS-3156, NeuroPôle, Strasbourg, France. [10] Department of Neurology, The Sean M. Healey and AMG Center for ALS at Mass General, Massachusetts General Hospital, Harvard Medical School, Boston, MA, USA. [11] Broad Institute of Harvard University and MIT, Cambridge, MA, USA. [12] Ulm University Medical Center, Department of Internal Medicine II, Ulm, Germany. [13] Munich Cluster for Systems Neurology (SyNergy), Munich, Germany. [14] These authors contributed equally: Jelena Scekic-Zahirovic, Inmaculada Sanjuan-Ruiz. [15] These authors jointly supervised this work: Sabine Liebscher, Luc Dupuis. ✉email: sabine.liebscher@med.uni-muenchen.de; ldupuis@unistra.fr

Amyotrophic lateral sclerosis (ALS) is the major adult motor neuron disease, with onset usually in the 6th and 7th decade of life and death due to respiratory insufficiency and progressive paralysis typically occurring 3–5 years after onset of motor symptoms[1–3]. Mutations in the Fused in Sarcoma gene (*FUS*), encoding an RNA-binding protein from the FET family[4,5], are associated with the most severe forms of ALS[6,7], clinically presenting with a very early onset and rapid disease progression[8,9]. ALS associated mutations in *FUS* are clustered in the C-terminal region of the FUS protein that includes the atypical PY nuclear localization sequence, and is required for protein entry into the nucleus[6,7,10–12]. The severity of the disease correlates with the degree of impairment of FUS nuclear import[11,12], and the most severe cases of ALS known to date, are indeed caused by mutations leading to the complete truncation of the PY-NLS[8,9].

A number of clinical and pathological studies suggest that FUS mislocalization to the cytoplasm and subsequent aggregation could be relevant beyond the few ALS-FUS cases. First, *FUS* mutations, although rare in non-ALS cases, have been found in cases with frontotemporal dementia, either isolated[13,14] or as an initial presentation of ALS-FTD[15,16], as well as in patients with initial chorea[17], mental retardation[18], psychosis or dementia[19], and essential tremor[20]. In the absence of *FUS* mutations, FUS mislocalization[21], or aggregation[22,23] were found to be widespread in sporadic ALS. FUS pathology also defines a subset of cases with FTD (FTD-FUS) with prominent atrophy of the caudate putamen[24–26], concomitant pathology of other FET proteins, such as TAF15 and EWSR1[12,27–30] and frequent psychiatric symptoms[28]. FUS aggregates have also been observed in spinocerebellar ataxia and Huntington's disease[31,32]. While FUS mislocalization appears to be a common feature in neurodegenerative diseases, its pathological consequences have not been thoroughly studied beyond motor neuron degeneration.

Neurons with FUS pathology show decreased levels of FUS in the nucleus, that might compromise a number of processes dependent on proper FUS levels such as transcription and splicing regulation or DNA damage repair[4]. Interestingly, loss of FUS alters the splicing of multiple mRNAs relevant to neuronal function[33,34], such as *MAPT*, encoding the TAU protein, and alters the stability of mRNAs, encoding relevant synaptic proteins such as GluA1 and SynGAP1[35–39]. However, loss of nuclear FUS levels is very efficiently compensated for by autoregulatory mechanisms as well as by other FET proteins, and loss of nuclear FUS remains limited as opposed to loss of nuclear TDP-43, observed in TDP-43 pathology[40]. Indeed, heterozygous *Fus* knock-in mice, which carry one mutant allele leading to cytoplasmic and not nuclear localization of FUS, only show marginal loss of nuclear FUS due to compensatory overexpression[10,41]. Beyond nuclear loss of function, accumulation of cytoplasmic FUS was found to be a critical event in ALS-FUS in multiple studies in mouse models. For instance, cytoplasmic FUS is necessary to cause motor neuron degeneration in ALS-FUS[10,41–46] as heterozygous *Fus* knock-in mouse models develop mild, late onset muscle weakness and motor neuron degeneration, but not haploinsufficient *Fus* knockout mice[10,41,46]. To date, there are few studies investigating whether the accumulation of cytoplasmic FUS might lead to phenotypes beyond motor neuron degeneration. Interestingly, FUS is also found at synaptic and dendritic sites[38,47–51], and Sahadevan, Hembach et al.[52] identify synaptic mRNA targets for FUS that are critical for synaptic formation, function and maintenance.

Here, we show that a partial cytoplasmic mislocalization of FUS in heterozygous *Fus* knock-in mice is sufficient to drive a panel of behavioral abnormalities, including locomotor hyperactivity and alterations in social interactions, which preceded motor neuron degeneration. Behavioral deficits were accompanied by ventricle enlargement and atrophy of several subcortical structures in the absence of widespread neuronal loss in the cortex. Mechanistically, we could identify a progressive increase in neuronal activity in the frontal cortex of *Fus* knock-in mice in vivo. Furthermore, we observed a coordinated downregulation of multiple genes related to synaptic function in the frontal cortex throughout adulthood, which were confirmed by ultrastructural and morphological defects of synapses. These synaptic defects were more profound in inhibitory compared to excitatory synapses and accompanied by increased levels of FUS protein as well as of 3 of its RNA targets (*Fus, Nrxn1*, and *Gabra1*) in synaptosomes of heterozygous *Fus* knock-in mice. Thus, FUS cytoplasmic enrichment is sufficient to trigger synaptic deficits, leading to increased neuronal activity and behavioral phenotypes. These findings suggest that FUS mislocalization could trigger deleterious phenotypes beyond impaired motor function that could be relevant for both ALS-FUS but also for other neurodegenerative diseases based on FUS mislocalization.

Results

Spontaneous locomotor hyperactivity in $Fus^{\Delta NLS/+}$ mice. Since FUS mislocalization and aggregation are observed in patients with various neurodegenerative diseases, we hypothesized that partial FUS cytoplasmic mislocalization in $Fus^{\Delta NLS/+}$ mice could be sufficient to cause a number of behavioral phenotypes. Two independent cohorts of mice were analyzed at 4 months of age, before the appearance of motor impairment[41] and 10 months of age. Evaluation of basal motor activity in a familiar environment showed significantly increased locomotor activity in $Fus^{\Delta NLS/+}$ mice over the 3 consecutive days of observation (Fig. 1a, b). Interestingly, this hyperactivity was observed throughout the entire night in 4-months-old $Fus^{\Delta NLS/+}$ mice (Fig. 1a), but only during late night hours in older $Fus^{\Delta NLS/+}$ mice (Fig. 1b). In the open field, ambulatory distance, duration of ambulation, mean speed and preference for peripheral quadrants over central quadrants were similar in 10-months-old $Fus^{\Delta NLS/+}$ mice and wild-type littermates, indicating the absence of hyperactivity in a novel environment (Supplementary Fig. 1a, b). To further study potential anxiety-related phenotypes in $Fus^{\Delta NLS/+}$ mice, we used the dark/light box test, based on the preference of mice for dark compartments over illuminated places. In this test, 10-months-old $Fus^{\Delta NLS/+}$ mice and $Fus^{+/+}$ mice showed a similar latency to enter, similar frequency of transitions and similar duration to explore illuminated compartment (Supplementary Fig. 1c). Thus, $Fus^{\Delta NLS/+}$ mice are hyperactive, but do not show evidence of anxious behaviors, at least at the ages tested.

Mildly compromised consolidation of spatial memory in $Fus^{\Delta NLS/+}$ mice. To explore the possibility that behavioral phenotypes of $Fus^{\Delta NLS/+}$ mice included spatial memory defects, we performed the Morris water maze test. This task requires hippocampal function, at least during acquisition and memory formation, but relies on a proper cortico-hippocampal dialog for longer retention times or remote memory retrieval (Fig. 1c)[53]. At 10 months of age, $Fus^{\Delta NLS/+}$ mice performed similarly well to their $Fus^{+/+}$ littermates regarding the distance travelled and latency to find the hidden platform over training days (Fig. 1d, e). We then performed a probe trial 18 days after the last training and observed that, although both genotypes searched significantly in the target quadrant compared to nontarget areas, $Fus^{\Delta NLS/+}$ mice displayed a slightly decreased performance to retrieve memory at this timepoint (Fig. 1f). Furthermore, $Fus^{\Delta NLS/+}$ mice lost their previous memory significantly faster than wild-type

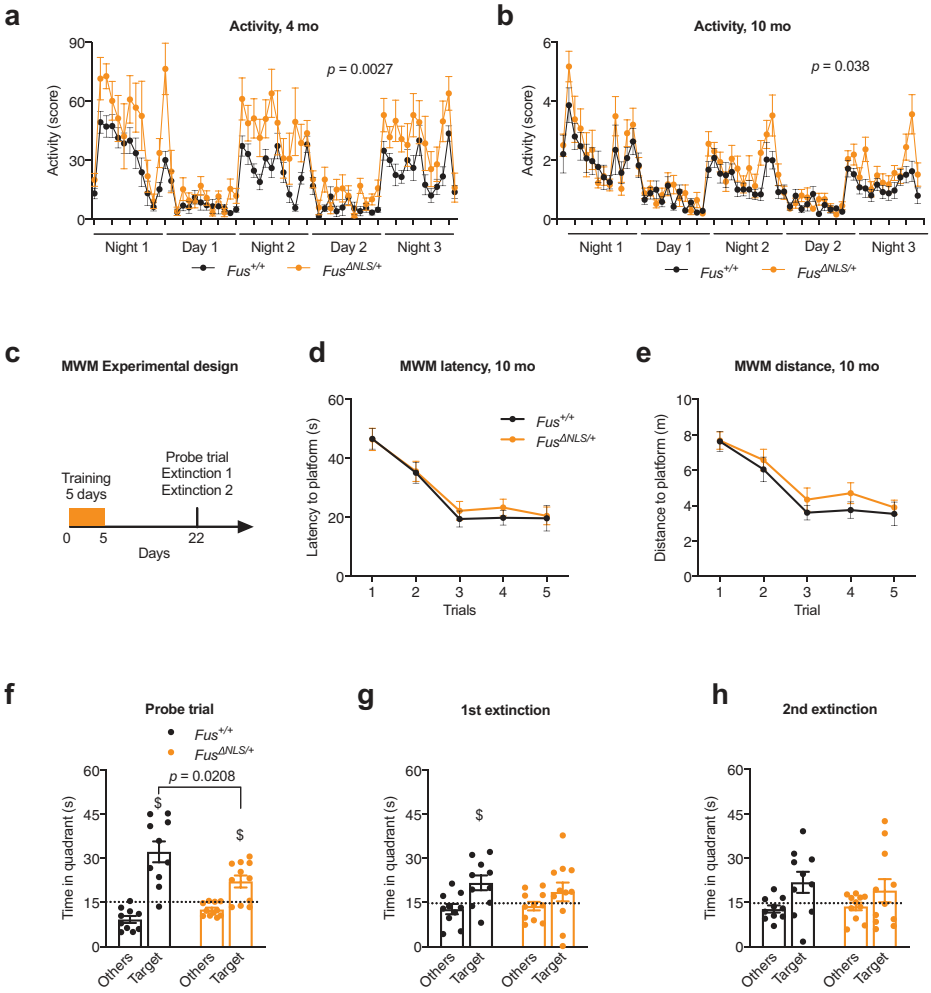

Fig. 1 *Fus*$^{\Delta NLS/+}$ mice display increased nocturnal spontaneous locomotor activity and cognitive defects. a, b Line graphs represent mice home cage activity-actimetry over three consecutive days at 4 months (**a**) and 10 months (**b**) of *Fus*$^{+/+}$ (black) and *Fus*$^{\Delta NLS/+}$ (orange) male mice $N = 11$ for *Fus*$^{+/+}$ and $N = 10$ for *Fus*$^{\Delta NLS/+}$ mice at 4 months and $N = 15$ for *Fus*$^{+/+}$ and $N = 14$ for *Fus*$^{\Delta NLS/+}$ mice at 10 months. Repeated measures Two-way ANOVA followed by Sidak for multiple comparisons, with time and genotype as variables. $P = 0.0027$ at 4 months and $p = 0.038$ at 10 months for genotype effect. Data are presented as mean ± SEM values of activity score per hour. **c** Schematic illustration of the Morris water maze (MWM) experimental strategy (paradigm). Mice were subjected to a five-day training period and tested for spatial memory retention in a probe trial (60 seconds) 18 days after the last acquisition. The probe trial was then followed by two extinction tests, performed at 2 h intervals. **d, e** Line graphs represent latency (in seconds) (**d**) and total distance swam (in meters) (**e**) to find the hidden platform during acquisition of 10-months-old *Fus*$^{+/+}$ (black) and *Fus*$^{\Delta NLS/+}$ (orange) male mice. Both genotypes improved similarly their performance between day 1 and 5. $N = 10$ for *Fus*$^{+/+}$ and $N = 11$ for *Fus*$^{\Delta NLS/+}$ mice. Data are presented as mean ± SEM values of four trials per day of training. A two-way repeated measure analysis of variance (ANOVA) (genotype * days) was conducted to determine the effect of genotype on learning over time. No significant effect of genotype is observed. **f** Bar graphs represent the time spent in the target quadrant (Target) and the average of the time spent in the other three quadrants (Others) during probe trial. Dashed line indicates chance level (15 seconds per quadrant; i.e., 25%). $N = 10$ for *Fus*$^{+/+}$ and $N = 11$ for *Fus*$^{\Delta NLS/+}$ mice. Data are presented as mean ± SEM. Both genotypes were significantly above random but *Fus*$^{\Delta NLS/+}$ mice performed significantly worse than *Fus*$^{+/+}$ littermates ($, $p < 0.01$, One sample *t*-test was used to compare to a chance level, Target quadrant: $p = 0.0008$ for *Fus*$^{+/+}$ and $p = 0.006$ for *Fus*$^{\Delta NLS/+}$). Genotype comparison was made using One-way ANOVA; $F(1,19) = 6.33$, $p = 0.0208$. **g, h** Bar graphs represent the time spent in quadrants (Target vs Others) during the first (**g**) and the second (**h**) extinction test ($, $p < 0.05$ vs chance levels). One-way ANOVA for genotype effect ($F(1,19) = 0.56$, $p = 0.46$) (**g**), ($F(1,19) = 0.27$, $p = 0.6$) (**h**) and One sample *t*-test was used to compare to a chance level, (Target quadrant: $p = 0.025$ for *Fus*$^{+/+}$ and $p = 0.22$ for *Fus*$^{\Delta NLS/+}$) (**g**), (Target quadrant: $p = 0.08$ for *Fus*$^{+/+}$ and $p = 0.09$ for *Fus*$^{\Delta NLS/+}$) (**h**). $N =$ 10 for *Fus*$^{+/+}$ and $N = 11$ for *Fus*$^{\Delta NLS/+}$ mice, with same mice as panel **f**. Data are presented as mean ± SEM. Source data are provided as a Source Data file.

mice, as they were searching randomly in a first extinction test performed 2 h after the probe trial, while wild-type mice still showed a significant more directed searching behaviour and preferred the target area over others (Fig. 1g). This suggests that consolidation of long-term memory was mildly compromised in *Fus*$^{\Delta NLS/+}$ mice. Lastly, both genotypes did not distinguish the target over the other quadrants in a second extinction test (Fig. 1h). Altogether, these data show that *Fus*$^{\Delta NLS/+}$ mice were able to learn but displayed impaired long-term memory in agreement with a dysfunction of cortical regions.

Social disinhibition in *Fus*$^{\Delta NLS/+}$ mice. Marked changes in personality and social behavior, such as social withdrawal or social disinhibition, obsessive-compulsive behaviors, euphoria or apathy are common in subjects with behavioral variant (bv)FTD, a disease with pronounced FUS mislocalization[54–56]. Social

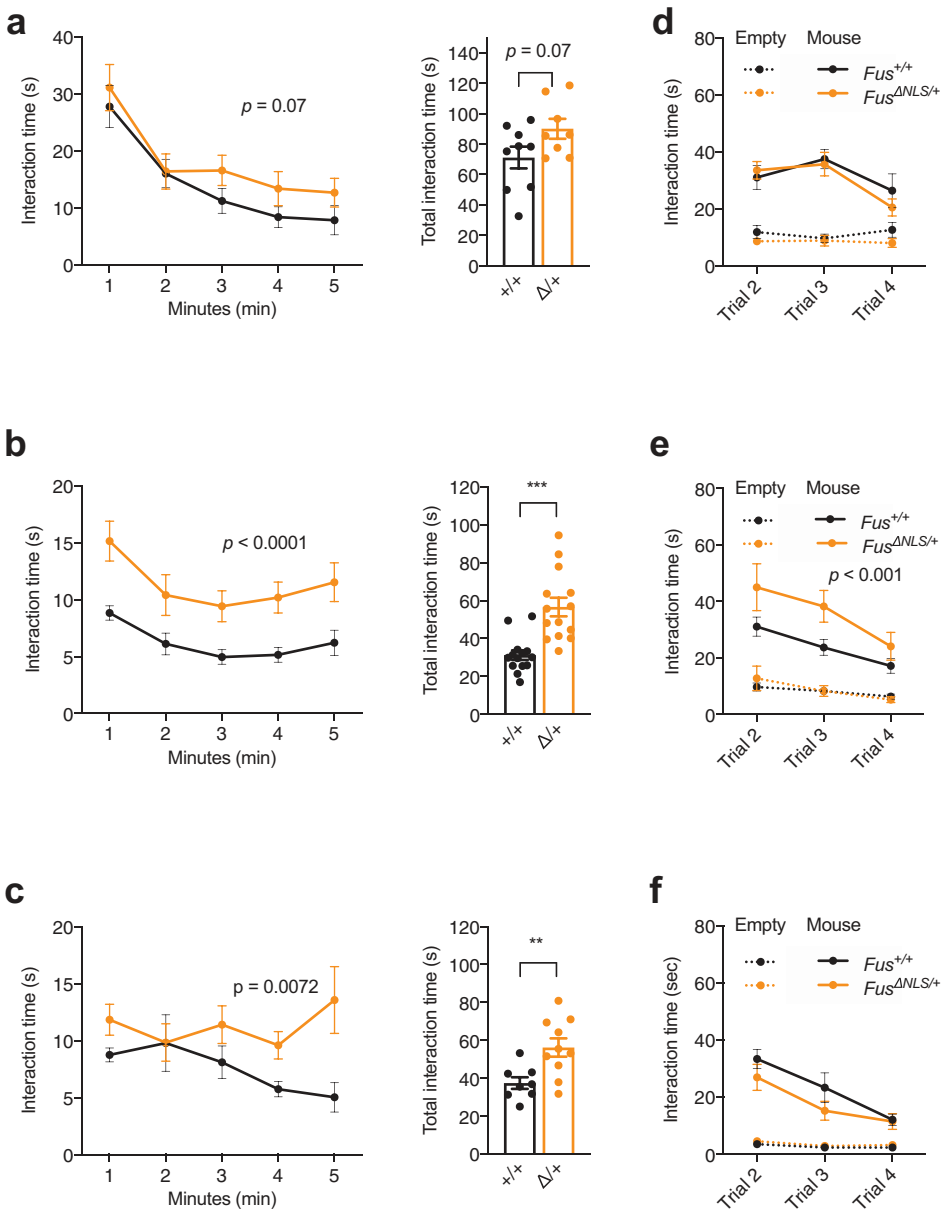

Fig. 2 Social behavior abnormalities in *Fus*$^{\Delta NLS/+}$ mice. a–c Line and bar graphs represent interaction time between resident (test) and intruder mice exclusively initiated by resident mouse in one-minute intervals (line graphs, on the left) or over the total time (bar graphs, on the right) during a 5 min resident-intruder test in home cage for 4 (**a**), 10 (**b**), and 22 (**c**) months-old *Fus*$^{+/+}$ (black) and *Fus*$^{\Delta NLS/+}$ (orange) male mice. Note that, young *Fus*$^{\Delta NLS/+}$ mice demonstrated a trend towards an increased social interest for intruder mouse (**a**) while older mice interacted with intruders significantly longer then *Fus*$^{+/+}$ (**b**, **c**) showing an age-dependent impairment of social behavior–disinhibition. All values are represented as mean ± SEM. At 4 months, $N = 9$ for *Fus*$^{+/+}$ and $N = 8$ for *Fus*$^{\Delta NLS/+}$ mice; At 10 months, $N = 14$ for *Fus*$^{+/+}$ and $N = 14$ for *Fus*$^{\Delta NLS/+}$ mice; At 22 months, $N = 8$ for *Fus*$^{+/+}$ and $N = 10$ for *Fus*$^{\Delta NLS/+}$ mice. Two-way repeated measures ANOVA followed by Sidak post-hoc test ($p = 0.07$ (4 months), $p < 0.001$ (10 months), and $p = 0.007$ (22 months) for genotype.effect); Two-sided Unpaired Student's *t*-test for total time $p = 0.07$ (4 months), $p < 0.001$ (10 months), and $p = 0.007$ (22 months)). **d**, **f** Line graphs represent sociability in the three-chamber test measured as interaction time with novel mice across three trials for *Fus*$^{+/+}$(black) and *Fus*$^{\Delta NLS/+}$ (orange) male mice at 4 (**d**), 10 (**e**), and 22 (**f**) months of age. Time exploring an empty cage (object) across trials is represented as dashed lines. At 4 months, $N = 9$ for *Fus*$^{+/+}$ and $N = 8$ for *Fus*$^{\Delta NLS/+}$ mice; At 10 months, $N = 14$ for *Fus*$^{+/+}$ and $N = 14$ for *Fus*$^{\Delta NLS/+}$ mice; At 22 months, $N = 8$ for *Fus*$^{+/+}$ and $N = 9$ for *Fus*$^{\Delta NLS/+}$ mice. Data are presented as mean ± SEM. Three-way ANOVA with Newman Keuls post-hoc test for multiple comparisons, $p =$ ns (4 months), $p < 0.001$ (10 months) and $p =$ ns (22 months) for genotype effect). Source data are provided as a Source Data file.

deficits were also reported in progranulin haploinsufficient mice, a mouse model of FTD[57]. To determine whether *Fus*$^{\Delta NLS/+}$ mice have social behavioral deficits, we first performed the resident-intruder test specific for evaluating sociability in mice. Interestingly, 4-months-old *Fus*$^{\Delta NLS/+}$ mice showed a trend towards longer interaction with the intruder mouse as compared with *Fus*$^{+/+}$ mice ($p = 0.07$) (Fig. 2a), that was significant at 10 months of age (Fig. 2b) and persisted until 22 months of age (Fig. 2c). Aggressive behavior was only observed at 4 months of age, and not affected by the *Fus* genotype (attack duration:

13.0 ± 1.4 s in $Fus^{+/+}$ mice vs 11.6 ± 1.0 s in $Fus^{\Delta NLS/+}$ mice, $p = 0.88$ two-sided unpaired Student's *t*-test). To further characterize the social behavioral impairment, we used a modified version of the three-chamber social paradigm. After a first trial of habituation using an empty setup, a novel mouse is introduced in a side compartment. The interactions initiated by the test mouse with either the novel mouse or the empty cage was quantified. Of most relevance, across the three consecutive trials (Trial 2, 3, and 4), we observed that 10-months-old $Fus^{\Delta NLS/+}$ mice consistently interacted more with the novel mouse than $Fus^{+/+}$ mice, in line with social disinhibition (Fig. 2e). This was not observed at 4 or 22 months of age (Fig. 2d–f). Importantly, mice of both genotypes spent more time interacting with the novel mouse than with the empty cage, indicating that mice could recognize its conspecific. The interaction time gradually decreased in later trials, suggesting progressive loss of social interest in the novel mouse, while it became familiar (Fig. 2d–f). Similar findings of social disinhibition in both resident-intruder test and three-chamber paradigms as a novel environment exclude the possibility that the observed increased social interactions resulted from locomotor hyperactivity in the home cage. Importantly, the olfactory function of $Fus^{\Delta NLS/+}$ mice was preserved, since results showed no differences between genotypes at 22 months of age in the time spent sniffing filter paper, covered with either attractive scent (vanilla) or an aversive scent (2-methyl butyrate) (Supplementary Fig. 2). These findings together with absence of major motor phenotype at that age (Supplementary Fig. 1a, b) indicated that social behavior is specifically affected in $Fus^{\Delta NLS/+}$ mice. Taken altogether, behavioral analyses of $Fus^{\Delta NLS/+}$ mice uncovered locomotor hyperactivity, cognitive deficits, and altered memory consolidation as well as selective impairment in sociability.

Increased spontaneous neuronal activity in $Fus^{\Delta NLS/+}$ mice in vivo. As the behavioral changes observed are highly reminiscent of frontal lobe dysfunction, we next asked whether neuronal activity is altered within that brain area. We thus examined spontaneous neuronal activity using in vivo two-photon calcium imaging (Fig. 3a–c). We studied neurons in cortical layer II/III of the frontal cortex expressing the genetically encoded calcium indicator GCaMP (delivered through an AAV vector) in mice at the age of 4 and 10 months (Fig. 3b). Indeed, we observed a significant increase in spontaneous activity, which worsened with age. While in 4-month-old mice the fraction of active neurons did not differ between $Fus^{+/+}$ and $Fus^{\Delta NLS/+}$ mice (Fig. 3d), there was a decrease in transient amplitudes (Fig. 3e) and an increase in transient frequency (Fig. 3f) in $Fus^{\Delta NLS/+}$ mice. In 10-month-old animals, this increase in activity was already evident at the level of the fraction of active cells in $Fus^{\Delta NLS/+}$ (Fig. 3g). Moreover, we observed an increase in the transient amplitudes (Fig. 3h) and also in the transient frequency (Fig. 3i) in $Fus^{\Delta NLS/+}$ mice compared to their $Fus^{+/+}$ littermates. Taken together, our data demonstrate an age dependent, strong increase in neuronal activity in vivo within the upper layers of frontal cortex of $Fus^{\Delta NLS/+}$ mice.

$Fus^{\Delta NLS/+}$ mice show ventricle enlargement and atrophy of subcortical structures but preserved cortical neurons. We next sought to understand the structural basis of behavioral and electrophysiological abnormalities in $Fus^{\Delta NLS/+}$ mice by employing MR imaging. FLASH MRI datasets for $Fus^{\Delta NLS/+}$ mice and $Fus^{+/+}$ littermates were processed for volumetric quantification using an in-house developed script[58], aimed at registering the MRI images to a template derived from the Allen Brain Atlas reference and then at parcellating the cerebral structures into hierarchically arranged volumes of interest, which can be interrogated for the volume of any region or group of regions (Fig. 4a, b). The overall intracranial volume (ICV) was comparable in $Fus^{\Delta NLS/+}$ and $Fus^{+/+}$ mice (Fig. 4c). However, upon normalization for the ICV, the volume of the brain parenchyma was significantly decreased in $Fus^{\Delta NLS/+}$ (by ~1.5%; average normalized volume was 98.52% for $Fus^{+/+}$ and 97.14% for $Fus^{\Delta NLS/+}$; Fig. 4d). Visual inspection of the MRI images revealed a substantial increase in the volume of lateral ventricles, which was confirmed by the registration algorithm and quantitated as an almost doubling of ventricular volumes (Fig. 4e). The ventriculomegaly was not associated with neocortical atrophy (Fig. 4f), but we identified a significant atrophy of the medial septum (Fig. 4g) and of the structures corresponding to the cortical subplate (including claustrum, endopiriform cortex and lateral, basomedial, basolateral, and posterior amygdalar nuclei; Fig. 4h). Only a nonsignificant trend for reduced volume was detected for hippocampus (9.06% for $Fus^{+/+}$ vs. 8.62% for $Fus^{\Delta NLS/+}$; $p = 0.15$; Two-sided Unpaired Student's *t*-test) and striatum (9.76% for $Fus^{+/+}$ vs. 9.89% for $Fus^{\Delta NLS/+}$; $p = 0.56$, Two-sided Unpaired Student's *t*-test). Interestingly, we also detected a significant degree of atrophy in the non-neocortical olfactory areas of the piriform cortex (2.48% for $Fus^{+/+}$ vs. 2.18% for $Fus^{\Delta NLS/+}$; $p = 0.0006$, Two-sided Unpaired Student's *t*-test). The lack of a prominent cortical atrophy phenotype was further confirmed by brain histology in $Fus^{\Delta NLS/+}$ mice at both 10 and 22 months of age. Cortical cytoarchitecture appeared preserved in $Fus^{\Delta NLS/+}$ mice, with normal lamination and no cortical thinning. The density of NeuN positive neurons in the frontal cortex was similar between $Fus^{\Delta NLS/+}$ mice and their wild-type littermates at 10 and 22 months of age (Fig. 4i, j).

Taken together, these data demonstrate a significant hydrocephalus ex vacuo in $Fus^{\Delta NLS/+}$, due to the atrophy of subcortical structures, such as the medial septum, several amygdalar nuclei, piriform areas, and tentatively the hippocampus.

Transcriptome of $Fus^{\Delta NLS/+}$ cortex points to defects in inhibitory neurotransmission and synapses. To understand the molecular basis of altered behavior in $Fus^{\Delta NLS/+}$ mice, we performed RNAseq on frontal cortex of 5- and 22-months-old $Fus^{\Delta NLS/+}$ mice and their wild-type littermates. Principal component analysis showed a clear separation between $Fus^{\Delta NLS/+}$ mice and their wild-type littermates at 22 months of age, while clustering was imperfect at 5 months of age, suggesting an exacerbation of the transcriptional differences between genotypes with age (Supplementary Fig. 3a).

Using a stringent analytical pipeline (FDR < 0.05), we did not identify differentially expressed genes between $Fus^{\Delta NLS/+}$ and $Fus^{+/+}$ mice at 5 and 22 months (Supplementary Fig. 3b). To ensure that the absence of differentially expressed genes was not due to the stringent calibration of *p*-values, we compared the 5-months and 22-months-old $Fus^{+/+}$ mice RNAseq datasets to probe age-related alterations. We were able to detect more than 2000 genes differentially expressed between 5- and 22-months-old wild-type mice, at a 5% false discovery rate, demonstrating that this approach can reliably detect changes in gene expression (Supplementary Fig. 3b).

To place gene expression changes in a systems-level framework, we performed weighted-gene coexpression network analysis (WGCNA) across all available $Fus^{\Delta NLS/+}$ and $Fus^{+/+}$ datasets, including 5 and 22-months RNAseq, as well as 1 and 6 months RNAseq datasets from Sahadevan et al.[52]. Potential batch effects were removed using a negative binomial regression model to estimate batch effects based on the count matrix[59] (Supplementary Fig. 3c) and allowed clustering between genotypes (Supplementary Fig. 3d). WGCNA analysis allowed us to

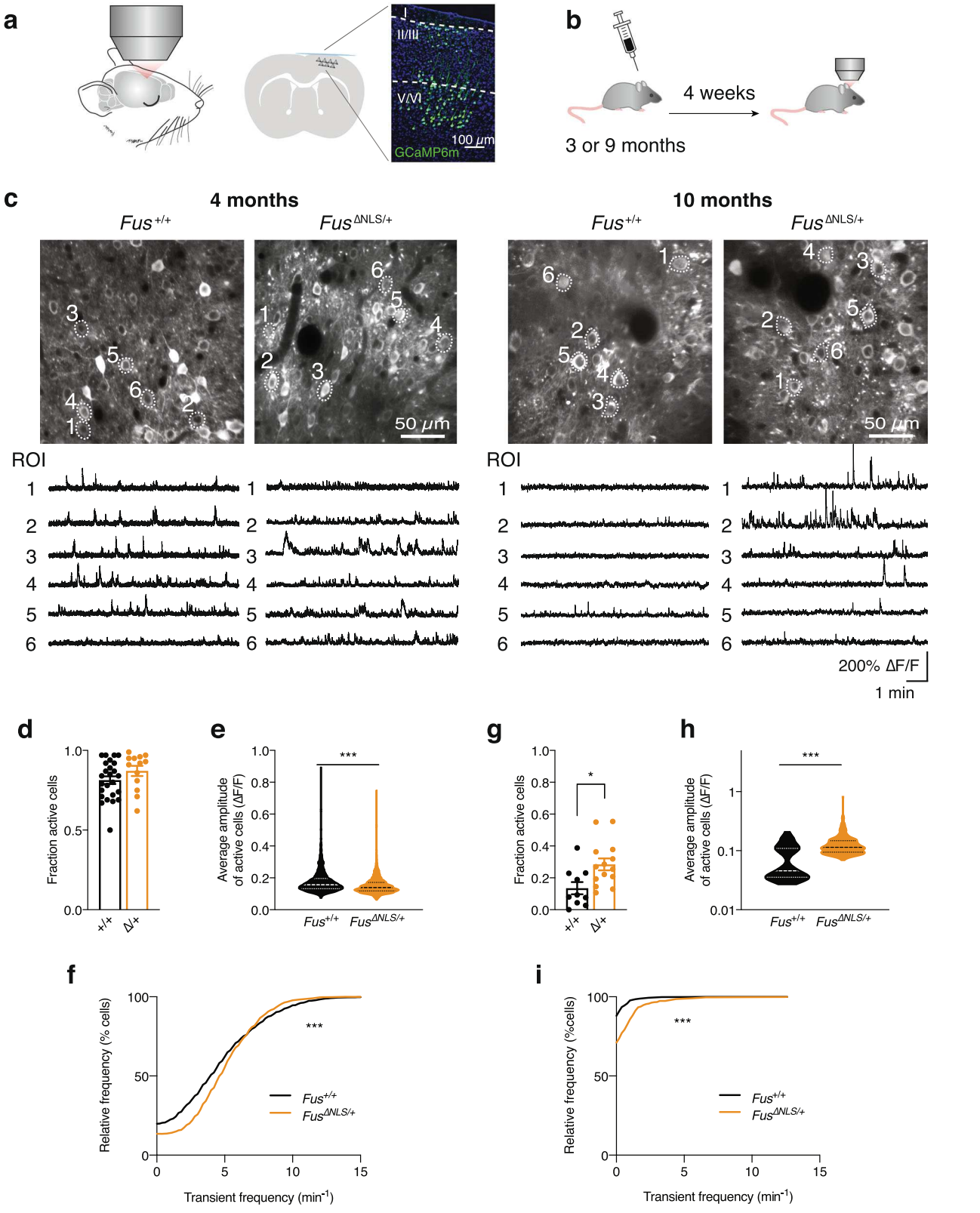

identify two mRNA modules significantly correlated with the genotype condition in cortex and labeled as turquoise and yellow modules according to the WGCNA conventions (Bonferroni-corrected $P < 0.05$; Fig. 5a, Supplementary Data 1). Cell-type enrichment analysis demonstrated that the turquoise module, but not the yellow module, was enriched in neuronally expressed genes (Fig. 5b). Indeed, the Turquoise module, downregulated in $Fus^{\Delta NLS/+}$ mice (Fig. 5c–e), was enriched in genes related to synaptic physiology and development, most notably of GABAergic and glutamatergic synapses (Fig. 5d). Hub genes of the turquoise module included one GABA receptor encoding genes such as *Gabrb1*, one glutamate receptor gene (*Grid2*) and genes

Fig. 3 Assessment of neuronal activity in *Fus*$^{\Delta NLS/+}$ mice in vivo. a Neuronal activity was monitored in frontal cortex of anesthetized mice. Scheme of coronal section, indicating the expression of GCaMP6s in cortex assessed through a cranial window. Magnified view of imaged cortical area demonstrates neuronal expression of GCaMP (green) across all cortical layers. **b** Timeline of experiments. Male and female mice were injected with AAV9-syn-jGCaMP7s (at 3 months of age) or AAV2/1-hsyn-GCaMP6m (at 9 months of age) into frontal cortex and implanted with a cranial window. In vivo imaging began 4 weeks after implantation. **c** Representative examples (average projections) of field of views (FOV) imaged in *Fus*$^{+/+}$ and *Fus*$^{\Delta NLS/+}$ mice at 4 months ($N = 8$ *Fus*$^{+/+}$ mice and $N = 3$ *Fus*$^{\Delta NLS/+}$ mice, left) and at 10 months ($N = 5$ *Fus*$^{+/+}$ mice and $N = 6$ *Fus*$^{\Delta NLS/+}$ mice, right) are shown together with fluorescence calcium traces of selected regions of interest (ROIs). **d** The fraction of active cells per FOV was not affected in 4-month-old *Fus*$^{\Delta NLS/+}$ mice. $N = 13$ FOVs in 3 *Fus*$^{\Delta NLS/+}$ and $N = 25$ FOVs in 8 *Fus*$^{+/+}$ mice. Data are presented as mean ± SEM $p = 0.1627$, Two-sided Unpaired Student's *t*-test. **e**, **f** The calcium transient frequencies (**e**) were increased while the average transient amplitudes (**f**) were decreased in *Fus*$^{\Delta NLS/+}$ mice. $N = 1107$ ROIs in 3 *Fus*$^{\Delta NLS/+}$ and $N = 2264$ ROIs in 8 *Fus*$^{+/+}$, superimposed by the median (**e**). Kolmogorov–Smirnov test, $^{***}p < 0.0001$ for both panel **e** and **f**. **g–i** The fraction of active cells per FOV (**g**) as well as (**h**) the frequencies and (**i**) the average amplitudes of calcium transients of each ROI were increased in 10-month-old *Fus*$^{\Delta NLS/+}$ mice. Data are individual FOVs (**g**; $N = 14$ FOVs in 6 *Fus*$^{\Delta NLS/+}$ and $N = 10$ FOVs in 5 *Fus*$^{+/+}$ mice) or individual ROIs (**h**, **i**; $N = 855$ ROIs in 6 *Fus*$^{\Delta NLS/+}$ and $N = 631$ ROIs in 5 *Fus*$^{+/+}$ mice) superimposed by the mean ± SEM (**g**) or the median (**h**, **i**). panel **g:** Two-tailed Unpaired Student's *t*-test, $^{*}p = 0.0126$; panel **h** and **i**: Kolmogorov–Smirnov test, $^{***}p < 0.0001$ for both panels. Source data are provided as a Source Data file.

tightly associated with synaptic development and autism (*Nrxn1, Lrfn5, Plcb1, Erc2, Frmpd4, Tanc2, Ctnnd2, Dmd*). Consistent with the known molecular function of FUS, the yellow module was enriched for genes related to RNA metabolism and processing and was progressively upregulated with age. Hub genes of this module comprise genes related to mRNA splicing (*Snrnp70, Ddx39b*, *Ilf3*), RNA transport (*Hnrnpl*, *Rbm3, Ipo4*), or RNA degradation (*Exosc10*) (Fig. 5f–h). Thus, transcriptome analysis points to the existence of synaptic defects in the frontal cortex of *Fus*$^{\Delta NLS/+}$ mice.

Synaptic defects in in *Fus*$^{\Delta NLS/+}$ mice. To independently validate potential synaptic defects in *Fus*$^{\Delta NLS/+}$ frontal cortex, we performed quantitative ultrastructural analysis of inhibitory (Fig. 6a) and excitatory (Fig. 6b) synapses in this brain region. Inhibitory synapses in layers II/III of the frontal cortex, identified by the presence of mitochondria on both sides of the synapse, showed major ultrastructural alterations in *Fus*$^{\Delta NLS/+}$ mice, with increased boutons sizes (Fig. 6c), longer active zones (Fig. 6d), prominently increased vesicle numbers (Fig. 6e), and increased distance of vesicles to the active zone as compared to wild-type synapses (Fig. 6f). Excitatory synapses, identified as asymmetrical, with a pronounced postsynaptic density, also showed ultrastructural alterations; however, in the opposite direction: excitatory synapses showed overall decreased bouton size, decreased length of the active zone, and decreased vesicle number in *Fus*$^{\Delta NLS/+}$ cortex (Fig. 6g–l). Importantly, ultrastructural alterations of excitatory synapses were less pronounced than those of inhibitory synapses.

To further explore morphological changes occurring at inhibitory synapses, we quantified the density and the cluster size of three inhibitory synaptic markers: the GABA transporter VGAT localized at the presynaptic site[60] and two receptors specifically expressed at the postsynaptic site of all GABA monoaminergic synapses[61], the postsynaptic scaffold protein Gephyrin[62] and the $GABA_A$ receptor containing α3 subunit ($GABA_A$Rα3). Pictures were acquired in cortical layer 1 to allow imaging of inhibitory synapses located on the apical dendrites of pyramidal neurons[63]. Consistent with the observed ultrastructural abnormalities, a significant decrease in all markers for inhibitory synapses was identified (Fig. 6k, l). This decrease in density was associated with a decrease in the size of the clusters for VGAT, $GABA_A$Rα3, and Gephyrin (Fig. 6m), suggesting a functional impairment of the remaining synapses.

We then sought to determine whether these defects in inhibitory synapses were caused or associated with the loss of inhibitory neurons and focused on parvalbumin-positive (PV) interneurons as the largest group of inhibitory interneurons in the cortex. Using immunohistochemistry, we did not detect differences in the number of PV neurons in the frontal cortex of *Fus*$^{\Delta NLS/+}$ mice neither at 10 nor at 22 months of age (Supplementary Fig. 4a–c). As a result of the ΔNLS mutation, FUS would be expected to accumulate in the cytoplasm of PV neurons as previously shown in other cell types[10,41,49]. We thus performed double immunostaining for FUS and parvalbumin and determined the nuclear/cytoplasmic ratio selectively in PV neurons. As shown in Supplementary Fig. 4d, e, cytoplasmic FUS staining was increased in PV neurons of *Fus*$^{\Delta NLS/+}$ compared to *Fus*$^{+/+}$ mice. Intriguingly, FUS cytoplasmic staining increased with age in wild-type PV interneurons, but remained significantly lower than in *Fus*$^{\Delta NLS/+}$ neurons. Altogether, these results demonstrate the existence of defects in cortical *Fus*$^{\Delta NLS/+}$ synapses, affecting inhibitory synapses more prominently, which could underlie the observed neuronal hyperexcitability (Fig. 3).

Synaptic accumulation of FUS and its RNA targets in *Fus*$^{\Delta NLS/+}$ cortex. To determine whether the observed phenotypes could be linked to a disrupted function of FUS at the synapse, we performed synaptosomal fractionation of the frontal cortex from 5-months-old *Fus*$^{\Delta NLS/+}$ mice. Obtained fractions were enriched in the synaptophysin protein (Fig. 7a–c, and Source data for uncropped western blots) and depleted in the nuclear lncRNA *Malat* (Fig. 7d), consistent with synaptic enrichment. In synaptosomes of *Fus*$^{\Delta NLS/+}$ mice, we observed an almost ten-fold increase in FUS content compared to wild-type synaptosomes, while the total or cytoplasmic FUS contents only increased 2–3 times (Fig. 7a–d). This increased FUS content was mostly due to mutant FUS synaptosomal accumulation, since it was not observed when using an antibody targeting the NLS of FUS (and thus not the mutant FUS ΔNLS protein) (Fig. 7a–d). FUS is known to bind a number of mRNAs, including *Fus* mRNA itself, as well as mRNAs important for (inhibitory) synaptic function such as *Nrxn1* or *Gabra1*[34]. Consistently, we observed increased levels of these 3 mRNAs in synaptosomal fractions of *Fus*$^{\Delta NLS/+}$ mice (Fig. 7e). This enrichment was relatively selective as 3 mRNAs encoding genes from the Turquoise module showed distinct patterns of synaptosomal enrichment: *Gabrb1* and *Grid2*, but not *Ctnnd2*, mRNAs showed clear synaptosomal enrichment, but only *Gabrb1* mRNA showed slightly elevated levels in *Fus*$^{\Delta NLS/+}$ synaptosomes. Collectively, our data show that defects in synapses, which are more pronounced in inhibitory synapses, and are related to synaptic FUS accumulation, likely causing the increased spontaneous neuronal activity and subsequent widespread behavioral abnormalities in *Fus*$^{\Delta NLS/+}$ mice.

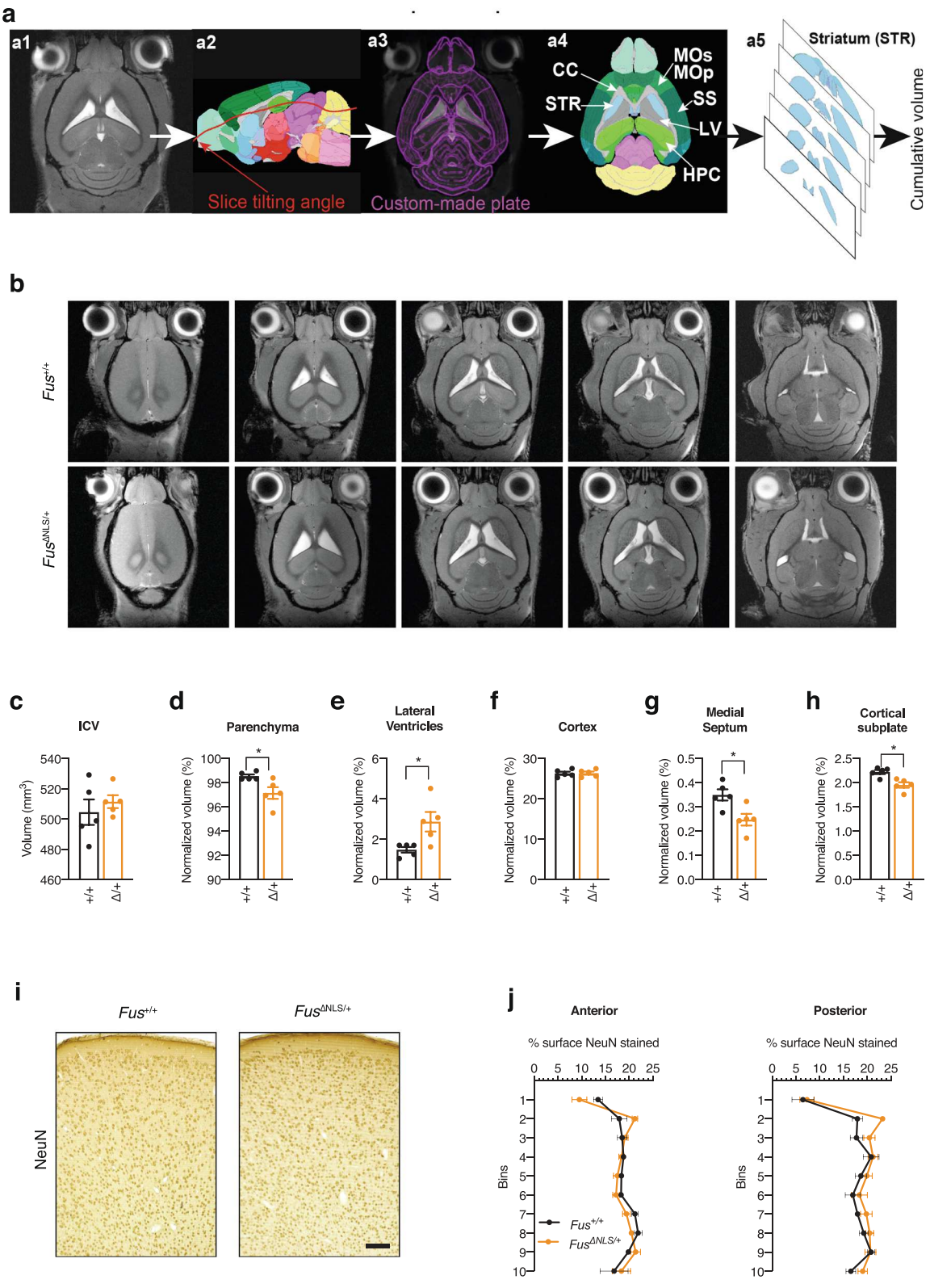

Discussion

In this study, we show that knock-in mice with cytoplasmic accumulation of FUS display widespread behavioral alterations, beyond motor symptoms. We further determine that FUS mislocalization leads to increased spontaneous neuronal activity in the cortex, indicative of neuronal hyperexcitability, that is associated with structural and ultrastructural alterations of inhibitory synapses. Last, we show that the FUS mutation alters FUS synaptic content and modifies synaptic levels of a subset of its RNA targets, possibly underlying the observed phenotypes. The

Fig. 4 Structural and histological brain analysis of *Fus*$^{+/+}$ and *Fus*$^{\Delta NLS/+}$ mice. a Representation of the workflow used to determine volumes of corresponding brain structures from MRI slices per each mouse by the custom-made *Fiji* macro plugin (upper row). **b** Representative MRI slice images of *Fus*$^{+/+}$ (upper row) and *Fus*$^{\Delta NLS/+}$ (lower row) male mice. **c–h** Bar graph showing intracranial volume (ICV) (**c**), normalized volume of the brain parenchyma (**d**), of lateral ventricles (**e**), cortex (**f**), medial septum (**g**), and cortical subplate (**h**) in *Fus*$^{\Delta NLS/+}$ vs *Fus*$^{+/+}$ mice. For panels **c**–**h**, $N = 5$ for *Fus*$^{+/+}$ and $N = 5$ for *Fus*$^{\Delta NLS/+}$ mice. Data are presented as mean ± SEM. Two-tailed Unpaired Student's *t*-test, **c**: $p = 0.4838$; **d**: $p = 0.0249$; **e**: $p = 0.0249$; **f**: 0.9489; **g**: $p = 0.0151$; **h**: $p = 0.0051$. **i** Representative image of NeuN immunohistochemistry at 22 months of age in *Fus*$^{+/+}$ ($N = 3$ mice) or *Fus*$^{\Delta NLS/+}$ ($N = 5$) male mice in the anterior region of the M1/M2 cerebral cortex. Scale bar: 100 µm. **j** Distribution of NeuN+ neurons in *Fus*$^{+/+}$ (black) or *Fus*$^{\Delta NLS/+}$ (orange) male mice, in anterior and posterior regions of the M1/M2 cerebral cortex. $N = 3$ for *Fus*$^{+/+}$ and $N = 5$ for *Fus*$^{\Delta NLS/+}$ mice. Source data are provided as a Source Data file.

timelines of the different experimental studies are summarized in Supplementary Fig. 5.

The notion that FUS mislocalization is a widespread pathological event in sporadic ALS, but also in many other neurological diseases, prompted us to investigate the behavioral phenotype of *Fus*$^{\Delta NLS/+}$ mice. While motor defects can be detected as early as 6 months of age and motor neuron degeneration is not detected before 18–22 months of age, we observed an early spontaneous locomotor hyperactivity in *Fus*$^{\Delta NLS/+}$ mice. In addition, we observed various defects in executive functions, including impaired remote long-term memory, and abnormal social interactions. Hyperactivity and social and executive dysfunctions have been previously documented in other mouse models of ALS/FTD. As such the transgenic overexpression of mutant FUS can e.g., cause hyperactivity and cognitive deficits[64]. Similar abnormalities are also observed in TDP-43 knock-in mice[65], C9ORF72 BAC transgenic mice[66], or Chmp2b transgenic mice[67], suggesting that ALS mutations commonly lead to various behavioral alterations in mouse models, that are dominant over motor dysfunction. These phenotypes seen in mouse models nicely recapitulate widespread cognitive and executive dysfunction typical of ALS[68,69] and support the clinical overlap between ALS and FTD[70].

The deficits in executive functions and social behavior that we observe in *Fus*$^{\Delta NLS/+}$ mice are particularly relevant for FTD. Increased ventricular volume[71–73] as well as atrophy of subcortical structures[73,74] were found in FTD patients and presymptomatic mutation carriers, strengthening the analogy to *Fus*$^{\Delta NLS/+}$ mice. Pathology of FUS and other FET proteins (TAF15 and EWRS1) is a hallmark of a subset of FTD cases (FTD-FET cases). In FTD-FET cases, FUS pathology is associated with nuclear clearance of the FUS protein in neurons with FUS aggregates, although this nuclear clearance is not as pronounced as in cases with TDP-43 pathology[40]. Importantly, the FUS protein is accompanied by several other proteins in FTD-FET pathological aggregates, including TAF15 and EWSR1, two other FET proteins, as well as Transportin 1[12,27–30]. Thus, the disease in FTD-FET patients could be driven by several non-mutually exclusive mechanisms, including cytoplasmic accumulation and/or aggregation of FUS, nuclear clearance of FUS and/or aggregation of co-deposited pathological proteins. Previous studies indicate that complete loss of FUS could be sufficient to lead to FTD like symptoms in mice, and this was consistent with the role of FUS in controlling the splicing of mRNAs relevant to FTD, such as *MAPT*, encoding the TAU protein, or in the stability of mRNAs encoding relevant synaptic proteins such as GluA1 and SynGAP1[35–39]. In *Fus*$^{\Delta NLS/+}$ mice, there is, however, a limited loss of nuclear FUS immunoreactivity[10,41] and no obvious FUS aggregates, ruling out that these pathological events might play a major role in the observed behavioral alterations. The quasi-normal levels of FUS in the nucleus are explained by the existence of potent autoregulatory mechanisms, which are able to largely buffer the effect of the mutation on nuclear FUS levels. Mislocalization of either TAF15 or EWSR1 is also unable to account for behavioral abnormalities as both of these proteins show normal localization in *Fus*$^{\Delta NLS/+}$ neurons, as well as ALS-FUS patients[30]. Together, our results show that FUS mislocalization alone is sufficient to trigger behavioral symptoms and suggest that this might be a major driver of disease pathophysiology in FTD-FET patients. Importantly, our findings do not exclude that at later stages of disease progression, loss of nuclear FUS function might occur as a result of collapsed autoregulatory mechanisms, thereby exacerbating neurological symptoms.

A major finding of this study is that *Fus*$^{\Delta NLS/+}$ mice develop morphological and ultrastructural synaptic defects. The combination of locomotor hyperactivity with social deficits, as observed in *Fus*$^{\Delta NLS/+}$ mice, is commonly observed in various mouse models with synaptic defects. For instance, mouse models of autism spectrum disorders, such as mice lacking the ProSAP/Shank proteins[75,76], display similar behavioral alterations. Our results point to a major defect in synapses, primarily affecting inhibitory synapses. This conclusion is supported by at least three main results: First, transcriptome analyses of the cerebral cortex show that genes related to synapses are affected. Second, the density of inhibitory synapses as well as the clusters size of three typical markers of inhibitory synapses (VGAT, $GABA_A$Ra3, and Gephyrin) are decreased. Third, inhibitory synapses are ultrastructurally abnormal, with increased size, increased number of vesicles and increased distance between vesicles and the active zone, which could be compensatory to their decreased density. Excitatory synapses were also abnormal, but their defects were minor compared to inhibitory synapses. Our data suggest that both the pre- and postsynaptic compartment of inhibitory synapses are affected by the *Fus* mutation. Indeed, the decrease in the density of Gephyrin positive puncta could reflect a disorganization of the postsynaptic density[77], potentially caused by decreased GABAR activity[78–80]. Decreased VGAT density, as well as increased bouton size or vesicle disorganization further suggest impairment of presynaptic GABAergic terminals. On its own, decreased VGAT density might reflect an overall reduction of inhibitory synapses throughout the cortical layers[81] and lead to impaired loading of GABA in the presynaptic vesicles[60]. Importantly, Sahadevan, Hembach and collaborators performed studies in *Fus*$^{\Delta NLS/+}$ mice at earlier ages and observed defects of inhibitory synapses, as early as 1 month of age, worsening at 6 months of age[52]. It is important to note that the disruption of inhibitory synapses can explain most of the detected behavioral and electrophysiological phenotypes observed in *Fus*$^{\Delta NLS/+}$ mice. Illustrating this, loss of *Gabra1*[82], or of *Gabra3*[83] are sufficient to lead to locomotor hyperactivity and the FUS target *Nrxn1* (encoding a key factor in the formation of GABAergic and glutamatergic synapses[84]), is critical in regulating locomotor activity and social behavior in mice[85,86]. Indeed, the deletion of all three neurexins from PV neurons is causing a decrease in the number of synapses of this neuronal type[87], in a manner similar to what is observed in *Fus*$^{\Delta NLS/+}$ mice.

Our current results do not allow to determine whether a specific subpopulation of inhibitory neurons would be more

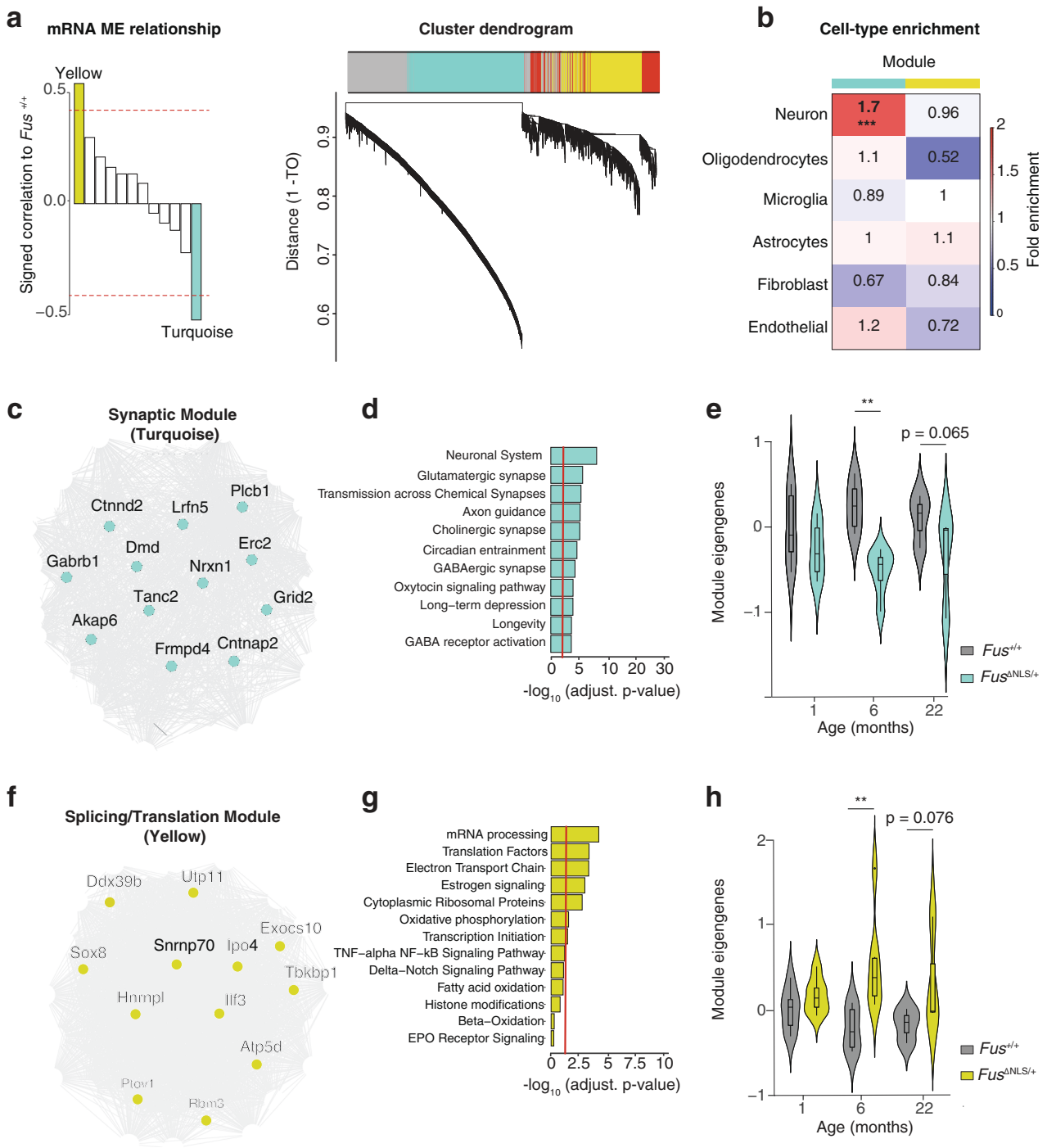

Fig. 5 mRNA coexpression network analysis pinpoints defects in inhibitory and excitatory synapses in *Fus*$^{\Delta NLS/+}$ mice. a Signed association (Pearson correlation) of the mRNA MEs with transgenic condition. Modules with positive values indicate increased expression in transgenic mice; modules with negative values indicate decreased expression in transgenic mice. The red dotted lines indicate Bonferroni-corrected $P < 0.05$ for multiple comparisons ($n = 12$ modules, $n = 16$ mice per group). **b** Cell-type enrichment of modules (average $n = 200$ genes) using mouse genes in mRNA modules (Fisher's two-tailed exact test, ***FDR $= 2 \times 10^{-5}$). **c** Coexpression network plot of the synaptic (turquoise) module. The top 12 hub genes are indicated by name. **d** Gene ontology term enrichment of the synaptic module using 1791 synaptic module genes. **e** Trajectory of the synaptic module in the cortex of *Fus*$^{\Delta NLS/+}$ mice across time. Boxplot show median and quartile distributions, the upper and lower lines representing the 75th and 25th percentiles, respectively. Two-way ANOVA, $F_{(1,24)} = 14.55$, $p = 0.0008$; $n = 4$–6 mice per group. **f** Coexpression network plot of the splicing/translation module. The top 12 hub genes are indicated by gene name. **g** GO term enrichment of the splicing/translation module using 1112 splicing/translation module genes. **h** Trajectory of the splicing/translation module in the cortex of *Fus*$^{\Delta NLS/+}$mice across time. Boxplot show median and quartile distributions, the upper and lower lines representing the 75th and 25th percentiles, respectively. Two-way ANOVA, $F_{(1,24)} = 11.92$, $p = 0.002$; $n = 4$–6 mice per group. The center line represents the median.

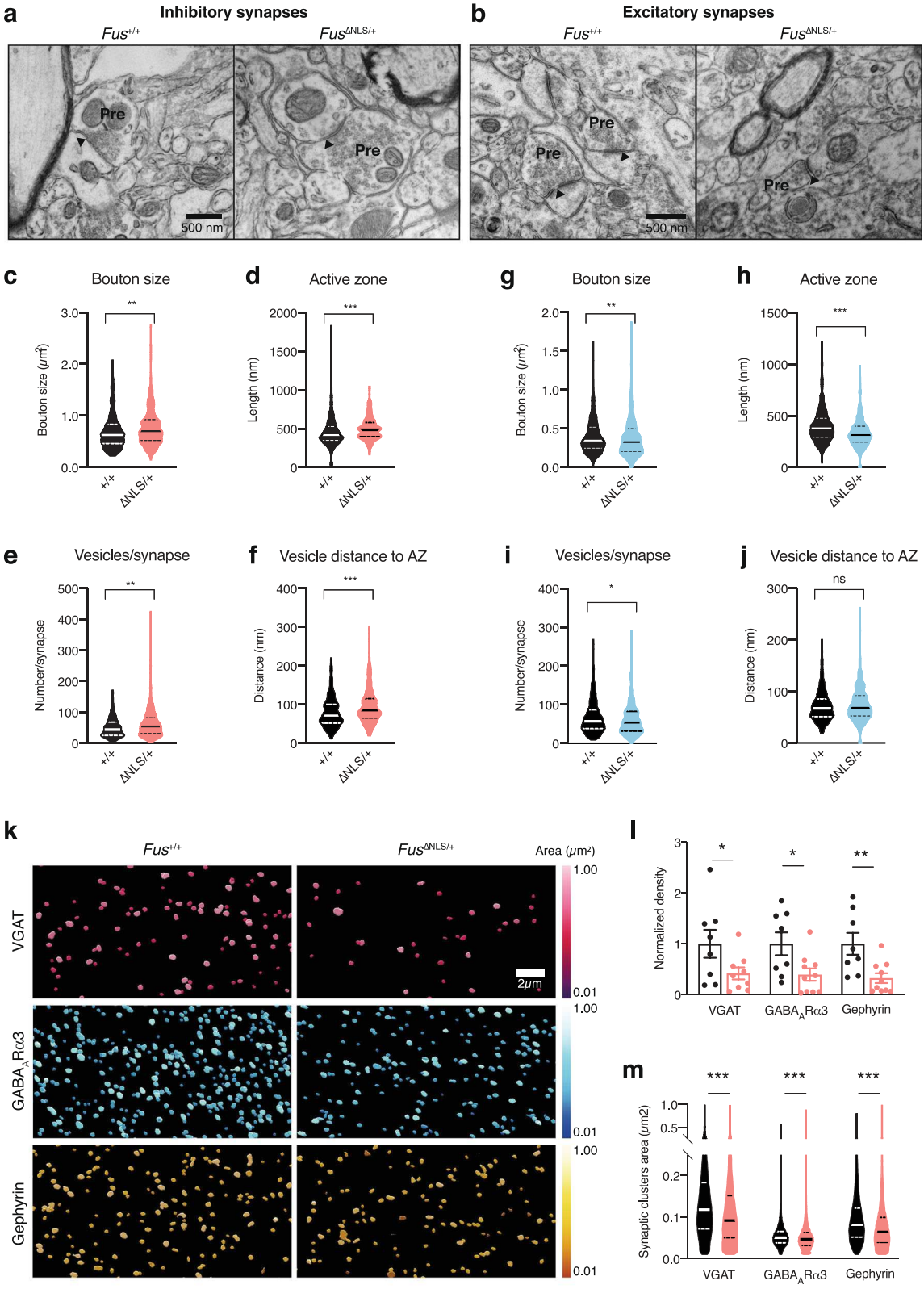

selectively affected in $Fus^{\Delta NLS/+}$ mice. PV interneurons are, however, a strong candidate according to the results of our studies, but also their involvement in TDP-43 knock-in mice[65], and in TDP-43 transgenic mice that display degeneration of hippocampal PV positive interneurons[88]. Functional impairment of PV interneurons might represent a unifying theme in ALS pathophysiology, as multiple electrophysiological studies demonstrate hypoexcitability of PV neurons in SOD1 and TDP-43 transgenic mouse models of ALS[89–92]. Others, however, found PV interneurons to be unaltered presymptomatically and to turn hyperexcitable during the symptomatic phase in the same $SOD1^{G93A}$ mouse model[93]. In either case, those changes in PV excitability were always accompanied by hyperexcitability of layer V pyramidal neurons[89–91,93]. These findings in mouse models nicely

Fig. 6 Defects in synapses in 22-months-old *Fus*$^{\Delta NLS/+}$ mice. a, **b** Representative image of transmission electron microscopy in *Fus*$^{+/+}$ or *Fus*$^{\Delta NLS/+}$ layer II/III of the motor cortex at 22 months of age showing inhibitory synapses (**a**) (as containing ≥1 mitochondrion on each side of the synapse) and excitatory synapses (**b**). Pre: presynaptic compartment; active zone is shown with an arrowhead. $N = 4$ *Fus*$^{+/+}$ mice (1 male and 3 females), and $N = 4$ *Fus*$^{\Delta NLS/+}$ mice (1 male and 3 females) have been analyzed. **c**–**f** Violin plot showing the distribution of bouton sizes (**c**), the length of active zones (**d**), the number of vesicles per synapse (**e**), and the distance of individual vesicles to the active zone (**f**) in inhibitory synapses of *Fus*$^{+/+}$ (black) or *Fus*$^{\Delta NLS/+}$ (orange) mice. For panels **c**–**f**, $N = 379$ synapses from 1 male and 3 female *Fus*$^{+/+}$ mice and $N = 387$ synapses from 1 male and 3 female *Fus*$^{\Delta NLS/+}$ mice were analyzed. Kolmogorov–Smirnov test. **c**: $p = 0.0016$; **d**: $p < 0.0001$; **e**: $p = 0.0010$; **f**: $p < 0.0001$. **g**–**j** Violin plot showing the distribution of bouton size (**g**), the length of active zone (**h**), the number of vesicles per synapse (**i**), and the distance of individual vesicles to the active zone (**j**) in excitatory synapses of *Fus*$^{+/+}$ (black) or *Fus*$^{\Delta NLS/+}$ (cyan) mice. For panels **g**–**j**, $N = 463$ synapses from 1 male and 3 female *Fus*$^{+/+}$ mice and $N = 490$ synapses from 1 male and 3 female *Fus*$^{\Delta NLS/+}$ mice were analyzed. Kolmogorov–Smirnov test. **g**: $p = 0.0038$; **h**: $p < 0.0001$; **i**: $p = 0.0362$; **j**: $p = 0.2182$. **k** Representative images of GABAARα3, Gephyrin and VGAT intensity in 22-months male mice, coded by area size (Imaris). $N = 3$ *Fus*$^{+/+}$ mice and $N = 4$ *Fus*$^{\Delta NLS/+}$ mice have been analyzed. **l** Bar graphs representing the density analysis for VGAT, GABAARα3, and Gephyrin comparing *Fus*$^{+/+}$ vs *Fus*$^{\Delta NLS/+}$ mice. (*Fus*$^{+/+}$ vs *Fus*$^{\Delta NLS/+}$, Mann–Whitney test, VGAT, $p = 0.0464$; GABAARα3, $p = 0.0217$; Gephyrin, $p = 0.0043$). $N = 8$ FOVs from 3 *Fus*$^{+/+}$ mice and $N = 9$ FOVs from 4 *Fus*$^{\Delta NLS/+}$ mice were analyzed for VGAT; $N = 8$ FOVs from 3 *Fus*$^{+/+}$ mice and $N = 10$ FOVs from 4 *Fus*$^{\Delta NLS/+}$ mice were analyzed for GABAARα3 and Gephyrin. Data are presented as mean ± SEM. Mann–Whitney, One tailed, VGAT: $p = 0.0464$; GABAARα3: $p = 0.0217$; Gephyrin: $p = 0.0043$. **m** Violin plot representing the analysis of the clusters size for VGAT, GABAARα3, and Gephyrin comparing *Fus*$^{+/+}$ vs *Fus*$^{\Delta NLS/+}$ mice. $N = 142{,}416$ synapses from 3 *Fus*$^{+/+}$ mice and $N = 115{,}151$ synapses from 4 *Fus*$^{\Delta NLS/+}$ mice were analyzed for VGAT; $N = 202{,}302$ synapses from 3 *Fus*$^{+/+}$ mice and $N = 99{,}464$ synapses from 4 *Fus*$^{\Delta NLS/+}$ mice were analyzed for GABAARα3; $N = 169{,}036$ synapses from 3 *Fus*$^{+/+}$ mice and $N = 68{,}422$ synapses from 4 *Fus*$^{\Delta NLS/+}$ mice were analyzed for Gephyrin. Kolmogorov–Smirnov test. VGAT: $p < 0.0001$; GABAARα3: $p < 0.0001$; Gephyrin: $p < 0.0001$. Source data are provided as a Source Data file.

recapitulate human ALS pathology, in which cortical hyperexcitability is a frequent and, most importantly, early finding in familial and sporadic cases, including FUS mutation carriers[16,94]. In line with these findings, we also observed a pronounced increase in spontaneous neuronal activity in vivo, which is highly indicative of hyperexcitable pyramidal neurons. While we cannot rule out cell autonomous alterations affecting the intrinsic excitability of pyramidal neurons, our histological, ultrastructural, and transcriptomic data strongly argue for defective inhibitory neurotransmission by PV interneurons. In summary, our results, along with others, support the notion that dysfunction of cortical PV interneurons contribute to neural circuit defects in ALS and FTD. Importantly, while we observe molecular and structural defects in inhibitory neurons, we did not observe a loss of PV cell bodies in *Fus*$^{\Delta NLS/+}$ mice, suggesting that the major defect resembles a synaptopathy rather than frank neuronal loss, consistent with other studies[51]. Altogether, our results identify a role for FUS in regulating GABAergic synapse structure and function. Since other major classes of inhibitory interneurons[95] were not investigated, we cannot exclude that somatostatin positive (SST) or HTR3A expressing interneurons are also affected, although to a lesser extent than PV neurons. Furthermore, our work also shows that this *Fus* mutation alters glutamatergic synapses, as judged from both WGCNA analysis of RNAseq (Fig. 5) and electron microscopy (Fig. 7). This is consistent with results from Sahadevan, Hembach et al.[52] providing evidence that FUS is also critically involved in glutamatergic synaptogenesis, at least during development, and is in line with previous studies[96]. Further work is required to disentangle the causes and consequences of GABAergic and glutamatergic impairment, and their respective mechanisms.

How can mutant FUS regulate inhibitory synaptic structure? We observe that the loss of the FUS NLS leads to an increased level of the mutant protein in purified synaptosomes. These results are consistent with results from Sahadevan, Hembach et al., where the authors identified a number of FUS synaptic RNA targets, and a subset of these were also increased in synaptosomes of *Fus*$^{\Delta NLS/+}$ mice. Interestingly, in both studies, several FUS synaptic targets are not modified in *Fus*$^{\Delta NLS/+}$ synaptosomes, including some related to GABAergic neurons. Sahadevan, Hembach and collaborators further demonstrate that at least a subset of these FUS synaptic RNA targets show increased stability in *Fus*$^{\Delta NLS/+}$ neurons. It seems thus reasonable to hypothesize that accumulation of synaptic FUS compromises synaptic homeostasis through altered stability of key synaptic RNAs, either through direct binding, or indirectly. This does not exclude additional mechanisms of toxicity for synaptic FUS, in particular effects on local synaptic translation[44,97], that could affect synaptic protein levels. Further work should focus on determining whether FUS might also regulate synaptic translation of specific proteins involved in inhibitory transmission, and whether rescuing synaptic defects in inhibitory neurons might translate into an efficient therapeutic strategy.

In summary, we show here that cytoplasmic accumulation of FUS leads to a major synaptopathy mainly in inhibitory neurons, that is accompanied by consistent behavioral and electrophysiological phenotypes. The identification of the mechanisms downstream of FUS' synaptic action might lead to efficient therapeutic strategies for FUS related neurodegenerative diseases.

Methods

Mouse models and behavioral analyses. Wild-type (*Fus*$^{+/+}$) and heterozygous (*Fus*$^{\Delta NLS/+}$) mice on a pure genetic background (C57BL/6 J), have been described previously[10], were bred and housed in the central animal facility of the Faculty of medicine of Strasbourg, with a regular 12-h light and dark cycle (light on at 7:00 am) under constant conditions (21 ± 1 °C; 60% humidity). Standard laboratory rodent food and water were available ad libitum throughout all experiments. Mice were genotyped by PCR of genomic DNA from tail biopsies using oligonucleotide primers (sequence provided in Supplementary Data 2)[10]. Mouse experiments were performed in compliance with all relevant ethical regulations for animal testing and researcher. All experiments were approved by local ethical committee from Strasbourg University (CREMEAS) under reference number AL/27/34/02/13 (behavior), by the Government of upper Bavaria (license number Az 55.2-1-54-2532-11-2016, two-photon microscopy) and by „Regierungspräsidium Tübingen" (animal license number 1431, MRI). Behavioral tests were done during the light phase (between 9 am and 5 pm) of their light/dark cycle except for indicated experiments. Until the mice reached the age when the behavioral tests were performed mice were group-housed. Once mice were single housed for the behavioral task they were kept individually for only a period necessary to finalize the set of behavioral experiments and in order to minimize possible negative effects of isolation, afterwards cohorts were sacrificed and processes for downstream analyses. Male mice of 4, 10, and 22 months of age were subjected to behavioral studies and data were analyzed blind to genotypes. The sex of the animals studied is indicated in each figure legend.

Spontaneous locomotor activity in the home cage–actimetry. Home cage activity was assessed according to previously published protocols[98]. Mice were placed individually in large transparent Makrolon cages (42 × 26 × 15 cm) adapted to the shelves of the testing device (eight cages/shelve). Two infrared light beams, passing through each cage, were targeted on two photocells, 2.5 cm above the cage floor

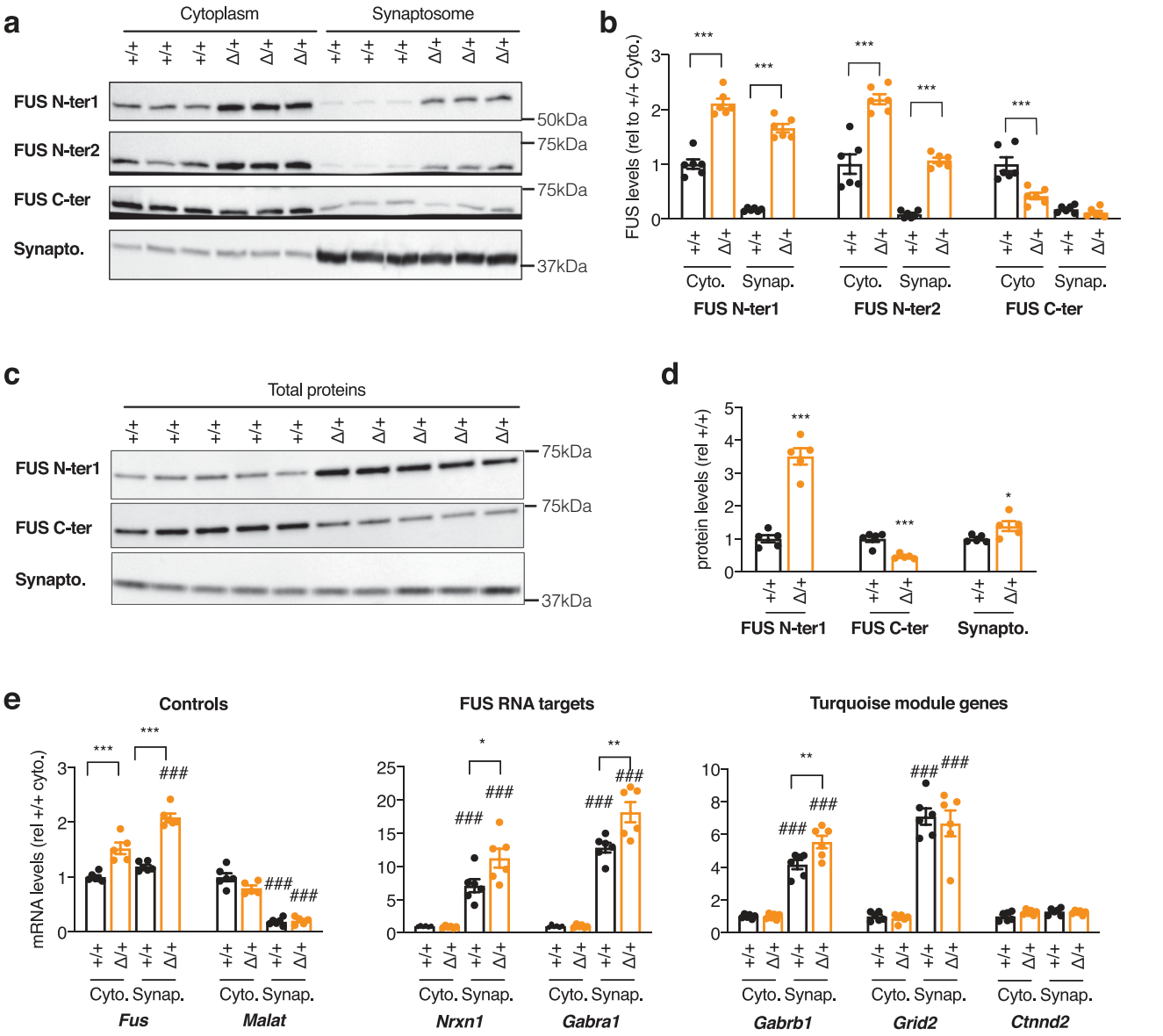

Fig. 7 FUS accumulates in synaptosomes of *Fus*$^{\Delta NLS/+}$ mice and alters synaptosomal levels of a subset of its targets. a, b Representative western blot images (**a**) and respective quantifications (**b**) of cytoplasmic (**a**, left) or synaptosome (**a**, right) extracts from *Fus*$^{+/+}$ (+/+) or *Fus*$^{\Delta NLS/+}$ (Δ/+) mice (4 months of age,) using two antibodies recognizing the N-terminal part of the FUS protein (FUS N-ter1 and FUS N-ter2), the C-terminal part of FUS (encoding the NLS, FUS C-ter) or synaptophysin protein to show enrichment in synaptic proteins in the synaptosome fraction. $N = 6$ *Fus*$^{+/+}$ mice and $N = 6$ *Fus*$^{\Delta NLS/+}$ mice were analyzed. Data are presented as mean ± SEM. One-Way ANOVA with Tukey post-hoc test. $^{***}p < 0.0001$ Please note that the FUS western blots were run on independent gels, to avoid stripping and reprobing on the same membrane for the same protein. Each of these gels were controlled for equal loading using StainFree markers, that are provided in the source data. **c, d** Representative western blot images (**c**) and respective quantifications (**d**) of total extracts (**c**) from *Fus*$^{+/+}$ (+/+) or *Fus*$^{\Delta NLS/+}$ (Δ/+) mice (4 months of age,) using the same antibodies as in panel **a**. $N = 5$ *Fus*$^{+/+}$ mice and $N = 5$ *Fus*$^{\Delta NLS/+}$ mice were analyzed. Data are presented as mean ± SEM. Two-tailed Unpaired Student's *t*-test. N-ter1: $p < 0.0001$; C-ter: *p*-value: $p = 0.0006$; Synaptophysin: $p = 0.0411$. **e** mRNA levels of the indicated genes in RNAs extracted from cytoplasmic (Cyto.) or synaptosome (Synap.) extracts from *Fus*$^{+/+}$ (+/+) or *Fus*$^{\Delta NLS/+}$ (Δ/+) frontal cortex from 4-months-old female mice as assessed using RT-qPCR. $N = 6$ *Fus*$^{+/+}$ mice and $N = 5$ *Fus*$^{\Delta NLS/+}$ mice were analyzed. Data are presented as mean ± SEM. Genes are grouped by categories (controls, established FUS RNA targets, and genes belonging to the Turquoise module). All quantifications are presented relative to the +/+ cytoplasmic RNA levels set to 1. One-way ANOVA with Tukey post-hoc test. *Fus:* $^{***}p < 0.0001$ vs corresponding wild-type fraction; $^{\#\#\#}p < 0.0001$ vs corresponding cytoplasmic fraction of the same genotype. *Malat:* $^{\#\#\#}p = 0.0001$ vs corresponding cytoplasmic fraction of the same genotype. *Nrxn1* $^{*}p = 0.0140$ vs corresponding wild-type fraction; $^{\#\#\#}p < 0.0001$ vs corresponding cytoplasmic fraction of the same genotype. *Gabra1:* $^{**}p = 0.0012$ vs corresponding wild-type fraction; $^{\#\#\#}p < 0.0001$ vs corresponding cytoplasmic fraction of the same genotype. *Gabrb1:* $^{**}p = 0.0029$ vs corresponding wild-type fraction; $^{\#\#\#}p < 0.0001$ vs corresponding cytoplasmic fraction of the same genotype. *Grid2:* $^{\#\#\#}p < 0.0001$ vs corresponding cytoplasmic fraction of the same genotype. *Ctnnd2:* no significant differences observed ($p > 0.05$). Source data are provided as a Source Data file.

level and 28 cm apart. The number of cage crossing was recorded automatically and was used to determine or score the spontaneous locomotor activity. The experiment began at 17.00 pm and after 2 h of habituation continued for 3 consecutive days for a complete 24 h nictemeral cycle (12 h dark and 12 h light).

Open field. The general exploratory locomotion and anxiety in a novel environment were tested during 15 min long sessions in the open field arena (72 × 72 × 36 cm) located in a test room and lit by a 600 lux for background lighting, according to published protocol[99]. The open maze was divided by lines into sixteen squares (18 × 18 cm). Each mouse was placed in the center of the arena and allowed to freely move while being video recorded. The recorded data were analyzed offline with EthoVision XT software system (Noldus Information Technology). The time spent in the center (four central quadrants) vs. the perimeter (12 peripheral quadrants) was used to measure anxiety, while the total distance traversed in the arena and average moving speed (mean velocity) was used to evaluate locomotor activity. For each mouse a movement heat map and trajectory tracking map that are representing a corresponding locomotor activity were made independently.

Dark/light box test. The light/dark box apparatus consisted of two Poly-Vinyl-Chloride (PVC) compartments of equal size (18.5 × 18.5 × 15 cm) one opaque and the other transparent, connected through an opaque tunnel (5 × 5.5 × 5 cm). The illumination of the transparent compartment was set at 400 lux. Each mouse was placed alone in the dark compartment and the mouse's behavior was recorded during 5 min with a video camcorder located ~150 cm above the center of the box. Test was conducted during the morning. The latency before the first transition into the light compartment, the number of transitions between the two compartments and the time spent in each compartment were tested to assess for anxiety level and exploratory behavior, as published previously[99].

Olfactory preference test. This test is designed to identify specific detection deficiencies and/or odor preference, namely the ability to sense attractive or aversive scents. After 30 min of habituation to empty cage with no bedding, each mouse was challenged with a filter paper embedded with two strong scents (vanilla and 2-methyl butyrate) or a neutral scent (water) was video recorded over 3 min. A 1-h pause in between the exposure to different scents was applied to each mouse using a procedure adapted from previously reported protocols[67,100]. The time the mouse spent sniffing the filter paper—the exploration time, is calculated post-hoc by an examiner blind to mouse genotype and condition. Those scents with the exploration time greater than water were designated as "attractive" while those with times less than water were termed "aversive".

Social interaction in the home cage (resident-intruder test). Social interaction was assessed in the home cage by a standard protocol[67,101]. Briefly, both resident and intruder mice were isolated and housed individually for 1 week before the task. After 30 min of habituation to the test room resident mouse was allowed to freely roam in his home cage without the cage top for 1 min. A novel male intruder mouse (nonlittermate of same background, same age, and similar weight) was then introduced in the opposite corner as the resident and allowed to interact for 5 min while videotaped. The total physical interaction, defined as the time during which the resident mouse actively explores the intruder was analyzed post-hoc. Only social activities, such as time spent investigating, grooming, following, sniffing etc. were quantified separately for each minute and for the whole time of the task and were differentiated from nonsocial/aggressive activities such as attacks, bites, and tail rattles.

Three-chamber social task. Specific social behaviors such as sociability and social recognition were analyzed by using three-chamber social task. The experimental procedure is adapted from Gascon E et al.[67]. The three-chamber box (59 × 39.5 × 21.5 cm) is made of transparent Plexiglas (Noldus Information Technology, Wageningen, The Netherlands) and is divided into three chambers (one middle and two side chambers) of equal size (18.5 × 39.5 cm) by the walls with a square opening (7 × 7 cm) that could be closed by a slide door. Each of the two side chambers contains a mobile wire cylinder shaped cage (20 × 10 cm diameter) that is made of transparent Plexiglas bars placed 6 mm apart. Cage is closed by the upper and lower lids.

Mice of both genotypes ($Fus^{+/+}$ and $Fus^{\Delta NLS/+}$) that were experimentally tested are referred to as the test mice and adult male unfamiliar mice of same background, age and weight used as the social stimulus are called novel mice. All mice were housed individually for 1 week before the test and were habituated to the testing room for at least 1 h before the start of behavioral tasks. One day prior to the testing, the novel mice were habituated to mobile wire cage for 5 min. The keeping of the novel mouse separated in a wire cage prevents aggressive and sexual activities, and in the same time ensures that any social interaction is initiated by the test mouse. Sessions were videotaped and visually analyzed post-hoc. The experimental procedure was carried out in four trials of 5 min each. After each trial, the mouse was returned to his home cage for 15 min. Trials were grouped into two consecutive parts.

Trial 1 (habituation): the test mouse was placed in the middle chamber and left to freely explore each of the three chambers: the empty middle or two sides' arenas containing the empty wire cages for 5 min.

Trials 2–4 (sociability, social recognition, social learning acquisition): the mouse was placed in the middle chamber, but an unfamiliar mouse (novel mouse) was placed into a wire cage in one of the side chambers (the wire cage in the other side-chamber remains empty). The test mouse had free access to all three chambers. The position of novel mouse and empty wired cage were alternated between trials. We quantified the time spent actively exploring a novel mouse or an empty cage by the test mouse as a social interaction time or an object exploration time, respectively. The longer time that test mouse spends in the close perimeter around the cage containing the novel mouse while actively interacting with it (staring, sniffing) compared to the empty cage—object, indicates social preference or social recognition as a result of the capability to differentiate a conspecific from an object. The motivation of the test mouse to spontaneously interact with novel mouse is considered as sociability which gradually decreased over trials as a result of social learning acquisition.

Water maze task. The water maze consisted of a circular pool (diameter 160 cm; height 60 cm) filled with water (21 ± 1 °C) made opaque by addition of a powdered milk (about 1.5 g/L). The habituation day consisted in one 4-trial session using a visible platform (diameter 11 cm, painted black, protruding 1 cm above the water surface and located in the South-East quadrant of the pool), starting randomly from each of the four cardinal points at the edge of the pool. During this habituation trial, a blue curtain surrounded the pool to prevent the use of distal cues and thus incidental encoding of spatial information. For the following days, the curtain was removed. Mice were given a 5-day training period (4 consecutive trials/day, maximum duration of a trial 60 seconds, inter-trial interval = 10–15 seconds) with a hidden platform located at a fixed position in the North-West quadrant. Animals were starting randomly from each of the four cardinal points at the edge of the pool and the sequence of the start points was randomized over days. Mice were tested for retention in a 18-days delay probe trial and two extinction tests: the first 2 h after probe trial and the second 2 h after the first. For the probe trial, the platform was removed; the mice were introduced in the pool from the North-East (a starting point never used during acquisition) and allowed a 60-seconds swimming time to explore the pool. Data were collected and computed by a video-tracking system (SMART; AnyMaze software). For the visible platform and training trials following parameters were used: the distance traveled and the latency time before reaching the platform and the average swimming speed. For the probe trial and extinction tests the time (in secondes) spent in the target quadrant (i.e., where the platform was located during acquisition) was analyzed[102].

Assessing neuronal activity by in vivo two-photon imaging

Cranial window implantation and virus injection. Mice of both sexes were implanted with a cranial window at 3 and 9 months of age (±10 days), respectively and received a stereotaxic injection of the genetically encoded calcium indicator (AAV2/1.hsyn.GCaMP6m.WPRE.SV40 diluted 1:6 in saline—10-month-old cohort or AAV9.syn.jGCaMP7s.WPRE diluted 1:6 in saline—4-month-old cohort (pGP-AAV-syn-jGCaMP7s-WPRE was a gift from Douglas Kim & GENIE Project, Addgene viral prep # 104487-AAV9; RRID:Addgene_104487)[103] into the primary motor cortex (M1)[104]. In brief, mice were first anesthetized with Fentanyl (0.05 mg/kg), Midazolam (5.0 mg/kg), and Metedomidin (0.5 mg/kg). A circular craniotomy with a 2 mm radius, centered at 1.7 mm lateral and 0.8 mm anterior to bregma, was performed, followed by the slow injection of a total of ~1 µl of the calcium indicator into three sites (~300 nl per site at 600 µm cortical depth). A 4 mm round glass coverslip (Warner Instruments) was placed over the cortex and sealed with UV-curable dental acrylic (Venus Diamond Flow, Heraeus Kulzer GmbH). A metal head bar was attached to the skull using dental acrylic (Paladur, Heraeus Kulzer GmbH), allowing for stable positioning during two-photon imaging.

Two-photon imaging in anesthetized mice. Four weeks following the cranial window implantation, in vivo two-photon imaging was performed within cortical layer II/III using a two-photon microscope (Hyperscope, Scientifica, equipped with an 8 kHz resonant scanner) at a frame rate of 30 Hz and a resolution of 512 × 512 pixels. Using a ×16 water-immersion objective (Nikon), stacks consisting of 15,000 frames (equivalent to ~8 min) were acquired, covering a field of view (FOV) of 300 × 300 µm. Light source was a Ti:Sapphire laser with a DeepSee pre-chirp unit (Spectra Physics MaiTai eHP)[104]. GCaMP was excited at 910 nm, with a laser power not exceeding 40 mW (typically 10–40 mW). In each mouse, two to five FOVs at cortical depths of 140–310 µm were imaged, yielding 2264 cells in $Fus^{+/+}$ ($n = 25$ experiments, 8 mice) and 1107 cells in $Fus^{\Delta NLS/+}$ ($n = 13$ experiments, 3 mice) at 4 months of age; and 631 cells in $Fus^{+/+}$ ($n = 10$ experiments, 5 mice) and 855 cells in $Fus^{\Delta NLS/+}$ mice ($n = 14$ experiments, 6 mice) at 10 months of age. During imaging, mice were anesthetized with 1.0–1.5 volume % isoflurane in pure O_2 at a flow rate of ~0.5 l/min, to maintain a respiratory rate in the range of 110–130 breaths per minute. Body temperature was maintained at 37 degrees using a physiological monitoring system (Harvard Apparatus).

Image processing and data analysis. All image analyses were performed in Matlab (Math Works) using custom-written routines[104]. In brief, full frame images were corrected for potential x and y brain displacement, and regions of interests (ROIs) were semi-automatically selected based on the maximum and mean projections of all frames. Fluorescence signals of all pixels within a selected ROI were averaged,

the intensity traces were low pass filtered at 10 Hz. Contamination from neuropil signals was accounted for using the following Eq. (1)[104],

$$\mathbf{F}_{\mathrm{ROI\_comp}} = \mathbf{F}_{\mathrm{ROI}} - 0.7 \times \mathbf{F}_{\mathrm{neuropil}} + 0.7 \times \mathrm{median}(\mathbf{F}_{\mathrm{neuropil}}) \quad (1)$$

F_{ROI_comp} stands for neuropil-compensated fluorescence of the ROI, F_{ROI}, and $F_{neuropil}$ represent the initial fluorescence signal of the ROI and the signal from the neuropil, respectively. A neuron was defined as 'active' if it displayed at least one prominent calcium transient over 20 frames (corresponding to ~0.7 seconds). The overall difference in the fraction of active cells between 4- and 10-month-old mice could be due to both age as well as the usage of the more sensitive calcium indicator GCaMP7s[105]. To compare the impact of the indicator alone, we also investigated a control 4 m age cohort expressing GCaMP6m, in which case the fraction of active cells was 81% and not different from the average observed in the *Fus*$^{+/+}$ control cohort used here (ranksum test, $p = 0.87$, 7 experiments in 3 mice).

Histological techniques. Male mice were anesthetized with intraperitoneal injection of 100 mg/kg ketamine chlorhydrate (Imalgène 1000®, Merial) and 5 mg/kg xylazine (Rompun 2%®, Bayer), and then transcardially perfused with cold PFA 4% in 0.01 M phosphate buffered saline (PBS). After dissection, brains were post-fixed for 24 h and then included in agar 4% and serial cuts of 40 µm thick were made using vibratome (Leica Biosystems, S2000).

Peroxidase immunohistochemistry. For peroxidase immunohistochemistry, sections were incubated 10 min with H_2O_2 3%, rinsed with PBS 1× and incubated with blocking solution (8% Horse serum, 0.3% Bovine Serum Albumin, 0.3% Triton, PBS-0.02% Thimerosal). Sections were rinsed, and then incubated with anti-mouse NeuN or anti-mouse parvalbumin (Millipore, MAB377, 1:100 and Sigma, P3088, 1:1000, respectively) overnight at room temperature. The second day, sections were rinsed and incubated for 2 h at room temperature with biotinylated donkey anti-mouse antibody (Jackson, 715-067-003, 1:500). After sections were rinsed, they were incubated for 1 h in horseradish peroxidase ABC kit (Vectastain ABC kit, PK-6100, Vector Laboratories Inc.), rinsed and incubated with DAB (Sigma, D5905). The enzymatic reaction was stopped by adding PBS 1X, rinsed with water and sections were mounted with DPX mounting medium (Sigma, O6522).

Quantification. Images were quantified using a homemade ImageJ plugin. A Region Of Interest (ROI) was first defined by the user as the M1/M2 regions of the cerebral cortex as defined by the Paxinos Atlas[106] using the following coordinates: interaural 4.06 mm; Bregma 0.26 mm. For NeuN immunohistochemistry, a second, more anterior region of M1/M2 cortex was also quantified with the following coordinates: Interaural: 5.74 mm, Bregma: 1.94 mm.

In this region, a semi-automated segmentation led to the identification of the labelled structures (cells or nuclei). Finally, the plugin subdivided the previous ROI into 10 subregions and measured either the number of objects per subregion or the proportion of each subregion that is covered by labelled structures.

Immunofluorescence. Sections were rinsed with PBS 1X then incubated with blocking solution (8% Goat serum, 0.3% Bovine Serum Albumin, 0.3% Triton, PBS-0.02% Thimérosal) overnight at 4 °C in primary antibody: rabbit anti-FUS antibody (ProteinTech, 11570-1-AP, 1:100) and mouse anti-parvalbumin antibody (Sigma, P3088, 1:1000). After three rinses in PBS, sections were incubated for 2 h at room temperature with Hoechst (Sigma, B2261, 1/50.000) and secondary antibody: Goat anti-mouse Alexa-488 secondary antibody (Invitrogen, A11034, 1:500) and goat anti-mouse Alexa-647 secondary antibody (Invitrogen, A21245, 1:500). Finally sections were subsequently washed with PBS (3 × 10 min) and mounted in Aqua/polymount (Polysciences, 18606).

Images were acquired along the Z axis (Z stacking) using a Zeiss AxioImage.M2 microscope equipped with a Plan-Apochromat ×20/0.8 objective, high performance B/W camera (Orca Flash4, Hamamatsu) and run by the Zeiss Zen2 software. Images were quantified using the ImageJ freeware. First, the user defined ROIs corresponding to the cytoplasm and nucleus or several PV positive cells at several Z positions. Then a homemade macro was used to calculate the ratio, in the green channel, of the cytoplasm intensity divided by the nucleus one.

Electron microscopy. Mice from both sexes were used for electron microscopy. Mice were anesthetized by intraperitoneal injection of 100 mg/kg ketamine chlorhydrate and 5 mg/kg xylazine and transcardially perfused with glutaraldehyde (2.5% in 0.1 M cacodylate buffer at pH 7.4). Brains were dissected and immersed in the same fixative overnight. After three rinses in Cacodylate buffer (EMS, 11650), serial cuts of 80 µm thick were made with vibratome. Slides were then post-fixed in 1% osmium in Cacodylate buffer 1 h at room temperature. Finally, tissues were dehydrated in graded ethanol series and embedded in Embed 812 (EMS, 13940). The ultrathin sections (50 nm) were cut with an ultramicrotome (Leica, EM UC7), counterstained with uranyl acetate (1% (w/v) in 50% ethanol) and observed with a Hitachi 7500 transmission electron microscope (Hitachi High Technologies Corporation, Tokyo, Japan) equipped with an AMT Hamamatsu digital camera (Hamamatsu Photonics, Hamamatsu City, Japan). Analysis of electron micrographs was performed as follows: 100 inhibitory synapses located in layers II/III were imaged per animal. Inhibitory synapses were identified as containing at least one mitochondrion in each synaptic bouton. Synapses morphometry was analyzed using ImageJ freeware (National Institute of Health), where each synaptic boutons' area was manually drawn as previously described[107]. An automated plugin was used to drawn and measure the active zones' length, the number of synaptic vesicles within each bouton and the distance of each vesicle to the active zone, being as the beeline from the vesicle to the active zone. All images were acquired in layer II/III of the M1/M2 regions of the cerebral cortex as defined by the Paxinos Atlas[106] using the following coordinates: interaural 4.06 mm; Bregma 0.26 mm.

Synaptic density in brain sections. Male mice were anesthetized by CO_2 inhalation before perfusion with PBS containing 4% paraformaldehyde and 4% sucrose. Brains were harvested and post-fixed overnight in the same fixative and then stored at 4 °C in PBS containing 30% sucrose. Sixty micrometers thick coronal sections were cut on a cryostat and processed for free-floating immunofluorescence staining. Brain sections were incubated with the indicated primary antibodies (Rabbit GABAAalpha3 antibody Synaptic Systems, 1:500; Mouse Gephyrin antibody Synaptic Systems, 1:500, Guinea pig VGAT antibody, Synaptic Systems, 1/500) for 48 h at 4 °C followed by secondary antibodies (1:1000) for 24 h at 4 °C. The antibodies were diluted in 1× Tris Buffer Saline solution containing 10% donkey serum, 3% BSA, and 0.25% Triton-X100. Sections were then mounted on slides with Prolong Diamond (Life Technologies) before confocal microscopy.

Confocal images were acquired on a Leica SP8 Falcon microscope using ×63 (NA 1.4) with a zoom power of 3. Images were acquired at a 2048 × 2048 pixel image resolution, yielding a pixel size of 30.05 nm. To quantify the density of synaptic markers, images were acquired in the molecular layer 1/2 of the primary motor cortex area, using the same parameters for all genotypes. Images were acquired from top to bottom with a Z step size of 500 nm. Images were deconvoluted using Huygens Professional software (Scientific Volume Imaging). Images were then analyzed as described[108]. Briefly, stacks were analyzed using the built-in particle analysis function in Fiji[109]. The size of the particles was defined according to previously published studies[77,110]. To assess the number of clusters, images were thresholded (same threshold per marker and experiment), and a binary mask was generated. A low size threshold of 0.01 um diameter and high pass threshold of 1 um diameter were applied. Top and bottom stacks were removed from the analysis to only keep the 40 middle stacks. For the analysis, the number of clusters per 40 z stacks was summed and normalized by the volume imaged (75153.8 µm^3). The density was normalized to the control group.

Structural MRI scans. Male mice were used for MRI studies. All data were acquired on a dedicated small bore animal scanner (Biospec 117/16, Bruker, Ettlingen, Germany) equipped with a cryogenically cooled two-element surface (MRI CryoProbeTM, Bruker BioSpec, Ettlingen, Germany) transmit/receive coil. Anatomical brain images were acquired in coronal slice orientation (30 slices) applying a gradient-echo (FLASH) sequence with acquisition parameters as: TE/TR 2.95/400 ms (TE = echo time, TR = repetition time), matrix 30 × 340 × 340, resolution 250 × 50 × 50 mm^3).

Anatomical annotation of brain MRI images was performed in *Fiji*[58] using custom-written routines. In brief, in order to generate a plate corresponding to a single MRI cross section (Figure 4a1) a macro was run to reslice a stack of sagittal plates pursued via the Scalable Brain Atlas[111] according to a manually defined tilting angle by means of the Dynamic Reslice *Fiji* plugin (Figure 4a2). Custom-made plates were then registered onto the corresponding MRI slice by the manual denotation of the major, easily recognizable anatomical landmarks with the Big Warp plugin (Figure 4a3). The thresholding of the warped RGB plates (Figure 4a4) according to the brain structure color code resulted in parcellation of the MRI cross section into single regions. Due to the marked ventriculomegaly, for lateral ventricles and medial septum only, a loss of resolution in the custom plates was noticeable upon warping, therefore these areas along with the entire brain cross section (in order to include olfactory bulbs and cerebellum for the overall intracranial volume) were manually delineated. Finally, region volumes were determined following Cavalieri's principle, i.e., the measurement of the scaled cumulative area was multiplied by the slice increment (Figure 4a5). The volumetric analysis was blinded and evaluated by the same investigator. Code used for volumetric quantification of MRI scans is provided in Supplementary Software.

RNAseq. RNAseq on frontal cortex was performed as previously described[10,41]. Briefly, RNA from cortex of 22-months-old male *Fus*$^{\Delta NLS/+}$ mice and their control littermates were extracted with TRIzol (Invitrogen). RNA quality was measured using the Agilent Bioanalyzer system or RNA screenTape (Agilent technologies) according to the manufacturer's recommendations. Samples were processed using the Illumina TruSeq single Stranded mRNA Sample Preparation Kit according to manufacturer's protocol. Generated cDNA libraries were sequenced using an Illumina HiSeq 2000 sequencer with 4–5 biological replicates sequenced per condition using single read, 50 cycle runs. RNA from the cortex of 5-months-old male *Fus* $^{\Delta NLS/+}$ and control littermate mice was extracted, and libraries were generated using the Illumina TruSeq single Stranded mRNA Sample Preparation Kit. The cDNA libraries were sequenced on a HiSeq 4000 with three biological replicates per condition using single-end 50 bp read. Total reads sequenced varies from 35 to 45 million reads. Complete QC report will be made publicly available.

Raw reads were mapped to the mouse reference genome GRCm38 with STAR version 2.7.0[112] and default parameters using Ensembl gene annotations (version 87). Gene-level abundance estimates were estimated using the option–quantMode geneCount in STAR. We filtered the lowly expressed genes wherein each gene was required to have at least 15 counts across all samples and used both exonic and intronic reads. The filtered set of genes was used for the PCA plot and differential expression analysis. Differential gene expression analysis was performed with the ARMOR workflow[113] and a cut off FDR value of 0.05 was set in both datasets. RNA samples sequenced in the present study from 5–6-months-old mice ($n = 10$) were pooled to the samples from Sahadevan et al., 2020, ($n = 6$).

Weighted-gene coexpression network analysis. Coexpression network analysis was performed using a user-friendly R WGCNA library[114]. We wanted to investigate mouse brain coexpression networks that are disease specific in $Fus^{\Delta NLS/+}$ mice. Biweighted midcorrelations were calculated for all pairs of genes, and then a signed similarity matrix was created. In the signed network, the similarity between genes reflects the sign of the correlation of their expression profiles. The signed similarity matrix was then raised to the power β to emphasize strong correlations and reduce the emphasis of weak correlations on an exponential scale. The resulting adjacency matrix was then transformed into a topological overlap matrix as describe[115]. After scaling the network (consensus scaling quantile = 0.2), a threshold power of 5 was chosen (because it was the smallest threshold that resulted in a scale-free R^2 fit of 0.9) and the consensus network was created by calculating the component-wise minimum values for topological overlap. Using 1 − TOM (dissTOM) as the distance measure, genes were hierarchically clustered. Initial module assignments were determined using the blockwiseModules function as follows: blockwiseModules(datExpr, power = 5,TOMType = "signed", minModuleSize = 30, networkType = "signed",deepSplit = 2, reassignThreshold = 0, mergeCutHeight = 0.35, numericLabels = TRUE, pamRespectsDendro = FALSE, saveTOMs = TRUE, verbose = 3). The resulting modules or groups of coexpressed genes were used to calculate the MEs or the first principal component of the module. MEs were correlated with different biological and technical traits like transgenic condition and batch to find disease-specific modules. Module hubs were defined by calculating module membership (kME) values, which are the Pearson correlations between each gene and each ME. Genes with a kME < 0.7 were removed from the module. Network visualization was done with the igraph package in R. Module definitions from the network analysis were used to create synthetic eigengenes for the 1-month, 6 months and 22-months timepoint and were used to understand the trajectory of various modules across timepoints.

Enrichment analyses using single-cell experiment data. To reduce false positives, we used FDR-adjusted *P*-values for multiple hypergeometric test comparisons. For cell-type enrichment analysis, we used an already published single-cell mouse brain dataset[116]. Finally, genes in network modules were characterized using EnrichR (version 1.2.5)[117].

Synaptosomal enrichment followed by RT-qPCR and western blotting. Frontal cortex was removed from the brains of 4-months-old female mice by micro-dissection, as previously described[118], harvested, rapidly frozen in liquid nitrogen and stored at −80 °C until use. Synaptosomal fraction was isolated using Syn-PER Synaptic Protein Extraction kit (Thermo Scientific, 87793) according to manufacturer's instructions.

On synaptosomal preparations, RNA was extracted using TRIzol reagent (Sigma–Aldrich, 93289). 1 µg of RNA was reverse transcribed using iScript Ready-to-use cDNA supermix (Bio-Rad, 1708841). Quantitative PCR (qPCR) was performed using SsoAdvanced Universal SYBR Green Supermix (Bio-Rad, 172574) and quantified with Bio-Rad CFX Manager software. Gene expression was normalized by computing a normalization factor by Genorm software using three standard genes *Pol2*, *Tbp*, and *Actn* for nervous tissue. Primer sequences are provided in Supplementary Data 2.

For western blotting cytosolic and synaptosomal fractions were prepared using the same protocol, and protein concentration was quantitated using the BCA protein assay kit (Pierce). Fifteen micrograms of proteins were loaded into a gradient 4–20% SDS-PAGE gel (Bio-Rad, 5678094) and transferred on a 0.45 µm nitrocellulose membrane (Bio-Rad) using a semi-dry Transblot Turbo system (Bio-Rad). Membranes were saturated with 10% nonfat milk in PBS and then probed with the following primary antibodies: Anti-Synaptophysin (Abcam, ab14692, 1:1000), Anti-FUS N-ter1 (ProteinTech, 11570, 1:1000), Anti-FUS N-ter2 (Bethyl, A300-293A, 1:2000), and Anti-FUS C-ter (Bethyl, A300-294A, 1:2000) all diluted in 3% nonfat milk in PBS. Blots were washed and incubated with anti-Rabbit secondary antibody conjugated with HRP (P.A.R.I.S, BI2407, 1:5000) for 2 hours. Membranes were washed several times and analyzed with chemiluminescence using ECL Lumina Forte (Millipore, WBLUF0500) using the Chemidoc XRS Imager (Bio-Rad). Total proteins were detected with a stain-free gel capacity and normalized. Uncropped western blot images and stain-free images are provided in supplementary figures.

Statistics. If not stated otherwise, data are presented as mean ± standard error of the mean (SEM). Statistical analyses were performed using GraphPad Prism 8 (GraphPad, CA). Unpaired *t*-test was used for comparison between two groups, one-way or two-way analysis of the variance (ANOVA), followed by Tukey's multiple comparison post-hoc test and two-way repeated measures (RM) ANOVA, followed by Sidak multiple comparison post-hoc test were applied for three or more groups. Distributions were compared using the Kolmogorov–Smirnov (KS) test. Results were considered significant when $p < 0.05$.

Reporting summary. Further information on research design is available in the Nature Research Reporting Summary linked to this article.

Data availability

Source data are provided with this paper as supplementary information. The RNAseq datasets that support the findings of this study have been deposited in GEO with the accession codes GSE166615. Source data are provided with this paper.

Code availability

The code used for MRI analysis is provided as supplementary files.

Received: 25 May 2020; Accepted: 13 April 2021;
Published online: 21 May 2021

References

1. Taylor, J. P., Brown, R. H. Jr. & Cleveland, D. W. Decoding ALS: from genes to mechanism. *Nature* **539**, 197–206 (2016).
2. Brown, R. H. Jr. & Al-Chalabi, A. Amyotrophic lateral sclerosis. *N. Engl. J. Med.* **377**, 162–172 (2017).
3. van Es, M. A. et al. Amyotrophic lateral sclerosis. *Lancet* **390**, 2084–2098 (2017).
4. Dormann, D. & Haass, C. TDP-43 and FUS: a nuclear affair. *Trends Neurosci.* **34**, 339–348 (2011).
5. Dormann, D. & Haass, C. Fused in sarcoma (FUS): an oncogene goes awry in neurodegeneration. *Mol. Cell Neurosci.* **56**, 475–486 (2013).
6. Kwiatkowski, T. J. Jr et al. Mutations in the FUS/TLS gene on chromosome 16 cause familial amyotrophic lateral sclerosis. *Science* **323**, 1205–1208 (2009).
7. Vance, C. et al. Mutations in FUS, an RNA processing protein, cause familial amyotrophic lateral sclerosis type 6. *Science* **323**, 1208–1211 (2009).
8. Waibel, S., Neumann, M., Rabe, M., Meyer, T. & Ludolph, A. C. Novel missense and truncating mutations in FUS/TLS in familial ALS. *Neurology* **75**, 815–817 (2010).
9. Waibel, S. et al. Truncating mutations in FUS/TLS give rise to a more aggressive ALS-phenotype than missense mutations: a clinico-genetic study in Germany. *Eur. J. Neurol.* **20**, 540–546 (2013).
10. Scekic-Zahirovic, J. et al. Toxic gain of function from mutant FUS protein is crucial to trigger cell autonomous motor neuron loss. *EMBO J.* **35**, 1077–1097 (2016).
11. Dormann, D. et al. ALS-associated fused in sarcoma (FUS) mutations disrupt Transportin-mediated nuclear import. *EMBO J.* **29**, 2841–2857 (2010).
12. Dormann, D. et al. Arginine methylation next to the PY-NLS modulates Transportin binding and nuclear import of FUS. *EMBO J.* **31**, 4258–4275 (2012).
13. Huey, E. D. et al. FUS and TDP43 genetic variability in FTD and CBS. *Neurobiol. Aging* **33**, 1016 e9–1016 17 (2012).
14. Van Langenhove, T. et al. Genetic contribution of FUS to frontotemporal lobar degeneration. *Neurology* **74**, 366–371 (2010).
15. Broustal, O. et al. FUS mutations in frontotemporal lobar degeneration with amyotrophic lateral sclerosis. *J. Alzheimers Dis.* **22**, 765–769 (2010).
16. Blair, I. P. et al. FUS mutations in amyotrophic lateral sclerosis: clinical, pathological, neurophysiological and genetic analysis. *J. Neurol. Neurosurg. Psychiatry* **81**, 639–645 (2010).
17. Flies, C. M. & Veldink, J. H. Chorea is a pleiotropic clinical feature of mutated fused-in-sarcoma in amyotrophic lateral sclerosis. *Amyotroph Lateral Scler Frontotemporal Degener* **21**, 309–311 (2020).
18. Yamashita, S. et al. Sporadic juvenile amyotrophic lateral sclerosis caused by mutant FUS/TLS: possible association of mental retardation with this mutation. *J. Neurol.* **259**, 1039–1044 (2012).
19. Yan, J. et al. Frameshift and novel mutations in FUS in familial amyotrophic lateral sclerosis and ALS/dementia. *Neurology* **75**, 807–814 (2010).
20. Merner, N. D. et al. Exome sequencing identifies FUS mutations as a cause of essential tremor. *Am. J. Hum. Genet.* **91**, 313–319 (2012).
21. Tyzack, G. E. et al. Widespread FUS mislocalization is a molecular hallmark of amyotrophic lateral sclerosis. *Brain* **142**, 2572–2580 (2019).

22. Deng, H. X. et al. FUS-immunoreactive inclusions are a common feature in sporadic and non-SOD1 familial amyotrophic lateral sclerosis. *Ann. Neurol.* **67**, 739–748 (2010).
23. Ikenaka, K. et al. Characteristic features of FUS inclusions in spinal motor neurons of sporadic amyotrophic lateral sclerosis. *J. Neuropathol. Exp. Neurol.* **79**, 370–377 (2020).
24. Snowden, J. S. et al. The most common type of FTLD-FUS (aFTLD-U) is associated with a distinct clinical form of frontotemporal dementia but is not related to mutations in the FUS gene. *Acta Neuropathol.* **122**, 99–110 (2011).
25. Seelaar, H. et al. Frequency of ubiquitin and FUS-positive, TDP-43-negative frontotemporal lobar degeneration. *J. Neurol.* **257**, 747–753 (2010).
26. Josephs, K. A. et al. Caudate atrophy on MRI is a characteristic feature of FTLD-FUS. *Eur. J. Neurol.* **17**, 969–975 (2010).
27. Suarez-Calvet, M. et al. Monomethylated and unmethylated FUS exhibit increased binding to Transportin and distinguish FTLD-FUS from ALS-FUS. *Acta Neuropathol.* **131**, 587–604 (2016).
28. Urwin, H. et al. FUS pathology defines the majority of tau- and TDP-43-negative frontotemporal lobar degeneration. *Acta Neuropathol.* **120**, 33–41 (2010).
29. Mackenzie, I. R. et al. Pathological heterogeneity in amyotrophic lateral sclerosis with FUS mutations: two distinct patterns correlating with disease severity and mutation. *Acta Neuropathol.* **122**, 87–98 (2011).
30. Neumann, M. et al. FET proteins TAF15 and EWS are selective markers that distinguish FTLD with FUS pathology from amyotrophic lateral sclerosis with FUS mutations. *Brain* **134**, 2595–2609 (2011).
31. Doi, H., Koyano, S., Suzuki, Y., Nukina, N. & Kuroiwa, Y. The RNA-binding protein FUS/TLS is a common aggregate-interacting protein in polyglutamine diseases. *Neurosci. Res.* **66**, 131–133 (2010).
32. Mori, S. et al. Expanded polyglutamine impairs normal nuclear distribution of fused in sarcoma and poly (rC)-binding protein 1 in Huntington's disease. *Neuropathology* **39**, 358–367 (2019).
33. Rogelj, B. et al. Widespread binding of FUS along nascent RNA regulates alternative splicing in the brain. *Sci. Rep.* **2**, 603 (2012).
34. Lagier-Tourenne, C. et al. Divergent roles of ALS-linked proteins FUS/TLS and TDP-43 intersect in processing long pre-mRNAs. *Nat. Neurosci.* **15**, 1488–1497 (2012).
35. Kino, Y. et al. FUS/TLS deficiency causes behavioral and pathological abnormalities distinct from amyotrophic lateral sclerosis. *Acta Neuropathol. Commun.* **3**, 24 (2015).
36. Orozco, D. et al. Loss of fused in sarcoma (FUS) promotes pathological Tau splicing. *EMBO Rep.* **13**, 759–764 (2012).
37. Ishigaki, S. et al. Altered Tau isoform ratio caused by loss of FUS and SFPQ function leads to FTLD-like phenotypes. *Cell Rep.* **18**, 1118–1131 (2017).
38. Yokoi, S. et al. 3'UTR length-dependent control of SynGAP isoform alpha2 mRNA by FUS and ELAV-like proteins promotes dendritic spine maturation and cognitive function. *Cell Rep.* **20**, 3071–3084 (2017).
39. Ishigaki, S. & Sobue, G. Importance of functional loss of FUS in FTLD/ALS. *Front. Mol. Biosci.* **5**, 44 (2018).
40. Neumann, M. & Mackenzie, I. R. A. Review: Neuropathology of non-tau frontotemporal lobar degeneration. *Neuropathol. Appl. Neurobiol.* **45**, 19–40 (2019).
41. Scekic-Zahirovic, J. et al. Motor neuron intrinsic and extrinsic mechanisms contribute to the pathogenesis of FUS-associated amyotrophic lateral sclerosis. *Acta Neuropathol.* **133**, 887–906 (2017).
42. Sun, S. et al. ALS-causative mutations in FUS/TLS confer gain- and loss-of-function by altered association with SMN and U1-snRNP. *Nat. Commun.* **6**, 6171 (2015).
43. Sun, S. et al. ALS-causative mutations in FUS/TLS confer gain and loss of function by altered association with SMN and U1-snRNP. *Nat. Commun.* **6**, 6171 (2015).
44. Lopez-Erauskin, J. et al. ALS/FTD-linked mutation in FUS suppresses intra-axonal protein synthesis and drives disease without nuclear loss-of-function of FUS. *Neuron* **100**, 816–830 e7 (2018).
45. Ling, S. C. et al. Overriding FUS autoregulation in mice triggers gain-of-toxic dysfunctions in RNA metabolism and autophagy-lysosome axis. *elife* **8**, e40811 (2019).
46. Devoy, A. et al. Humanized mutant FUS drives progressive motor neuron degeneration without aggregation in 'FUSDelta14' knockin mice. *Brain* **140**, 2797–2805 (2017).
47. So, E. et al. Mitochondrial abnormalities and disruption of the neuromuscular junction precede the clinical phenotype and motor neuron loss in hFUSWT transgenic mice. *Hum. Mol. Genet.* **27**, 463–474 (2018).
48. Schoen, M. et al. Super-resolution microscopy reveals presynaptic localization of the ALS/FTD related protein FUS in hippocampal neurons. *Front. Cell Neurosci.* **9**, 496 (2015).
49. Picchiarelli, G. et al. FUS-mediated regulation of acetylcholine receptor transcription at neuromuscular junctions is compromised in amyotrophic lateral sclerosis. *Nat. Neurosci.* **22**, 1793–1805 (2019).
50. Deshpande, D. et al. Synaptic FUS localization during motoneuron development and its accumulation in human ALS synapses. *Front. Cell Neurosci.* **13**, 256 (2019).
51. Sephton, C. F. et al. Activity-dependent FUS dysregulation disrupts synaptic homeostasis. *Proc. Natl Acad. Sci. USA* **111**, E4769–E4778 (2014).
52. Sahadevan, S. et al. Synaptic FUS accumulation triggers early misregulation of synaptic RNAs in a mouse model of ALS. https://doi.org/10.1038/s41467-021-23188-8. (2021).
53. Frankland, P. W. & Bontempi, B. The organization of recent and remote memories. *Nat. Rev. Neurosci.* **6**, 119–130 (2005).
54. Neary, D., Snowden, J. & Mann, D. Frontotemporal dementia. *Lancet Neurol.* **4**, 771–780 (2005).
55. Bang, J., Spina, S. & Miller, B. L. Frontotemporal dementia. *Lancet* **386**, 1672–1682 (2015).
56. Piguet, O., Hornberger, M., Mioshi, E. & Hodges, J. R. Behavioural-variant frontotemporal dementia: diagnosis, clinical staging, and management. *Lancet Neurol.* **10**, 162–172 (2011).
57. Roberson, E. D. Mouse models of frontotemporal dementia. *Ann. Neurol.* **72**, 837–849 (2012).
58. Schindelin, J. et al. Fiji: an open-source platform for biological-image analysis. *Nat. Methods* **9**, 676–682 (2012).
59. Zhang, Y., Parmigiani, G. & Johnson, W. E. ComBat-seq: batch effect adjustment for RNA-seq count data. *NAR Genom. Bioinform.* **2**, lqaa078 (2020).
60. Wojcik, S. M. et al. A shared vesicular carrier allows synaptic corelease of GABA and glycine. *Neuron* **50**, 575–587 (2006).
61. Fritschy, J. M. & Mohler, H. GABAA-receptor heterogeneity in the adult rat brain: differential regional and cellular distribution of seven major subunits. *J. Comp. Neurol.* **359**, 154–194 (1995).
62. Choii, G. & Ko, J. Gephyrin: a central GABAergic synapse organizer. *Exp. Mol. Med.* **47**, e158 (2015).
63. Kubota, Y., Karube, F., Nomura, M. & Kawaguchi, Y. The diversity of cortical inhibitory synapses. *Front. Neural Circuits* **10**, 27 (2016).
64. Shiihashi, G. et al. Dendritic homeostasis disruption in a novel frontotemporal dementia mouse model expressing cytoplasmic fused in sarcoma. *EBioMedicine* **24**, 102–115 (2017).
65. White, M. A. et al. TDP-43 gains function due to perturbed autoregulation in a Tardbp knock-in mouse model of ALS-FTD. *Nat. Neurosci.* **21**, 552–563 (2018).
66. Jiang, J. et al. Gain of toxicity from ALS/FTD-linked repeat expansions in C9ORF72 is alleviated by antisense oligonucleotides targeting GGGGCC-containing RNAs. *Neuron* **90**, 535–550 (2016).
67. Gascon, E. et al. Alterations in microRNA-124 and AMPA receptors contribute to social behavioral deficits in frontotemporal dementia. *Nat. Med.* **20**, 1444–1451 (2014).
68. Goldstein, L. H. & Abrahams, S. Changes in cognition and behaviour in amyotrophic lateral sclerosis: nature of impairment and implications for assessment. *Lancet Neurol.* **12**, 368–380 (2013).
69. Beeldman, E. et al. The cognitive profile of behavioural variant FTD and its similarities with ALS: a systematic review and meta-analysis. *J. Neurol. Neurosurg. Psychiatry* **89**, 995–1002 (2018).
70. Ling, S. C., Polymenidou, M. & Cleveland, D. W. Converging mechanisms in ALS and FTD: disrupted RNA and protein homeostasis. *Neuron* **79**, 416–438 (2013).
71. Tavares, T. P. et al. Ventricular volume expansion in presymptomatic genetic frontotemporal dementia. *Neurology* **93**, e1699–e1706 (2019).
72. Knopman, D. S. et al. Brain and ventricular volumetric changes in frontotemporal lobar degeneration over 1 year. *Neurology* **72**, 1843–1849 (2009).
73. Manera, A. L., Dadar, M., Collins, D. L., Ducharme, S. & Frontotemporal Lobar Degeneration Neuroimaging Initiative. Deformation based morphometry study of longitudinal MRI changes in behavioral variant frontotemporal dementia. *Neuroimage Clin.* **24**, 102079 (2019)..
74. Convery, R. S. et al. Basal forebrain atrophy in frontotemporal dementia. *Neuroimage Clin.* **26**, 102210 (2020).
75. Schmeisser, M. J. et al. Autistic-like behaviours and hyperactivity in mice lacking ProSAP1/Shank2. *Nature* **486**, 256–260 (2012).
76. Peixoto, R. T., Wang, W., Croney, D. M., Kozorovitskiy, Y. & Sabatini, B. L. Early hyperactivity and precocious maturation of corticostriatal circuits in Shank3B(-/-) mice. *Nat. Neurosci.* **19**, 716–724 (2016).
77. Craig, A. M., Banker, G., Chang, W., McGrath, M. E. & Serpinskaya, A. S. Clustering of gephyrin at GABAergic but not glutamatergic synapses in cultured rat hippocampal neurons. *J. Neurosci.* **16**, 3166–3177 (1996).
78. Dejanovic, B. et al. Palmitoylation of gephyrin controls receptor clustering and plasticity of GABAergic synapses. *PLoS Biol.* **12**, e1001908 (2014).
79. Tretter, V. et al. Molecular basis of the gamma-aminobutyric acid A receptor alpha3 subunit interaction with the clustering protein gephyrin. *J. Biol. Chem.* **286**, 37702–37711 (2011).

80. Mukherjee, J. et al. The residence time of GABA(A)Rs at inhibitory synapses is determined by direct binding of the receptor alpha1 subunit to gephyrin. *J. Neurosci.* **31**, 14677–14687 (2011).
81. Lin, T. W. et al. Regulation of synapse development by Vgat deletion from ErbB4-positive interneurons. *J. Neurosci.* **38**, 2533–2550 (2018).
82. Borghese, C. M. et al. An isoflurane- and alcohol-insensitive mutant GABA(A) receptor alpha(1) subunit with near-normal apparent affinity for GABA: characterization in heterologous systems and production of knockin mice. *J. Pharmacol. Exp. Ther.* **319**, 208–218 (2006).
83. Yee, B. K. et al. A schizophrenia-related sensorimotor deficit links alpha 3-containing GABAA receptors to a dopamine hyperfunction. *Proc. Natl Acad. Sci. USA* **102**, 17154–17159 (2005).
84. Graf, E. R., Zhang, X., Jin, S. X., Linhoff, M. W. & Craig, A. M. Neurexins induce differentiation of GABA and glutamate postsynaptic specializations via neuroligins. *Cell* **119**, 1013–1026 (2004).
85. Grayton, H. M., Missler, M., Collier, D. A. & Fernandes, C. Altered social behaviours in neurexin 1alpha knockout mice resemble core symptoms in neurodevelopmental disorders. *PLoS ONE* **8**, e67114 (2013).
86. Sudhof, T. C. Synaptic neurexin complexes: a molecular code for the logic of neural circuits. *Cell* **171**, 745–769 (2017).
87. Chen, L. Y., Jiang, M., Zhang, B., Gokce, O. & Sudhof, T. C. Conditional deletion of all neurexins defines diversity of essential synaptic organizer functions for neurexins. *Neuron* **94**, 611–625 e4 (2017).
88. Tsuiji, H. et al. TDP-43 accelerates age-dependent degeneration of interneurons. *Sci. Rep.* **7**, 14972 (2017).
89. Khademullah, C. S. et al. Cortical interneuron-mediated inhibition delays the onset of amyotrophic lateral sclerosis. *Brain* **143**, 800–810 (2020).
90. Zhang, W. et al. Hyperactive somatostatin interneurons contribute to excitotoxicity in neurodegenerative disorders. *Nat. Neurosci.* **19**, 557–559 (2016).
91. Clark, R. M., Brizuela, M., Blizzard, C. A. & Dickson, T. C. Reduced excitability and increased neurite complexity of cortical interneurons in a familial mouse model of amyotrophic lateral sclerosis. *Front. Cell Neurosci.* **12**, 328 (2018).
92. Gunes, Z. I., Kan, V. W. Y., Ye, X. & Liebscher, S. Exciting complexity: the role of motor circuit elements in ALS pathophysiology. *Front. Neurosci.* **14**, 573 (2020).
93. Kim, J. et al. Changes in the excitability of neocortical neurons in a mouse model of amyotrophic lateral sclerosis are not specific to corticospinal neurons and are modulated by advancing disease. *J. Neurosci.* **37**, 9037–9053 (2017).
94. Geevasinga, N., Menon, P., Ozdinler, P. H., Kiernan, M. C. & Vucic, S. Pathophysiological and diagnostic implications of cortical dysfunction in ALS. *Nat. Rev. Neurol.* **12**, 651–661 (2016).
95. Lim, L., Mi, D., Llorca, A. & Marin, O. Development and functional diversification of cortical interneurons. *Neuron* **100**, 294–313 (2018).
96. Udagawa, T. et al. FUS regulates AMPA receptor function and FTLD/ALS-associated behaviour via GluA1 mRNA stabilization. *Nat. Commun.* **6**, 7098 (2015).
97. Yasuda, K. et al. The RNA-binding protein Fus directs translation of localized mRNAs in APC-RNP granules. *J. Cell Biol.* **203**, 737–746 (2013).
98. Moreau, P. H., Cosquer, B., Jeltsch, H., Cassel, J. C. & Mathis, C. Neuroanatomical and behavioral effects of a novel version of the cholinergic immunotoxin mu p75-saporin in mice. *Hippocampus* **18**, 610–622 (2008).
99. Gould, T. D. *Mood and Anxiety Related Phenotypes in Mice* (Humana Press, 2009).
100. Witt, R. M., Galligan, M. M., Despinoy, J. R. & Segal, R. Olfactory behavioral testing in the adult mouse. *J. Vis. Exp.* **23**, 949 (2009).
101. Winslow, J. T. Mouse social recognition and preference. *Curr. Protoc. Neurosci.* 10.1002/0471142301.ns0816s22 (2003).
102. Cholvin, T. et al. Dorsal hippocampus and medial prefrontal cortex each contribute to the retrieval of a recent spatial memory in rats. *Brain Struct. Funct.* **221**, 91–102 (2016).
103. Chen, T. W. et al. Ultrasensitive fluorescent proteins for imaging neuronal activity. *Nature* **499**, 295–300 (2013).
104. Liebscher, S., Keller, G. B., Goltstein, P. M., Bonhoeffer, T. & Hubener, M. Selective persistence of sensorimotor mismatch signals in visual cortex of behaving Alzheimer's disease mice. *Curr. Biol.* **26**, 956–964 (2016).
105. Dana, H. et al. High-performance calcium sensors for imaging activity in neuronal populations and microcompartments. *Nat. Methods* **16**, 649–657 (2019).
106. Paxinos, G. & Franklin, K. B. J. *The Mouse Brain in Stereotaxic Coordinates* (Academic Press/Elsevier, 2001).
107. Dorgans, K. et al. Short-term plasticity at cerebellar granule cell to molecular layer interneuron synapses expands information processing. *elife* **8**, e41586 (2019).
108. De Rossi, P. et al. Aberrant accrual of BIN1 near Alzheimer's disease amyloid deposits in transgenic models. *Brain Pathol.* **29**, 485–501 (2019).
109. Rueden, C. T. et al. ImageJ2: ImageJ for the next generation of scientific image data. *BMC Bioinformatics* **18**, 529 (2017).
110. Specht, C. G. et al. Quantitative nanoscopy of inhibitory synapses: counting gephyrin molecules and receptor binding sites. *Neuron* **79**, 308–321 (2013).
111. Bakker, R., Tiesinga, P. & Kotter, R. The Scalable Brain Atlas: instant web-based access to public brain atlases and related content. *Neuroinformatics* **13**, 353–366 (2015).
112. Dobin, A. et al. STAR: ultrafast universal RNA-seq aligner. *Bioinformatics* **29**, 15–21 (2013).
113. Orjuela, S., Huang, R., Hembach, K. M., Robinson, M. D. & Soneson, C. ARMOR: An Automated Reproducible MOdular Workflow for Preprocessing and Differential Analysis of RNA-seq Data. *G3 (Bethesda)* **9**, 2089–2096 (2019).
114. Langfelder, P. & Horvath, S. WGCNA: an R package for weighted correlation network analysis. *BMC Bioinformatics* **9**, 559 (2008).
115. Li, A. & Horvath, S. Network neighborhood analysis with the multi-node topological overlap measure. *Bioinformatics* **23**, 222–231 (2007).
116. Ximerakis, M. et al. Single-cell transcriptomic profiling of the aging mouse brain. *Nat. Neurosci.* **22**, 1696–1708 (2019).
117. Kuleshov, M. V. et al. Enrichr: a comprehensive gene set enrichment analysis web server 2016 update. *Nucleic Acids Res.* **44**, W90–W97 (2016).
118. Spijker, S. in *Neuroproteomics* (ed. Li, K. W.) 23–26 (Humana Press, 2011).

Acknowledgements

We thank the Imaging Platform of the CRBS (PIC-STRA UMS 38, Inserm, Unistra) and the Plateforme Imagerie In Vitro de Strasbourg for their help in performing imaging for this study. This work was funded by Agence Nationale de la Recherche (ANR-16-CE92-0031 to A.L.B. and L.D., ANR-16-CE16-0015 to L.D., ANR-19-CE17-0016 to L.D.), by Fondation pour la recherche médicale (FRM, DEQ20180339179), Axa Research Funds (rare diseases award 2019, to L.D.), Fondation Thierry Latran (HypmotALS, to L.D. and F.R. and TRiALS to F.R.), Radala Foundation (F.R.), MNDA (Dupuis/Apr16/852-791 to L.D.), ALSA (2235, 3209, and 8075 to L.D. and C.L.T.), Target ALS (to C.L.T.), NINDS/NIH R01-NS108769 (to C.L.T.) Deutsche Forschungsgemeinschaft (DFG, German Research Foundation) under Germany's Excellence Strategy within the framework of the Munich Cluster for Systems Neurology—EXC 2145 SyNergy—ID 390857198 (S.L.), under individual grants no. 431995586, 443642953, 446067541 (F.R.) and under the SonderForschungsBereich (SFB) 1149/2 (251293561 to F.R.), Emmy Noether Programme (S.L.), the Deutsche Gesellschaft für Muskelkranke e.V. (S.L.), and the Graduate School for Systemic Neurosciences GSN-LMU (V.K.). C.L.T. is the recipient of the Araminta Broch-Healey Endowed Chair in ALS. The collaborative work between L.D. and M.P. laboratories was funded by ARSLA (2016). I.S.R. was funded by the Région Grand Est (France).

Author contributions

J.S.Z. and I.S.R. performed behavioral analysis with help of R.C., L.T., and G.P. I.S.R. and J.S.Z. performed histology, imaging, and electron microscopy with help of P.D.R., M.J., P.K., V.D., and S.D.G. V.K. performed in vivo calcium imaging. S.M. performed RNAseq analysis, with the help of S.S., K.M.H., N.M., C.L.T., and M.P. D.W. performed and analyzed MRI with the help of J.S.Z., H.P.M., S.A., J.K., V.R., A.L., and F.R. S.D. performed synaptosomal extractions, western blotting and RT-qPCR with the help of I.S.R. and G.P. A.L., A.L.B., F.R., M.P., C.L.T., S.L., and L.D. secured funding. M.P., C.L.T., S.L., and L.D. designed and coordinated experiments. J.S.Z., I.S.R., S.L., and L.D. wrote the manuscript.

Funding

Open Access funding enabled and organized by Projekt DEAL.

Competing interests

The authors declare no competing interests.

Additional information

Supplementary information The online version contains supplementary material available at https://doi.org/10.1038/s41467-021-23187-9.

Correspondence and requests for materials should be addressed to S.L. or L.D.

Peer review information *Nature Communications* thanks Abraham Acevedo-Arozena, Sami Barmada and the other, anonymous, reviewer(s) for their contribution to the peer review of this work. Peer reviewer reports are available.

Reprints and permission information is available at http://www.nature.com/reprints

Publisher's note Springer Nature remains neutral with regard to jurisdictional claims in published maps and institutional affiliations.

Open Access This article is licensed under a Creative Commons Attribution 4.0 International License, which permits use, sharing, adaptation, distribution and reproduction in any medium or format, as long as you give appropriate credit to the original author(s) and the source, provide a link to the Creative Commons license, and indicate if changes were made. The images or other third party material in this article are included in the article's Creative Commons license, unless indicated otherwise in a credit line to the material. If material is not included in the article's Creative Commons license and your intended use is not permitted by statutory regulation or exceeds the permitted use, you will need to obtain permission directly from the copyright holder. To view a copy of this license, visit http://creativecommons.org/licenses/by/4.0/.

© The Author(s) 2021

EBioMedicine 41 (2019) 38–39

Contents lists available at ScienceDirect

EBioMedicine

journal homepage: www.ebiomedicine.com

EBioMedicine
Published by THE LANCET

Commentary

The dark side of HDAC inhibition in ALS

Anne-Laurence Boutillier [a], Laura Tzeplaeff [a,b], Luc Dupuis [b,*]

[a] Université de Strasbourg, CNRS UMR 7364, Laboratoire de Neuroscience Cognitives et Adaptatives (LNCA), Strasbourg, France
[b] Université de Strasbourg, Inserm, UMR-S1118, Strasbourg, France

In this article of *EBioMedicine*, Viviana Moresi and colleagues provide genetic evidence that skeletal muscle HDAC4 exerts a protective role for neuromuscular junction and muscle innervation in amyotrophic lateral sclerosis (ALS) [1].

HDACs are enzymes able to remodel the chromatin through histone deacetylation. The hypothesis that alterations in chromatin remodeling participates in ALS progression comes from studies published 10 years ago showing that ALS disease progression in a mouse model is associated with a loss of the histone acetyl transferase CBP and decreased histone acetylation in motor neurons at disease onset [2]. However, counteracting pharmacologically decreased histone acetylation by broad HDAC inhibition had a moderate effect on whole animal survival [3,4]. More particularly, such treatment efficiently protected motor neuron cell bodies, and slightly delayed the onset of motor decline, but was unable to prevent disruption of neuromuscular junctions [5]. It is therefore likely that HDAC inhibitors might negatively influence other cell types involved in ALS. Pigna and collaborators show here that muscle HDAC4 is a strong candidate for these negative effects of HDAC inhibition.

HDAC4 is a member of the class IIa family that is devoid of deacetylase activity, and likely leads to histone desacetylation through binding of Class I HDACs [6]. In neurons, HDAC4 is predominantly cytoplasmic, particularly concentrated in dendritic spines [7]. Specific neuronal loss of HDAC4 leads to defects in motor coordination, learning and anxiety disorder [8]. HDAC4 is also expressed in muscle, and has a critical developmental role through inhibition of the transcriptional activity of MEF2 [9]. HDAC4 is highly upregulated upon denervation, as occurs in ALS, and is enriched at neuromuscular junctions where it activates the subsynaptic gene expression program [10,11]. Muscle specific deletion of HDAC4 thus leads to defective induction of subsynaptic gene expression but without impacting muscle mass [12,13]. Surprisingly, such manipulation also leads to better muscle reinnervation after nerve injury, in part through relieving the expression of FGF-related retrograde signals to motor neurons [14]. In patients, high muscle HDAC4 expression was correlated to faster disease progression [15]. Given the broad roles of HDAC4 in the different cell-types, it was difficult to predict whether HDAC4 loss would be beneficial or deleterious in ALS.

Pigna and collaborators here used an elegant genetic strategy to dissect the role of HDAC4 in muscle in a mouse model of ALS. Using a conditional allele of *Hdac4*, they ablated HDAC4 in muscle through crossing with transgenic mice expressing CRE under the *Myog* promoter, and introduced a transgene allowing expression of mutant SOD1, a cause of familial ALS. They observed that muscle HDAC4 deletion exacerbates a number of disease parameters in this model: acceleration of weight loss, muscle atrophy and weakness leading to acceleration of disease onset although overall survival remained unaffected. Consistent with a critical role of HDAC4 in neuromuscular junction, muscle HDAC4 ablation led to smaller and more frequently denervated neuromuscular synapses in mutant SOD1 mice, and potently blunted the induction of the so-called denervation response mounted by muscle in response to inactivity. Notably, no effect was observed on motor neuron survival. Muscle proteolytic pathways were also less activated in ALS mice without muscle HDAC4. Interestingly, HDAC4 ablation led to transcriptional dysregulations related to metabolism, ubiquitin-dependent catabolism and skeletal muscle response to denervation, including the upregulation of mitochondrial uncoupling protein 1, whose muscle expression is sufficient to recapitulate most of the observed effects in these animals [16]. As an overall conclusion of the study, Pigna and collaborators demonstrate that the pathways activated by HDAC4 in muscle during ALS are responsible for compensatory reinnervation through the myogenin pathway. Ablation of this key player in the pathway blunts this response and negatively affects NMJ response to denervation, while potentially inducing hypermetabolism.

The study by Pigna and collaborators provides an elegant demonstration why class IIa HDAC inhibition may not be suitable to protect the neuromuscular function in ALS, consistent with a recent study that showed only a transient protection of motor performance after treatment of the same ALS model with the class II specific HDAC inhibitor MC1568 [17]. The current study also nicely confirms 10 years old studies using the pan-HDAC inhibitor valproic acid that potently protected motor neurons, likely via class I HDACs inhibition-dependent effects, but did not prevent NMJ denervation at late stages, possibly because of class IIa HDACs inhibition-dependent effects. In the context of ALS, recent work has shown that HDAC6 inhibitors could provide interesting protection in various mouse models [18] and inhibitors of class I HDACs remain also interesting targets for neuronal protection, especially as HDAC1 appears as a downstream target of both FUS and TDP-43 related ALS. Future work in this area should focus on increasing selectivity of HDAC inhibitors, and ameliorate targeting of the CNS to avoid the deleterious effects of HDAC inhibition in the periphery.

DOI of original article: https://doi.org/10.1016/j.ebiom.2019.01.038.
* Corresponding author.
E-mail address: ldupuis@neuro-cnrs.unistra.fr (L. Dupuis).

https://doi.org/10.1016/j.ebiom.2019.02.039
2352-3964/© 2019 The Authors. Published by Elsevier B.V. This is an open access article under the CC BY-NC-ND license (http://creativecommons.org/licenses/by-nc-nd/4.0/).

Author's contribution

ALB, LT and LD performed literature search and wrote the manuscript.

Conflict of interest

The authors declare no conflict of interest.

Acknowledgments

The authors apologize to the many researchers whose work is not specifically referenced due to space limitations. The authors are supported by Inserm, CNRS, Unistra, ANR-16-CE92-0031 (EPIFUS), ANR-16-CE16-0015 (ToFU), Alsace Alzheimer 67, France Alzheimer (AAP SM 2017 #1664), Fondation pour la recherche médicale and Axa Banque Patrimoniale research fund.

References

[1] Pigna E, Simonazzi E, Sanna K, Bernadzki KM, Proszynski T, Heil C, et al. Histone deacetylase 4 protects from denervation and skeletal muscle atrophy in a murine model of amyotrophic lateral sclerosis. EBioMedicine 2019. https://doi.org/10.1016/j.ebiom.2019.01.038.
[2] Rouaux C, Jokic N, Mbebi C, Boutillier S, Loeffler JP, Boutillier AL. Critical loss of CBP/p300 histone acetylase activity by caspase-6 during neurodegeneration. EMBO J 2003;22(24):6537–49.
[3] Petri S, Kiaei M, Kipiani K, Chen J, Calingasan NY, Crow JP, et al. Additive neuroprotective effects of a histone deacetylase inhibitor and a catalytic antioxidant in a transgenic mouse model of amyotrophic lateral sclerosis. Neurobiol Dis 2006;22(1):40–9.
[4] Sugai F, Yamamoto Y, Miyaguchi K, Zhou Z, Sumi H, Hamasaki T, et al. Benefit of valproic acid in suppressing disease progression of ALS model mice. Eur J Neurosci 2004;20(11):3179–83.
[5] Rouaux C, Panteleeva I, Rene F, Gonzalez de Aguilar JL, Echaniz-Laguna A, Dupuis L, et al. Sodium valproate exerts neuroprotective effects in vivo through CREB-binding protein-dependent mechanisms but does not improve survival in an amyotrophic lateral sclerosis mouse model. J Neurosci 2007;27(21):5535–45.
[6] Lahm A, Paolini C, Pallaoro M, Nardi MC, Jones P, Neddermann P, et al. Unraveling the hidden catalytic activity of vertebrate class IIa histone deacetylases. Proc Natl Acad Sci U S A 2007;104(44):17335–40.
[7] Darcy MJ, Calvin K, Cavnar K, Ouimet CC. Regional and subcellular distribution of HDAC4 in mouse brain. J Comp Neurol 2010;518(5):722–40.
[8] Kim MS, Akhtar MW, Adachi M, Mahgoub M, Bassel-Duby R, Kavalali ET, et al. An essential role for histone deacetylase 4 in synaptic plasticity and memory formation. J Neurosci 2012;32(32):10879–86.
[9] Miska EA, Karlsson C, Langley E, Nielsen SJ, Pines J, Kouzarides T. HDAC4 deacetylase associates with and represses the MEF2 transcription factor. EMBO J 1999;18(18):5099–107.
[10] Cohen TJ, Waddell DS, Barrientos T, Lu Z, Feng G, Cox GA, et al. The histone deacetylase HDAC4 connects neural activity to muscle transcriptional reprogramming. J Biol Chem 2007;282(46):33752–9.
[11] Tang H, Macpherson P, Marvin M, Meadows E, Klein WH, Yang XJ, et al. A histone deacetylase 4/myogenin positive feedback loop coordinates denervation-dependent gene induction and suppression. Mol Biol Cell 2009;20(4):1120–31.
[12] Moresi V, Williams AH, Meadows E, Flynn JM, Potthoff MJ, McAnally J, et al. Myogenin and class II HDACs control neurogenic muscle atrophy by inducing E3 ubiquitin ligases. Cell 2010;143(1):35–45.
[13] Choi MC, Cohen TJ, Barrientos T, Wang B, Li M, Simmons BJ, et al. A direct HDAC4-MAP kinase crosstalk activates muscle atrophy program. Mol Cell 2012;47(1):122–32.
[14] Williams AH, Valdez G, Moresi V, Qi X, McAnally J, Elliott JL, et al. MicroRNA-206 delays ALS progression and promotes regeneration of neuromuscular synapses in mice. Science 2009;326(5959):1549–54.
[15] Bruneteau G, Simonet T, Bauche S, Mandjee N, Malfatti E, Girard E, et al. Muscle histone deacetylase 4 upregulation in amyotrophic lateral sclerosis: potential role in reinnervation ability and disease progression. Brain 2013;136:2359–68 Pt 8.
[16] Dupuis L, Gonzalez de Aguilar JL, Echaniz-Laguna A, Eschbach J, Rene F, Oudart H, et al. Muscle mitochondrial uncoupling dismantles neuromuscular junction and triggers distal degeneration of motor neurons. PLoS One 2009;4(4):e5390.
[17] Buonvicino D, Felici R, Ranieri G, Caramelli R, Lapucci A, Cavone L, et al. Effects of class II-selective histone deacetylase inhibitor on neuromuscular function and disease progression in SOD1-ALS mice. Neuroscience 2018;379:228–38.
[18] Guo W, Naujock M, Fumagalli L, Vandoorne T, Baatsen P, Boon R, et al. HDAC6 inhibition reverses axonal transport defects in motor neurons derived from FUS-ALS patients. Nat Commun 2017;8(1):861.

BIBLIOGRAPHY

A

Abdulla, S., Machts, J., Kaufmann, J., Patrick, K., Kollewe, K., Dengler, R., Heinze, H.-J., Petri, S., Vielhaber, S., and Nestor, P.J. (2014). Hippocampal degeneration in patients with amyotrophic lateral sclerosis. Neurobiology of Aging *35*, 2639–2645.

Abramzon, Y.A., Fratta, P., Traynor, B.J., and Chia, R. (2020). The Overlapping Genetics of Amyotrophic Lateral Sclerosis and Frontotemporal Dementia. Frontiers in Neuroscience *14*, 42.

Achour, M., Le Gras, S., Keime, C., Parmentier, F., Lejeune, F.-X., Boutillier, A.-L., Néri, C., Davidson, I., and Merienne, K. (2015). Neuronal identity genes regulated by super-enhancers are preferentially down-regulated in the striatum of Huntington's disease mice. Human Molecular Genetics *24*, 3481–3496.

Akirav, I., and Maroun, M. (2006). Ventromedial Prefrontal Cortex Is Obligatory for Consolidation and Reconsolidation of Object Recognition Memory. Cerebral Cortex *16*, 1759–1765.

Alarcón, J.M., Malleret, G., Touzani, K., Vronskaya, S., Ishii, S., Kandel, E.R., and Barco, A. (2004). Chromatin Acetylation, Memory, and LTP Are Impaired in CBP+/− Mice: A Model for the Cognitive Deficit in Rubinstein-Taybi Syndrome and Its Amelioration. Neuron *42*, 947–959.

Alcalá-Vida, R., Seguin, J., Lotz, C., Molitor, A.M., Irastorza-Azcarate, I., Awada, A., Karasu, N., Bombardier, A., Cosquer, B., Skarmeta, J.L.G., et al. (2021). Age-related and disease locus-specific mechanisms contribute to early remodelling of chromatin structure in Huntington's disease mice. Nat Commun *12*, 364.

Alfieri, J.A., Silva, P.R., and Igaz, L.M. (2016). Early Cognitive/Social Deficits and Late Motor Phenotype in Conditional Wild-Type TDP-43 Transgenic Mice. Front Aging Neurosci *8*, 310.

Allis, C.D., Berger, S.L., Cote, J., Dent, S., Jenuwien, T., Kouzarides, T., Pillus, L., Reinberg, D., Shi, Y., Shiekhattar, R., et al. (2007). New Nomenclature for Chromatin-Modifying Enzymes. Cell *131*, 633–636.

Alzheimer, A. (1911). über eigenartige Krankheitsfälle des späteren Alters. Z. f. d. g. Neur. u. Psych. *4*, 356.

Arenas, A., Chen, J., Kuang, L., Barnett, K.R., Kasarskis, E.J., Gal, J., and Zhu, H. (2020). Lysine acetylation regulates the RNA binding, subcellular localization and inclusion formation of FUS. Human Molecular Genetics *29*, 2684–2697.

Arias, J., Alberts, A.S., Brindle, P., Claret, F.X., Smeal, T., Karin, M., Feramisco, J., and Montminy, M. (1994). Activation of cAMP and mitogen responsive genes relies on a common nuclear factor. Nature *370*, 226–229.

Armstrong, R.A., Gearing, M., Bigio, E.H., Cruz-Sanchez, F.F., Duyckaerts, C., Mackenzie, I.R.A., Perry, R.H., Skullerud, K., Yokoo, H., and Cairns, N.J. (2011a). The spectrum and severity

of FUS-immunoreactive inclusions in the frontal and temporal lobes of ten cases of neuronal intermediate filament inclusion disease. Acta Neuropathol *121*, 219–228.

Armstrong, R.A., Gearing, M., Bigio, E.H., Cruz-Sanchez, F.F., Duyckaerts, C., Mackenzie, I.R.A., Perry, R.H., Skullerud, K., Yokoo, H., and Cairns, N.J. (2011b). Spatial patterns of FUS-immunoreactive neuronal cytoplasmic inclusions (NCI) in neuronal intermediate filament inclusion disease (NIFID). J Neural Transm (Vienna) *118*, 1651–1657.

Atkins, E.R., Bulsara, M.K., and Panegyres, P.K. (2012). The natural history of early-onset dementia: the Artemis Project. BMJ Open *2*, e001764.

B

Baade, I., Hutten, S., Sternburg, E.L., Pörschke, M., Hofweber, M., Dormann, D., and Kehlenbach, R.H. (2021). The RNA-binding protein FUS is chaperoned and imported into the nucleus by a network of import receptors. Journal of Biological Chemistry *296*, 100659.

Baechtold, H., Kuroda, M., Sok, J., Ron, D., Lopez, B.S., and Akhmedov, A.T. (1999). Human 75-kDa DNA-pairing Protein Is Identical to the Pro-oncoprotein TLS/FUS and Is Able to Promote D-loop Formation *. Journal of Biological Chemistry *274*, 34337–34342.

Bahari-Javan, S., Maddalena, A., Kerimoglu, C., Wittnam, J., Held, T., Bähr, M., Burkhardt, S., Delalle, I., Kügler, S., Fischer, A., et al. (2012). HDAC1 Regulates Fear Extinction in Mice. J. Neurosci. *32*, 5062–5073.

Balendra, R., and Isaacs, A.M. (2018). C9orf72-mediated ALS and FTD: multiple pathways to disease. Nat Rev Neurol *14*, 544–558.

Barker, G.R.I., and Warburton, E.C. (2011). When Is the Hippocampus Involved in Recognition Memory? J. Neurosci. *31*, 10721–10731.

Barrett, L.E., Bockstaele, E.J.V., Sul, J.Y., Takano, H., Haydon, P.G., and Eberwine, J.H. (2006). Elk-1 associates with the mitochondrial permeability transition pore complex in neurons. PNAS *103*, 5155–5160.

Barski, A., Cuddapah, S., Cui, K., Roh, T.-Y., Schones, D.E., Wang, Z., Wei, G., Chepelev, I., and Zhao, K. (2007). High-Resolution Profiling of Histone Methylations in the Human Genome. Cell *129*, 823–837.

Bäumer, D., Hilton, D., Paine, S.M.L., Turner, M.R., Lowe, J., Talbot, K., and Ansorge, O. (2010). Juvenile ALS with basophilic inclusions is a FUS proteinopathy with FUS mutations(e–Pub ahead of print). Neurology *75*, 611–618.

Belly, A., Moreau-Gachelin, F., Sadoul, R., and Goldberg, Y. (2005). Delocalization of the multifunctional RNA splicing factor TLS/FUS in hippocampal neurones: exclusion from the nucleus and accumulation in dendritic granules and spine heads. Neuroscience Letters *379*, 152–157.

Belzil, V.V., Langlais, J.-S., Daoud, H., Dion, P.A., Brais, B., and Rouleau, G.A. (2012). Novel FUS deletion in a patient with juvenile amyotrophic lateral sclerosis. Arch. Neurol. *69*, 653–656.

Belzil, V.V., Bauer, P.O., Prudencio, M., Gendron, T.F., Stetler, C.T., Yan, I.K., Pregent, L., Daughrity, L., Baker, M.C., Rademakers, R., et al. (2013). Reduced C9orf72 gene expression in c9FTD/ALS is caused by histone trimethylation, an epigenetic event detectable in blood. Acta Neuropathol *126*, 895–905.

Benito, E., Urbanke, H., Ramachandran, B., Barth, J., Halder, R., Awasthi, A., Jain, G., Capece, V., Burkhardt, S., Navarro-Sala, M., et al. (2015). HDAC inhibitor–dependent transcriptome and memory reinstatement in cognitive decline models. J Clin Invest *125*, 3572–3584.

Bennett, S.A., Tanaz, R., Cobos, S.N., and Torrente, M.P. (2019). Epigenetics in amyotrophic lateral sclerosis: a role for histone post-translational modifications in neurodegenerative disease. Translational Research *204*, 19–30.

Bernstein, B.E., Mikkelsen, T.S., Xie, X., Kamal, M., Huebert, D.J., Cuff, J., Fry, B., Meissner, A., Wernig, M., Plath, K., et al. (2006). A Bivalent Chromatin Structure Marks Key Developmental Genes in Embryonic Stem Cells. Cell *125*, 315–326.

Besnard, A., Galan, B., Vanhoutte, P., and Caboche, J. (2011). Elk-1 a Transcription Factor with Multiple Facets in the Brain. Front. Neurosci. *5*.

Bicks, L.K., Koike, H., Akbarian, S., and Morishita, H. (2015). Prefrontal Cortex and Social Cognition in Mouse and Man. Frontiers in Psychology *6*, 1805.

Biffi, G., Tannahill, D., McCafferty, J., and Balasubramanian, S. (2013). Quantitative visualization of DNA G-quadruplex structures in human cells. Nature Chem *5*, 182–186.

Birsa, N., Bentham, M.P., and Fratta, P. (2020). Cytoplasmic functions of TDP-43 and FUS and their role in ALS. Seminars in Cell & Developmental Biology *99*, 193–201.

Bisler, S., Schleicher, A., Gass, P., Stehle, J.H., Zilles, K., and Staiger, J.F. (2002). Expression of c-Fos, ICER, Krox-24 and JunB in the whisker-to-barrel pathway of rats: time course of induction upon whisker stimulation by tactile exploration of an enriched environment. Journal of Chemical Neuroanatomy *23*, 187–198.

Blair, I.P., Williams, K.L., Warraich, S.T., Durnall, J.C., Thoeng, A.D., Manavis, J., Blumbergs, P.C., Vucic, S., Kiernan, M.C., and Nicholson, G.A. (2010). FUS mutations in amyotrophic lateral sclerosis: clinical, pathological, neurophysiological and genetic analysis. Journal of Neurology, Neurosurgery & Psychiatry *81*, 639–645.

Blanco-García, N., Asensio-Juan, E., Cruz, X. de la, and Martínez-Balbás, M.A. (2009). Autoacetylation Regulates P/CAF Nuclear Localization *. Journal of Biological Chemistry *284*, 1343–1352.

Blazon, M. (2018). REGULATION OF GABA RELEASE BY PRESYNAPTIC CAV2.2 IN THE BASOLATERAL AMYGDALA AND INFRALIMBIC CORTEX. Undefined.

Blechingberg, J., Holm, I.E., and Nielsen, A.L. (2012). Characterization and expression analysis in the developing embryonic brain of the porcine FET family: FUS, EWS, and TAF15. Gene *493*, 27–35.

Bontempi, B., Laurent-Demir, C., Destrade, C., and Jaffard, R. (1999). Time-dependent reorganization of brain circuitry underlying long-term memory storage. Nature *400*, 671–675.

Bourke, S.C., Tomlinson, M., Williams, T.L., Bullock, R.E., Shaw, P.J., and Gibson, G.J. (2006). Effects of non-invasive ventilation on survival and quality of life in patients with amyotrophic lateral sclerosis: a randomised controlled trial. The Lancet Neurology *5*, 140–147.

Bousiges, O., Vasconcelos, A.P. de, Neidl, R., Cosquer, B., Herbeaux, K., Panteleeva, I., Loeffler, J.-P., Cassel, J.-C., and Boutillier, A.-L. (2010). Spatial Memory Consolidation is Associated with Induction of Several Lysine-Acetyltransferase (Histone Acetyltransferase) Expression Levels and H2B/H4 Acetylation-Dependent Transcriptional Events in the Rat Hippocampus. Neuropsychopharmacology *35*, 2521–2537.

Boutillier, A.-L., Tzeplaeff, L., and Dupuis, L. (2019). The dark side of HDAC inhibition in ALS. EBioMedicine *41*, 38–39.

Boxer, A.L., Gold, M., Huey, E., Gao, F.-B., Burton, E.A., Chow, T., Kao, A., Leavitt, B.R., Lamb, B., Grether, M., et al. (2013). Frontotemporal degeneration, the next therapeutic frontier: Molecules and animal models for frontotemporal degeneration drug development. Alzheimer's & Dementia *9*, 176–188.

Broening, H.W., Morford, L.L., Inman-Wood, S.L., Fukumura, M., and Vorhees, C.V. (2001). 3,4-Methylenedioxymethamphetamine (Ecstasy)-Induced Learning and Memory Impairments Depend on the Age of Exposure during Early Development. J. Neurosci. *21*, 3228–3235.

Broustal, O., Camuzat, A., Guillot-Noël, L., Guy, N., Millecamps, S., Deffond, D., Lacomblez, L., Golfier, V., Hannequin, D., Salachas, F., et al. (2010). FUS Mutations in Frontotemporal Lobar Degeneration with Amyotrophic Lateral Sclerosis. Journal of Alzheimer's Disease : JAD *22*, 765–769.

Bruijn, L.I., Houseweart, M.K., Kato, S., Anderson, K.L., Anderson, S.D., Ohama, E., Reaume, A.G., Scott, R.W., and Cleveland, D.W. (1998). Aggregation and Motor Neuron Toxicity of an ALS-Linked SOD1 Mutant Independent from Wild-Type SOD1. Science *281*, 1851–1854.

Burg, T., Rossaert, E., Moisse, M., Van Damme, P., and Van Den Bosch, L. (2021). Histone Deacetylase Inhibition Regulates Lipid Homeostasis in a Mouse Model of Amyotrophic Lateral Sclerosis. Int J Mol Sci *22*, 11224.

Burke, K.A., Janke, A.M., Rhine, C.L., and Fawzi, N.L. (2015). Residue-by-Residue View of In Vitro FUS Granules that Bind the C-Terminal Domain of RNA Polymerase II. Molecular Cell *60*, 231–241.

C

Cammarota, M., Bevilaqua, L.R., Ardenghi, P., Paratcha, G., Levi de Stein, M., Izquierdo, I., and Medina, J.H. (2000). Learning-associated activation of nuclear MAPK, CREB and Elk-1, along with Fos production, in the rat hippocampus after a one-trial avoidance learning: abolition by NMDA receptor blockade. Brain Res Mol Brain Res *76*, 36–46.

Carlezon, W.A., Duman, R.S., and Nestler, E.J. (2005). The many faces of CREB. Trends in Neurosciences *28*, 436–445.

Cassel, J.-C., de Vasconcelos, A.P., Loureiro, M., Cholvin, T., Dalrymple-Alford, J.C., and Vertes, R.P. (2013). The reuniens and rhomboid nuclei: Neuroanatomy, electrophysiological characteristics and behavioral implications. Prog Neurobiol *111*, 34–52.

Cations, M., Draper, B., Low, L.-F., Radford, K., Trollor, J., Brodaty, H., Sachdev, P., Gonski, P., Broe, G.A., and Withall, A. (2018). Non-Genetic Risk Factors for Degenerative and Vascular Young Onset Dementia: Results from the INSPIRED and KGOW Studies. J Alzheimers Dis *62*, 1747–1758.

Cavigelli, M., Dolfi, F., Claret, F.X., and Karin, M. (1995). Induction of c-fos expression through JNK-mediated TCF/Elk-1 phosphorylation. EMBO J *14*, 5957–5964.

Chatterjee, S., Cassel, R., Schneider-Anthony, A., Merienne, K., Cosquer, B., Tzeplaeff, L., Halder Sinha, S., Kumar, M., Chaturbedy, P., Eswaramoorthy, M., et al. (2018). Reinstating plasticity and memory in a tauopathy mouse model with an acetyltransferase activator. EMBO Molecular Medicine *10*, e8587.

Chatterjee, S., Angelakos, C.C., Bahl, E., Hawk, J.D., Gaine, M.E., Poplawski, S.G., Schneider-Anthony, A., Yadav, M., Porcari, G.S., Cassel, J.-C., et al. (2020). The CBP KIX domain regulates long-term memory and circadian activity. BMC Biology *18*, 155.

Chen, K., Bennett, S.A., Rana, N., Yousuf, H., Said, M., Taaseen, S., Mendo, N., Meltser, S.M., and Torrente, M.P. (2018). Neurodegenerative Disease Proteinopathies Are Connected to Distinct Histone Post-translational Modification Landscapes. ACS Chem. Neurosci. *9*, 838–848.

Chew, J., Gendron, T.F., Prudencio, M., Sasaguri, H., Zhang, Y.-J., Castanedes-Casey, M., Lee, C.W., Jansen-West, K., Kurti, A., Murray, M.E., et al. (2015). C9ORF72 repeat expansions in mice cause TDP-43 pathology, neuronal loss, and behavioral deficits. Science *348*, 1151–1154.

Cholvin, T., Loureiro, M., Cassel, R., Cosquer, B., Herbeaux, K., de Vasconcelos, A.P., and Cassel, J.-C. (2016). Dorsal hippocampus and medial prefrontal cortex each contribute to the retrieval of a recent spatial memory in rats. Brain Struct Funct *221*, 91–102.

Christidi, F., Karavasilis, E., Velonakis, G., Ferentinos, P., Rentzos, M., Kelekis, N., Evdokimidis, I., and Bede, P. (2018). The Clinical and Radiological Spectrum of Hippocampal Pathology in Amyotrophic Lateral Sclerosis. Front. Neurol. *9*.

Christidi, F., Karavasilis, E., Rentzos, M., Velonakis, G., Zouvelou, V., Xirou, S., Argyropoulos, G., Papatriantafyllou, I., Pantolewn, V., Ferentinos, P., et al. (2019). Hippocampal pathology in amyotrophic lateral sclerosis: selective vulnerability of subfields and their associated projections. Neurobiology of Aging *84*, 178–188.

Clark, R.E., Zola, S.M., and Squire, L.R. (2000). Impaired Recognition Memory in Rats after Damage to the Hippocampus. J. Neurosci. *20*, 8853–8860.

Cobos, S.N., Bennett, S.A., and Torrente, M.P. (2019). The impact of histone post-translational modifications in neurodegenerative diseases. Biochimica et Biophysica Acta (BBA) - Molecular Basis of Disease *1865*, 1982–1991.

Collins, B.E., Sweatt, J.D., and Greer, C.B. (2019a). Broad domains of histone 3 lysine 4 trimethylation are associated with transcriptional activation in CA1 neurons of the hippocampus during memory formation. Neurobiology of Learning and Memory *161*, 149–157.

Collins, B.E., Greer, C.B., Coleman, B.C., and Sweatt, J.D. (2019b). Histone H3 lysine K4 methylation and its role in learning and memory. Epigenetics & Chromatin *12*, 7.

Crozat, A., Åman, P., Mandahl, N., and Ron, D. (1993). Fusion of CHOP to a novel RNA-binding protein in human myxoid liposarcoma. Nature *363*, 640.

Cruzalegui, F.H., Cano, E., and Treisman, R. (1999). ERK activation induces phosphorylation of Elk-1 at multiple S/T-P motifs to high stoichiometry. Oncogene *18*, 7948–7957.

Cullinan, W.E., Herman, J.P., Battaglia, D.F., Akil, H., and Watson, S.J. (1995). Pattern and time course of immediate early gene expression in rat brain following acute stress. Neuroscience *64*, 477–505.

D

Dalley, J.W., Cardinal, R.N., and Robbins, T.W. (2004). Prefrontal executive and cognitive functions in rodents: neural and neurochemical substrates. Neuroscience & Biobehavioral Reviews *28*, 771–784.

Darovic, S., Mihevc, S.P., Župunski, V., Gunčar, G., Štalekar, M., Lee, Y.-B., Shaw, C.E., and Rogelj, B. (2015). Phosphorylation of C-terminal tyrosine residue 526 in FUS impairs its nuclear import. J Cell Sci *128*, 4151–4159.

Dash, P.K., Orsi, S.A., and Moore, A.N. (2005). Sequestration of serum response factor in the hippocampus impairs long-term spatial memory. J Neurochem *93*, 269–278.

Daumas, S., Ceccom, J., Halley, H., Francés, B., and Lassalle, J.-M. (2009). Activation of metabotropic glutamate receptor type 2/3 supports the involvement of the hippocampal mossy fiber pathway on contextual fear memory consolidation. Learn. Mem. *16*, 504–507.

Davis, S., Vanhoutte, P., Pages, C., Caboche, J., and Laroche, S. (2000). The MAPK/ERK cascade targets both Elk-1 and cAMP response element-binding protein to control long-term potentiation-dependent gene expression in the dentate gyrus in vivo. J Neurosci *20*, 4563–4572.

DeJesus-Hernandez, M., Mackenzie, I.R., Boeve, B.F., Boxer, A.L., Baker, M., Rutherford, N.J., Nicholson, A.M., Finch, N.A., Flynn, H., Adamson, J., et al. (2011). Expanded GGGGCC Hexanucleotide Repeat in Noncoding Region of C9ORF72 Causes Chromosome 9p-Linked FTD and ALS. Neuron *72*, 245–256.

Deng, H.-X., Zhai, H., Bigio, E.H., Yan, J., Fecto, F., Ajroud, K., Mishra, M., Ajroud-Driss, S., Heller, S., Sufit, R., et al. (2010). FUS-immunoreactive inclusions are a common feature in sporadic and non-SOD1 familial amyotrophic lateral sclerosis. Annals of Neurology *67*, 739–748.

Deng, J., Yang, M., Chen, Y., Chen, X., Liu, J., Sun, S., Cheng, H., Li, Y., Bigio, E.H., Mesulam, M., et al. (2015). FUS Interacts with HSP60 to Promote Mitochondrial Damage. PLoS Genet *11*, e1005357.

Deng, Q., Holler, C.J., Taylor, G., Hudson, K.F., Watkins, W., Gearing, M., Ito, D., Murray, M.E., Dickson, D.W., Seyfried, N.T., et al. (2014). FUS is Phosphorylated by DNA-PK and Accumulates in the Cytoplasm after DNA Damage. J. Neurosci. *34*, 7802–7813.

DeVito, L.M., and Eichenbaum, H. (2010). Distinct contributions of the hippocampus and medial prefrontal cortex to the "what–where–when" components of episodic-like memory in mice. Behavioural Brain Research *215*, 318–325.

Devoy, A., Kalmar, B., Stewart, M., Park, H., Burke, B., Noy, S.J., Redhead, Y., Humphrey, J., Lo, K., Jaeger, J., et al. (2017). Humanized mutant FUS drives progressive motor neuron degeneration without aggregation in 'FUSDelta14' knockin mice. Brain *140*, 2797–2805.

Dini Modigliani, S., Morlando, M., Errichelli, L., Sabatelli, M., and Bozzoni, I. (2014). An ALS-associated mutation in the FUS 3′-UTR disrupts a microRNA–FUS regulatory circuitry. Nat Commun *5*, 4335.

Doi, H., Okamura, K., Bauer, P.O., Furukawa, Y., Shimizu, H., Kurosawa, M., Machida, Y., Miyazaki, H., Mitsui, K., Kuroiwa, Y., et al. (2008). RNA-binding Protein TLS Is a Major Nuclear Aggregate-interacting Protein in Huntingtin Exon 1 with Expanded Polyglutamine-expressing Cells. J. Biol. Chem. *283*, 6489–6500.

Doi, H., Koyano, S., Suzuki, Y., Nukina, N., and Kuroiwa, Y. (2010). The RNA-binding protein FUS/TLS is a common aggregate-interacting protein in polyglutamine diseases. Neuroscience Research *66*, 131–133.

Doria, J.G., Souza, J.M. de, Silva, F.R., Olmo, I.G., Carvalho, T.G., Alves-Silva, J., Ferreira-Vieira, T.H., Santos, J.T., Xavier, C.Q.S., Silva, N.C., et al. (2018). The mGluR5 positive allosteric modulator VU0409551 improves synaptic plasticity and memory of a mouse model of Huntington's disease. Journal of Neurochemistry *147*, 222–239.

Dormann, D., Rodde, R., Edbauer, D., Bentmann, E., Fischer, I., Hruscha, A., Than, M.E., Mackenzie, I.R.A., Capell, A., Schmid, B., et al. (2010). ALS-associated fused in sarcoma (FUS) mutations disrupt Transportin-mediated nuclear import. The EMBO Journal *29*, 2841–2857.

Dormann, D., Madl, T., Valori, C.F., Bentmann, E., Tahirovic, S., Abou-Ajram, C., Kremmer, E., Ansorge, O., Mackenzie, I.R.A., Neumann, M., et al. (2012). Arginine methylation next to the PY-NLS modulates Transportin binding and nuclear import of FUS. The EMBO Journal *31*, 4258–4275.

Dubue, J.D., McKinney, T.L., Treit, D., and Dickson, C.T. (2015). Intrahippocampal Anisomycin Impairs Spatial Performance on the Morris Water Maze. J. Neurosci. *35*, 11118–11124.

E

Ederle, H., Funk, C., Abou-Ajram, C., Hutten, S., Funk, E.B.E., Kehlenbach, R.H., Bailer, S.M., and Dormann, D. (2018). Nuclear egress of TDP-43 and FUS occurs independently of Exportin-1/CRM1. Sci Rep *8*, 7084.

Enslen, H., Raingeaud, J., and Davis, R.J. (1998). Selective Activation of p38 Mitogen-activated Protein (MAP) Kinase Isoforms by the MAP Kinase Kinases MKK3 and MKK6 *. Journal of Biological Chemistry *273*, 1741–1748.

Euston, D.R., Gruber, A.J., and McNaughton, B.L. (2012). The Role of Medial Prefrontal Cortex in Memory and Decision Making. Neuron *76*, 1057–1070.

F

Farrelly, L.A., Thompson, R.E., Zhao, S., Lepack, A.E., Lyu, Y., Bhanu, N.V., Zhang, B., Loh, Y.-H.E., Ramakrishnan, A., Vadodaria, K.C., et al. (2019). Histone serotonylation is a permissive modification that enhances TFIID binding to H3K4me3. Nature *567*, 535–539.

Fecto, F., and Siddique, T. (2011). Making Connections: Pathology and Genetics Link Amyotrophic Lateral Sclerosis with Frontotemporal Lobe Dementia. J Mol Neurosci *45*, 663.

Fischer, A. (2019). The Role of Dynamic Histone Modifications in Learning Behavior. Curr Top Behav Neurosci *42*, 127–157.

Frankland, P.W., and Bontempi, B. (2005). The organization of recent and remote memories. Nature Reviews Neuroscience *6*, 119–130.

Fujii, R., and Takumi, T. (2005). TLS facilitates transport of mRNA encoding an actin-stabilizing protein to dendritic spines. Journal of Cell Science *118*, 5755–5765.

Fujii, R., Okabe, S., Urushido, T., Inoue, K., Yoshimura, A., Tachibana, T., Nishikawa, T., Hicks, G.G., and Takumi, T. (2005). The RNA Binding Protein TLS Is Translocated to Dendritic Spines by mGluR5 Activation and Regulates Spine Morphology. Current Biology *15*, 587–593.

G

Gardiner, M., Toth, R., Vandermoere, F., Morrice, N.A., and Rouse, J. (2008). Identification and characterization of FUS/TLS as a new target of ATM. Biochem J *415*, 297–307.

Gascon, E., Lynch, K., Ruan, H., Almeida, S., Verheyden, J.M., Seeley, W.W., Dickson, D.W., Petrucelli, L., Sun, D., Jiao, J., et al. (2014). Alterations in microRNA-124 and AMPA receptors contribute to social behavioral deficits in frontotemporal dementia. Nat Med *20*, 1444–1451.

Gasparini, L., Terni, B., and Spillantini, M.G. (2007). Frontotemporal Dementia with Tau Pathology. NDD *4*, 236–253.

Geevasinga, N., Menon, P., Özdinler, P.H., Kiernan, M.C., and Vucic, S. (2016). Pathophysiological and diagnostic implications of cortical dysfunction in ALS. Nat Rev Neurol *12*, 651–661.

Gerbino, V., Carrì, M.T., Cozzolino, M., and Achsel, T. (2013). Mislocalised FUS mutants stall spliceosomal snRNPs in the cytoplasm. Neurobiology of Disease *55*, 120–128.

Golimstok, A., Cámpora, N., Rojas, J.I., Fernandez, M.C., Elizondo, C., Soriano, E., and Cristiano, E. (2014). Cardiovascular risk factors and frontotemporal dementia: a case-control study. Transl Neurodegener *3*, 13.

Gonzalez, A., Mannen, T., Çağatay, T., Fujiwara, A., Matsumura, H., Niesman, A.B., Brautigam, C.A., Chook, Y.M., and Yoshizawa, T. (2021). Mechanism of karyopherin-β2 binding and nuclear import of ALS variants FUS(P525L) and FUS(R495X). Sci Rep *11*, 3754.

Gordon, E., Rohrer, J.D., and Fox, N.C. (2016). Advances in neuroimaging in frontotemporal dementia. Journal of Neurochemistry *138*, 193–210.

Gorkin, D.U., Qiu, Y., Hu, M., Fletez-Brant, K., Liu, T., Schmitt, A.D., Noor, A., Chiou, J., Gaulton, K.J., Sebat, J., et al. (2019). Common DNA sequence variation influences 3-dimensional conformation of the human genome. Genome Biol *20*, 255.

Gregory, J.M., Fagegaltier, D., Phatnani, H., and Harms, M.B. (2020). Genetics of Amyotrophic Lateral Sclerosis. Curr Genet Med Rep *8*, 121–131.

Gregory, R.I., Yan, K., Amuthan, G., Chendrimada, T., Doratotaj, B., Cooch, N., and Shiekhattar, R. (2004). The Microprocessor complex mediates the genesis of microRNAs. Nature *432*, 235–240.

Guan, J.-S., Haggarty, S.J., Giacometti, E., Dannenberg, J.-H., Joseph, N., Gao, J., Nieland, T.J.F., Zhou, Y., Wang, X., Mazitschek, R., et al. (2009). HDAC2 negatively regulates memory formation and synaptic plasticity. Nature *459*, 55–60.

Guenther, M.G., Jenner, R.G., Chevalier, B., Nakamura, T., Croce, C.M., Canaani, E., and Young, R.A. (2005). Global and Hox-specific roles for the MLL1 methyltransferase. PNAS *102*, 8603–8608.

Guo, W., Naujock, M., Fumagalli, L., Vandoorne, T., Baatsen, P., Boon, R., Ordovás, L., Patel, A., Welters, M., Vanwelden, T., et al. (2017). HDAC6 inhibition reverses axonal transport defects in motor neurons derived from FUS-ALS patients. Nature Communications *8*, 861.

Guzman, K.M., Brink, L.E., Rodriguez-Bey, G., Bodnar, R.J., Kuang, L., Xing, B., Sullivan, M., Park, H.J., Koppes, E., Zhu, H., et al. (2020). Conditional depletion of Fus in oligodendrocytes leads to motor hyperactivity and increased myelin deposition associated with Akt and cholesterol activation. Glia *68*, 2040–2056.

H

Halbach, O. von B. und, Zacher, C., Gass, P., and Unsicker, K. (2006). Age-related alterations in hippocampal spines and deficiencies in spatial memory in mice. Journal of Neuroscience Research *83*, 525–531.

Hicks, G.G., Singh, N., Nashabi, A., Mai, S., Bozek, G., Klewes, L., Arapovic, D., White, E.K., Koury, M.J., Oltz, E.M., et al. (2000). Fus deficiency in mice results in defective B-lymphocyte development and activation, high levels of chromosomal instability and perinatal death. Nat Genet *24*, 175–179.

Hnisz, D., Abraham, B.J., Lee, T.I., Lau, A., Saint-André, V., Sigova, A.A., Hoke, H.A., and Young, R.A. (2013). Super-Enhancers in the Control of Cell Identity and Disease. Cell *155*, 934–947.

Ho, W.Y., Chang, J.-C., Tyan, S.-H., Yen, Y.-C., Lim, K., Tan, B.S.Y., Ong, J., Tucker-Kellogg, G., Wong, P., Koo, E., et al. (2019). FUS-mediated dysregulation of Sema5a, an autism-related gene, in FUS mice with hippocampus-dependent cognitive deficits. Hum Mol Genet.

Ho, W.Y., Agrawal, I., Tyan, S.-H., Sanford, E., Chang, W.-T., Lim, K., Ong, J., Tan, B.S.Y., Moe, A.A.K., Yu, R., et al. (2021). Dysfunction in nonsense-mediated decay, protein homeostasis, mitochondrial function, and brain connectivity in ALS-FUS mice with cognitive deficits. Acta Neuropathologica Communications *9*, 9.

Hodges, J.R., Davies, R., Xuereb, J., Kril, J., and Halliday, G. (2003). Survival in frontotemporal dementia. Neurology *61*, 349–354.

Hoover, W.B., and Vertes, R.P. (2007). Anatomical analysis of afferent projections to the medial prefrontal cortex in the rat. Brain Struct Funct *212*, 149–179.

Huang, C., Zhou, H., Tong, J., Chen, H., Liu, Y.-J., Wang, D., Wei, X., and Xia, X.-G. (2011). FUS Transgenic Rats Develop the Phenotypes of Amyotrophic Lateral Sclerosis and Frontotemporal Lobar Degeneration. PLOS Genetics *7*, e1002011.

Huang, C., Tong, J., Bi, F., Wu, Q., Huang, B., Zhou, H., and Xia, X.-G. (2012). Entorhinal cortical neurons are the primary targets of FUS mislocalization and ubiquitin aggregation in FUS transgenic rats. Human Molecular Genetics *21*, 4602–4614.

Huang, E.J., Zhang, J., Geser, F., Trojanowski, J.Q., Strober, J.B., Dickson, D.W., Brown, R.H., Shapiro, B.E., and Lomen-Hoerth, C. (2010). Extensive FUS-immunoreactive Pathology in Juvenile Amyotrophic Lateral Sclerosis with Basophilic Inclusions. Brain Pathol *20*, 1069–1076.

Huang, G., Li, H., and Zhang, H. (2020). Abnormal Expression of Mitochondrial Ribosomal Proteins and Their Encoding Genes with Cell Apoptosis and Diseases. Int J Mol Sci *21*, 8879.

Humphrey, J., Birsa, N., Milioto, C., McLaughlin, M., Ule, A.M., Robaldo, D., Eberle, A.B., Kräuchi, R., Bentham, M., Brown, A.-L., et al. (2020). FUS ALS-causative mutations impair FUS autoregulation and splicing factor networks through intron retention. Nucleic Acids Res *48*, 6889–6905.

Husi, H., Ward, M.A., Choudhary, J.S., Blackstock, W.P., and Grant, S.G.N. (2000). Proteomic analysis of NMDA receptor–adhesion protein signaling complexes. Nature Neuroscience *3*, 661–669.

Husmann, D., and Gozani, O. (2019). Histone lysine methyltransferases in biology and disease. Nat Struct Mol Biol *26*, 880–889.

I

Ikenaka, K., Ishigaki, S., Iguchi, Y., Kawai, K., Fujioka, Y., Yokoi, S., Abdelhamid, R.F., Nagano, S., Mochizuki, H., Katsuno, M., et al. (2020). Characteristic Features of FUS Inclusions in Spinal Motor Neurons of Sporadic Amyotrophic Lateral Sclerosis. Journal of Neuropathology & Experimental Neurology *79*, 370–377.

Ingre, C., Roos, P.M., Piehl, F., Kamel, F., and Fang, F. (2015). Risk factors for amyotrophic lateral sclerosis. Clin Epidemiol *7*, 181–193.

Ishaque, A., Mah, D., Seres, P., Luk, C., Eurich, D., Johnston, W., Yang, Y.-H., and Kalra, S. (2018). Evaluating the cerebral correlates of survival in amyotrophic lateral sclerosis. Annals of Clinical and Translational Neurology *5*, 1350–1361.

Ishigaki, S., Masuda, A., Fujioka, Y., Iguchi, Y., Katsuno, M., Shibata, A., Urano, F., Sobue, G., and Ohno, K. (2012). Position-dependent FUS-RNA interactions regulate alternative splicing events and transcriptions. Sci Rep *2*.

Ishigaki, S., Fujioka, Y., Okada, Y., Riku, Y., Udagawa, T., Honda, D., Yokoi, S., Endo, K., Ikenaka, K., Takagi, S., et al. (2017). Altered Tau Isoform Ratio Caused by Loss of FUS and SFPQ Function Leads to FTLD-like Phenotypes. Cell Reports *18*, 1118–1131.

Ishiguro, A., Kimura, N., Watanabe, Y., Watanabe, S., and Ishihama, A. (2016). TDP-43 binds and transports G-quadruplex-containing mRNAs into neurites for local translation. Genes Cells *21*, 466–481.

Iwata, A., Miura, S., Kanazawa, I., Sawada, M., and Nukina, N. (2001). α-Synuclein forms a complex with transcription factor Elk-1. Journal of Neurochemistry *77*, 239–252.

Jaiswal, M.K. (2019). Riluzole and edaravone: A tale of two amyotrophic lateral sclerosis drugs. Medicinal Research Reviews *39*, 733–748.

J

Ji, A.-L., Zhang, X., Chen, W.-W., and Huang, W.-J. (2017). Genetics insight into the amyotrophic lateral sclerosis/frontotemporal dementia spectrum. Journal of Medical Genetics *54*, 145–154.

Jiang, J., Zhu, Q., Gendron, T.F., Saberi, S., McAlonis-Downes, M., Seelman, A., Stauffer, J.E., Jafar-nejad, P., Drenner, K., Schulte, D., et al. (2016). Gain of toxicity from ALS/FTD-linked repeat expansions in C9ORF72 is alleviated by antisense oligonucleotides targeting GGGGCC-containing RNAs. Neuron *90*, 535–550.

Jiang, X., Zhang, T., Wang, H., Wang, T., Qin, M., Bao, P., Wang, R., Liu, Y., Chang, H.-C., Yan, J., et al. (2018). Neurodegeneration-associated FUS is a novel regulator of circadian gene expression. Translational Neurodegeneration *7*, 24.

Joardar, A., Manzo, E., and Zarnescu, D.C. (2017). Metabolic Dysregulation in Amyotrophic Lateral Sclerosis: Challenges and Opportunities. Curr Genet Med Rep *5*, 108–114.

Jones, B.F., and Witter, M.P. (2007). Cingulate cortex projections to the parahippocampal region and hippocampal formation in the rat. Hippocampus *17*, 957–976.

Josephs, K.A., Whitwell, J.L., Parisi, J.E., Petersen, R.C., Boeve, B.F., Jack, C.R., and Dickson, D.W. (2010). Caudate atrophy on MRI is a characteristic feature of FTLD-FUS. Eur J Neurol *17*, 969–975.

Jul, P., Volbracht, C., de Jong, I.E.M., Helboe, L., Elvang, A.B., and Pedersen, J.T. (2016). Hyperactivity with Agitative-Like Behavior in a Mouse Tauopathy Model. Journal of Alzheimer's Disease *49*, 783–795.

Jun, M.-H., Ryu, H.-H., Jun, Y.-W., Liu, T., Li, Y., Lim, C.-S., Lee, Y.-S., Kaang, B.-K., Jang, D.-J., and Lee, J.-A. (2017). Sequestration of PRMT1 and Nd1-L mRNA into ALS-linked FUS mutant R521C-positive aggregates contributes to neurite degeneration upon oxidative stress. Scientific Reports *7*, 40474.

Jutzi, D., Campagne, S., Schmidt, R., Reber, S., Mechtersheimer, J., Gypas, F., Schweingruber, C., Colombo, M., von Schroetter, C., Loughlin, F.E., et al. (2020). Aberrant interaction of FUS with the U1 snRNA provides a molecular mechanism of FUS induced amyotrophic lateral sclerosis. Nat Commun *11*, 6341.

K

Kabashi, E., Valdmanis, P.N., Dion, P., Spiegelman, D., McConkey, B.J., Velde, C.V., Bouchard, J.-P., Lacomblez, L., Pochigaeva, K., Salachas, F., et al. (2008). TARDBP mutations in individuals with sporadic and familial amyotrophic lateral sclerosis. Nat Genet *40*, 572–574.

Kai, M. (2016). Roles of RNA-Binding Proteins in DNA Damage Response. International Journal of Molecular Sciences *17*, 310.

Kanai, Y., Dohmae, N., and Hirokawa, N. (2004). Kinesin Transports RNA: Isolation and Characterization of an RNA-Transporting Granule. Neuron *43*, 513–525.

Kaur, S.J., McKeown, S.R., and Rashid, S. (2016). Mutant SOD1 mediated pathogenesis of Amyotrophic Lateral Sclerosis. Gene *577*, 109–118.

Kelle, D., Kırımtay, K., Selçuk, E., and Karabay, A. (2019). Elk1 affects katanin and spastin proteins via differential transcriptional and post-transcriptional regulations. PLOS ONE *14*, e0212518.

Kennedy, M.B. (2016). Synaptic Signaling in Learning and Memory. Cold Spring Harb Perspect Biol *8*, a016824.

Kerimoglu, C., Agis-Balboa, R.C., Kranz, A., Stilling, R., Bahari-Javan, S., Benito-Garagorri, E., Halder, R., Burkhardt, S., Stewart, A.F., and Fischer, A. (2013). Histone-Methyltransferase MLL2 (KMT2B) Is Required for Memory Formation in Mice. J. Neurosci. *33*, 3452–3464.

Kerimoglu, C., Sakib, M.S., Jain, G., Benito, E., Burkhardt, S., Capece, V., Kaurani, L., Halder, R., Agís-Balboa, R.C., Stilling, R., et al. (2017). KMT2A and KMT2B Mediate Memory Function by Affecting Distinct Genomic Regions. Cell Reports *20*, 538–548.

Kesner, R.P., and Ragozzino, M.E. (2003). The role of the prefrontal cortex in object-place learning: a test of the attribute specificity model. Behav Brain Res *146*, 159–165.

Kim, M.-S., Akhtar, M.W., Adachi, M., Mahgoub, M., Bassel-Duby, R., Kavalali, E.T., Olson, E.N., and Monteggia, L.M. (2012). An Essential Role for Histone Deacetylase 4 in Synaptic Plasticity and Memory Formation. J. Neurosci. *32*, 10879–10886.

Kino, Y., Washizu, C., Aquilanti, E., Okuno, M., Kurosawa, M., Yamada, M., Doi, H., and Nukina, N. (2011). Intracellular localization and splicing regulation of FUS/TLS are variably affected by amyotrophic lateral sclerosis-linked mutations. Nucleic Acids Res *39*, 2781–2798.

Kino, Y., Washizu, C., Kurosawa, M., Yamada, M., Miyazaki, H., Akagi, T., Hashikawa, T., Doi, H., Takumi, T., Hicks, G.G., et al. (2015). FUS/TLS deficiency causes behavioral and pathological abnormalities distinct from amyotrophic lateral sclerosis. Acta Neuropathol Commun *3*.

Kitamura, T., Ogawa, S.K., Roy, D.S., Okuyama, T., Morrissey, M.D., Smith, L.M., Redondo, R.L., and Tonegawa, S. (2017). Engrams and circuits crucial for systems consolidation of a memory. Science *356*, 73–78.

Kleefstra, T., Schenck, A., Kramer, J.M., and van Bokhoven, H. (2014). The genetics of cognitive epigenetics. Neuropharmacology *80*, 83–94.

Klein, M.M., Cholvin, T., Cosquer, B., Salvadori, A., Le Mero, J., Kourouma, L., Boutillier, A.-L., Pereira de Vasconcelos, A., and Cassel, J.-C. (2019). Ventral midline thalamus lesion prevents persistence of new (learning-triggered) hippocampal spines, delayed neocortical spinogenesis, and spatial memory durability. Brain Struct Funct *224*, 1659–1676.

Kondo, K., Mashima, T., Oyoshi, T., Yagi, R., Kurokawa, R., Kobayashi, N., Nagata, T., and Katahira, M. (2018). Plastic roles of phenylalanine and tyrosine residues of TLS/FUS in complex formation with the G-quadruplexes of telomeric DNA and TERRA. Sci Rep *8*, 2864.

Kornmann, B., Schaad, O., Bujard, H., Takahashi, J.S., and Schibler, U. (2007). System-Driven and Oscillator-Dependent Circadian Transcription in Mice with a Conditionally Active Liver Clock. PLOS Biology *5*, e34.

Kouzine, F., Wojtowicz, D., Baranello, L., Yamane, A., Nelson, S., Resch, W., Kieffer-Kwon, K.-R., Benham, C.J., Casellas, R., Przytycka, T.M., et al. (2017). Permanganate/S1 Nuclease Footprinting Reveals Non-B DNA Structures with Regulatory Potential across a Mammalian Genome. Cell Systems *4*, 344-356.e7.

Kuroda, M., Sok, J., Webb, L., Baechtold, H., Urano, F., Yin, Y., Chung, P., de Rooij, D.G., Akhmedov, A., Ashley, T., et al. (2000). Male sterility and enhanced radiation sensitivity in TLS(-/-) mice. EMBO J *19*, 453–462.

Kuruvilla, M.S., Green, J.R., Ayaz, H., and Murman, D.L. (2013). Neural correlates of cognitive decline in ALS: An fNIRS study of the prefrontal cortex. Cogn Neurosci *4*, 115–121.

Kwiatkowski, T.J., Bosco, D.A., LeClerc, A.L., Tamrazian, E., Vanderburg, C.R., Russ, C., Davis, A., Gilchrist, J., Kasarskis, E.J., Munsat, T., et al. (2009). Mutations in the FUS/TLS Gene on Chromosome 16 Cause Familial Amyotrophic Lateral Sclerosis. Science *323*, 1205–1208.

Kwok, R.P.S., Lundblad, J.R., Chrivia, J.C., Richards, J.P., Bächinger, H.P., Brennan, R.G., Roberts, S.G.E., Green, M.R., and Goodman, R.H. (1994). Nuclear protein CBP is a coactivator for the transcription factor CREB. Nature *370*, 223–226.

L

Lagier-Tourenne, C., Polymenidou, M., and Cleveland, D.W. (2010). TDP-43 and FUS/TLS: emerging roles in RNA processing and neurodegeneration. Hum Mol Genet *19*, R46–R64.

Lagier-Tourenne, C., Polymenidou, M., Hutt, K.R., Vu, A.Q., Baughn, M., Huelga, S.C., Clutario, K.M., Ling, S.-C., Liang, T.Y., Mazur, C., et al. (2012). Divergent roles of ALS-linked proteins FUS/TLS and TDP-43 intersect in processing long pre-mRNAs. Nat Neurosci *15*, 1488–1497.

Langston, R.F., and Wood, E.R. (2010). Associative recognition and the hippocampus: Differential effects of hippocampal lesions on object-place, object-context and object-place-context memory. Hippocampus *20*, 1139–1153.

Latif-Hernandez, A., Shah, D., Ahmed, T., Lo, A.C., Callaerts-Vegh, Z., Van der Linden, A., Balschun, D., and D'Hooge, R. (2016). Quinolinic acid injection in mouse medial prefrontal cortex affects reversal learning abilities, cortical connectivity and hippocampal synaptic plasticity. Sci Rep *6*, 36489.

Lavaur, J., Bernard, F., Trifilieff, P., Pascoli, V., Kappes, V., Pages, C., Vanhoutte, P., and Caboche, J. (2007). A TAT DEF Elk-1 Peptide Regulates the Cytonuclear Trafficking of Elk-1 and Controls Cytoskeleton Dynamics. Journal of Neuroscience *27*, 14448–14458.

Lebert, F., Stekke, W., Hasenbroekx, C., and Pasquier, F. (2004). Frontotemporal dementia: a randomised, controlled trial with trazodone. Dement Geriatr Cogn Disord *17*, 355–359.

Lepack, A.E., Werner, C.T., Stewart, A.F., Fulton, S.L., Zhong, P., Farrelly, L.A., Smith, A.C.W., Ramakrishnan, A., Lyu, Y., Bastle, R.M., et al. (2020). Dopaminylation of histone H3 in ventral tegmental area regulates cocaine seeking. Science *368*, 197–201.

Lerga, A., Hallier, M., Delva, L., Orvain, C., Gallais, I., Marie, J., and Moreau-Gachelin, F. (2001). Identification of an RNA Binding Specificity for the Potential Splicing Factor TLS. J. Biol. Chem. *276*, 6807–6816.

Li, C., Wang, H., Yin, Z., Fang, P., Xiao, R., Xiang, Y., Wang, W., Li, Q., Huang, B., Huang, J., et al. (2021). Ligand-induced native G-quadruplex stabilization impairs transcription initiation. Genome Res.

Lin, Y., Mori, E., Kato, M., Xiang, S., Wu, L., Kwon, I., and McKnight, S.L. (2016). Toxic PR Poly-Dipeptides Encoded by the C9orf72 Repeat Expansion Target LC Domain Polymers. Cell *167*, 789-802.e12.

Lin, Y., Currie, S.L., and Rosen, M.K. (2017). Intrinsically disordered sequences enable modulation of protein phase separation through distributed tyrosine motifs. Journal of Biological Chemistry *292*, 19110–19120.

Ling, S.-C., Polymenidou, M., and Cleveland, D.W. (2013). Converging Mechanisms in ALS and FTD: Disrupted RNA and Protein Homeostasis. Neuron *79*, 416–438.

Liu, M.-N., Lau, C.-I., and Lin, C.-P. (2019). Precision Medicine for Frontotemporal Dementia. Front. Psychiatry *10*.

Liu, X., Niu, C., Ren, J., Zhang, J., Xie, X., Zhu, H., Feng, W., and Gong, W. (2013). The RRM domain of human fused in sarcoma protein reveals a non-canonical nucleic acid binding site. Biochimica et Biophysica Acta (BBA) - Molecular Basis of Disease *1832*, 375–385.

Logroscino, G., Traynor, B.J., Hardiman, O., Chiò, A., Mitchell, D., Swingler, R.J., Millul, A., Benn, E., Beghi, E., and Eurals, F. (2010). Incidence of amyotrophic lateral sclerosis in Europe. Journal of Neurology, Neurosurgery & Psychiatry *81*, 385–390.

Logroscino, G., Tortelli, R., Rizzo, G., Marin, B., Preux, P.M., and Malaspina, A. (2015). Amyotrophic Lateral Sclerosis: An Aging-Related Disease. Curr Geri Rep *4*, 142–153.

Lopez, J., Herbeaux, K., Cosquer, B., Engeln, M., Muller, C., Lazarus, C., Kelche, C., Bontempi, B., Cassel, J.-C., and Vasconcelos, A.P. de (2012). Context-dependent modulation of hippocampal and cortical recruitment during remote spatial memory retrieval. Hippocampus *22*, 827–841.

López-Erauskin, J., Tadokoro, T., Baughn, M.W., Myers, B., McAlonis-Downes, M., Chillon-Marinas, C., Asiaban, J.N., Artates, J., Bui, A.T., Vetto, A.P., et al. (2018). ALS/FTD-Linked Mutation in FUS Suppresses Intra-axonal Protein Synthesis and Drives Disease Without Nuclear Loss-of-Function of FUS. Neuron *100*, 816-830.e7.

Loughlin, F.E., Lukavsky, P.J., Kazeeva, T., Reber, S., Hock, E.-M., Colombo, M., Schroetter, C.V., Pauli, P., Cléry, A., Mühlemann, O., et al. (2019). The Solution Structure of FUS Bound to RNA Reveals a Bipartite Mode of RNA Recognition with Both Sequence and Shape Specificity. Molecular Cell *73*, 490-504.e6.

Ludolph, A.C., Dorst, J., Dreyhaupt, J., Weishaupt, J.H., Kassubek, J., Weiland, U., Meyer, T., Petri, S., Hermann, A., Emmer, A., et al. (2020). Effect of High-Caloric Nutrition on Survival in Amyotrophic Lateral Sclerosis. Annals of Neurology *87*, 206–216.

Lueptow, L.M. (2017). Novel Object Recognition Test for the Investigation of Learning and Memory in Mice. JoVE (Journal of Visualized Experiments) e55718.

Luo, Y., Blechingberg, J., Fernandes, A.M., Li, S., Fryland, T., Børglum, A.D., Bolund, L., and Nielsen, A.L. (2015). EWS and FUS bind a subset of transcribed genes encoding proteins enriched in RNA regulatory functions. BMC Genomics *16*.

Luukkainen, L., Bloigu, R., Moilanen, V., and Remes, A.M. (2015). Epidemiology of Frontotemporal Lobar Degeneration in Northern Finland. DEE *5*, 435–441.

Lysikova, E.A., Kukharsky, M.S., Chaprov, K.D., Vasilieva, N.A., Roman, A.Y., Ovchinnikov, R.K., Deykin, A.V., Ninkina, N., and Buchman, V.L. (2019). Behavioural impairments in mice of a novel FUS transgenic line recapitulate features of frontotemporal lobar degeneration. Genes, Brain and Behavior *18*, e12607.

M

Machamer, J.B., Woolums, B.M., Fuller, G.G., and Lloyd, T.E. (2018). FUS causes synaptic hyperexcitability in Drosophila dendritic arborization neurons. Brain Research *1693*, 55–66.

Machts, J., Vielhaber, S., Kollewe, K., Petri, S., Kaufmann, J., and Schoenfeld, M.A. (2018). Global Hippocampal Volume Reductions and Local CA1 Shape Deformations in Amyotrophic Lateral Sclerosis. Front. Neurol. *9*.

Mackenzie, I.R., Nicholson, A.M., Sarkar, M., Messing, J., Purice, M.D., Pottier, C., Annu, K., Baker, M., Perkerson, R.B., Kurti, A., et al. (2017). TIA1 mutations in amyotrophic lateral sclerosis and frontotemporal dementia promote phase separation and alter stress granule dynamics. Neuron *95*, 808-816.e9.

Mackenzie, I.R.A., Foti, D., Woulfe, J., and Hurwitz, T.A. (2008). Atypical frontotemporal lobar degeneration with ubiquitin-positive, TDP-43-negative neuronal inclusions. Brain *131*, 1282–1293.

Madabhushi, R., Gao, F., Pfenning, A.R., Pan, L., Yamakawa, S., Seo, J., Rueda, R., Phan, T.X., Yamakawa, H., Pao, P.-C., et al. (2015). Activity-Induced DNA Breaks Govern the Expression of Neuronal Early-Response Genes. Cell *161*, 1592–1605.

Maei, H.R., Zaslavsky, K., Teixeira, C.M., and Frankland, P.W. (2009). What is the most sensitive measure of water maze probe test performance? Front. Integr. Neurosci. *3*.

Manns, J.R., and Eichenbaum, H. (2009). A cognitive map for object memory in the hippocampus. Learn. Mem. *16*, 616–624.

Mantovan, M.C., Baggio, L., Barba, G.D., Smith, P., Pegoraro, E., Soraru', G., Bonometto, P., and Angelini, C. (2003). Memory deficits and retrieval processes in ALS1. European Journal of Neurology *10*, 221–227.

March, Z.M., King, O.D., and Shorter, J. (2016). Prion-like domains as epigenetic regulators, scaffolds for subcellular organization, and drivers of neurodegenerative disease. Brain Research *1647*, 9–18.

Marogianni, C., Rikos, D., Provatas, A., Dadouli, K., Ntellas, P., Tsitsi, P., Patrinos, G., Dardiotis, E., Hadjigeorgiou, G., and Xiromerisiou, G. (2019). The role of C9orf72 in neurodegenerative disorders: a systematic review, an updated meta-analysis, and the creation of an online database. Neurobiology of Aging *84*, 238.e25-238.e34.

Marr (1971). Simple memory: a theory for archicortex. Philosophical Transactions of the Royal Society of London. B, Biological Sciences.

Marzi, S.J., Leung, S.K., Ribarska, T., Hannon, E., Smith, A.R., Pishva, E., Poschmann, J., Moore, K., Troakes, C., Al-Sarraj, S., et al. (2018). A histone acetylome-wide association study of Alzheimer's disease identifies disease-associated H3K27ac differences in the entorhinal cortex. Nat Neurosci *21*, 1618–1627.

Mastrocola, A.S., Kim, S.H., Trinh, A.T., Rodenkirch, L.A., and Tibbetts, R.S. (2013). The RNA-binding Protein Fused in Sarcoma (FUS) Functions Downstream of Poly(ADP-ribose) Polymerase (PARP) in Response to DNA Damage. J. Biol. Chem. *288*, 24731–24741.

Masuda, A., Takeda, J., Okuno, T., Okamoto, T., Ohkawara, B., Ito, M., Ishigaki, S., Sobue, G., and Ohno, K. (2015). Position-specific binding of FUS to nascent RNA regulates mRNA length. Genes Dev. *29*, 1045–1057.

Mathis, C. (2018). The value of the object recognition paradigm in investigating animal models of Alzheimer's disease: Advances and future directions. In Handbook of Object Novelty Recognition, Vol. 27, (San Diego, CA, US: Elsevier Academic Press), pp. 307–330.

Maurice, T., Duclot, F., Meunier, J., Naert, G., Givalois, L., Meffre, J., Célérier, A., Jacquet, C., Copois, V., Mechti, N., et al. (2008). Altered Memory Capacities and Response to Stress in p300/CBP-Associated Factor (PCAF) Histone Acetylase Knockout Mice. Neuropsychopharmacol *33*, 1584–1602.

Mayr, B., and Montminy, M. (2001). Transcriptional regulation by the phosphorylation-dependent factor CREB. Nat Rev Mol Cell Biol *2*, 599–609.

McCarthy, A., Lonergan, R., Olszewska, D.A., O'Dowd, S., Cummins, G., Magennis, B., Fallon, E.M., Pender, N., Huey, E.D., Cosentino, S., et al. (2015). Closing the tau loop: the missing tau mutation. Brain *138*, 3100–3109.

Mehta, P. (2018). Prevalence of Amyotrophic Lateral Sclerosis — United States, 2015. MMWR Morb Mortal Wkly Rep *67*.

Mejzini, R., Flynn, L.L., Pitout, I.L., Fletcher, S., Wilton, S.D., and Akkari, P.A. (2019). ALS Genetics, Mechanisms, and Therapeutics: Where Are We Now? Front. Neurosci. *0*.

Merienne, N., Meunier, C., Schneider, A., Seguin, J., Nair, S.S., Rocher, A.B., Gras, S.L., Keime, C., Faull, R., Pellerin, L., et al. (2019). Cell-Type-Specific Gene Expression Profiling in Adult Mouse Brain Reveals Normal and Disease-State Signatures. Cell Reports *26*, 2477-2493.e9.

Merner, N.D., Girard, S.L., Catoire, H., Bourassa, C.V., Belzil, V.V., Rivière, J.-B., Hince, P., Levert, A., Dionne-Laporte, A., Spiegelman, D., et al. (2012). Exome Sequencing Identifies FUS Mutations as a Cause of Essential Tremor. The American Journal of Human Genetics *91*, 313–319.

Mishra, S.K., Tawani, A., Mishra, A., and Kumar, A. (2016). G4IPDB: A database for G-quadruplex structure forming nucleic acid interacting proteins. Sci Rep *6*, 38144.

Mitchell, J.C., McGoldrick, P., Vance, C., Hortobagyi, T., Sreedharan, J., Rogelj, B., Tudor, E.L., Smith, B.N., Klasen, C., Miller, C.C.J., et al. (2013). Overexpression of human wild-type FUS causes progressive motor neuron degeneration in an age- and dose-dependent fashion. Acta Neuropathol *125*, 273–288.

Morlando, M., Dini Modigliani, S., Torrelli, G., Rosa, A., Di Carlo, V., Caffarelli, E., and Bozzoni, I. (2012). FUS stimulates microRNA biogenesis by facilitating co-transcriptional Drosha recruitment. EMBO J *31*, 4502–4510.

Morris, R. (1984). Developments of a water-maze procedure for studying spatial learning in the rat. Journal of Neuroscience Methods *11*, 47–60.

Morris, R.G., Garrud, P., Rawlins, J.N., and O'Keefe, J. (1982). Place navigation impaired in rats with hippocampal lesions. Nature *297*, 681–683.

Munoz, D.G., Neumann, M., Kusaka, H., Yokota, O., Ishihara, K., Terada, S., Kuroda, S., and Mackenzie, I.R. (2009). FUS pathology in basophilic inclusion body disease. Acta Neuropathol *118*, 617.

Munter, J. de, Babaevskaya, D., Wolters, E.C., Pavlov, D., Lysikova, E., Kalueff, A.V., Gorlova, A., Oplatchikova, M., Pomytkin, I.A., Proshin, A., et al. (2020). Molecular and behavioural abnormalities in the FUS-tg mice mimic frontotemporal lobar degeneration: Effects of old and new anti-inflammatory therapies. Journal of Cellular and Molecular Medicine *24*, 10251–10257.

Murakami, T., Qamar, S., Lin, J.Q., Schierle, G.S.K., Rees, E., Miyashita, A., Costa, A.R., Dodd, R.B., Chan, F.T.S., Michel, C.H., et al. (2015). ALS/FTD Mutation-Induced Phase Transition of FUS Liquid Droplets and Reversible Hydrogels into Irreversible Hydrogels Impairs RNP Granule Function. Neuron *88*, 678–690.

Murray, M.E., DeJesus-Hernandez, M., Rutherford, N.J., Baker, M., Duara, R., Graff-Radford, N.R., Wszolek, Z.K., Ferman, T.J., Josephs, K.A., Boylan, K.B., et al. (2011). Clinical and neuropathologic heterogeneity of c9FTD/ALS associated with hexanucleotide repeat expansion in C9ORF72. Acta Neuropathol *122*, 673–690.

N

Nadel, L., and Moscovitcht, M. (1997). Memory consolidation, retrograde amnesia and the hippocampal complex. 11.

Nakaya, T., Alexiou, P., Maragkakis, M., Chang, A., and Mourelatos, Z. (2013). FUS regulates genes coding for RNA-binding proteins in neurons by binding to their highly conserved introns. RNA *19*, 498–509.

Naumann, M., Pal, A., Goswami, A., Lojewski, X., Japtok, J., Vehlow, A., Naujock, M., Günther, R., Jin, M., Stanslowsky, N., et al. (2018). Impaired DNA damage response signaling by FUS-NLS mutations leads to neurodegeneration and FUS aggregate formation. Nat Commun *9*, 1–17.

Neary, D., Snowden, J.S., Gustafson, L., Passant, U., Stuss, D., Black, S., Freedman, M., Kertesz, A., Robert, P.H., Albert, M., et al. (1998). Frontotemporal lobar degeneration: A consensus on clinical diagnostic criteria. Neurology *51*, 1546–1554.

Neary, D., Snowden, J., and Mann, D. (2005). Frontotemporal dementia. The Lancet Neurology *4*, 771–780.

Neumann, M., Sampathu, D.M., Kwong, L.K., Truax, A.C., Micsenyi, M.C., Chou, T.T., Bruce, J., Schuck, T., Grossman, M., Clark, C.M., et al. (2006). Ubiquitinated TDP-43 in Frontotemporal Lobar Degeneration and Amyotrophic Lateral Sclerosis. Science *314*, 130–133.

Neumann, M., Roeber, S., Kretzschmar, H.A., Rademakers, R., Baker, M., and Mackenzie, I.R.A. (2009). Abundant FUS-immunoreactive pathology in neuronal intermediate filament inclusion disease. Acta Neuropathol *118*, 605.

Neumann, M., Bentmann, E., Dormann, D., Jawaid, A., DeJesus-Hernandez, M., Ansorge, O., Roeber, S., Kretzschmar, H.A., Munoz, D.G., Kusaka, H., et al. (2011). FET proteins TAF15 and EWS are selective markers that distinguish FTLD with FUS pathology from amyotrophic lateral sclerosis with FUS mutations. Brain *134*, 2595–2609.

Nissen, L.J., Gelly, J.-C., and Hipskind, R.A. (2001). Induction-independent Recruitment of CREB-binding Protein to the c-fos Serum Response Element through Interactions between the Bromodomain and Elk-1 *. Journal of Biological Chemistry *276*, 5213–5221.

Niu, C., Zhang, J., Gao, F., Yang, L., Jia, M., Zhu, H., and Gong, W. (2012). FUS-NLS/Transportin 1 Complex Structure Provides Insights into the Nuclear Targeting Mechanism of FUS and the Implications in ALS. PLOS ONE *7*, e47056.

Nolan, S.O., and Lugo, J.N. (2018). Reversal learning paradigm reveals deficits in cognitive flexibility in the Fmr1 knockout male mouse. F1000Res *7*, 711.

O

Okamoto, K., Murakami, N., Kusaka, H., Yoshida, M., Hashizume, Y., Nakazato, Y., Matsubara, E., and Hirai, S. (1992). Ubiquitin-positive intraneuronal inclusions in the extramotor cortices of presenile dementia patients with motor neuron disease. J Neurol *239*, 426–430.

Oliveira, A.M.M., Hawk, J.D., Abel, T., and Havekes, R. (2010). Post-training reversible inactivation of the hippocampus enhances novel object recognition memory. Learn Mem *17*, 155–160.

Olney, R.K., Murphy, J., Forshew, D., Garwood, E., Miller, B.L., Langmore, S., Kohn, M.A., and Lomen-Hoerth, C. (2005). The effects of executive and behavioral dysfunction on the course of ALS. Neurology *65*, 1774–1777.

Onohara, A., Koh, K., Nagasaka, T., Shindo, K., Kato, M., Aoki, M., and Takiyama, Y. (2015). Japanese amyotrophic lateral sclerosis patient with learning disabilities with a deletion mutation in the C-terminal of the *FUS/TLS* gene. Neurol Clin Neurosci *3*, 192–193.

Orozco, D., and Edbauer, D. (2013). FUS-mediated alternative splicing in the nervous system: consequences for ALS and FTLD. J Mol Med *91*, 1343–1354.

Orozco, D., Tahirovic, S., Rentzsch, K., Schwenk, B.M., Haass, C., and Edbauer, D. (2012). Loss of fused in sarcoma (FUS) promotes pathological Tau splicing. EMBO Rep *13*, 759–764.

P

Packard, M.G., and Knowlton, B.J. (2002). Learning and memory functions of the Basal Ganglia. Annu Rev Neurosci *25*, 563–593.

Park, S.-Y., and Kim, J.-S. (2020). A short guide to histone deacetylases including recent progress on class II enzymes. Exp Mol Med *52*, 204–212.

Parker, D., Ferreri, K., Nakajima, T., LaMorte, V.J., Evans, R., Koerber, S.C., Hoeger, C., and Montminy, M.R. (1996). Phosphorylation of CREB at Ser-133 induces complex formation with CREB-binding protein via a direct mechanism. Mol Cell Biol *16*, 694–703.

Patel, A., Lee, H.O., Jawerth, L., Maharana, S., Jahnel, M., Hein, M.Y., Stoynov, S., Mahamid, J., Saha, S., Franzmann, T.M., et al. (2015). A Liquid-to-Solid Phase Transition of the ALS Protein FUS Accelerated by Disease Mutation. Cell *162*, 1066–1077.

Peleg, S., Sananbenesi, F., Zovoilis, A., Burkhardt, S., Bahari-Javan, S., Agis-Balboa, R.C., Cota, P., Wittnam, J.L., Gogol-Doering, A., Opitz, L., et al. (2010). Altered Histone Acetylation Is Associated with Age-Dependent Memory Impairment in Mice. Science *328*, 753–756.

PENFIELD, W., and MILNER, B. (1958). Memory Deficit Produced by Bilateral Lesions in the Hippocampal Zone. A.M.A. Archives of Neurology & Psychiatry *79*, 475–497.

Pereira, G.C., Sanchez, L., Schaughency, P.M., Rubio-Roldán, A., Choi, J.A., Planet, E., Batra, R., Turelli, P., Trono, D., Ostrow, L.W., et al. (2018). Properties of LINE-1 proteins and repeat element expression in the context of amyotrophic lateral sclerosis. Mobile DNA *9*, 35.

Picchiarelli, G., Demestre, M., Zuko, A., Been, M., Higelin, J., Dieterlé, S., Goy, M.-A., Mallik, M., Sellier, C., Scekic-Zahirovic, J., et al. (2019). FUS-mediated regulation of acetylcholine receptor transcription at neuromuscular junctions is compromised in amyotrophic lateral sclerosis. Nat Neurosci *22*, 1793–1805.

PICK, A. (1892). Uber die Beziehungen der senilen Hirnatrophie zur Aphasie. Prag Med Wochenschr *17*, 165–167.

Pigna, E., Simonazzi, E., Sanna, K., Bernadzki, K.M., Proszynski, T., Heil, C., Palacios, D., Adamo, S., and Moresi, V. (2019). Histone deacetylase 4 protects from denervation and skeletal muscle atrophy in a murine model of amyotrophic lateral sclerosis. EBioMedicine *40*, 717–732.

Prasad, A., Bharathi, V., Sivalingam, V., Girdhar, A., and Patel, B.K. (2019). Molecular Mechanisms of TDP-43 Misfolding and Pathology in Amyotrophic Lateral Sclerosis. Front. Mol. Neurosci. *0*.

Q

Qiu, H., Lee, S., Shang, Y., Wang, W.-Y., Au, K.F., Kamiya, S., Barmada, S.J., Finkbeiner, S., Lui, H., Carlton, C.E., et al. (2014). ALS-associated mutation FUS-R521C causes DNA damage and RNA splicing defects. J Clin Invest *124*, 981–999.

Quinn, J.J., Ma, Q.D., Tinsley, M.R., Koch, C., and Fanselow, M.S. (2008). Inverse temporal contributions of the dorsal hippocampus and medial prefrontal cortex to the expression of long-term fear memories. Learn Mem *15*, 368–372.

R

Rabbitts, T.H., Forster, A., Larson, R., and Nathan, P. (1993). Fusion of the dominant negative transcription regulator CHOP with a novel gene FUS by translocation t(12;16) in malignant liposarcoma. Nat Genet *4*, 175–180.

Radford, R.A., Morsch, M., Rayner, S.L., Cole, N.J., Pountney, D.L., and Chung, R.S. (2015). The established and emerging roles of astrocytes and microglia in amyotrophic lateral sclerosis and frontotemporal dementia. Front Cell Neurosci *9*.

Rasmussen Eid, H., Rosness, T.A., Bosnes, O., Salvesen, Ø., Knutli, M., and Stordal, E. (2019). Smoking and Obesity as Risk Factors in Frontotemporal Dementia and Alzheimer's Disease: The HUNT Study. Dement Geriatr Cogn Dis Extra *9*, 1–10.

Reber, S., Stettler, J., Filosa, G., Colombo, M., Jutzi, D., Lenzken, S.C., Schweingruber, C., Bruggmann, R., Bachi, A., Barabino, S.M., et al. (2016). Minor intron splicing is regulated by FUS and affected by ALS-associated FUS mutants. The EMBO Journal *35*, 1504–1521.

Remaud, J., Ceccom, J., Carponcy, J., Dugué, L., Menchon, G., Pech, S., Halley, H., Francés, B., and Dahan, L. (2014). Anisomycin injection in area CA3 of the hippocampus impairs both short-term and long-term memories of contextual fear. Learn Mem *21*, 311–315.

Renton, A.E., Majounie, E., Waite, A., Simón-Sánchez, J., Rollinson, S., Gibbs, J.R., Schymick, J.C., Laaksovirta, H., van Swieten, J.C., Myllykangas, L., et al. (2011). A Hexanucleotide Repeat Expansion in C9ORF72 Is the Cause of Chromosome 9p21-Linked ALS-FTD. Neuron *72*, 257–268.

Renton, A.E., Chiò, A., and Traynor, B.J. (2014). State of play in amyotrophic lateral sclerosis genetics. Nat Neurosci *17*, 17–23.

Restivo, L., Vetere, G., Bontempi, B., and Ammassari-Teule, M. (2009). The Formation of Recent and Remote Memory Is Associated with Time-Dependent Formation of Dendritic Spines in the Hippocampus and Anterior Cingulate Cortex. J. Neurosci. *29*, 8206–8214.

Rhoads, S.N., Monahan, Z.T., Yee, D.S., and Shewmaker, F.P. (2018). The Role of Post-Translational Modifications on Prion-Like Aggregation and Liquid-Phase Separation of FUS. Int J Mol Sci *19*.

Rippon, G.A., Scarmeas, N., Gordon, P.H., Murphy, P.L., Albert, S.M., Mitsumoto, H., Marder, K., Rowland, L.P., and Stern, Y. (2006). An Observational Study of Cognitive Impairment in Amyotrophic Lateral Sclerosis. Archives of Neurology *63*, 345–352.

Rodriguez-Ortiz, C.J., Hoshino, H., Cheng, D., Liu-Yescevitz, L., Blurton-Jones, M., Wolozin, B., LaFerla, F.M., and Kitazawa, M. (2013). Neuronal-Specific Overexpression of a Mutant Valosin-Containing Protein Associated with IBMPFD Promotes Aberrant Ubiquitin and TDP-43 Accumulation and Cognitive Dysfunction in Transgenic Mice. Am J Pathol *183*, 504–515.

Roeber, S., Mackenzie, I.R.A., Kretzschmar, H.A., and Neumann, M. (2008). TDP-43-negative FTLD-U is a significant new clinico-pathological subtype of FTLD. Acta Neuropathol *116*, 147.

Rosen, D.R., Siddique, T., Patterson, D., Figlewicz, D.A., Sapp, P., Hentati, A., Donaldson, D., Goto, J., O'Regan, J.P., Deng, H.-X., et al. (1993). Mutations in Cu/Zn superoxide dismutase gene are associated with familial amyotrophic lateral sclerosis. Nature *362*, 59–62.

Rossaert, E., Pollari, E., Jaspers, T., Van Helleputte, L., Jarpe, M., Van Damme, P., De Bock, K., Moisse, M., and Van Den Bosch, L. (2019). Restoration of histone acetylation ameliorates disease and metabolic abnormalities in a FUS mouse model. Acta Neuropathologica Communications *7*, 107.

Rosso, S.M. (2003). Medical and environmental risk factors for sporadic frontotemporal dementia: a retrospective case-control study. Journal of Neurology, Neurosurgery & Psychiatry *74*, 1574–1576.

Roze, E., Bettuing, S., Deyts, C., Marcon, E., Brami-Cherrier, K., Pagès, C., Humbert, S., Mérienne, K., and Caboche, J. (2008). Mitogen- and stress-activated protein kinase-1 deficiency is involved in expanded-huntingtin-induced transcriptional dysregulation and striatal death. The FASEB Journal *22*, 1083–1093.

Rulten, S.L., Rotheray, A., Green, R.L., Grundy, G.J., Moore, D.A.Q., Gómez-Herreros, F., Hafezparast, M., and Caldecott, K.W. (2014). PARP-1 dependent recruitment of the amyotrophic lateral sclerosis-associated protein FUS/TLS to sites of oxidative DNA damage. Nucleic Acids Res *42*, 307–314.

S

Sabari, B.R., Zhang, D., Allis, C.D., and Zhao, Y. (2017). Metabolic regulation of gene expression through histone acylations. Nat Rev Mol Cell Biol *18*, 90–101.

Sahadevan, S., Hembach, K.M., Tantardini, E., Pérez-Berlanga, M., Hruska-Plochan, M., Megat, S., Weber, J., Schwarz, P., Dupuis, L., Robinson, M.D., et al. (2021). Synaptic FUS accumulation triggers early misregulation of synaptic RNAs in a mouse model of ALS. Nat Commun *12*, 3027.

Salinas, S., Briançon-Marjollet, A., Bossis, G., Lopez, M.-A., Piechaczyk, M., Jariel-Encontre, I., Debant, A., and Hipskind, R.A. (2004). SUMOylation regulates nucleo-cytoplasmic shuttling of Elk-1. Journal of Cell Biology *165*, 767–773.

Sama, R.R.K., Ward, C.L., and Bosco, D.A. (2014). Functions of FUS/TLS From DNA Repair to Stress Response: Implications for ALS. ASN Neuro *6*.

Sama, R.R.K., Fallini, C., Gatto, R., McKeon, J.E., Song, Y., Rotunno, M.S., Penaranda, S., Abdurakhmanov, I., Landers, J.E., Morfini, G., et al. (2017). ALS-linked FUS exerts a gain of toxic function involving aberrant p38 MAPK activation. Scientific Reports *7*, 115.

Sananbenesi, F., Fischer, A., Schrick, C., Spiess, J., and Radulovic, J. (2002). Phosphorylation of hippocampal Erk-1/2, Elk-1, and p90-Rsk-1 during contextual fear conditioning: interactions between Erk-1/2 and Elk-1. Mol Cell Neurosci *21*, 463–476.

Sand, L.G.L., Szuhai, K., and Hogendoorn, P.C.W. (2015). Sequencing Overview of Ewing Sarcoma: A Journey across Genomic, Epigenomic and Transcriptomic Landscapes. Int J Mol Sci *16*, 16176–16215.

Sanjuan-Ruiz, I., Govea-Perez, N., McAlonis-Downes, M., Dieterle, S., Megat, S., Dirrig-Grosch, S., Picchiarelli, G., Piol, D., Zhu, Q., Myers, B., et al. (2021). Wild-type FUS corrects ALS-like disease induced by cytoplasmic mutant FUS through autoregulation. Molecular Neurodegeneration *16*, 61.

Savage, A.L., Wilm, T.P., Khursheed, K., Shatunov, A., Morrison, K.E., Shaw, P.J., Shaw, C.E., Smith, B., Breen, G., Al-Chalabi, A., et al. (2014). An Evaluation of a SVA Retrotransposon in the FUS Promoter as a Transcriptional Regulator and Its Association to ALS. PLoS One *9*, e90833.

Scandaglia, M., Lopez-Atalaya, J.P., Medrano-Fernandez, A., Lopez-Cascales, M.T., Blanco, B. del, Lipinski, M., Benito, E., Olivares, R., Iwase, S., Shi, Y., et al. (2017). Loss of Kdm5c Causes Spurious Transcription and Prevents the Fine-Tuning of Activity-Regulated Enhancers in Neurons. Cell Reports *21*, 47–59.

Scaramuzzino, C., Monaghan, J., Milioto, C., Jr, N.A.L., Maltare, A., Aggarwal, T., Casci, I., Fackelmayer, F.O., Pennuto, M., and Pandey, U.B. (2013). Protein Arginine Methyltransferase 1 and 8 Interact with FUS to Modify Its Sub-Cellular Distribution and Toxicity In Vitro and In Vivo. PLOS ONE *8*, e61576.

Scekic-Zahirovic, J., Sendscheid, O., El Oussini, H., Jambeau, M., Sun, Y., Mersmann, S., Wagner, M., Dieterlé, S., Sinniger, J., Dirrig-Grosch, S., et al. (2016). Toxic gain of function from mutant FUS protein is crucial to trigger cell autonomous motor neuron loss. EMBO J *35*, 1077–1097.

Scekic-Zahirovic, J., Oussini, H.E., Mersmann, S., Drenner, K., Wagner, M., Sun, Y., Allmeroth, K., Dieterlé, S., Sinniger, J., Dirrig-Grosch, S., et al. (2017). Motor neuron intrinsic and extrinsic mechanisms contribute to the pathogenesis of FUS-associated amyotrophic lateral sclerosis. Acta Neuropathol *133*, 887–906.

Scekic-Zahirovic, J., Sanjuan-Ruiz, I., Kan, V., Megat, S., De Rossi, P., Dieterlé, S., Cassel, R., Jamet, M., Kessler, P., Wiesner, D., et al. (2021). Cytoplasmic FUS triggers early behavioral alterations linked to cortical neuronal hyperactivity and inhibitory synaptic defects. Nat Commun *12*, 3028.

Schneider, A., Chatterjee, S., Bousiges, O., Selvi, B.R., Swaminathan, A., Cassel, R., Blanc, F., Kundu, T.K., and Boutillier, A.-L. (2013). Acetyltransferases (HATs) as Targets for Neurological Therapeutics. Neurotherapeutics *10*, 568–588.

Schoen, M., Reichel, J.M., Demestre, M., Putz, S., Deshpande, D., Proepper, C., Liebau, S., Schmeisser, M.J., Ludolph, A.C., Michaelis, J., et al. (2015). Super-Resolution Microscopy

Reveals Presynaptic Localization of the ALS/FTD Related Protein FUS in Hippocampal Neurons. Front Cell Neurosci *9*, 496.

Schueller, E., Paiva, I., Blanc, F., Wang, X.-L., Cassel, J.-C., Boutillier, A.-L., and Bousiges, O. (2020). Dysregulation of histone acetylation pathways in hippocampus and frontal cortex of Alzheimer's disease patients. European Neuropsychopharmacology *33*, 101–116.

Schwartz, J.C., Ebmeier, C.C., Podell, E.R., Heimiller, J., Taatjes, D.J., and Cech, T.R. (2012). FUS binds the CTD of RNA polymerase II and regulates its phosphorylation at Ser2. Genes Dev *26*, 2690–2695.

Scoville, W.B., and Milner, B. (1957). Loss of Recent Memory After Bilateral Hippocampal Lesions. Journal of Neurology, Neurosurgery & Psychiatry *20*, 11–21.

Seelaar, H., Klijnsma, K.Y., de Koning, I., van der Lugt, A., Chiu, W.Z., Azmani, A., Rozemuller, A.J.M., and van Swieten, J.C. (2010). Frequency of ubiquitin and FUS-positive, TDP-43-negative frontotemporal lobar degeneration. J Neurol *257*, 747–753.

Semon, R.W. (1921). The mneme (London, New York: G. Allen & Unwin ltd.).

Sephton, C.F., Tang, A.A., Kulkarni, A., West, J., Brooks, M., Stubblefield, J.J., Liu, Y., Zhang, M.Q., Green, C.B., Huber, K.M., et al. (2014). Activity-dependent FUS dysregulation disrupts synaptic homeostasis. PNAS *111*, E4769–E4778.

Shang, Y., and Huang, E.J. (2016). Mechanisms of FUS mutations in familial amyotrophic lateral sclerosis. Brain Research *1647*, 65–78.

Sharma, A., Lyashchenko, A.K., Lu, L., Nasrabady, S.E., Elmaleh, M., Mendelsohn, M., Nemes, A., Tapia, J.C., Mentis, G.Z., and Shneider, N.A. (2016a). ALS-associated mutant FUS induces selective motor neuron degeneration through toxic gain of function. Nat Commun *7*.

Sharma, A., Lyashchenko, A.K., Lu, L., Nasrabady, S.E., Elmaleh, M., Mendelsohn, M., Nemes, A., Tapia, J.C., Mentis, G.Z., and Shneider, N.A. (2016b). ALS-associated mutant FUS induces selective motor neuron degeneration through toxic gain of function. Nat Commun *7*, 10465.

Sheng, M., and Greenberg, M.E. (1990). The regulation and function of c-fos and other immediate early genes in the nervous system. Neuron *4*, 477–485.

Shiihashi, G., Ito, D., Arai, I., Kobayashi, Y., Hayashi, K., Otsuka, S., Nakajima, K., Yuzaki, M., Itohara, S., and Suzuki, N. (2017). Dendritic Homeostasis Disruption in a Novel Frontotemporal Dementia Mouse Model Expressing Cytoplasmic Fused in Sarcoma. EBioMedicine *24*, 102–115.

Smith, A.R., Smith, R.G., Macdonald, R., Marzi, S.J., Burrage, J., Troakes, C., Al-Sarraj, S., Mill, J., and Lunnon, K. (2021). The histone modification H3K4me3 is altered at the ANK1 locus in Alzheimer's disease brain. Future Science OA *7*, FSO665.

Smith, E.F., Shaw, P.J., and De Vos, K.J. (2019). The role of mitochondria in amyotrophic lateral sclerosis. Neuroscience Letters *710*, 132933.

Snowden, J.S. (2001). Distinct behavioural profiles in frontotemporal dementia and semantic dementia. Journal of Neurology, Neurosurgery & Psychiatry *70*, 323–332.

Snowden, J.S., Hu, Q., Rollinson, S., Halliwell, N., Robinson, A., Davidson, Y.S., Momeni, P., Baborie, A., Griffiths, T.D., Jaros, E., et al. (2011). The most common type of FTLD-FUS (aFTLD-U) is associated with a distinct clinical form of frontotemporal dementia but is not related to mutations in the FUS gene. Acta Neuropathol *122*, 99–110.

Spiegel, J., Cuesta, S.M., Adhikari, S., Hänsel-Hertsch, R., Tannahill, D., and Balasubramanian, S. (2021). G-quadruplexes are transcription factor binding hubs in human chromatin. Genome Biology *22*, 117.

Squire, L.R., Genzel, L., Wixted, J.T., and Morris, R.G. (2015). Memory Consolidation. Cold Spring Harb Perspect Biol *7*, a021766.

Stoppel, C.M., Vielhaber, S., Eckart, C., Machts, J., Kaufmann, J., Heinze, H.-J., Kollewe, K., Petri, S., Dengler, R., Hopf, J.-M., et al. (2014). Structural and functional hallmarks of amyotrophic lateral sclerosis progression in motor- and memory-related brain regions. NeuroImage: Clinical *5*, 277–290.

Suárez-Calvet, M., Neumann, M., Arzberger, T., Abou-Ajram, C., Funk, E., Hartmann, H., Edbauer, D., Kremmer, E., Göbl, C., Resch, M., et al. (2016). Monomethylated and unmethylated FUS exhibit increased binding to Transportin and distinguish FTLD-FUS from ALS-<Emphasis Type="Italic">FUS</Emphasis>. Acta Neuropathol *131*, 587–604.

Suberbielle, E., Sanchez, P.E., Kravitz, A.V., Wang, X., Ho, K., Eilertson, K., Devidze, N., Kreitzer, A.C., and Mucke, L. (2013). Physiologic brain activity causes DNA double-strand breaks in neurons, with exacerbation by amyloid-β. Nature Neuroscience *16*, 613–621.

Sugiura, T., Sakurai, K., and Nagano, Y. (2007). Intracellular characterization of DDX39, a novel growth-associated RNA helicase. Experimental Cell Research *313*, 782–790.

Sukhanova, M.V., Singatulina, A.S., Pastré, D., and Lavrik, O.I. (2020). Fused in Sarcoma (FUS) in DNA Repair: Tango with Poly(ADP-ribose) Polymerase 1 and Compartmentalisation of Damaged DNA. Int J Mol Sci *21*, 7020.

Sun, S., Ling, S.-C., Qiu, J., Albuquerque, C.P., Zhou, Y., Tokunaga, S., Li, H., Qiu, H., Bui, A., Yeo, G.W., et al. (2015). ALS-causative mutations in FUS/TLS confer gain and loss of function by altered association with SMN and U1-snRNP. Nature Communications *6*, 6171.

Svetoni, F., Frisone, P., and Paronetto, M.P. (2016). Role of FET proteins in neurodegenerative disorders. RNA Biology *13*, 1089–1102.

Svetoni, F., De Paola, E., La Rosa, P., Mercatelli, N., Caporossi, D., Sette, C., and Paronetto, M.P. (2017). Post-transcriptional regulation of FUS and EWS protein expression by miR-141 during neural differentiation. Hum Mol Genet *26*, 2732–2746.

Swarup, V., Phaneuf, D., Bareil, C., Robertson, J., Rouleau, G.A., Kriz, J., and Julien, J.-P. (2011). Pathological hallmarks of amyotrophic lateral sclerosis/frontotemporal lobar degeneration in transgenic mice produced with TDP-43 genomic fragments. Brain *134*, 2610–2626.

Swinnen, B., and Robberecht, W. (2014). The phenotypic variability of amyotrophic lateral sclerosis. Nat Rev Neurol *10*, 661–670.

T

Takahama, K., Takada, A., Tada, S., Shimizu, M., Sayama, K., Kurokawa, R., and Oyoshi, T. (2013). Regulation of Telomere Length by G-Quadruplex Telomere DNA- and TERRA-Binding Protein TLS/FUS. Chemistry & Biology *20*, 341–350.

Takeda, T., Uchihara, T., Mochizuki, Y., Mizutani, T., and Iwata, M. (2007). Memory deficits in amyotrophic lateral sclerosis patients with dementia and degeneration of the perforant pathway: A clinicopathological study. Journal of the Neurological Sciences *260*, 225–230.

Takeda, T., Uchihara, T., Arai, N., Mizutani, T., and Iwata, M. (2008). Progression of hippocampal degeneration in amyotrophic lateral sclerosis with or without memory impairment: distinction from Alzheimer disease. Acta Neuropathol *117*, 35.

Tan, A.Y., Riley, T.R., Coady, T., Bussemaker, H.J., and Manley, J.L. (2012). TLS/FUS (translocated in liposarcoma/fused in sarcoma) regulates target gene transcription via single-stranded DNA response elements. PNAS *109*, 6030–6035.

Tang, G.-B., Zeng, Y.-Q., Liu, P.-P., Mi, T.-W., Zhang, S.-F., Dai, S.-K., Tang, Q.-Y., Yang, L., Xu, Y.-J., Yan, H.-L., et al. (2017). The Histone H3K27 Demethylase UTX Regulates Synaptic Plasticity and Cognitive Behaviors in Mice. Frontiers in Molecular Neuroscience *10*, 267.

Teixeira, C.M., Pomedli, S.R., Maei, H.R., Kee, N., and Frankland, P.W. (2006). Involvement of the Anterior Cingulate Cortex in the Expression of Remote Spatial Memory. J. Neurosci. *26*, 7555–7564.

Terryn, J., Verfaillie, C.M., and Van Damme, P. (2021). Tweaking Progranulin Expression: Therapeutic Avenues and Opportunities. Frontiers in Molecular Neuroscience *14*, 157.

Thompson, P.R., Wang, D., Wang, L., Fulco, M., Pediconi, N., Zhang, D., An, W., Ge, Q., Roeder, R.G., Wong, J., et al. (2004). Regulation of the p300 HAT domain via a novel activation loop. Nat Struct Mol Biol *11*, 308–315.

Tian, X., Zhang, S., Liu, H.-M., Zhang, Y.-B., Blair, C.A., Mercola, D., Sassone-Corsi, P., and Zi, X. (2013). Histone Lysine-Specific Methyltransferases and Demethylases in Carcinogenesis: New Targets for Cancer Therapy and Prevention. Curr Cancer Drug Targets *13*, 558–579.

Tibshirani, M., Tradewell, M.L., Mattina, K.R., Minotti, S., Yang, W., Zhou, H., Strong, M.J., Hayward, L.J., and Durham, H.D. (2015). Cytoplasmic sequestration of FUS/TLS associated with ALS alters histone marks through loss of nuclear protein arginine methyltransferase 1. Hum Mol Genet *24*, 773–786.

Tonegawa, S., Morrissey, M.D., and Kitamura, T. (2018). The role of engram cells in the systems consolidation of memory. Nat Rev Neurosci *19*, 485–498.

Tong, L., Balazs, R., Thornton, P.L., and Cotman, C.W. (2004). β-Amyloid Peptide at Sublethal Concentrations Downregulates Brain-Derived Neurotrophic Factor Functions in Cultured Cortical Neurons. J. Neurosci. *24*, 6799–6809.

Tradewell, M.L., Yu, Z., Tibshirani, M., Boulanger, M.-C., Durham, H.D., and Richard, S. (2012). Arginine methylation by PRMT1 regulates nuclear-cytoplasmic localization and toxicity of FUS/TLS harbouring ALS-linked mutations. Hum Mol Genet *21*, 136–149.

Trojer, P., and Reinberg, D. (2007). Facultative Heterochromatin: Is There a Distinctive Molecular Signature? Molecular Cell *28*, 1–13.

Tsai, K.-J., Yang, C.-H., Fang, Y.-H., Cho, K.-H., Chien, W.-L., Wang, W.-T., Wu, T.-W., Lin, C.-P., Fu, W.-M., and Shen, C.-K.J. (2010). Elevated expression of TDP-43 in the forebrain of mice is sufficient to cause neurological and pathological phenotypes mimicking FTLD-U. Journal of Experimental Medicine *207*, 1661–1673.

Tsai, Y.-L., Coady, T.H., Lu, L., Zheng, D., Alland, I., Tian, B., Shneider, N.A., and Manley, J.L. (2020). ALS/FTD-associated protein FUS induces mitochondrial dysfunction by preferentially sequestering respiratory chain complex mRNAs. Genes Dev *34*, 785–805.

Turner, M.R., Al-Chalabi, A., Chio, A., Hardiman, O., Kiernan, M.C., Rohrer, J.D., Rowe, J., Seeley, W., and Talbot, K. (2017). Genetic screening in sporadic ALS and FTD. J Neurol Neurosurg Psychiatry *88*, 1042–1044.

Tyzack, G.E., Luisier, R., Taha, D.M., Neeves, J., Modic, M., Mitchell, J.S., Meyer, I., Greensmith, L., Newcombe, J., Ule, J., et al. (2019). Widespread FUS mislocalization is a molecular hallmark of amyotrophic lateral sclerosis. Brain *142*, 2572–2580.

U

Udagawa, T., Fujioka, Y., Tanaka, M., Honda, D., Yokoi, S., Riku, Y., Ibi, D., Nagai, T., Yamada, K., Watanabe, H., et al. (2015). FUS regulates AMPA receptor function and FTLD/ALS-associated behaviour via GluA1 mRNA stabilization. Nat Commun *6*, 1–13.

Urwin, H., Josephs, K.A., Rohrer, J.D., Mackenzie, I.R., Neumann, M., Authier, A., Seelaar, H., Van Swieten, J.C., Brown, J.M., Johannsen, P., et al. (2010). FUS pathology defines the majority of tau- and TDP-43-negative frontotemporal lobar degeneration. Acta Neuropathol *120*, 33–41.

Usman, U., Choi, C., Camicioli, R., Seres, P., Lynch, M., Sekhon, R., Johnston, W., and Kalra, S. (2011). Mesial Prefrontal Cortex Degeneration in Amyotrophic Lateral Sclerosis: A High-Field Proton MR Spectroscopy Study. American Journal of Neuroradiology *32*, 1677–1680.

V

Van Deerlin, V.M., Leverenz, J.B., Bekris, L.M., Bird, T.D., Yuan, W., Elman, L.B., Clay, D., Wood, E.M., Chen-Plotkin, A.S., Martinez-Lage, M., et al. (2008). TARDBP mutations in amyotrophic lateral sclerosis with TDP-43 neuropathology: a genetic and histopathological analysis. Lancet Neurol *7*, 409–416.

Vance, C., Rogelj, B., Hortobágyi, T., Vos, K.J.D., Nishimura, A.L., Sreedharan, J., Hu, X., Smith, B., Ruddy, D., Wright, P., et al. (2009). Mutations in FUS, an RNA Processing Protein, Cause Familial Amyotrophic Lateral Sclerosis Type 6. Science *323*, 1208–1211.

Vance, C., Scotter, E.L., Nishimura, A.L., Troakes, C., Mitchell, J.C., Kathe, C., Urwin, H., Manser, C., Miller, C.C., Hortobágyi, T., et al. (2013). ALS mutant FUS disrupts nuclear

localization and sequesters wild-type FUS within cytoplasmic stress granules. Hum Mol Genet *22*, 2676–2688.

Vashishtha, M., Ng, C.W., Yildirim, F., Gipson, T.A., Kratter, I.H., Bodai, L., Song, W., Lau, A., Labadorf, A., Vogel-Ciernia, A., et al. (2013). Targeting H3K4 trimethylation in Huntington disease. PNAS *110*, E3027–E3036.

Vertes, R.P. (2004). Differential projections of the infralimbic and prelimbic cortex in the rat. Synapse *51*, 32–58.

Vorobyov, V., Deev, A., Sengpiel, F., Nebogatikov, V., and Ustyugov, A.A. (2021). Cortical and Striatal Electroencephalograms and Apomorphine Effects in the FUS Mouse Model of Amyotrophic Lateral Sclerosis. J Alzheimers Dis *81*, 1429–1443.

W

Wang, H., and Hegde, M.L. (2020). Molecular Basis of DNA Repair Defects in FUS-Associated ALS: Implications of a New Paradigm and Its Potential as Therapeutic Target (IntechOpen).

Wang, H., Guo, W., Mitra, J., Hegde, P.M., Vandoorne, T., Eckelmann, B.J., Mitra, S., Tomkinson, A.E., Bosch, L.V.D., and Hegde, M.L. (2018). Mutant FUS causes DNA ligation defects to inhibit oxidative damage repair in Amyotrophic Lateral Sclerosis. Nat Commun *9*, 1–18.

Wang, W.-H., Cheng, L.-C., Pan, F.-Y., Xue, B., Wang, D.-Y., Chen, Z., and Li, C.-J. (2011). Intracellular Trafficking of Histone Deacetylase 4 Regulates Long-Term Memory Formation. The Anatomical Record *294*, 1025–1034.

Wang, W.-Y., Pan, L., Su, S.C., Quinn, E.J., Sasaki, M., Jimenez, J.C., Mackenzie, I.R.A., Huang, E.J., and Tsai, L.-H. (2013). Interaction of FUS and HDAC1 regulates DNA damage response and repair in neurons. Nature Neuroscience *16*, 1383–1391.

Wang, X., Arai, S., Song, X., Reichart, D., Du, K., Pascual, G., Tempst, P., Rosenfeld, M.G., Glass, C.K., and Kurokawa, R. (2008a). Induced ncRNAs allosterically modify RNA-binding proteins in cis to inhibit transcription. Nature *454*, 126–130.

Wang, X., Schwartz, J.C., and Cech, T.R. (2015). Nucleic acid-binding specificity of human FUS protein. Nucleic Acids Res *43*, 7535–7543.

Wang, X.-L., Kooijman, S., Gao, Y., Tzeplaeff, L., Cosquer, B., Milanova, I., Wolff, S.E.C., Korpel, N., Champy, M.-F., Petit-Demoulière, B., et al. (2021). Microglia-specific knock-down of Bmal1 improves memory and protects mice from high fat diet-induced obesity. Mol Psychiatry.

Wang, Z., Zang, C., Rosenfeld, J.A., Schones, D.E., Barski, A., Cuddapah, S., Cui, K., Roh, T.-Y., Peng, W., Zhang, M.Q., et al. (2008b). Combinatorial patterns of histone acetylations and methylations in the human genome. Nat Genet *40*, 897–903.

Wang, Z., Zang, C., Cui, K., Schones, D.E., Barski, A., Peng, W., and Zhao, K. (2009). Genome-wide mapping of HATs and HDACs reveals distinct functions in active and inactive genes. Cell *138*, 1019–1031.

Ward, C.L., Boggio, K.J., Johnson, B.N., Boyd, J.B., Douthwright, S., Shaffer, S.A., Landers, J.E., Glicksman, M.A., and Bosco, D.A. (2014). A loss of FUS/TLS function leads to impaired cellular proliferation. Cell Death & Disease *5*, e1572.

Wheeler, D.W., White, C.M., Rees, C.L., Komendantov, A.O., Hamilton, D.J., and Ascoli, G.A. (2015). Hippocampome.org: a knowledge base of neuron types in the rodent hippocampus. ELife *4*, e09960.

Williams, K.L., Topp, S., Yang, S., Smith, B., Fifita, J.A., Warraich, S.T., Zhang, K.Y., Farrawell, N., Vance, C., Hu, X., et al. (2016). CCNF mutations in amyotrophic lateral sclerosis and frontotemporal dementia. Nat Commun *7*, 11253.

Wisman, L.A.B., Sahin, G., Maingay, M., Leanza, G., and Kirik, D. (2008). Functional Convergence of Dopaminergic and Cholinergic Input Is Critical for Hippocampus-Dependent Working Memory. J. Neurosci. *28*, 7797–7807.

Wood, M.A., Kaplan, M.P., Park, A., Blanchard, E.J., Oliveira, A.M.M., Lombardi, T.L., and Abel, T. (2005). Transgenic mice expressing a truncated form of CREB-binding protein (CBP) exhibit deficits in hippocampal synaptic plasticity and memory storage. Learn. Mem. *12*, 111–119.

Y

Yamashita, S., Mori, A., Sakaguchi, H., Suga, T., Ishihara, D., Ueda, A., Yamashita, T., Maeda, Y., Uchino, M., and Hirano, T. (2012). Sporadic juvenile amyotrophic lateral sclerosis caused by mutant FUS/TLS: possible association of mental retardation with this mutation. J. Neurol. *259*, 1039–1044.

Yan, J., Wang, H., Liu, Y., and Shao, C. (2008). Analysis of Gene Regulatory Networks in the Mammalian Circadian Rhythm. PLOS Computational Biology *4*, e1000193.

Yan, J., Deng, H.-X., Siddique, N., Fecto, F., Chen, W., Yang, Y., Liu, E., Donkervoort, S., Zheng, J.G., Shi, Y., et al. (2010). Frameshift and novel mutations in FUS in familial amyotrophic lateral sclerosis and ALS/dementia. Neurology *75*, 807–814.

Yang, L., Gal, J., Chen, J., and Zhu, H. (2014). Self-assembled FUS binds active chromatin and regulates gene transcription. PNAS *111*, 17809–17814.

Yap, E.-L., and Greenberg, M.E. (2018). Activity-Regulated Transcription: Bridging the Gap between Neural Activity and Behavior. Neuron *100*, 330–348.

Yasuda, K., Clatterbuck-Soper, S.F., Jackrel, M.E., Shorter, J., and Mili, S. (2017). FUS inclusions disrupt RNA localization by sequestering kinesin-1 and inhibiting microtubule detyrosination. J Cell Biol *216*, 1015–1034.

Young, J.C., Hoogenraad, N.J., and Hartl, F.U. (2003). Molecular chaperones Hsp90 and Hsp70 deliver preproteins to the mitochondrial import receptor Tom70. Cell *112*, 41–50.

Z

Zangenehpour, S., and Chaudhuri, A. (2002). Differential induction and decay curves of c-fos and zif268 revealed through dual activity maps. Molecular Brain Research *109*, 221–225.

Zhang, J., Ji, F., Liu, Y., Lei, X., Li, H., Ji, G., Yuan, Z., and Jiao, J. (2014). Ezh2 Regulates Adult Hippocampal Neurogenesis and Memory. J. Neurosci. *34*, 5184–5199.

Zhang, X., Wang, F., Hu, Y., Chen, R., Meng, D., Guo, L., Lv, H., Guan, J., and Jia, Y. (2020). In vivo stress granule misprocessing evidenced in a FUS knock-in ALS mouse model. Brain *143*, 1350–1367.

Zhou, Y., Liu, S., Liu, G., Öztürk, A., and Hicks, G.G. (2013). ALS-Associated FUS Mutations Result in Compromised FUS Alternative Splicing and Autoregulation. PLoS Genet *9*, e1003895.

Zhu, H., Belcher, M., and van der Harst, P. (2011). Healthy aging and disease: role for telomere biology? Clin Sci (Lond) *120*, 427–440.

Zhu, Y., Vidaurre, O.G., Adula, K.P., Kezunovic, N., Wentling, M., Huntley, G.W., and Casaccia, P. (2017). Subcellular Distribution of HDAC1 in Neurotoxic Conditions Is Dependent on Serine Phosphorylation. J. Neurosci. *37*, 7547–7559.

Zou, Z.-Y., Cui, L.-Y., Sun, Q., Li, X.-G., Liu, M.-S., Xu, Y., Zhou, Y., and Yang, X.-Z. (2013). De novo FUS gene mutations are associated with juvenile-onset sporadic amyotrophic lateral sclerosis in China. Neurobiology of Aging *34*, 1312.e1-1312.e8.

Zou, Z.-Y., Zhou, Z.-R., Che, C.-H., Liu, C.-Y., He, R.-L., and Huang, H.-P. (2017). Genetic epidemiology of amyotrophic lateral sclerosis: a systematic review and meta-analysis. J Neurol Neurosurg Psychiatry *88*, 540–549.

VERSION FRANCAISE

(Extraits choisis)

AVANT PROPOS

Les travaux de cette thèse sont focalisés sur le rôle de la protéine Fused in sarcoma (FUS) et son implication dans les déficits de mémoire, ainsi que les altérations transcriptomiques et épigénomiques associées, dans le contexte de deux maladies neurodégénératives : La sclérose latérale amyotrophique (SLA) et la démence frontotemporale (DFT).

La SLA est caractérisée par la mort prédominante des neurones moteurs supérieurs dans le cortex moteur et des neurones moteurs inférieurs dans la moelle épinière. Ces patients présentent une faiblesse musculaire progressive qui aboutit fréquemment à une insuffisance respiratoire et provoque le décès des patients dans les 2 à 5 ans suivant l'apparition des symptômes. La DFT est la deuxième démence précoce la plus fréquente après la maladie d'Alzheimer. Les patients présentent une atrophie corticale et une mort neuronale prédominantes dans le cortex frontal et temporal, accompagnées de troubles comportementaux et du langage. Malgré leurs différences au niveau symptomatique, la SLA et la DFT font partie du même spectre en raison de leurs caractéristiques communes en matière de neuropathologie et de causes génétiques. Parmi tous les patients atteints de DFT et de SLA, environ 30 % présentent simultanément (1) un déficit moteur et (2) une déficience cognitive ou des critères de démence. Ces patients sont mal caractérisés dans la littérature et sont généralement associés à une aggravation de la progression de la maladie et à une durée de vie plus courte.

Plusieurs mutations se trouvant dans le gène codant pour la protéine de liaison à l'ADN/ARN Fused in sarcoma (FUS) ont été associées à l'apparition précoce et à des cas graves de SLA familiale (5 %) et à un petit nombre de cas sporadiques (1 %). Chez ces patients, la protéine FUS, qui est nucléaire en conditions physiologiques, est mal localisée et se retrouve sous forme agrégée dans le cytoplasme. Une telle anomalie de FUS est également observée dans des cas de SLA sans mutation, ainsi que dans des cas sporadiques de DFT (10%).

La protéine FUS est impliquée dans toutes les étapes de l'expression génétique, y compris la transcription, l'épissage alternatif et le transport de l'ARNm. FUS a également été associé aux voies de réparation des lésions de l'ADN, aux modifications épigénétiques et à plusieurs fonctions

neuronales et synaptiques. Cependant, la manière dont les mutations de FUS affectent ces voies nucléaires reste largement méconnue.

Ce manuscrit est composé d'une introduction qui vise à présenter les concepts majeurs sur lesquels repose ma thèse. Tout d'abord, j'ai commencé par introduire les concepts d'apprentissage et de la mémoire, puis j'ai présenté les modifications épigénétiques post-traductionnelles des histones et leur rôle dans le processus de mémoire. Pour continuer, j'ai décrit la SLA et la DFT et me suis concentré sur les patients FUS au sein de la SLA et de la DFT avant de donner une introduction complète sur les fonctions physiologiques de la protéine FUS. Enfin, en deux parties indépendantes, j'ai présenté les altérations comportementales observées dans les différents modèles de souris liées à FUS et les altérations épigénétiques associées aux dysfonctionnements de FUS. La section d'introduction sera suivie des objectifs de ma thèse et de mes contributions scientifiques présentées sous forme de deux articles en préparations. Comme aucune de nos études n'a encore été publiée, j'ai ensuite discuté de la signification de nos résultats dans une discussion générale. La première partie de la discussion est principalement axée sur la caractérisation des altérations comportementales observées dans notre modèle de souris (principalement la discussion de la contribution scientifique 2). La deuxième partie vise à exposer les mécanismes potentiels qui sous-tendent les altérations moléculaires et comportementales en présence de la mutation FUS (principalement la discussion de la contribution scientifique 1). Dans la troisième et dernière partie, je discute de la validité de notre modèle dans le spectre SLA-DFT et de l'implication de nos résultats en termes d'approches thérapeutiques existantes visant particulièrement l’épigénétiques.

Au cours de ma thèse, j'ai eu la chance de collaborer à un autre article qui montre que la mauvaise localisation de FUS est suffisante pour induire des défauts synaptiques corticaux qui pourraient conduire à des symptômes similaires à ceux de la DFT dans notre modèle de souris (Scekic-Zahirovic et al., 2021). J'ai également participé à la rédaction d'un commentaire qui discute de l'effet négatif potentiel du traitement via des inhibiteurs d'HDAC dans le contexte de la SLA (Boutillier et al., 2019). Ces deux études sont discutées dans la partie discussion et sont disponibles dans la section annexe. La section Annexe comprend également deux articles publiés auxquels j'ai participé le long de ma thèse. Les informations détaillées sur ma contribution dans ces articles sont exposées au début de la section Annexe.

OBJECTIFS DE LA THESE

La mauvaise localisation cytoplasmique de FUS est liée à la sclérose latérale amyotrophique (SLA) et à la démence frontotemporale (DFT). Parmi ses multiples rôles physiologiques, FUS est impliqué dans l'expression des gènes, les modifications épigénétiques et les fonctions synaptiques. Nous avons émis l'hypothèse que la mauvaise localisation de FUS dans la SLA/DFT influencerait les régulations épigénétiques et la transcription associée, impactant finalement les fonctions neuronales et les capacités cognitives. Au cours des 4 années de ma thèse, nous avons particulièrement abordé ces questions dans l'hippocampe, une région cérébrale clé impliquée dans la mémoire.

Nous avons réalisé nos études sur des souris *Fus*$^{\Delta NLS/+}$, un modèle de souris knock-in portant une mutation troncatoire de FUS, développé au laboratoire de Mr Dupuis. L'utilisation d'un modèle de souris présentant une copie unique de la mutation est similaire à la situation génétique des patients SLA-FUS. En outre, les souris *Fus*$^{\Delta NLS/+}$ présentent une mauvaise localisation cytoplasmique de la protéine FUS, comme cela est observé chez les patients atteints de SLA et de DFT.

Pour comprendre les altérations présentent au sein de l'hippocampe dans le cadre des pathologiques liées à FUS et la relation de cette protéine avec les processus de mémoire, les travaux de thèse ont été déclinés en quatre objectifs :

1) Quelle est l'étendue des déficits cognitifs chez les souris *Fus*$^{\Delta NLS/+}$?

2) Les informations transcriptomiques (en conditions basales ou pendant la formation de la mémoire) et épigénomiques (en conditions basales) sont-elles altérées dans l'hippocampe des souris *Fus*$^{\Delta NLS/+}$?

3) Où FUS se fixe-t-il sur le génome ? La mutation de FUS a-t-elle un impact sur la liaison de FUS à la chromatine chez les souris Fus$^{\Delta NLS/+}$?

4) Les altérations épigénomiques sont-elles associées à des changements d'accessibilité de la chromatine ?

Mes contributions scientifiques sont détaillées en deux grandes sections qui sont présentées dans les pages suivantes en tant que deux articles en préparations. Notre étude principale, présentée ci-après comme la contribution scientifique 1 en préparation, vise à caractériser les altérations hippocampiques et les changements épigénétiques et transcriptomiques associés observés chez les souris *Fus*$^{\Delta NLS/+}$. Pour ce faire, nous avons utilisé plusieurs techniques de séquençage de nouvelle génération (RNA-seq, ChIP-seq et ATAC-seq) et nous avons réalisé des analyses épigénomiques et de régions chromatiniennes ouvertes spécifiquement dans les noyaux neuronaux hippocampiques isolés par FACS. Ma deuxième contribution scientifique, vise à réaliser une analyse complète des altérations comportementales/cognitives présentes chez les souris Fus$^{\Delta NLS/+}$ et à mieux caractériser le modèle. Dans cet article, nous avons testé l'activité locomotrice, l'anxiété, la flexibilité cognitive mais aussi différents aspects de la mémoire (ex : mémoire spatiale et mémoire procédurale), ainsi que différentes composantes de la mémoire de type épisodique (Quoi ? Où ? Quand ?).

I. Les analyses comportementales des souris *Fus*$^{\Delta NLS/+}$ révèlent une diminution globale de l'apprentissage et de la mémoire qui reflète des altérations dans différentes régions du cerveau et différents types de cellules.

L'article de Scekic-Zahirovic et collaborateurs auquel j'ai participé (voir Scekic-Zahirovic et al., 2021 dans "Annexes"), s'est concentré sur les altérations comportementales associées aux dysfonctionnements corticaux. Nous avons démontré une hyperactivité ainsi que des dysfonctionnements sociaux et exécutifs chez ces souris. Ces altérations étaient principalement liées à des défauts des neurones inhibiteurs dans le cortex frontal. Dans les études présentées ici, nous avons réalisé une caractérisation complète des fonctions cognitives chez les souris SLA/DFT *Fus*$^{\Delta NLS/+}$ à un stade précoce (4-5 mois). En nous concentrant sur les altérations de l'hippocampe dans le modèle de souris *Fus*$^{\Delta NLS/+}$, nous avons d'abord observé que les souris présentaient un retard des performances d'acquisition et des altérations de rétention de la mémoire dans le MWM, associé à une diminution des épines matures et à une altération de l'expression génique induite par l'apprentissage dans l'hippocampe (altérations glutamatergiques et GABAergiques) (voir contribution expérimentale 1). Dans une seconde étude, (voir contribution expérimentale 2), nous avons exploré plusieurs autres aspects liés à la mutation FUSΔNLS, notamment l'anxiété et la mémoire spatiale et procédurale. Nous avons également effectué des tests liés aux l'objets qui permettent d'investiguer divers aspects des composantes de la mémoire : « Quoi ? » « Où ?» et « Quand ?». Ainsi, nous avons confirmé des altérations hippocampiques et proposé des altérations plus étendues qui toucheraient différentes régions parahippocampiques et du striatum. En conclusion, même si les souris *Fus*$^{\Delta NLS/+}$ sont capables de réussir la plupart des tâches, elles démontrent une diminution globale de l'apprentissage et de la mémoire et sont même incapables d'associé les composantes du « quoi » et du « où » ainsi que de déterminer quel élément a été expérimenté en premier. Ainsi, notre modèle de souris met en évidence un dysfonctionnement généralisé dans plusieurs régions cérébrales, suggérant que l'on devrait se concentrer davantage sur ces régions cérébrales chez les patients atteints de SLA/DFT.

1) L'hyperactivité, un symptôme précoce de la DFT chez les souris *Fus*$^{\Delta NLS/+}$.

Nos études démontrent une hyperactivité chez les souris *Fus*$^{\Delta NLS/+}$ à l'âge de 3, 4 et 10 mois. Ces symptômes semblent encore plus marqués à l'âge précoce de 3 mois. Dans la littérature, la surexpression transgénique de FUS mutant entraîne également une hyperactivité (Shiihashi et al., 2017). Les symptômes d'hyperactivité sont également observés dans d'autres modèles murins de DFT tels que le modèle Tau (Jul et al., 2016) et un modèle *C9ORF72* (Chew et al., 2015), et pourraient refléter l'hyperactivité sans but observée dans la forme désinhibée des patients atteints de DFT comportementale (Neary et al., 2005 ; Snowden et al., 2011). Un comportement ritualiste/répétitif est également une caractéristique commune des patients atteints de la DFT-FUS qui présentent principalement la variante comportementale de la DFT (Snowden et al., 2011). Cette activité locomotrice accrue peut également être une conséquence de l'hyperexcitabilité corticale précoce observée chez les patients atteints de SLA (Geevasinga et al., 2016). Par conséquent, les études actuelles du laboratoire de Mr Dupuis analyse l'électrocorticographie chez les souris *Fus*$^{\Delta NLS/+}$. De manière intéressante, l'augmentation du phénotype locomoteur est également observée lorsque FUS est réduit par injection de shRNA dans l'hippocampe (Udagawa et al., 2015), ce qui indique une possible implication de l'hippocampe dans l'hyperactivité médiée par FUS. L'hyperactivité pourrait aussi être déclenchée par le dysfonctionnement du FUS dans des types cellulaires spécifiques, par exemple les oligodendrocytes (Guzman et al., 2020). Ceci est particulièrement important au vu du rôle émergent des cellules gliales dans la SLA et la DFT (Radford et al., 2015) et de la dérégulation des oligodendrocytes dans la moelle épinière de notre modèle de souris *Fus*$^{\Delta NLS/+}$ (Scekic-Zahirovic et al., 2017).

Dans notre étude, nous avons également démontré que les souris *Fus*$^{\Delta NLS/+}$ présentaient une diminution significative de leur poids par rapport à leurs congénères WT, ce qui pourrait être en lien avec l'augmentation de l'activité locomotrice. Une autre hypothèse serait une diminution de la prise alimentaire et/ou des altérations métaboliques chez les souris *Fus*$^{\Delta NLS/+}$. En effet, les patients atteints de SLA présentent des anomalies métaboliques (Joardar et al., 2017) et un complément alimentaire enrichi en lipides est associé à une augmentation de la survie chez les patients atteints de SLA à progression rapide (Ludolph et al., 2020).

2) Dysfonctionnement de l'hippocampe chez les souris *Fus*$^{\Delta NLS/+}$.

Dans la littérature, les patients atteints de DFT sont décrits comme ayant une mémoire épisodique et des compétences visuospatiales relativement épargnées (Liu et al., 2019). Cependant, notre étude a démontré que les souris *Fus*$^{\Delta NLS/+}$ présentent une altération de l'hippocampe. Nous avons observé une acquisition diminuée dans le test spatial du MWM dans deux cohortes indépendantes de souris à l'âge de 5 mois. Nous avons également confirmé une altération de la mémoire à deux âges différents (5 et 10 mois), à deux moments différents de l'acquisition de l'apprentissage (3 ou 4 jours) et durant des étapes de consolidation différentes (Mémoire à long terme (MLT) récente et éloigné). Nous avons ainsi démontré que autant l'acquisition que la MLT récente et éloigné étaient réduites chez les souris *Fus*$^{\Delta NLS/+}$. D'autres modèles de souris SLA/DFT, mimant par exemple la pathologie TDP43, démontrent des altérations spatiales (Swarup et al., 2011 ; Tsai et al., 2010). De même, un modèle exprimant le mutant humain FUS présente des altérations spatiales dans le labyrinthe de Barnes et le MWM (Ho et al., 2021 ; Huang et al., 2012). Les altérations hippocampiques sont également détaillées dans plusieurs études effectuées sur des souris exprimant une forme mutant de FUS humain (Shiihashi et al., 2017 ; López-Erauskin et al., 2018 ; Ho et al., 2019 ; Sahadevan et al., 2021). De plus, nos analyses ont démontré une diminution de la morphologie des épines matures dans la région hippocampique CA1 des souris *Fus*$^{\Delta NLS/+}$ et une expression génique glutamatergique et GABAergique anormale induite par l'apprentissage. De manière intéressante, dans le MWM, indépendamment du temps de rappel de la mémoire, nous avons observé une diminution de la capacité des souris *Fus*$^{\Delta NLS/+}$ à localiser précisément la plateforme. Dans la littérature, l'altération de la neurogenèse a été décrite comme responsable du manque de précision (Clelland et al., 2009 ; Garthe et al., 2009). Dans la littérature, l'altération de la neurogenèse n'a été décrite que chez les souris présentant une diminution de la protéine FUS (Ishigaki et al., 2017). Il n'est cependant pas connu quelle serait l'implication de la mutation de FUS dans ce processus. Pour répondre à cette question, nous analysons actuellement la prolifération et la survie des neurones chez les souris *Fus*$^{\Delta NLS/+}$ après injection de BrdU.

Alors que l'atrophie du cortex temporal est un aspect caractérisé des patients FTD, seules quelques études se sont concentrées sur l'altération de l'hippocampe chez les patients atteint de SLA (Christidi et al., 2019 ; Stoppel et al., 2014 ; Takeda et al., 2008). A la lumière de nos résultats,

nous proposons que les analyses de l'hippocampe pourraient être critiques dans le contexte de la maladie SLA-DTF, notamment dans le contexte particulier de FUS où la littérature est encore plus absente.

3) Et qu'en est-il du réseau para-hippocampique chez les souris *Fus*$^{\Delta NLS/+}$?

Nos études ont également évalué des tests liés aux objets afin d'examiner divers aspects des composantes de la mémoire " Quoi, Où et Quand ". La plupart des précédents modèles de souris exprimant FUS humain ont démontré une altération de la reconnaissance d'un nouvel objet (Ho et al., 2021 ; López-Erauskin et al., 2018 ; Munter et al., 2020). Des résultats similaires ont été observés dans d'autres modèles de souris SLA et/ou DFT, comme dans les modèles de souris TDP43 (Alfieri et al., 2016 ; Rodriguez-Ortiz et al., 2013 ; Tsai et al., 2010). Nous avons démontré ici que l'expression du mutant murin FUSΔNLS est associée à une légère diminution de la reconnaissance de nouveaux objets ainsi que de la localisation d'objets. Cependant, même avec une performance diminuée, les souris *Fus*$^{\Delta NLS/+}$ sont parfaitement capables de discriminer un objet nouveau ou déplacé. En revanche, nous avons démontré l'incapacité des souris *Fus*$^{\Delta NLS/+}$ à associer les informations de l'objet « Quoi ? » et du lieu « Où ? » ou à déterminer quel élément a été expérimenté en premier, révélant ainsi une légère altération des réseaux cérébraux "Quoi" et "Où" indépendamment et une déficience prédominante des réseaux cérébraux " Quoi et Où" et "Quoi et Quand". Dans la littérature, chaque composante de la mémoire peut être associée à des interactions entre différentes régions du cerveau et différents réseaux cérébraux.
Le succès du NOR, qui teste la composante "Quoi", est associé au cortex périrhinal (identité de l'objet), au cortex entorhinal latéral et au mPFC pour le rappel de la mémoire de 24 heures (Akirav et Maroun, 2006). Les régions cérébrales associées à la capacité de localiser les objets dans la tâche OL sont en partie l'hippocampe (Barker et Warburton, 2011 ; Oliveira et al., 2010), le subiculum et le cortex entorhinal médian (lié au contexte). La tâche OIP, qui teste la mémoire associative objet-emplacement et l'association de l'identité ("Quoi") et de l'emplacement ("Où") d'un objet, repose sur le cortex entorhinal. La tâche TOM, qui teste l'ordre dans lequel les objets ont été présentés, s'est avérée dépendre de l'hippocampe (Barker et Warburton, 2011), du cortex périrhinal et du cortex mPFC (Barker et Warburton, 2011). Pour plus d'informations, voir le chapitre "The Value of the Object Recognition Paradigm in Investigating Animal Models of

Alzheimer's Disease: Advances and Future Directions" dans Handbook of Behavioral Neuroscience (Mathis, 2018).

Ainsi, notre recherche amène une preuve supplémentaire concernant les altérations du réseau hippocampique chez les souris *Fus*$^{\Delta NLS/+}$. Cependant, nous proposons ici que la mutation de FUS puisse également avoir un impact plus étendu sur les régions parahippocampiques.

4) Altérations corticales chez les souris *Fus*$^{\Delta NLS/+}$.

Les modules corticaux, et en particulier le mPFC, sont étroitement liés à la mémoire à long terme (MLT), (Bicks et al., 2015 ; Frankland et Bontempi, 2005 ; Tonegawa et al., 2018). Dans le MWM, notre modèle de souris démontre une diminution de la rétention de la MLT à la fois pour le temps récent (24 heures) et éloigné (30 jours). De plus, même si les souris *Fus*$^{\Delta NLS/+}$ sont capables de discriminer un nouvel objet dans le NOR, elles montrent une légère diminution par rapport à leurs congénères WT, y compris dans la MLT récente de 24 heures. De manière intéressante, une étude précédente de Scekic-Zahirovic et al. de 2021, à laquelle j'ai participé, a mis en évidence une anomalie du comportement social à 4, 10 et 22 mois et une diminution de la consolidation de la MLT éloigné à l'âge de 10 mois chez les souris *Fus*$^{\Delta NLS/+}$, reflétant toutes deux des altérations du cortex frontal (Scekic-Zahirovic et al., 2021).

Des modifications du comportement social ont également été observées dans d'autres modèles de souris exprimant FUS mutant humain (López-Erauskin et al., 2018 ; Lysikova et al., 2019 ; Sephton et al., 2014) ou dans un modèle de souris C9ORF72 (Jiang et al., 2016) et CHMP2B SLA et/ou DFT (Gascon et al., 2014). Ces résultats sont en accord avec la désinhibition sociale présente dans la forme désinhibée des patients de type DFT comportementale où une atrophie prédominante du lobe orbitofrontal-temporal est observée (Snowden, 2001 ; Neary et al., 2005). Dans le cas particulier de la DFT-FUS, on observe également un déclin précoce du comportement social (Roeber et al., 2008).

Concernant l'altération de la consolidation de la mémoire, plusieurs autres études sur des souris exprimant FUS humain démontrent une altération de la mémoire lors de conditionnement à la peur (Shiihashi et al., 2017 ; López-Erauskin et al., 2018 ; Ho et al., 2019, 2021) et une altération

de la reconnaissance d'un nouvel animal (Shiihashi et al., 2017) ou objet (López-Erauskin et al., 2018 ; Munter et al., 2020 ; Ho et al., 2021). De telles altérations de la mémoire sont également observées dans d'autres modèles de souris de DFT, par exemple en surexprimant une forme sauvage de TDP-43 (Alfieri et al., 2016), en surexprimant la protéine Tau mutante humaine (Chatterjee et al., 2018) ou en exprimant VCP mutant humain (Rodriguez-Ortiz et al., 2013). Dans la littérature, les patients atteints de DFT démontrent des dysfonctionnements exécutifs avec des difficultés de planification, de maintien d'une attention soutenue, de la mémorisation des instructions et de la gestion de tâches multiples, dépendant du cortex frontal mais avec une préservation relative de la mémoire épisodique et des compétences visuospatiales (Liu et al., 2019). Un dysfonctionnement de l'attention et de la mémoire est également observé chez les patients présentant une neuropathologie de type DFT-FUS (Roeber et al., 2008). Ceci est en accord avec notre modèle puisque les souris *Fus*$^{\Delta NLS/+}$ sont capables de se souvenir de l'emplacement de la plateforme dans le MWM mais démontrent une réduction significative de cette mémoire par rapport aux souris sauvages. Des altérations corticales et des troubles cognitifs sont également décrits chez les patients atteints de SLA pure et de SLA-DFT (Mantovan et al., 2003 ; Rippon et al., 2006 ; Usman et al., 2011). Ainsi, des altérations corticales sont observées à la fois chez les patients atteints de SLA et de DFT et sont présentes chez les souris *Fus*$^{\Delta NLS/+}$.

L'altération de la rétention de la MLT et l'altération sociale chez les souris *Fus*$^{\Delta NLS/+}$, ont été proposées comme étant le résultat d'un défaut synaptique, en partie dû aux synapses inhibitrices (Sahadevan et al., 2021 ; Scekic-Zahirovic et al., 2021). L'expression d'un mutant humain FUS dans différents modèles murins est en effet associée à une diminution de la ramification dendritique et des épines dans le cortex (Sephton et al., 2014 ; Shiihashi et al., 2017). Cependant, il n'y a pas d'étude concernant l'altération spécifique des neurones inhibiteurs dans le modèle FUS ALS-FTD.

5) Les souris *Fus*$^{\Delta NLS/+}$ présentent des altérations striatales en accord avec la maladie FTD-FUS.

Pour finir, nous nous sommes intéressés au rôle du FUS dans la mémoire procédurale (savoir comment/apprentissage des habitudes) en utilisant le paradigme du double H (Kirch et al., 2015). Nous avons démontré que les souris *Fus*$^{\Delta NLS/+}$ ont une acquisition retardée dans le double H. Cependant, après 5 jours, les souris *Fus*$^{\Delta NLS/+}$ ont des performances similaires à celles de leurs

congénères sauvages et elles ne présentent pas d'altération de la mémoire procédurale. Nous avons donc conclu que la mutation de FUS peut induire un apprentissage procédural plus lent qui peut être compensé par un surentraînement des souris. L'apprentissage procédural dépend principalement du striatum (Packard et Knowlton, 2002). Cette structure est mal caractérisée dans les différents modèles de souris SLA/DFT. Néanmoins, une expression des gènes perturbée dans le striatum est observée dans un modèle de souris knockout FUS (Kino et al., 2015), ce qui suggère que FUS jouerait également un rôle dans le striatum. Comme indication supplémentaire de l'altération striatale dans la maladie SLA/DFT, des souris exprimant la protéine FUS humaine tronquée ont montré un spectre EEG altéré dans le striatum dès l'âge de 2 et 5 mois (Vorobyov et al., 2021). Il est intéressant de noter que l'atrophie striatale est une caractéristique des patients atteints de la DFT-FUS (Josephs et al., 2010) principalement associée à la forme stéréotypée des formes comportementales de la DFT (Snowden et al., 2011).

Dans l'ensemble, nos différentes études ont proposé une altération cérébrale plus répandue dans le spectre de la SLA-DFT que celle décrite précédemment. Nous avons observé des dysfonctionnements corticaux, hippocampiques, parahippocampiques et du striatum, probablement dus à une altération de la fonction des différents types de cellules neuronales et gliales. De plus, les altérations cognitives sont présentes à un âge précoce dans notre modèle de souris *Fus*$^{\Delta NLS/+}$ et sont présentes bien avant les symptômes moteurs de la SLA (Scekic-Zahirovic et al., 2017, 2021). Le laboratoire de Mr Dupuis travaille actuellement sur un nouveau modèle de souris conditionnel exprimant la mutation *Fus*ΔNLS uniquement à l'âge adulte. Ce modèle permettra de mieux comprendre l'implication du dysfonctionnement de FUS dans les neurones des patients porteurs d'une mutation génétique (avec implication développementale de FUS) vs les patients développant des FUSopathies sporadiques ne présentant aucune mutation du gène FUS. Nous pensons qu'une caractérisation et une étude plus approfondies de l'implication du FUS mutant dans les différentes régions du cerveau et les différents types de cellules pourraient aider à identifier des changements précoces et ainsi identifier des markers moléculaires dans le contexte de la SLA-DFT.

II. Mécanismes potentiels à l'origine des altérations **moléculaires et comportementales chez les souris FUS$^{\Delta NLS/+}$.**

Dans la présente étude, nous avons démontré un retard des performances d'acquisition et une altération de la rétention de la mémoire dépendante de l'hippocampe chez les souris porteuses de la mutation hétérozygote *Fus*$^{\Delta NLS}$. Nous avons en outre montré que ces altérations comportementales s'accompagnaient de dérégulations structurelles (épines en champignon) et transcriptionnelles dans la région hippocampique. Les souris *Fus*$^{\Delta NLS/+}$ et leurs congénères sauvages présentent en effet une expression génique différentielle au cours du processus de consolidation de la mémoire. Malgré peu de changements d'expression génique dans la condition HC, nous avons observé que la chromatine présente déjà de nombreuses altérations épigénomiques. Nous avons observé un enrichissement accru des marques actives (H3K4me3, H4K12ac et H3K27ac) et un enrichissement réduit de la marque répressive H3K27me3 dans les neurones isolés de l'hippocampe. Les différents groupes de HMEG (Histone Mark-Enriched Genes) montrent une augmentation discrète de leur expression, suggérant que la mutation FUSΔNLS a un impact à la fois sur la conformation de la chromatine et sur l'expression des gènes. De manière importante, nous avons également identifié les potentiels gènes cibles de FUS par des analyses ChIP-seq. FUS est principalement liés aux gènes du ribosome mitochondrial et révélé une liaison préférentielle aux niveau des motifs de la famille ETS (GGAA). En parallèle, nous avons démontré que la liaison à l'ADN de plusieurs facteurs de transcription était altérée dans l'hippocampe des souris *Fus*$^{\Delta NLS/+}$ parmi lesquels les membres ETS Elk1 et Elk3 sont affectés. Ainsi, nos données montrent que la mutation *Fus*$^{\Delta NLS}$ influence l'organisation de la chromatine, en particulier celle de la chromatine active, avec un impact significatif sur le transcriptome induit par l'apprentissage et d'autres altérations comportementales par une mécanistique qui pourrait être dépendante de la famille des facteurs de transcription ETS.

1) Les effets de la mutation du FUS se produisent-ils par un mécanisme direct de FUS dans le noyau ?

Notre étude démontre que malgré la troncation du domaine NLS, la protéines FUS$^{\Delta NLS}$ est retrouvée dans le noyau et représentent même 40-50% de la fraction totale de FUS nucléaire, sans changement significatif de la quantité totale de FUS nucléaire (Figure 5A-C). L'entrée du

mutant FUS$^{\Delta NLS}$ a déjà été décrite précédemment (Sanjuan-Ruiz et al., 2021) et il a été proposé qu'elle soit médiée par deux mécanismes différents. Premièrement, l'import nucléaire de FUS mutant peut être médiée par la protéine FUS WT elle-même, puisque FUS WT et mutants interagissent ensemble (Vance et al., 2013 ; Qiu et al., 2014). Deuxièmement, même si l'import nucléaire de FUS est principalement médiée par la région NLS, la région RGG seule est également capable d'interagir avec la transportine 1 (Dormann et al., 2010) et d'autres récepteurs d'importation nucléaire (Baade et al., 2021 ; Gonzalez et al., 2021). Étant donné que dans les cultures cellulaires, FUS se lie à l'ADN (Yang et al., 2014) et interagit avec RNApol II pour réguler la transcription des gènes (Schwartz et al., 2012), nous avons donc soupçonné que les interactions FUS-ADN pourraient être altérées si FUS mutant était présents dans le noyau. Notre étude ChIP-seq réalisée avec un anticorps capable de reconnaître la totalité des protéines FUS au niveau de leur domaine N-terminal montre que, quelle que soit la présence de protéines FUS WT et/ou ΔNLS, elles peuvent lier des régions génomiques identiques (Figure S9). A notre connaissance, notre étude ChIP-seq est la première à déchiffrer la distribution génomique précise de FUS dans les cellules du cerveau, plus précisément dans l'hippocampe. Nous avons constaté que FUS était principalement localisé au niveau des TSS des gènes, de manière similaire aux résultats obtenus par Schwartz et ses collaborateurs dans les cellules HEK293 (Schwartz et al., 2012). Cependant, alors qu'ils ont décrit une liaison généralisée de FUS sur le génome des cellules HEK293 (9731 gènes, représentant 68% des gènes exprimés), nous avons observé une liaison significative de FUS à 386 régions génomiques. Ces différences pourraient être dues à une fonction différente de FUS dans différents tissus/stades du développement ou expression postnatals (Blechingberg et al., 2012 ; Schoen et al., 2015). Le matériel de départ, qui était des cultures cellulaires pour Schwartz et al. (2012) et des tissus hippocampiques dans notre étude, peut également avoir été influencé différemment par l'étape de fixation protéine-ADN et/ou l'anticorps utilisé, et il est alors possible que notre immunoprécipitation de la chromatine n'ait capturé que les fragments d'ADN avec la plus grande quantité de FUS lié. Cependant, nous avons observé que plus de 90% des gènes cibles liés à FUS dans les cellules hippocampiques étaient similaires à ceux observés dans les cultures de cellules musculaires (C2C12), en utilisant la même technique et les mêmes anticorps (Picchiarelli et al, non publié). Ceci suggère un rôle commun du FUS dans les différents tissus.

En termes d'annotation fonctionnelle, ces gènes cibles de FUS ont été associés au métabolisme de l'ARN, à la traduction/ribosome et aux gènes liés aux mitochondries. Ces termes sont en accord avec les différentes fonctions de FUS. Le rôle de FUS dans le métabolisme de l'ARN, y compris la transcription, l'épissage, la polyadénylation, le traitement des miRNA et le transport de l'ARN est bien décrit dans l'introduction et dans plusieurs excellentes revues (Lagier-Tourenne et al., 2010 ; Ling et al., 2013 ; Birsa et al., 2020).

Plusieurs hypothèses peuvent expliquer les altérations génomiques induites par la mutation FUS et l'impact sur les processus d'apprentissage et de mémoire.

L'hypothèse des mitochondries. De manière intéressante, nous avons observé que FUS se lie à un grand nombre de gènes codant pour des protéines ribosomales mitochondriales (Mrpl et Mrps) (Fig. 5H). Ces protéines sont codées par le génome nucléaire, synthétisées dans le cytoplasme et transportées dans la mitochondrie pour être assemblées en ribosomes mitochondriaux. Les protéines Mrp traduisent 13 protéines codées par le génome mitochondrial qui jouent toutes un rôle indirect dans la chaîne respiratoire mitochondriale. Une expression anormale de Mrpl est associée à un trouble du métabolisme mitochondrial et à des dysfonctionnements cellulaires (Huang et al., 2020). Plus intéressant encore, FUS cible le gène Mrpl3, qui est lié aux maladies neurodégénératives et aux troubles de la mémoire dans un modèle de souris à mutation spontanée (Cahill et al., 2020). Ainsi, nous proposons que l'expression altérée des gènes cibles de FUS tels que les gènes Mrpl, ainsi que les gènes codant pour les enzymes du complexe I mitochondrial, pourrait directement conduire à une altération des fonctions mitochondriales et sous-tendre les déficits de mémoire des souris *Fus*$^{\Delta NLS/+}$ .En effet, les fonctions mitochondriales représentent des facteurs cruciaux pour la formation adéquate des épines dendritiques des neurones hippocampiques nouvellement formés au cours de la neurogenèse adulte (Arrázola et al., 2019 ; Richetin et al., 2017). La neurogenèse adulte est associée à la mémoire de précision hippocampique (Clelland et al., 2009 ; Garthe et al., 2009), qui est impactée chez nos souris *Fus*$^{\Delta NLS/+}$.

En accord avec cette hypothèse, le laboratoire de Mr Dupuis a observé une morphologie mitochondriale altérée dans les C2C12 exprimant moins de FUS par siRNA (Picchiarelli et al, non publié). Un autre modèle de souris FUS Knock In a démontré une altération de l'expression des gènes, principalement des gènes mitochondriaux, à un âge avancé (12 mois), alors qu'aucune

altération n'a été observée à un jeune âge (3 mois) (Devoy et al., 2017). A noter que 48 de nos gènes cibles de FUS sont en commun avec les gènes dérégulés chez ces souris âgées, dont certains gènes Mrp (Devoy et al., 2017). Dans la littérature, des formes anormales, des raccourcissements, des fragmentations et des dommages de la mitochondrie ont été observés lors de l'expression de FUS mutant humain dans des cultures de cellules neuronales (Deng et al., 2015 ; Tradewell et al., 2012), dans des jonctions neuro-musculaires pré- et postsynaptiques de souris exprimant FUS humain (Sharma et al., 2016) et dans des échantillons de cerveau FTLD-FUS (Deng et al., 2015). Deng et ses collaborateurs ont en outre proposé que l'anomalie mitochondriale pourrait être multifactorielle et que l'un des mécanisme pourrait impliquer la protéine chaperonne HSP60 et entraîner une translocation accrue de FUS dans les mitochondries. De manière intéressante, nos données Chip-seq FUS dans l'hippocampe démontrent la liaison de FUS sur le gène Hsp90, une autre protéine chaperonne impliquée dans la translocation des protéines vers les mitochondries (Young et al., 2003). De plus, les ARNm de Hsp90 interagissent également avec la protéine FUS mutante humaine (Tsai et al., 2020). Ainsi, nous pouvons spéculer que le FUS mutant pourrait modifier sa propre entrée dans la mitochondrie, ainsi que l'entrée d'autres protéines, par une régulation directe du gène et de l'ARNm Hsp90. D'autres implications de FUS mutant concernant les dysfonctionnements mitochondriaux dans le contexte de la SLA sont décrites dans ces revues (Smith et al., 2019 ; Birsa et al., 2020). Dans l'ensemble, notre Chip-seq FUS montre des preuves accrues d'un rôle direct du FUS mutant sur le processing de l'ARN et sur les dysfonctionnements mitochondriaux dans le spectre de la SLA-FTD.

L'hypothèse du " partenaire transcriptionnel " De manière surprenante, aucun changement significatif de la liaison de FUS à l'ADN n'a été identifié sur le génome des *Fus*$^{\Delta NLS/+}$. Ainsi, si FUS est correctement localisé sur le génome des souris *Fus*$^{\Delta NLS/+}$, comment pouvons-nous expliquer les altérations transcriptionnelles et comportementales dans notre modèle ? Nous avons constaté que les gènes liés à FUS étaient globalement plus exprimés dans l'hippocampe des souris *Fus*$^{\Delta NLS/+}$ que dans l'hippocampe des souris sauvages (Figure 5J). Cependant, un par un, aucun de ces gènes cibles n'a montré une up-régulation significative. Nous ne pouvons donc que spéculer sur un scénario possible impliqué dans les dérégulations induites par FUS. Il a été démontré que FUS se lie directement au domaine C-terminal de RNAPol2 et module la quantité de phosphorylation Ser2 présente près des TSS des gènes (Schwartz et al., 2012). L'effet de la

mutation FUS$^{\Delta NLS}$ sur ces interactions n'est pas connu dans notre modèle, mais une perte de fonction pourrait entraîner une hyperphosphorylation de la RNApol2 Ser2 au niveau des TSS des gènes liés et modifier leur taux de transcription. Ce qui se passe dans notre modèle n'est pas clair et devrait être complété par des ChIP-seq ciblés réalisés avec les différentes formes de Phospho-RNApol2. Il faut noter que le cluster 3 des gènes liés à FUS (faible liaison) était enrichi en gènes liés au complexe ARN polymérase II/ TFIIH, soulignant une régulation par FUS des gènes de la machinerie transcriptionnelle centrale. De telles altérations peuvent être en accord avec les niveaux inférieurs de transcription (en particulier ceux des IEG) mesurés après l'entraînement dans notre étude transcriptomique (Figure 2). Une autre hypothèse est que FUS est une protéine capable de médier la séparation de phase liquide-liquide (décrite dans l'introduction) et de créer un microenvironnement de manière réversible. Certains mutants de FUS ont des difficultés à inverser cette situation, ce qui entraîne un environnement moins dynamique (Murakami et al., 2015 ; Patel et al., 2015). Ainsi, si la formation des microenvironnements de FUS sont altérées dans notre modèle, cela pourrait influencer la façon dont FUS recrute et interagit avec l'appareil transcriptionnel pendant l'initiation de la transcription, ce qui modifierait davantage la transcription des gènes (Yang et al., 2014).

L'hypothèse Elk1/3. De manière frappante, les analyses des motifs liées aux promoteurs de nos données ChIP-seq de FUS ont démontré une liaison presque exclusive de FUS sur les motifs de la famille ETS (GGAA) (Figure 5I). De plus, nos données ATAC-seq ont mis en évidence une liaison altérée de plusieurs facteurs de transcription, parmi lesquels la liaison d'Elk1 et d'Elk3, membres de la famille ETS, était significativement réduite. Elk1, est fortement impliqué dans les processus d'apprentissage et de mémoire, voir la revue (Besnard et al., 2011). Une étude a rapporté que l'inhibition spécifique de la phosphorylation d'Elk1, et sa translocation nucléaire subséquente, était associée à un défaut dans l'expression des gènes induite par le glutamate, notamment des IEGs portant des sites SRE sur leurs promoteurs, comme c-fos ou junB (Lavaur et al., 2007). De manière intéressante, en conditions d'apprentissage, nos données RNA-seq ont démontré une expression réduite d'un groupe de gènes incluant les gènes précoces immédiats chez les souris *Fus*$^{\Delta NLS/+}$ par rapport à leurs congénères sauvages (voir par exemple l'expression de *Junb* sur la Figure 2E). Une diminution des membres nucléaires de la famille Elk dans les neurones hippocampiques FUS est également en accord avec nos données ATAC-seq montrant une diminution de la liaison aux loci génomiques Elk1/Elk3 (Figure 6A). En effet, si le FUS muté ΔNLS

pouvait se lier à Elk1/3 soit dans le cytoplasme soit dans le noyau, il pourrait directement empêcher la liaison correcte d'Elk1/3 à ses éléments réactifs dans les gènes liés à l'apprentissage et à la mémoire. Ainsi, l'altération des interactions entre FUS et Elk1/Elk3 ou d'autres membres de la famille ETS (et d'autres facteurs de transcription) pourrait constituer un mécanisme potentiel sous-jacent aux modifications transcriptomiques et comportementales du modèle de souris *Fus*$^{\Delta NLS/+}$.

Notre étude a démontré que la présence de la mutation FUS$^{\Delta NLS}$ est associée à un large éventail de changements épigénétiques. Il reste à comprendre comment ces modifications épigénétiques se produisent et comment elles affectent le processus d'apprentissage. Dans notre modèle, nous avons observé un enrichissement accru des marques d'histones associées aux régions de chromatine ouverte et à la transcription des gènes (H4K12ac, H3K4me3 & H3K27) et un enrichissement réduit des marques d'histones associées à la compaction de la chromatine et à l'extinction des gènes (H3K27me3). Le groupe d'HMEG associé aux marques actives inclut des gènes hautement exprimés qui présentent une augmentation significative de leur expression chez les souris *Fus*$^{\Delta NLS/+}$ (Figure 4A & Figure S8A, B). FUS est connu pour se lier aux histones acétyltransférases CBP et p300 (Wang et al., 2008) et à certaines isoformes de HDACs (Wang et al., 2013 ; Arenas et al., 2020) et cette liaison peut être compromise par la mutation du domaine NLS C-term de FUS. Cela pourrait contribuer aux altérations épigénomiques (statut d'acétylation/méthylation des histones) sur les sites spécifiques que nous avons déchiffrés. L'intégration des modifications épigénétiques et des altérations transcriptomiques a permis de mettre en évidence des dysfonctionnements de la synapse glutamatergique au cours du processus d'apprentissage (Figure D1). En effet, après 3 jours d'entraînement dans le labyrinthe aquatique de Morris, parmi les 288 DEG uniquement régulés à la hausse dans l'hippocampe des souris FUS (Figure 2D), 121 colocalisent avec H3K4me3 HMEG, 138 avec H4K12ac HMEG et 24 avec H3K27ac HMEG (Figure D1). Parmi les gènes affectés par les 3 marques d'histones on trouve *Grin2a*, *Grin2b*, *Gria2* ou *Lrrc7*. Ces résultats suggèrent que les modifications de la chromatine induites par FUS mutant sont suffisantes pour promouvoir de manière inappropriée la transcription de ces gènes hautement exprimés dans l'hippocampe lorsque les animaux sont mis au défi (ici par un entraînement spatial), car leurs niveaux d'expression n'étaient pas modifiés chez les souris WT en apprentissage. Il est intéressant de noter que parmi les DEG uniquement régulés à la hausse en réponse à l'apprentissage chez les souris WT, certains d'entre eux colocalisent également avec les HMEG (52 avec H3K4me3 HMEG, 63 avec H4K12ac HMEG et 8

avec H3K27ac HMEG) trouvés chez les souris FUS, mais leur expression n'est pas significativement modifiée en condition basal (RNA-seq data, HC). Ces gènes ne présentent pas une signature "neuronale/synaptique" mais plutôt " transcriptionnelle ", comme par exemple quatre membres de la famille ETS (*Ets2, Etv1, Etv3, Etv5*) qui présentent des niveaux accrus de H4K12ac à leur TSS (et de H3K4me3 pour *Ets2*). Ceci indique la coexistence de différents mécanismes, conduisant au dysfonctionnement de la transcription des gènes et plus particulièrement des membres ETS chez les souris FUS.

Autres... Enfin, l'intégration des gènes cibles de FUS avec les HMEG actif a révélé 9 gènes en commun pour H3K27ac, 59 gènes en commun pour H3K4me3, 133 gènes en commun avec H4K12ac, parmi lesquels 5 étaient communs aux trois marques (Figure D2). De façon intéressante, les analyses fonctionnelles de ces gènes ont révélé que plus de la moitié d'entre eux codent pour des protéines nucléaires, parmi lesquelles un lien fort a pu être trouvé, en utilisant les analyses d'expression génique STRING, sur un nœud central associé à la transcription/expression des gènes et à la liaison à l'ADN. Ce nœud comprend d'une part les enzymes Kmt2a/Kdm2b et d'autre part le répresseur transcriptionnel YY1 et le facteur de transcription Myc.

Kmt2a/Kdm2b méthylent/déméthylent spécifiquement H3K4 et sont donc directement concernés par les dysrégulations que nous observons au niveau épigénomique chez les souris $Fus^{\Delta NLS/+\ /+}$. De plus, l'expression du gène *Kmt2a* est significativement induite chez les souris $Fus^{\Delta NLS/+\ +}$ après l'entraînement dans le MWM, ce qui indique un nouveau lien putatif entre la liaison à l'ADN de FUS, la dysrégulation épigénomique et l'altération transcriptionnelle chez les souris $Fus^{\Delta NLS/+}$ .Ce mécanisme pourrait même être dépendant d'un membre de la famille des ETS, puisque EWS, une autre protéine de la famille FET est proposée pour agir en collaboration avec ETS et p300 HAT pour se lier à H3K4me3 et H3K27ac et réguler l'expression d'autres modificateurs d'histones, dans des lignées cellulaires du Sarcome d'Ewing (Sand et al., 2015). Enfin, il a été récemment montré que les souris *Kmt2a* conditionnel KO présentent des dysfonctionnements de la mémoire (Kerimoglu et al., 2017). De manière intéressante, les neurones hippocampiques présentant un Knock down de Kmt2a présentent des niveaux de H3K4me3 diminués sur les TSS des gènes qui sont spécifiquement enrichis pour les séquence ayant un consensus ETS (Kerimoglu et al., 2017).

De manière intrigante, FUS, YY1 et Myc ont été associés aux quadruplexes de guanine de l'ADN (G4) (Li et al., 2021 ; Mishra et al., 2016 ; Spiegel et al., 2021), une structure secondaire à quatre brins riches en guanine. La formation de structures G4 a été décrite à l'origine dans des cellules humaines (Biffi et al., 2013), puis cartographiée dans les promoteurs de gènes hautement exprimés/actifs dans des cellules des mammifères (Kouzine et al., 2017). Il est intéressant de noter que la région RGG de FUS interagit avec la structure G4, présente dans les télomères (Kondo et al., 2018). Récemment, TDP-43 a également été décrit comme une protéine de liaison G4 interagissant avec la transcription riche en GGGGCC du gène C9ORF72 impliqué dans la SLA (Ishiguro et al., 2016). Si la mutation de FUS peut ou non altérer directement la formation de quadruplex G4, ou indirectement via l'altération de la conformation du promoteur de protéines spécifiques interagissant avec G4, telles que YY1 et Myc dans l'hippocampe, est une hypothèse passionnante (et spéculative) qui reste à tester chez les souris *Fus*$^{\Delta NLS/+}$.

Ensemble, ces résultats soulignent que FUS peut réguler l'environnement transcriptionnel au niveau des TSS des gènes hautement exprimés (co-partenaires, marques d'histones, structure chromatinienne 3D) plutôt que la transcription, mais qui seraient capable de promouvoir la transcription de gènes inappropriés lors de l'activation (ici l'apprentissage).

2) Les effets de la mutation de FUS se produisent-ils par un mécanisme indirect de FUS dans le cytoplasme ?

En plus de la présence du FUS mutant dans le noyau, notre étude a démontré une augmentation du FUS cytoplasmique, principalement composé du FUS$^{\Delta NLS}$ mutant (Figure 5A-C). Cette observation a déjà été décrite dans nos études précédentes (Scekic-Zahirovic et al., 2017, 2021 ; Sanjuan-Ruiz et al., 2021) ainsi que dans d'autres modèles de souris FUS Knock In (Devoy et al., 2017 ; Zhang et al., 2020). FUS est étroitement contrôlé par des mécanismes d'autorégulation (Zhou et al., 2013 ; Dini Modigliani et al., 2014 ; Humphrey et al., 2020). Cependant, la présence de FUS mutant est associée à une perturbation de l'autorégulation de FUS et à une augmentation de l'expression de FUS dans le cytoplasme. Cela a également été démontré dans notre modèle de souris *Fus*$^{\Delta NLS/+}$ (Sanjuan-Ruiz et al., 2021). Dans le compartiment cytoplasmique, FUS est associé à plusieurs fonctions telles que le transport axonal (Sama et al., 2014) et la localisation subcellulaire, la traduction locale, la stabilisation et/ou la dégradation de plusieurs ARNm liés à

la synapse (Fujii et al., 2005 ; Udagawa et al., 2015). Ainsi, FUS interagit avec de nombreuses protéines dans le cytoplasme. Il est intéressant de noter que plusieurs modifications de ces mécanismes ont été attribués à la séquestration cytoplasmique des protéines en raison d'une interaction accrue avec FUS mutant. Par exemple, l'expression du mutant R521C de FUS dans les cellules HEK293 montre une augmentation de deux fois sa demi-vie et une stabilité d'interaction accrue par rapport au FUS WT (Qiu et al., 2014). Ainsi, en présence de différentes mutations de FUS, on observe une séquestration de la kinésine-1 (Yasuda et al., 2017), de plusieurs ARNm (Tsai et al., 2020), mais aussi une séquestration et une mauvaise localisation cytoplasmique de plusieurs composants du spliceosome (Gerbino et al., 2013 ; Jutzi et al., 2020 ; Reber et al., 2016) et de HDAC1 (Scekic-Zahirovic et al., 2016). Ces informations conduisent à deux hypothèses. Une première hypothèse pourrait être que le FUS mutant favorise une interaction avec une protéine cytoplasmique qui modifierait son recrutement et sa localisation dans le cytoplasme (perte de fonction). Dans notre modèle, nous pouvons supposer que FUS mutant peut altérer la localisation d'autres enzymes modificatrices d'histones comme celle décrite par exemple pour HDAC1 (Scekic-Zahirovic et al., 2016), entraînant ainsi des changements dans les différentes marques d'histones associées à la chromatine ouverte et à la transcription et impactant finalement l'expression génique. Une autre hypothèse pourrait être que dans notre modèle, FUS mutant pourrait interagir avec les différents membres de la famille ETS ou d'autres partenaires transcriptionnels (également discuté ci-dessus). Cette idée est soutenue par une découverte récente montrant une interaction directe entre FUS et le membre ETV5 de la famille ETS (Picchiarelli et al., 2019). Il est intéressant de noter que la séquestration de SRF, un partenaire d'Elk1, est suffisante pour perturber la mémoire spatiale à long terme dans le MWM (Dash et al., 2005).

Enfin, l'interaction accrue de l'ARNm avec FUS mutant pourrait expliquer pourquoi des altérations structurelles et comportementales sont observées chez les souris *Fus*$^{\Delta NLS/+}$ sans changements majeurs dans l'expression génique. Par conséquent, l'ARNm pourrait être présent en quantité satisfaisante dans la cellule sans être au bon endroit pour la transcription. En effet, un modèle exprimant FUS mutant a démontré une diminution significative de la synthèse protéique intra-axonale (López-Erauskin et al., 2018) et un CLIP-seq de FUS réalisé dans le cortex du modèle de souris *Fus*$^{\Delta NLS/+}$ a démontré que FUS interagit avec plusieurs ARNm glutamatergiques et GABAergiques à l'emplacement de la synapse (Sahadevan et al., 2021). Dans

nos données de RNA-seq, ces ARNs sont inchangés en condition HC. Cependant, Sahadevan et ses collaborateurs ne trouvent qu'une faible corrélation entre les changements d'expression des gènes et des ARNm cibles CLIP-seq, ce qui suggère que l'interaction FUS-ARNm pourrait être modifiée dans notre modèle sans changements visibles au niveau transcriptomique. En condition d'apprentissage, nous avons observé de manière intéressante 12 gènes en commun clairement associés à la synapse glutamatergique entre les gènes uniquement régulés à la hausse chez les souris FUS et le CLIP-seq de FUS (par exemple, *Gria2*, *Gria3*) (Figure D3). Ainsi, l'augmentation spécifique de l'expression des gènes neuronaux/synaptiques uniquement observée chez les souris *Fus*$^{\Delta NLS/+}$ en condition d'apprentissage peut provenir d'une stabilisation accrue entre FUS et l'ARNm dans le compartiment cytoplasmique. Comme mentionné précédemment, FUS fait partie de la machinerie du spliceosome et est impliqué dans l'épissage alternatif (Lagier-Tourenne et al., 2012). Par conséquent, le niveau total d'ARNm pourrait être inchangé dans notre modèle, mais cela n'exclut pas des différences dans les variants d'épissage qui pourraient entraîner une altération morphologique et comportementale dans le modèle de souris *Fus*$^{\Delta NLS/+}$ .Par exemple, FUS se lie au pré-ARN de Tau dans le cerveau des souris et régule l'épissage alternatif de l'exon 10 (Orozco et al., 2012). L'inclusion accrue de l'exon 10 est associée à l'expression prédominante de l'isoforme Tau 4R et à la DFT (McCarthy et al., 2015). Ainsi, des analyses plus approfondies sur les variantes d'épissage devraient être menées dans l'hippocampe des souris *Fus*$^{\Delta NLS/+}$ pour répondre à cette question.

De plus, pour pouvoir conclure correctement sur l'altération de l'expression génique chez les souris *Fus*$^{\Delta NLS/+}$, nous devons prendre en considération que la quantité d'ARNm dans la cellule dépend de la dynamique entre la synthèse et la dégradation de l'ARNm. Ainsi, si les deux mécanismes étaient altérés dans le même sens dans notre modèle, il en résulterait un ARN total inchangé mais qui pourrait avoir un impact sur l'activation neuronale et la réponse comportementale des souris.

Les différentes hypothèses dans lesquelles FUS peut réguler les altérations transcriptionnelles sont récapitulées dans la Figure D4.

III. Validité du modèle, conséquences pour les patients atteints de SLA-DFT et perspectives thérapeutiques.

Pour être considérées comme un modèle animal valide du spectre de la SLA-DFT, nos souris *Fus*$^{\Delta NLS/+}$ doivent répondre à trois critères : homologie ou similarité étiologique (validité de construction), isomorphisme ou similarité des symptômes (validité de face), prédictivité ou réactivité pharmacologique identique (validité prédictive) (Willner, 1984).

L'utilisation d'un modèle de souris à copie unique est très analogue à la situation génétique des patients FUS-SLA, la plupart des mutations étant présentes dans la région C-terminale de la protéine FUS, y compris le domaine NLS (Shang et Huang, 2016). Les mutations de FUS conduisent à une délocalisation cytoplasmique de FUS et à des agrégats pathologiques, principalement localisés dans le cytoplasme dans les cas de SLA familial (Kwiatkowski et al., 2009 ; Vance et al., 2009) et de SLA sporadique (Bäumer et al., 2010 ; Zou et al., 2013). Une mauvaise localisation cytoplasmique de FUS, en l'absence de mutations de FUS, est observée dans plusieurs cas de SLA familial et sporadique (Tyzack et al., 2019 ; Ikenaka et al., 2020). Des agrégats cytoplasmiques de FUS sont également trouvés dans un large sous-ensemble de patients atteints de DFT (Urwin et al., 2010). Dans l'ensemble, notre modèle de souris récapitule la mutation hétérozygote présente chez les patients FUS SLA familiaux et la délocalisation cytoplasmique observée à la fois chez les patients SLA et DFT. Il est à noter que ce modèle pourrait également être d'une grande importance pour comprendre d'autres maladies liées à FUS, regroupé sous le terme FUSopathies. En effet, des mutations de FUS sont également observées dans la maladie du tremblement essentiel (Merner et al., 2012) et en l'absence de mutation, une délocalisation cytoplasmique ou une agrégation du FUS est observée dans les maladies à polyglutamine telles que l'ataxie spino-cérébelleuse (Doi et al., 2010) et la maladie d'Huntington (Doi et al., 2008). Par conséquent, nous pensons que notre modèle offre une bonne homologie, car il reflète plusieurs causes (1) l'état de la mutation et (2) la mislocalisation cytoplasmique, observée dans la SLA-FTD et d'autres FUSopathies.

Nos études démontrent que la mutation de FUS est responsable de plusieurs changements comportementaux accompagnés de changements physiologiques et moléculaires dans l'hippocampe, en particulier de grands changements dans les marques épigénétiques des

histones et dans la dérégulation des gènes en réponse à l'apprentissage. Dans la littérature, il est clairement établi que les patients atteints de DFT présentent des altérations frontales et temporales, et on pourrait penser que les changements comportementaux chez les souris *Fus*$^{\Delta NLS/+}$ reflètent principalement la pathologie de la DFT. Cependant, de plus en plus de preuves démontrent un retard mental et des difficultés d'apprentissage (Bäumer et al., 2010 ; Belzil et al., 2012 ; Fecto et Siddique, 2011 ; Huang et al., 2010 ; Onohara et al., 2015 ; Yamashita et al., 2012 ; Yan et al., 2010 ; Zou et al., 2013) ainsi qu'une DFT concomitante (Blair et al., 2010 ; Broustal et al., 2010 ; Yan et al., 2010) chez les patients atteints de SLA. Les agrégats cytoplasmiques de FUS sont en effet présents non seulement dans les motoneurones de la moelle épinière mais aussi dans le cortex frontal (Kwiatkowski et al., 2009). Cependant, la plupart des études se concentrent sur l'agrégation du FUS dans les motoneurones de la moelle épinière ou dans le cortex moteur, et à notre connaissance, il n'existe aucune étude concernant l'agrégation du FUS dans d'autres régions du cerveau. Chez les patients SLA non FUS, l'hippocampe est connu pour être affecté et atrophié (Neumann et al., 2006 ; Takeda et al., 2007, 2008 ; Abdulla et al., 2014 ; Christidi et al., 2018 ; Machts et al., 2018 ; Christidi et al., 2019). Ces dernières années, une attention particulière a été portée au développement d'outils de dépistage cognitif sensibles, afin de mettre en évidence les dysfonctionnements cognitifs chez les patients atteints de SLA (Gosselt et al., 2020). Cependant, le fait que la SLA-FUS soit principalement associée à des cas de SLA juvéniles sévères et à progression rapide (Yamashita et al., 2012 ; Zou et al., 2013) peut expliquer pourquoi nous disposons de si peu d'informations concernant les altérations comportementales et hippocampiques dans ce contexte : la progression de la maladie est si rapide qu'elle ne permet pas une caractérisation précise au-delà du dysfonctionnement moteur. Dans l'ensemble, notre modèle de souris *Fus*$^{\Delta NLS/+}$ démontre un bon isomorphisme pour étudier la similitude des symptômes dans la DFT, et pourrait aider à mieux caractériser la pathologie hippocampique potentiellement présymptomatique dans la SLA.

Nos résultats ont-ils des conséquences sur les stratégies thérapeutiques futures ? Nous avons démontré que plusieurs marques d'histones étaient altérées chez les souris *Fus*$^{\Delta NLS/+}$. Nous avons observé un enrichissement des marques d'histones associées à une chromatine active (acétylation, méthylation). Le but de ma thèse était principalement de mieux comprendre la fonction de FUS dans le cerveau plutôt que la découverte de nouvelles cibles thérapeutiques. Cependant, les altérations épigénomiques sont largement décrites dans la littérature dans le

contexte des maladies neurodégénératives, et plusieurs études se concentrent sur la régulation de l'épigénome via l'utilisation de molécules spécifiques. Ces molécules, principalement basés sur des inhibiteurs d'HDAC et des activateurs de HAT, ont la capacité de restaurer les déficits de mémoire dans différents modèles de souris de la maladie d'Alzheimer (Alarcón et al., 2004 ; Peleg et al., 2010 ; Benito et al., 2015 ; Chatterjee et al., 2018) ou de restaurer les fonctions métaboliques et lipidiques dans la moelle épinière d'un autre modèle de souris SLA-DFT exprimant FUS humain (Guo et al., 2017 ; Burg et al., 2021). Cependant, ce type de stratégie pourrait ne pas convenir pour traiter les dysfonctionnements de l'hippocampe dans notre modèle de souris, car les inhibiteurs d'HDAC et les activateurs de HAT pourraient entraîner des niveaux d'acétylation encore plus élevés. FUS mutant est associé à une diminution des niveaux d'acétylation dans la moelle épinière murine (Burg et al., 2021) et dans les motoneurones de cultures primaires de moelle épinière (Tibshirani et al., 2015), alors que nous avons observé une augmentation de l'acétylation dans l'hippocampe dans cette étude. Il est donc probable que les inhibiteurs d'HDAC/activateurs d'HAT puissent affecter positivement certaines cellules tout en influençant négativement d'autres types de cellules impliquées dans la physiopathologie de la SLA et de la DFT. De plus, alors que les souris déficientes en HDAC2 présentent une facilitation de la mémoire et un nombre accru de synapses dans les tâches d'apprentissage contextuel de la peur et de mémoire spatiale (Guan et al., 2009), la perte spécifique de HDAC4 dans les neurones entraîne des défauts de coordination motrice et d'apprentissage ainsi qu'une augmentation des comportements de type anxieux (Kim et al., 2012). Nous avons discuté plus en détail de l'effet potentiellement négatif des inhibiteurs d'HDAC dans un commentaire qui se situe dans la section annexe de cette thèse (Boutillier et al., 2019).

Au final, il est encore trop tôt pour conclure à la prédictivité et à la réactivité pharmacologique identique dans le modèle de souris *Fus*$^{\Delta NLS/+}$ puisqu'aucun traitement n'est actuellement disponible pour traiter les altérations épigénétiques dans la maladie SLA-DFT. Cibler l'acétylation pourrait être une approche prometteuse dans certaines circonstances, mais des molécules qui interagissent avec des cibles plus précises, ou le développement d'un traitement local spécifique aux motoneurones ou aux régions corticales pourraient être nécessaires pour traiter les altérations épigénétiques dans le contexte des maladies SLA-DFT.

Université de Strasbourg

École Doctorale des Sciences de la Vie et de la Santé STRASBOURG

Laura TZEPLAEFF

Memory dysfunctions and associated epigenetic and transcriptomic changes in an ALS/FTD mouse model linked to a FUS mutation

Summary:

FUS protein dysfunction is linked to Amyotrophic lateral sclerosis (ALS) and Frontotemporal dementia (FTD), two fatal neurodegenerative diseases. Mutation in the FUS gene has been linked to ALS, while FUS cytoplasmic mislocalization is observed in both ALS and FTD patients. The FUS protein is involved with all steps of gene expression, including transcription, alternative splicing, and mRNA transport. FUS has also been associated to DNA damage repair pathways, epigenetic modifications, and several neuronal functions. To date, whether and how FUS mutation can impact neuronal functions such as learning and memory processes though transcriptomic, and genome wide epigenetic changes has never been studied. We first show that FUS mice bearing FUS mutation present several forms of cognitive disabilities. Second, our study demonstrates that FUS is able to bind specific loci on DNA, likely ETS/ELK promoter responsive elements present at the TSS of highly expressed genes. We further show that the truncated FUS mutation results in a wide range of epigenomic changes, likely underlying subsequent transcriptional alterations that are significantly measurable on the hippocampal transcriptome of trained mice. Such alterations may support the discrete but widespread memory deficits observed in the FUS mouse model. These studies highlight the impact of FUS mutation in a structure such as the hippocampus, generally less studied in ALS or FTD, but crucial in memory processes.

Keywords: amyotrophic lateral sclerosis, frontotemporal dementia, FUS, epigenetic, learning-induced transcriptome, hippocampus, neurons, behavioral characterization.

Résumé :

La dérégulation de la protéine FUS est liée à la sclérose latérale amyotrophique (SLA) et à la démence frontotemporale (DFT), deux maladies neurodégénératives mortelles. La mutation du gène FUS est liée à la SLA, tandis que la mauvaise localisation cytoplasmique de la protéine FUS est observée chez les patients atteints de SLA et de DFT. La protéine FUS est impliquée dans toutes les étapes de l'expression génétique, y compris la transcription, l'épissage alternatif et le transport de l'ARNm. FUS est également impliqué dans les voies de réparation des dommages de l'ADN, les modifications épigénétiques et dans plusieurs fonctions neuronales. Jusqu'à présent, on n'a jamais étudié si et comment la mutation de FUS pouvait avoir un impact sur les processus neuronaux tel que l'apprentissage et de mémoire par le biais de changements transcriptomiques et épigénétiques à l'échelle du génome. Notre étude montre que FUS est capable de se lier à des loci spécifiques sur l'ADN au niveau de la TSS de gènes hautement exprimés, probablement sur des éléments du promoteur liant les facteurs de transcription ETS/ELK. Nous montrons que la mutation FUS entraîne de nombreuses modifications épigénomiques, probablement à l'origine d'altérations transcriptionnelles mesurables dans l'hippocampe de souris entraînées. Ces altérations pourraient sous-tendre les déficits de mémoire discrets mais généralisés observés dans le modèle de souris FUS. Ces études mettent en évidence l'impact de la mutation de FUS dans une structure telle que l'hippocampe, généralement moins étudiée dans la SLA ou la DFT, mais cruciale dans les processus de mémoire.

Mots Clés : sclérose latérale amyotrophique, démence frontotemporale, FUS, epigenetique, transcriptome induit par l'apprentissage, hippocampe, neurones, caractérisation comportementale.